

**Understanding and modelling of motion sickness and its individual differences for the comfortable control of automated vehicles**

Irmak, T.

**DOI**

[10.4233/uuid:6a97e555-a39f-48b1-be2d-612b6f5510b7](https://doi.org/10.4233/uuid:6a97e555-a39f-48b1-be2d-612b6f5510b7)

**Publication date**

2022

**Document Version**

Final published version

**Citation (APA)**

Irmak, T. (2022). *Understanding and modelling of motion sickness and its individual differences for the comfortable control of automated vehicles*. [Dissertation (TU Delft), Delft University of Technology]. <https://doi.org/10.4233/uuid:6a97e555-a39f-48b1-be2d-612b6f5510b7>

**Important note**

To cite this publication, please use the final published version (if applicable). Please check the document version above.

**Copyright**

Other than for strictly personal use, it is not permitted to download, forward or distribute the text or part of it, without the consent of the author(s) and/or copyright holder(s), unless the work is under an open content license such as Creative Commons.

**Takedown policy**

Please contact us and provide details if you believe this document breaches copyrights. We will remove access to the work immediately and investigate your claim.

**UNDERSTANDING AND MODELLING OF  
MOTION SICKNESS AND ITS INDIVIDUAL  
DIFFERENCES FOR THE COMFORTABLE  
CONTROL OF AUTOMATED VEHICLES**



# UNDERSTANDING AND MODELLING OF MOTION SICKNESS AND ITS INDIVIDUAL DIFFERENCES FOR THE COMFORTABLE CONTROL OF AUTOMATED VEHICLES

## Dissertation

for the purpose of obtaining the degree of doctor  
at Delft University of Technology  
by the authority of the Rector Magnificus, prof. dr. ir. T.H.J.J van der Hagen,  
Chair of the Board for Doctorates  
to be defended publicly on  
Monday 16 May 2022 at 10:00 o'clock

by

**Tuğrul IRMAK**

Master of Engineering in Mechanical Engineering, University of Bristol,  
Bristol, The United Kingdom  
born in Üsküdar, Turkey.



This dissertation has been approved by the promotor

promotor: Dr.ir. R. Happee

copromotor: Dr.ir. D.M. Pool

Composition of the doctoral committee:

Rector Magnificus	chairperson
Dr.ir. R. Happee	Delft University of Technology, promotor
Dr.ir. D.M. Pool	Delft University of Technology, copromotor

*Independent members:*

Prof.dr.ir. M. Mulder	Delft University of Technology
Prof.dr. P. Vink	Delft University of Technology
Prof.dr. J.E. Bos	Vrije Universiteit Amsterdam
Prof.dr. T. Wada	Nara Institute of Science and Technology

*Reserve Members:*

Prof.dr. D.M. Gavrilă	Delft University of Technology
-----------------------	--------------------------------

*Other Members:*

Prof.dr. H. Bülthoff	Max-Planck-Institut für biologische Kybernetik
----------------------	--

Dr. Ksander N. de Winkel contributed significantly to the realisation of the thesis.

Keywords: motion sickness, motion perception, mathematical modelling, individual differences, parameter estimation, automated vehicles

Printed by: Ridderprint

Cover design: Anna Bleeker

Copyright © 2022 by T. Irmak

ISBN 978-94-6458-238-3

An electronic version of this dissertation is available at

<http://repository.tudelft.nl/>.

*The desire for safety stands against every great and noble enterprise*

Tacitus



# CONTENTS

<b>Summary</b>	<b>xi</b>
<b>1 Introduction</b>	<b>1</b>
1.1 Motion Sickness and the Automation Revolution . . . . .	1
1.2 The Brain as an Observer. . . . .	3
1.3 Properties of Motion Sickness . . . . .	6
1.4 Observer Theory and Motion Sickness . . . . .	8
1.5 Conflict to Sickness. . . . .	10
1.6 Research Objective . . . . .	11
1.7 Approach . . . . .	12
1.8 Thesis Outline . . . . .	12
1.8.1 Chapter 2: Objective and Subjective Quantification of Individual and Group Responses to Sickening Stimuli . . . . .	12
1.8.2 Chapter 3: Amplitude and Temporal Dynamics of Motion Sickness . . . . .	14
1.8.3 Chapter 4: Individual Motion Perception Parameters and Motion Sickness Frequency Sensitivity in Fore-Aft Motion . . . . .	14
1.8.4 Chapter 5: Validation of Perception Models for Motion Sickness Prediction . . . . .	15
1.9 Scope . . . . .	15
<b>2 Objective and Subjective Quantification of Individual and Group Responses to Sickening Stimuli</b>	<b>17</b>
2.1 Abstract. . . . .	18
2.2 Introduction . . . . .	18
2.3 Methods. . . . .	20
2.3.1 Participants . . . . .	20
2.3.2 Apparatus. . . . .	21
2.3.3 Task & Stimuli . . . . .	21
2.3.4 Instrumentation for Physiological Measurements . . . . .	23
2.3.5 Data Pre-processing . . . . .	23
2.3.6 Data Analysis. . . . .	25
2.4 Results . . . . .	28
2.4.1 Experiment 1: Internal-External Vision Group Response. . . . .	28
2.4.2 Experiment 2: Model fit . . . . .	30
2.4.3 Experiment 2: Repeatability of Individual Responses . . . . .	31
2.4.4 Experiment 2: Hypersensitivity . . . . .	33
2.4.5 Experiment 2: Influence of Parameters . . . . .	33

2.4.6	Experiment 1 & Experiment 2: Kinematic and Physiological Variables . . . . .	33
2.5	Discussion . . . . .	36
2.5.1	Internal-External Vision . . . . .	36
2.5.2	Repeatability and Oman's Model . . . . .	37
2.5.3	Kinematic and Physiological Variables . . . . .	38
2.5.4	Implications. . . . .	40
2.6	Conclusion . . . . .	40
<b>3</b>	<b>Amplitude and Temporal Dynamics of Motion Sickness</b>	<b>43</b>
3.1	Abstract . . . . .	44
3.2	Introduction . . . . .	44
3.3	Methods. . . . .	47
3.3.1	Ethics Statement . . . . .	47
3.3.2	Participants . . . . .	47
3.3.3	Apparatus. . . . .	47
3.3.4	Task . . . . .	47
3.3.5	Quantifying sickness . . . . .	48
3.3.6	Sickness Model . . . . .	49
3.3.7	Statistical Analysis . . . . .	51
3.4	Results . . . . .	52
3.4.1	Group-level Observations . . . . .	52
3.4.2	Oman Model . . . . .	52
3.4.3	Amplitude Cross Validation . . . . .	58
3.4.4	Sickness Forecasting . . . . .	58
3.5	Discussion . . . . .	61
3.5.1	Group-level Observations . . . . .	62
3.5.2	Individual-level Modelling . . . . .	63
3.5.3	Limitations . . . . .	66
3.6	Conclusion . . . . .	67
<b>4</b>	<b>Individual Motion Perception Parameters and Motion Sickness Frequency Sensitivity in Fore-aft Motion</b>	<b>69</b>
4.1	Abstract . . . . .	70
4.2	Introduction . . . . .	70
4.3	Methods. . . . .	74
4.3.1	Ethics Statement . . . . .	74
4.3.2	Participants . . . . .	74
4.3.3	Apparatus. . . . .	74
4.3.4	Task & Stimuli . . . . .	75
4.3.5	Data Reduction . . . . .	78
4.3.6	Peak Frequency of Sickness . . . . .	82
4.4	Results . . . . .	83
4.4.1	Perception Experiment . . . . .	83
4.4.2	Sickness Experiment . . . . .	83
4.4.3	Sickness and Perception . . . . .	87

---

4.5	Discussion . . . . .	88
4.5.1	Quantifying Sickness . . . . .	90
4.5.2	Group Sickness Sensitivity . . . . .	90
4.5.3	Individual Sickness Sensitivity . . . . .	91
4.5.4	Perception and Sickness . . . . .	92
4.5.5	Limitations . . . . .	93
4.6	Conclusion . . . . .	94
<b>5</b>	<b>Validation of Perception Models for Motion Sickness Prediction</b>	<b>97</b>
5.1	Abstract . . . . .	98
5.2	Introduction . . . . .	98
5.3	Models & Methods . . . . .	102
5.3.1	Models . . . . .	102
5.3.2	Motion Sickness Accumulation Model . . . . .	108
5.3.3	Model Tuning . . . . .	109
5.3.4	Model Validation for Sickness . . . . .	111
5.4	Model Tuning Results . . . . .	112
5.4.1	Fit to Empirical Perception Time-Domain Data . . . . .	112
5.4.2	Perception Frequency Responses . . . . .	115
5.4.3	Fit to Empirical Sickness Frequency Sensitivities . . . . .	115
5.5	Sickness Validation . . . . .	119
5.5.1	Subjective Vertical Model . . . . .	120
5.5.2	Multi-Sensory Observer Model . . . . .	122
5.5.3	Particle Filter Model . . . . .	122
5.6	Discussion . . . . .	122
5.6.1	Perception . . . . .	123
5.6.2	Sickness . . . . .	124
5.6.3	Future Work . . . . .	127
5.7	Conclusion . . . . .	128
<b>6</b>	<b>Discussion &amp; Recommendations</b>	<b>131</b>
6.1	Discussion . . . . .	132
6.1.1	Part I: Quantitative Analysis of Individual Differences . . . . .	132
6.1.2	Part II: Modelling the Temporal Dynamics of Motion Sickness . . . . .	134
6.1.3	Part III: Modelling the Dynamics of Sensory Conflict . . . . .	136
6.1.4	Implications & Recommendations . . . . .	138
6.2	General Conclusion . . . . .	141
	<b>References</b>	<b>143</b>
<b>A</b>	<b>Appendix of Chapter 3</b>	<b>163</b>
A.1	Individual Normalised MISC Rate . . . . .	163
A.2	Model Fits to All Individual Responses . . . . .	164
A.3	Sickness Forecasting . . . . .	165

---

<b>B</b>	<b>Appendix of Chapter 4</b>	<b>169</b>
B.1	Perception Experiment Responses . . . . .	170
B.2	MSOM Model Fits to Perception Responses . . . . .	172
B.3	Cross-over Frequency . . . . .	174
B.4	Sickness Experiment Responses . . . . .	175
B.5	Fixed Effect Model Residuals . . . . .	176
<b>C</b>	<b>Appendix of Chapter 5</b>	<b>177</b>
C.1	Motion Implementation . . . . .	177
C.2	Conflict Power . . . . .	179
C.3	SVM Lateral and Vertical Response Derivation . . . . .	180
C.4	MSOM Lateral Response Derivation . . . . .	182
	<b>Acknowledgements</b>	<b>185</b>
	<b>List of Publications</b>	<b>191</b>

# SUMMARY

By 2050 a large proportion of the cars on our roads will be self-driving and completely automated. We will no longer be driving these vehicles, but will be transported comfortably as passengers. We will be able to indulge in all sorts of media items in our vehicles, do work, or even just relax and sleep. Indeed, these fully automated vehicles will have a clear positive impact on everybody's lives. That is, if people do not become too motion sick to enjoy the ride.

It is known that drivers of vehicles do not get motion sick because they are in control of the vehicle and, hence, can anticipate upcoming motions. However, many passengers, which we will all eventually become, do experience motion sickness. This is particularly an issue when their eyes are off the road and when they are engaged in other activities. With a rising prospect of motion sickness, these activities may no longer seem attractive. Moreover, motion sickness increases workload and decreases cognitive performance, which means that those wishing to use their commuting time in cognitively demanding activities will be less productive in them.

With full automation, it is hoped that vehicle control systems can be optimised to reduce sickening motions to the lowest feasible level, whilst also achieving adequate vehicle performance in terms of, for instance, journey time. However, at this moment we don't yet have a good model of motion sickness that would enable such optimization. For example, route planning algorithms generally optimise for the shortest time, while some have recently started to optimise for the least polluting route. For this optimisation, the algorithm needs to have, amongst other things, traffic information, the roads, their lengths and legally allowable speeds, with all such information encapsulated in a general mathematical model. There is, however, no analogous model of motion sickness that can be used to optimise our vehicle's behaviour for the lowest passenger sickness incidence. A mathematical model in this sense is a set of equations that tell us how sickening a certain pattern of motion will be. A pattern of motion could be the vehicle taking a turn, switching a lane, stopping at a traffic light; anything that makes the vehicle change speed or direction. By being able to predict how much sickness will result from certain manoeuvres, the vehicle can be programmed to perform these manoeuvres in the least sickening manner.

One problem with developing mathematical models for motion sickness minimisation is that there is a great variability in how motion sickness manifests itself in individuals. This means that the motion sickness symptoms, their accumulation and even the nature of the motions that cause sickness are highly individual. Therefore, any algorithm meant for vehicle control must take the individual as the subject of its concern.

Prior to this thesis, the individual was not seen as a feasible unit of study. Instead, literature mainly focused on group-level responses. However, because motion sickness is so variable, it is likely that optimising group-averaged criteria, will



not optimise for group-averaged comfort. Instead, individualisation is needed. This need directly shaped the objective of this thesis, which was to *understand and model motion sickness accumulation and its individual differences for the comfortable control of automated vehicles*.

In this thesis, this objective was addressed in the three main parts:

1. *Quantitative analysis of individual differences*
2. *Modelling the temporal dynamics of motion sickness*
3. *Modelling the dynamics of sensory conflict*

This thesis describes four different human-subject experiments performed to systematically study the effects of: visual viewing condition, acceleration amplitude and acceleration frequency on the accumulation of motion sickness. Uniquely, to best measure individual differences, all experiments were done using a within-subject design. Temporal variations in the level of motion sickness in these experiments were measured using the MIsery SScale (MISC), a well-known subjective rating scale for motion sickness.

Two of the experiments (see chapter 2) were conducted on-road, using a passenger vehicle. Here, participants were exposed to a sickening drive in the form of repeated slaloms. Experiment 1 compared two visual conditions, internal (where the outside vehicle view was occluded) and external vision (where the participants were requested to look outside), while the second experiment focused only on internal vision. In both experiments, physiological and postural signals were recorded. From Experiment 1, it was found that internal vision was more sickening compared to external vision. This was likely related to the reduction in anticipatory cues. Experiment 2 tested hypersensitivity with a second exposure a few minutes after the first drive and tested repeatability of individuals' sickness responses by measuring these two exposures three times in three successive sessions. As a result, the existence of hypersensitivity that occurs as a consequence of motion sickness exposure was confirmed. Moreover, the Oman model of nausea was fitted to the MISC data. The Oman model is a control-theoretic model of motion sickness accumulation and the only one that is able to describe the hypersensitivity seen in Experiment 2. Due to rest periods between motion stimuli (e.g. traffic lights), modelling hypersensitivity is particularly important to vehicular transport. From the Oman model, it was determined that individuals have repeatable accumulation of motion sickness over time, where the variation in intra-individual motion susceptibility was small. This shows that the individual is, in fact, a feasible unit to study motion sickness and that day-to-day variations do not swamp the measurements of the desired signal. From the pooled physiological and postural signals in Experiment 1 and Experiment 2, it can be concluded that the galvanic skin response (sweating) was the only significant physiological correlate of motion sickness, but that despite their various drawbacks, subjective ratings remain a superior motion sickness metric.

In Experiment 3, which is the subject of chapter 3, the SIMONA Research Simulator at TU Delft's Aerospace Faculty was used. Here, the effect of motion amplitude

on sickness accumulation was studied. This experiment, unlike the prior two, was performed with eyes-open in darkness. The results showed that within an individual, sickness (given as MISC ratings) increased linearly with acceleration amplitude, a finding consistent with the group response. As a consequence of this experiment, for the first time, the Oman model was thoroughly validated in its predictions for multiple acceleration amplitudes and its parameter values were determined. This was done by fitting the Oman model to the MISC data. The resulting median parameter values were: 66.2 and 502.4 for the fast and slow time constants, 70.8 and 0.4 for the gain and non-linear output power scaling. Results also showed that individuals may display convergent or divergent sickness trajectories, and have a propensity for one over the other, with current methods of modelling sickness accumulation being best suited for the convergent trajectories.

Similar to Experiment 3, Experiment 4, which is the subject of chapter 4, was also simulator-based and with the same visual condition of eyes-open in darkness. In this experiment, the Cable-Robot Simulator at Max Planck Institute for Biological Cybernetics was used to investigate the effect of frequency on motion sickness susceptibility. Moreover, another simulator at the same research facility, the Cyber-Motion Simulator, was used to investigate motion perception parameters of the participants. In this experiment, individual frequency sensitivities were found to be distinctly different from the group sensitivity. Certain participants were more susceptible to lower, others to mid and higher frequencies. However, there was no clear peak in the group-level sensitivity when averaged across all individuals. This means that a "one size fits all" approach is suboptimal for motion sickness mitigation. Moreover, it was found that the overall sickness susceptibility to fore-aft motions was highly correlated ( $r = 0.74$ ) to the subjective vertical time constant that was measured in the Cyber-Motion Simulator.

It is generally hypothesised that motion sickness is caused by sensory conflicts that arise from a difference between incoming sensory signals and those signals expected by the brain. In chapters 2 and 3, the temporal dynamics of motion sickness were studied using simple motions in one direction. This meant that the internal sensory conflict could be assumed to be proportional to the accelerations experienced. In chapter 5 of this thesis, the sensory conflict term is instead derived from 6-D dynamic models of motion perception. To this end, three state-of-the-art motion perception models from literature were assessed: the Subjective Vertical Model, the Multi-sensory Observer Model and the Particle Filter model. As a result of this work, it was found that these available motion perception models did not generalise well across multiple motion paradigms to describe observed motion sickness. The most commonly used model of motion sickness, the Subjective Vertical model, provided the best specific fits to empirically observed group-level motion sickness frequency sensitivity to horizontal and vertical plane accelerations. However, the Subjective Vertical model did show important deviations from the observer framework from which sensory conflicts are derived, and the perceptual correlates to its variables were not clear. As a consequence of this model comparison, two crucial mechanisms for motion sickness prediction were identified. The first mechanism is an active estimation of the magnitude of gravity, which was found to be the only feasible way

of explaining motion sickness caused by vertical accelerations. The second mechanism identified was the somatogravic effect, as mediated by the two-way coupling between the semicircular canals and the otoliths. This was found to be important to model the differences in the frequency sensitivities between vertical and horizontal plane accelerations. Indeed, Experiment 4 empirically confirmed the relevance of the somatogravic effect for overall sickness susceptibility towards horizontal plane accelerations.

This thesis has achieved its main objective of increasing our understanding of motion sickness and its individual differences, as well as furthering motion sickness modelling capabilities. The experimental and modelling results of this thesis provide a firm foundation that will accelerate future research. For example, by showing that individuals have repeatable motion sickness responses and that individual dynamics can be captured by models of motion sickness accumulation, this thesis has opened the door for closed-loop identification of the dynamics driving sickness at the individual level. This will expedite the data bottleneck that currently hampers motion sickness research. Moreover, this thesis revealed that contemporary motion sickness models have difficulties in predicting sickness in those conditions they were not explicitly fitted to. It is argued that probabilistic models of sensory integration may represent motion sickness in a more emergent manner and ultimately provide better insights that may be used to design more comfortable automated vehicle controllers.

# 1

## INTRODUCTION

### 1.1. MOTION SICKNESS AND THE AUTOMATION REVOLUTION

The hyperbolic trajectory of technological growth (Roodman, 2020) has given many wonders and promises many more. One latest fruit of this process is automated vehicles. Completely self-driving vehicles are expected to reach 50% of market share by 2050 (Kyriakidis et al., 2015; Wadud et al., 2016). In Europe, the average vehicle occupancy rates for passenger cars is 1.7, indicating that it is mostly the driver that is in the vehicle (Fiorello et al., 2016). Automated vehicles are envisioned by society to be the embodiment of freedom, liberating the driver from the monotonous task of driving and allowing them to make use of otherwise unproductive travel time. Indeed, surveys reveal that approximately 40% of respondents would like to use this time to engage in cognitively demanding tasks such as working or reading (Kyriakidis et al., 2015).

For 30% of the population (Schmidt et al., 2020), however, this metamorphosis from driver to passenger prompts forth the atavistic malady (Huppert et al., 2017) of motion sickness. The driver does what the passenger can not, that is, to almost perfectly anticipate and initiate upcoming motions of the vehicle (Östh et al., 2014). The control over ego-motion, whether through a vehicle or one's own limbs, almost always suppresses motion sickness (Rolnick and Lubow, 2007). It is also the case that removing the driving task allows people to engage in non-driving activities. These activities require a shift of the visual focus from the road, to the inside of the vehicle. The reduction in visual information not only reduces one's ability to anticipate future motions of the vehicle (Griffin and Newman, 2004a), but also creates sensory rearrangement. That is, the brain is troubled by the contradictory existence of stationary visual stimuli and active sensation of movement caused by the vehicle and registered by the senses of balance, the vestibular system (Diels and Bos, 2016).

Motion sickness is a multisymptomatic syndrome that is often characterised in humans by initial symptoms such as headache, dizziness, sweating, stomach awareness and nausea (Bertolini and Straumann, 2016). These symptoms usually then progress in severity before culminating in retching and emesis (Bos et al., 2005). Most vertebrates suffer from motion sickness, including dogs (Wang and Chinn, 1956), cats (Hickman et al., 2008), rats (Mitchell et al., 1977), frogs (Wassersug et al., 1993) and even fish (Bauerle et al., 2004), though how motion sickness manifests differs

considerably between species. Rats for instance are incapable of emesis, though they do display conditioned gaping (Parker, 2014), likewise vomiting response in frogs can be delayed by hours after the end of the sickening motion stimulus (Naitoh et al., 2001). Motion sickness is, therefore, phylogenetically old. So old, in fact, it predates the evolution of the mammalian cochlea, our hearing apparatus (Manley, 2012). The fact that this apparently maladaptive response is evolutionarily conserved, leads some researchers (Bowins, 2010) to believe it might have a beneficial function. This adaptationist view was first put forth in the toxin detection hypothesis, formulated by Treisman (1977). Here, it is thought that the vestibular organ is a back-up to the chemoreceptors in the stomach and works to detect sensory rearrangement that might occur due to the consumption of a toxic substance. Symptoms that promote avoidance and expulsion of consumables, such as stomach awareness, taste aversion and vomiting, are clearly in line with this hypothesis. Other researchers take a more pluralist view and argue that motion sickness is likely an unintended, undesirable by-product of the useful process of state-estimation and motion perception employed by the brain (Oman, 2012). Moreover, given that motion sickness does not occur under natural conditions, but exclusively in artificial ones, it is not surprising that there was no selection against it.

The aim of motion sickness research is to understand the aetiology of motion sickness in detail and leverage this knowledge to improve, among many other things, passenger comfort in automated vehicles. This may seem like a vain research aim for some. However, it should be noted that some people are affected to such a degree as to avoid passive vehicular travel (Dai et al., 2010; Saunders, 1976). Indeed, certain ethnicities are known to have higher motion sickness susceptibility than others (Klosterhalfen et al., 2005) and there seems to be disparate impact of sex on the experience of motion sickness (Golding, 2006; Koslucher et al., 2015), with females being more susceptible than males. Therefore, reduction in motion sickness promotes the inclusivity of the technology, increasing its overall utility. To minimise motion sickness subject to vehicle motions, one must be able to express motion sickness as a function of these motions. This functional relationship between the input motions and ensuing sickness yields itself readily to mathematical treatment in the form of control-theoretic models. These models may then be used to predict the expected sickness for a given motion profile. With the driver now becoming the passenger it allows for the optimization of the automated drive through various technologies such as active suspension, motion planning and even route planning algorithms (Htike et al., 2020; Li and Hu, 2021).

There are, however, inherent challenges in operationalising a phenomenon such as motion sickness. For instance, unlike mass, energy, pressure or temperature, there is no natural unit of motion sickness. This means it is usually measured using subjective ratings such as the MIserY SScale (MISC) (Bos et al., 2005) which is an ordinal scale of sickness severity. The subjective nature of the measurements makes it hard to quantify motion sickness. Moreover, there is a spectacular degree of inter-individual variability in the manifestation of motion sickness. This variability is due to individual differences in autonomic sensitivity and prior motion exposure (Golding, 2006). Lastly, there is substantial delay between the motions and the resulting motion sick-

ness symptoms, making conventional system identification methods difficult to employ. Despite these hurdles, many excellent studies have demonstrated feasible approaches to quantitative modelling of motion sickness (Wada, 2021; Khalid et al., 2011b; Kamiji et al., 2007; Bos and Bles, 1998, 2002b; Zupan et al., 1994; Oman, 1991). These studies highlight the link between motion perception and motion sickness via the *observer* framework, where motion sickness is thought to be due to the conflict between internally predicted or expected sensory information, and the realised sensory information reported by the senses.

### 1.2. THE BRAIN AS AN OBSERVER

From the mutual exclusivity of knowing both the position and momentum of an elementary particle, to the length and severity of the next viral wave, uncertainty and ambiguity permeate through our physical reality. Sensory information transduced by the sensory apparatus of any organism is also subject to this uncertainty. One line of evidence for this comes from experiments on the response of retinal ganglion cell to light, which is probabilistic in nature (Barlow and Levick, 1971). Any noise that is innate to the sensor, whether it be quantum mechanical, in the case of retinal ganglion cells, or mechanical, such as that transduced by the otolith organs of the vestibular apparatus, will be subject to amplification due to conversion to an electrical signal (transduction noise) (Lillywhite and Laughlin, 1979). Even further along the processing pipeline, noise is present at all neural synapses (Rusakov et al., 2020).

In addition to being noisy, sensory signals can often be ambiguous. This is where multiple interpretations of the same sensory stimulus exist. One accessible example of this sensory ambiguity comes from the study of multistable imagery, examples of which are shown in Figure 1.1. In these images, there are two mutually exclusive interpretations of the same sensory input (Sterzer et al., 2009). Perception, may therefore, oscillate between the two possible interpretations, switching from every few seconds to tens of seconds with great degree of individual variability (Kornmeier et al., 2009). Examples of multistability exist for all the senses. One example the reader is encouraged to try is the “*Verbal Transformation Effect*” (Schwartz et al., 2012). In this, rapidly repeated vocalisation of the word “life” provides auditory stimuli that is fully compatible with both “fly” and “life”. The reader will notice that there is spontaneous switching between the two interpretations.

Similar ambiguities also exist for spatial orientation and motion perception. For instance, when participants are moved in the fore-aft direction using low-frequency accelerations in the absence of vision, participants may perceive: direct horizontal translation, going over a hill, and being swung on a swing (Wertheim et al., 2001). This is a manifestation of the tilt-translation ambiguity (Wood et al., 2007), and just like the visual and auditory bistable phenomena, differing interpretations emerge spontaneously. Although unlike the visual and auditory phenomena, the switching from one interpretation to another happens more slowly, over the course of minutes. In the absence of vision, this ambiguity is caused by the ambiguous sensory information provided by the otoliths of the vestibular system.

The otoliths are composed of bio-crystals named otoconia that lie above hair cells’ hair bundles known as stereocilia (Nam, 2017). The stereocilia themselves are at-

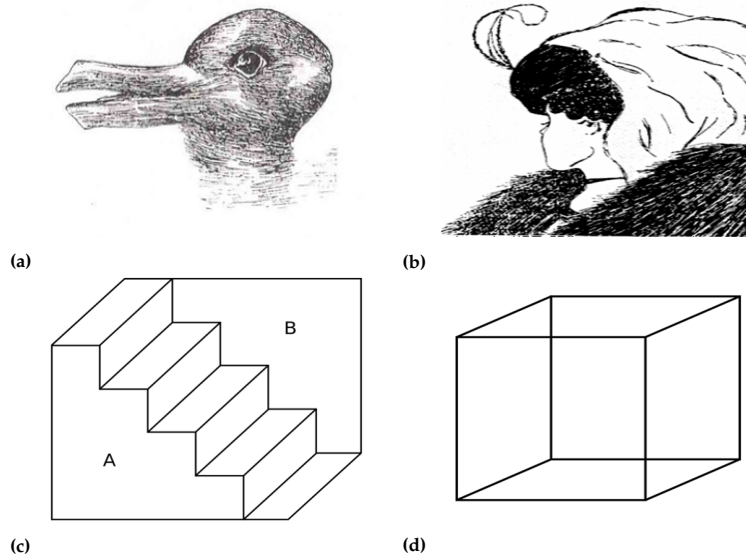


**Fig. 1.1** Examples of multistable sensory information, in this case, visual information. (a) and (b) are bistable images that illicit recognition ambiguity. (a) has two equilibrium states, a rabbit facing right and a duck facing left. Likewise, (b), known as “My wife and my mother-in-law” is also bistable, with the wife facing away from the reader and the mother-in-law facing toward the reader. (c) and (d) are examples of bistability in perception of object orientation in 3D. (c) shows both a staircase descending from left to right, but also the same staircase turned upside down. Likewise, (d), known as the “Necker cube” shows a cube that can be interpreted to have either the lower-left or the upper-right square as its front side

tached firmly to the otoconial gel. Upon acceleration of the head, the hair cells and the epithelial layer they are embedded in move with the head. Due to inertia, there is a consequent deflection of the stereocilia connecting the hair cells to the otoconial mass. This deflection is proportional to the acceleration experienced (Nam, 2017). However, due to Einstein’s equivalence principle, inertial acceleration cannot be discriminated from acceleration due to gravity (Merfeld et al., 2005a). Therefore, the otoliths report the inherently ambiguous gravito-inertial acceleration (also referred to as “specific force”). In the case of low-frequency fore-aft accelerations, this allows for multiple perceptual interpretations consisting of inertial only (fore-aft) motion, rotation, or a combination thereof.

The existence of multistable perception highlights an important fact about the connectivity of the brain. This is the existence of a hierarchical organisation (Wang et al., 2013) composed of: forward connections running from lower brain areas, such as the sensory periphery, to higher cortical areas, as well as backward connections running from higher cortical areas, to lower (Friston, 2005). The higher areas are thought to have an internal representation of the cause of a given sensory stimulus (Huang and Rao, 2011). Here, “predictions” encoded at the higher levels are compared with the sensory stimuli represented at the lower levels. The resulting *prediction errors* update the higher level predictions. The synergy between internal



predictions, sensory input and consequent prediction errors allows for inferences to be made about the causes of uncertain sensory data. The contemporary formulation of this hypothesized mode of operation is known as “*Predictive Coding*”, and was initially developed to model the neural activity in the visual cortex (Rao and Ballard, 1999).

As discussed previously, sensory information in regard to motion perception and spatial orientation is also inherently ambiguous and noisy. The brain must therefore infer, or as commonly named in control theoretic literature, *observe*, the cause of a given sensory stimulus. For spatial orientation, the cause it must observe is the real kinematic states of the organism, namely; angular orientation with respect to gravity, angular velocity, translational velocity and other such kinematic states (Bos and Bles, 2002b). There is strong neural evidence to indicate that the brain employs methods of *internal modelling* and prediction errors also for spatial orientation and motion perception (Laurens et al., 2013; Angelaki et al., 2004; Laurens and Angelaki, 2017).

Angelaki et al. (2004) for instance, identified motion sensitive neurons in the vestibular nuclei and the rostral fastigial nucleus whose firing rates were indicative of tilt-translation ambiguity resolution. Likewise, Laurens et al. (2013) recorded simple spike activity from both the nodulus/uvula Purkinje cells and the rostral fastigial nucleus during Tilt-While Rotating stimulation (TWR). TWR produces a false perception of translation, as well as a translational vestibular ocular reflex (tVOR). tVOR is an involuntary translation of the eyes in proportion to the stimulus, which can be measured reliably using video-oculography. The authors showed that the tVOR was predicted accurately by the internal model framework, and that the simple spike activity in these brain regions quantitatively matched the internal model predictions. Lastly, neurons in the vestibular nuclei and the rostral fastigial nucleus (regions of the brain thought to be involved in internal modelling) respond preferentially to passive motions, and that expected sensory consequences of active movement cancel out any reference signal from the semicircular canal and otolith inputs (Cullen, 2018). These studies provide strong support for the use of internal models by the brain to account for sensory noise and ambiguity in motion perception and spatial orientation.

A simple example of how internal modelling via prediction errors work to observe real kinematic states is the velocity storage mechanism. During constant velocity earth vertical yaw rotation, the rate of neural spikes originating from the hair cells of the semicircular canals decay toward baseline in 4-5 s (Paulin and Hoffman, 2019). This is because of the viscosity of endolymph fluid flow and elasticity of the cupula (Paulin and Hoffman, 2019).

To approximately observe the true angular velocity of the head, the semicircular canal measures the angular velocity of the head,  $\omega_h$ . This can be represented by a high-pass filter expressed in the form of a transfer function (Merfeld et al., 1999). The sensed angular velocity  $\omega_{hs}$  is then compared to the output of the internal model, which is the predicted sensed angular velocity,  $\hat{\omega}_{hs}$ . Through the feedback with observer gain  $K_{\omega_c}$ , the prediction error, or the conflict between the two drives the observed angular velocity  $\hat{\omega}_h$ , until the actual sensed and internally estimated ve-



locities match. This creates an extension in the time constants of angular velocity perception, compared to the raw semicircular canal signal.

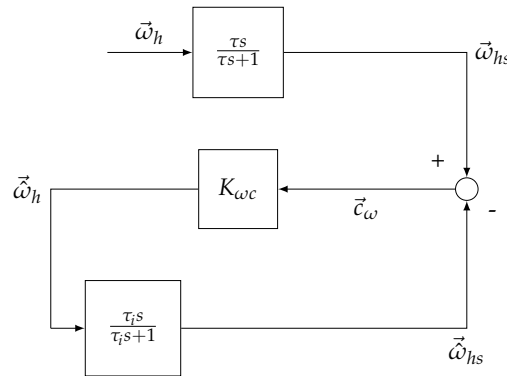


**Fig. 1.2** This figure illustrates the observer framework, which uses an internal model along with prediction errors to better approximate the real angular velocity of the head, despite the low bandwidth of the imperfect sensor

The observer framework which explicitly uses internal models and prediction errors presented here is widely used in models of human motion perception and spatial orientation, where it is employed to observe all relevant kinematic state variables.

### 1.3. PROPERTIES OF MOTION SICKNESS

In the 1960s, the consensus cause of motion sickness was intra- and inter-sensory conflict (Guedry Jr, 1970; Steele, 1961; Kennedy et al., 1965). Intra-sensory conflict is sensory conflict between the otoliths and the semicircular canals of the vestibular apparatus. Inter-sensory conflict is between the visual, somatosensory and vestibular sensory cues. However, this interpretation did not explain some listed fundamental properties of motion sickness:

#### Properties of Motion Sickness

- Organisms without a functioning vestibular system do not get sick from inertial motions
- Exposure to sickening motions leads to habituation to these motions
- Ego-motion does not cause motion sickness
- There is large inter-individual variation in sickness dynamics

The first property, “Organisms without a functioning vestibular system do not get motion sick from inertial motions” is the most fundamental property of motion sick-

ness and highlights the key role of the vestibular system. Evidence for this property comes from studies on patients with bilateral labyrinthectomy, who report a complete absence of motion sickness due to inertial motions (Golding, 2006). Moreover, patients with labyrinthine lesions show decreased motion sickness sensitivity (Dai et al., 2003, 2007). In these patients with vestibular deficits, the brain no longer receives the innately ambiguous and imperfect signals from both the otoliths or the semicircular canals. Therefore, the underlying kinematic states that would have produced the absent sensory information cannot be observed, thus preventing the sensory conflict from ever arising. Although critical for inertially induced motion sickness, the presence of a functioning vestibular system is not required for sickness induced by purely visual stimuli (Johnson and Sunahara, 1999). This means that even though adequate modelling of the vestibular system is essential for predicting motion sickness caused by automated vehicles, one must not discount the fact that motion sickness in general is a multisensory phenomenon, and requires integration of all sensory modalities.

The second property of motion sickness is that *“Exposure to sickening motions leads to habituation to these motions”*. This was the first property that historically linked motion sickness to the observer framework (Reason, 1978). Novel motion environments are thought to cause prediction errors between the sensed and expected sensory information. Reason (1978) used the word *“neural store”* to refer to the internal model from which the observer derives the expected sensory information. This prediction error slowly updates the internal model until the incident sensory information from the novel environment is no longer novel, but as expected. This habituation happens over the span of days (McCauley et al., 1976; Wood et al., 1994) and also has a large degree of inter-individual variability.

The third property, *“Self-motion does not cause motion sickness”*, just as the second, points to the importance of internal models. For self-induced motions, the observer has a copy of the control signal that is used to manipulate one’s actuators (Oman, 1982). This control signal acts like an address, facilitating easy acquisition of the expected sensory signal from the internal model, enabling the organism to perfectly anticipate oncoming sensory information. This explains why drivers rarely get sick (Schmidt et al., 2020). The importance of anticipation is further supported by experiments using a yoked design (Lackner, 2014). In these experiments, a master-slave joystick setup allowed one participant to drive the motion and the other to anticipate it. Sickness levels were not significantly different between the participants that were driving the motion and the participants who could anticipate the oncoming motions from the mechanically coupled joystick.

The fourth property is that *“There is large inter-individual variation in sickness dynamics”*. This variation is introduced in multiple places. For instance, the size and dynamics of the vestibular sensors vary between individuals (Wang et al., 2013). Likewise, there will also be differences in the internal model predictions subject to historical motions encountered by a given individual (Golding, 2006). Lastly, variation is introduced at the final level, where prediction errors are integrated over time into motion sickness symptoms. It can be the case that some individuals are more sensitive to prediction errors than other individuals, and so experience more

sickness. For a motion sickness model to be biologically feasible, it must capture this individual variability. Not only is this scientifically important, but it is also important for the usability of these models for comfort optimisation. This is because correlations, which seem strong at the group level, may not actually hold at the individual level. This is known as the "*Ecological Inference Fallacy*" (Freedman, 1999) and could mean that motion comfort algorithms, despite being developed with averaged population responses in mind, may on average fail for a given individual.

#### 1.4. OBSERVER THEORY AND MOTION SICKNESS

Oman (1982) was able to capture these properties of motion sickness in his observer based approach, as illustrated in Figure 1.3. In this approach, the desired kinematic state is compared with the estimated current state, and the resulting error is used to compute a control signal which is sent to the actuators. The A and B blocks shown here describe the real physics of the system, where the 'system' in this case is the head. The physical effect of actuators is summed with the effect of the current state on the system and integrated over time to yield the true state in the next time point. These true internal states are then measured by the sensory apparatus. The sensory information, or the afference signal, is then compared with the expected sensory signal. The expected sensory signal is computed in the same way. Here, the control signal that was sent to the actuators is also sent to an internal model of the real physics, given by  $\hat{A}$  and  $\hat{B}$ . The brain computes the expected sensory effect of this control signal. The conflict between the expected sensory afference and the real sensory afference helps the estimated states track the true internal states and updates the internal model parameters. A wide range of papers (Bos and Bles, 1998; Dai et al., 2010; Oman, 1982) have suggested that the conflicts that occur are then also integrated over time to drive motion sickness development.

Some authors (Wada, 2021; Kamiji et al., 2007) have built upon this conceptual framework. Bos and Bles (1998) famously developed their "Subjective Vertical Conflict" model (SVM), where the authors argued that as gravity is a fixed property of terrestrial living, organisms rely on it to provide a reliable frame of reference for navigation and orientation in three-dimensional space (Mackrout et al., 2019). Therefore, motion sickness is likely caused by a conflict between the sensed gravity and the internally estimated gravity. This model (Bos and Bles, 1998) was fitted to the group empirical sickness sensitivities obtained by O'Hanlon and McCauley (1973), who investigated the percentage of participants that vomited due to vertical accelerations as a function of frequency and acceleration amplitude. The SVM was able to reliably match the vertical acceleration sickness data. Since this seminal paper, there have been attempts to account for sickness produced by: horizontal plane accelerations (Khalid et al., 2011b), other multi-degree of freedom stimuli (Kamiji et al., 2007), as well as the effect of anticipation (Wada, 2021). However, these approaches have had a mixed degree of success, with most models fitting well to single degrees-of-freedom (dof) motion stimuli, but generalising suboptimally to multiple degrees-of-freedom.

Vehicular transport exposes passengers to these multiple degrees-of-freedom. Cornering, accelerating and decelerating causes noticeable accelerations in the hor-

## 1.4. OBSERVER THEORY AND MOTION SICKNESS

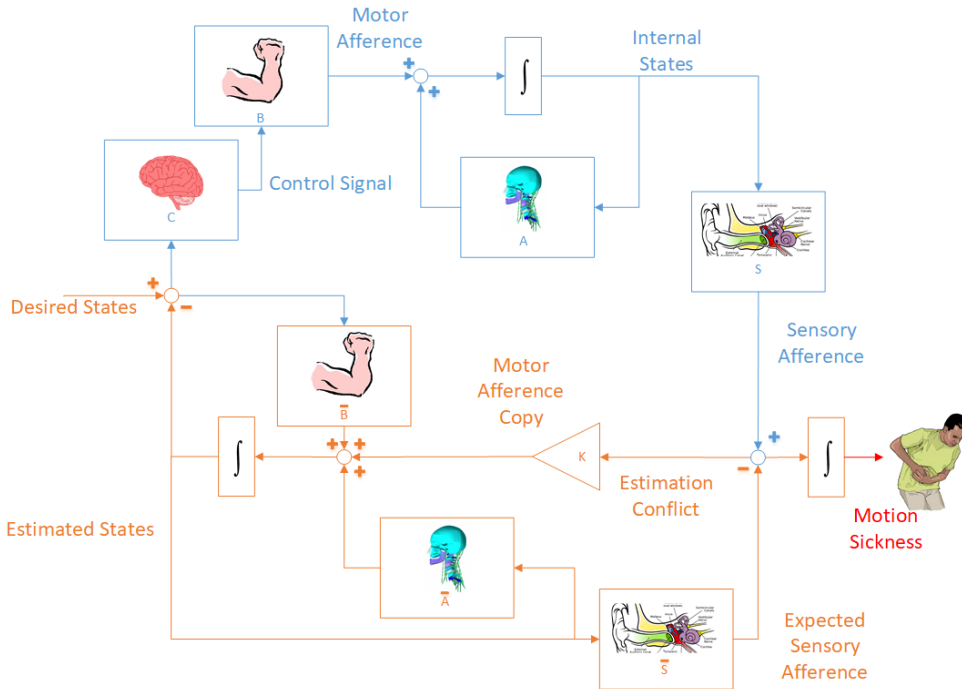


**Fig. 1.3** Observer framework proposed by Oman (1982) to account for the observed properties of motion sickness development. The left part (blue & red) describes motion generation and state estimation. The right part (green) describes motion sickness development as function of sensory conflict (see also Fig 1.4)

horizontal plane. Moreover, these horizontal plane accelerations may cause roll and pitch of the vehicle body, but also the passengers themselves inside the vehicle. Due to the large number of dof, and their possible interactions, experimentation is too costly. Instead, the most promising approach is likely through a combination of experimentation and modelling using the observer framework.

As shown in Figure 1.3, the observer framework ties motion sickness to motion perception through the errors in the estimation of true kinematic states. Studies (Dai et al., 2003, 2007; Tanguy et al., 2008; Young et al., 2003) have mainly explored this by evaluating the relationship between motion sickness susceptibility and the velocity storage mechanism, shown in Figure 1.2. These studies have identified a strong correlation between the time constant of velocity storage and susceptibility to cross-coupled coriolis. Other perceptual parameters, such as the dynamics of the subjective vertical, which is thought to modulate the tilt-translation ambiguity present during low frequency fore-aft accelerations (Wertheim et al., 2001), has received less attention. Furthermore, to date, frequency sensitivity to motion sickness and motion perception parameters have not been concurrently evaluated. In particular, it has not been proven that individual motion perception parameters correlate to individual motion sickness sensitivities. Evaluating this would enable better accounting of

motion sickness.

## 1.5. CONFLICT TO SICKNESS

The observer illustrated in Figure 1.3 uses sensory expectancy conflict as a way of obtaining better estimates of the internal states. The conflict signal is also thought to drive motion sickness, with different authors treating the conflict in different ways. In [Bos and Bles \(1998\)](#), the absolute value of the conflict is first scaled using a Hill function. This means that conflict takes on a sigmoidal scaling, with low values tending to zero and high values tending to one. The scaled conflict is then passed through a leaky integrator, whose output is the percentage of people that vomited. This approach has a number of limitations. Firstly, it conflates what is the internal dynamics that leads to sickness at an individual level given by the scaled sensory conflict, and the averaged group sickness dynamics. For a physiologically valid model of motion sickness, the final sickness predictions should map to individual sickness trajectories, not group-averaged ones. Secondly, due to its binary nature, the prediction of vomiting incidence is less useful for ride comfort optimisation than the prediction of motion sickness symptoms on a finer scale of increasing severity. Lastly, the parameters of the model have to be identified for each type of motion stimulus, which is inconvenient for complex motions.

The model of nausea proposed by [Oman \(1991\)](#) addresses these shortcomings. In this model, the absolute value of the conflict signal is input to a more physiologically plausible model of sickness. This model is composed of two paths, see Figure 1.4, the *slow* and the *fast* path. The slow path increases slowly, with a time constant that is approximately an order of magnitude longer than that of the fast path, and is thought to be hormonal. The fast path, acts on a shorter timescale than the slow path and is thought to be neural. The input to the fast path is the absolute value of the sensory conflict multiplied by the current value of the slow path. The scaling of the gain of the fast path by the slow path makes the model non-linear, and so allows it to describe the phenomenon of *hypersensitivity*. Hypersensitivity occurs when individuals who have been recently made sick are sensitised to further motions, such as to become sick much quicker than during their initial exposure ([Golding and Stott, 1997](#)). This effect is likely due to an increase in the levels of sickness mediating compounds ([Oman, 1991](#)). Indeed, among others, studies have reported an increase in adrenocorticotrophic hormone, cortisol and antidiuretic hormone after motion sickness ([Otto et al., 2005](#)). Unfortunately, it is not clear which endocrine responses contribute to the aetiology of motion sickness and which are irrelevant or parallel. Lastly, the outputs of both paths are summed to give an overall sickness rating as the model output (see Figure 1.4). It should be noted that the Oman model is an abstraction of the true physiological process underpinning the accumulation of motion sickness symptoms. On a biological level, neither the nature of the neural path nor the emetic linkage to the vomiting and nausea centres are at this time confirmed.

In addition to these biological unknowns, there are also knowledge gaps on the model level. For instance, although the Oman model is a promising candidate for the link between sensory conflict and motion sickness symptoms it has not been vali-

## 1.6. RESEARCH OBJECTIVE

dated and the parameters that govern its dynamics have not been estimated from experimental data. Moreover, although the purpose of using an individualised model of symptom development is clear, it is not clear whether individual sickness responses are sufficiently "repeatable" as to allow modelling them using this approach. Assessing repeatability also gives an indication for whether important information on the dynamics of sickness can be determined from within individual correlations, which is a source of data that has often been overlooked in motion sickness research. Lastly, it is not certain how well the Oman model generalises to mixed acceleration environments such as traffic, where different amplitudes of sensory conflict are encountered.

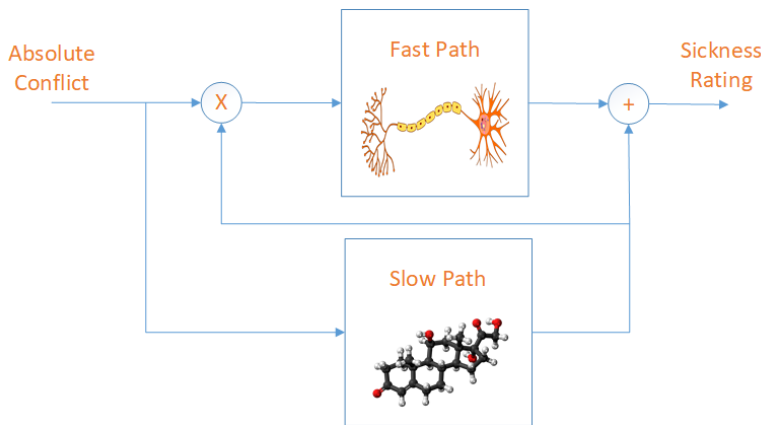


**Fig. 1.4** The figure illustrates the Oman model of nausea. It is made up of two paths; the slow and the fast path. The slow path is a hormonal path and is thought to accumulate slower than the fast path, which is a neural path. Both the slow path and the fast path may be represented by a second order system with repeated roots. The slow path is the gain to the fast path and the output of the two paths are summed to give a sickness rating

## 1.6. RESEARCH OBJECTIVE

To summarise, though there exists a large body of literature regarding the aetiology of motion sickness, mathematical modelling and model-based prediction of motion sickness accumulation over time itself is still in its infancy. While models using the observer framework have been formulated to describe population-level motion sickness due to mainly single degree-of-freedom motions, investigation of the relationship between motion perception and motion sickness for individuals using classical system identification methods is scarce. Moreover, current models require extensions to be able to predict the time evolution of motion sickness in multiple, coupled degrees-of-freedom motions with mixed amplitudes. Lastly, sickening motion experienced in traffic usually come in clusters, i.e. stop and go traffic separated by waiting at a traffic light. This makes modelling hypersensitivity also very important. Therefore, the objective for this thesis is:

**Thesis Objective**

Understanding and modelling of motion sickness accumulation and its individual differences for the comfortable control of automated vehicles.

## 1.7. APPROACH

The thesis objective is actualised via the three-part process described below:

- I **Quantitative Analysis of Individual Differences:** Large variation in individual susceptibility to motion sickness is a widely cited fact. Despite this, motion sickness dynamics at the individual level have not been quantitatively assessed. Such an assessment is important to avoid the pitfalls associated with inferring individual behaviour from group behaviour. This step is therefore crucial for developing personalised motion algorithms in automated vehicles.
- II **Modelling the Temporal Dynamics of Motion Sickness:** The mapping from sensory conflict to motion sickness symptoms is complex and non-linear. The model by [Oman \(1990b\)](#) is the most advanced model proposed to capture this complexity. However, its parameters have not been determined and its generalisability to different motion stimuli is unclear. This part aims to use the Oman model of Nausea to study the temporal dynamics of individuals. At the same time, it aims to assess model validity to different motion stimuli and improve it where possible and needed.
- III **Modelling the Dynamics of Sensory Conflict:** Prior to mapping sensory conflict to motion sickness, one must ascertain sensory conflict terms associated with a motion stimulus. This part aims to review the currently available means of modelling motion sickness via the observer framework. It compares various models, to find the best existing model for motion sickness prediction. Moreover, various perceptual mechanisms that generate the sensory conflict terms that might contribute to motion sickness modelling are identified.

## 1.8. THESIS OUTLINE

The three-part approach outlined above is presented in the chapters of this dissertation. The relationship between the chapters, the secondary questions and objectives, as well as each part of the approach used to advance the main aim of the thesis, is illustrated diagrammatically in [Figure 1.5](#).

### 1.8.1. CHAPTER 2: OBJECTIVE AND SUBJECTIVE QUANTIFICATION OF INDIVIDUAL AND GROUP RESPONSES TO SICKENING STIMULI

Chapter 2 describes two experiments that evaluated the temporal evolution of motion sickness in a highly dynamic sickening drive in a passenger vehicle. Experiment

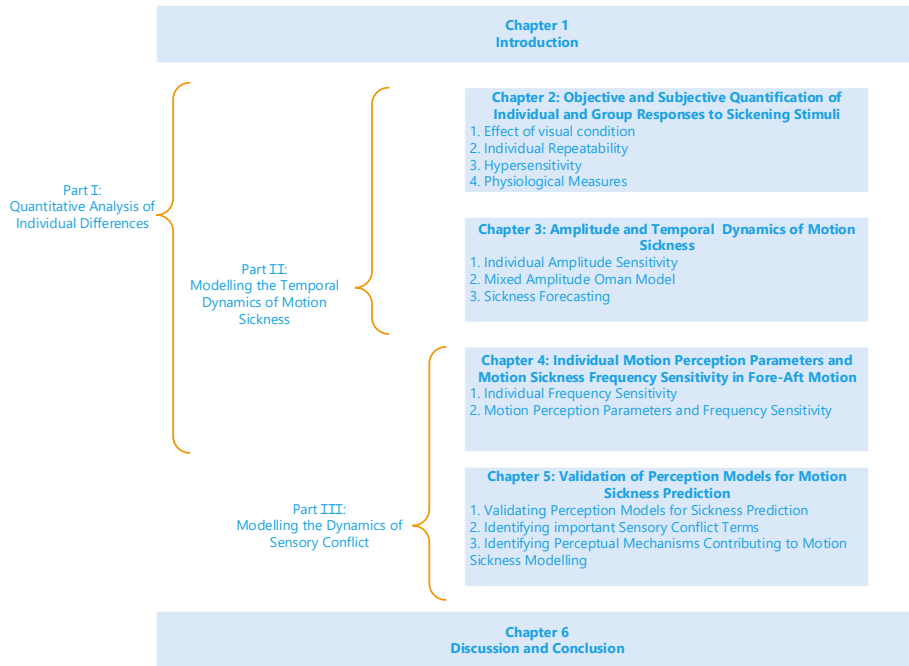


**Fig. 1.5** This figure illustrates the outline of the thesis with respect to the three part research approach taken in section 1.7 and their relationship to each of the chapters described in detail in section 1.8

1 studied the effect of internal and external visual condition on the development of motion sickness. Experiment 2 studied hypersensitivity caused by second motion exposure. Importantly, in Experiment 2, the trial-to-trial repeatability of the time evolution of sickness was studied using the Oman model. Lastly, physiological measures such as heart rate (HR), heart rate variability (HRV), galvanic skin resistance (GSR) as well as postural responses such as head roll were collected to ascertain whether they could be used as objective measures of motion sickness.

Results showed that internal vision was more sickening compared to external vision, with evidence pointing towards qualitatively different dynamics in the sickness evolution, possibly mediated by the elevated amplitude of the sensory conflict in the internal vision condition. Furthermore, hypersensitivity was observed and could be modelled accurately by the Oman model. The Oman model itself could be simplified such that the responses were described well by only two parameters, rather than the five used in the original formulation, to individual participants. Trial-to-trial repeatability was high, with individual level modelling based on the simplified Oman model providing results that were more accurate than group-level modelling. This was indicative of the sickness response being largely a deterministic function of the encountered motions. Lastly, the GSR was the only objective measure that correlated with motion sickness. Here, both the tonic and phasic components had a large



correlation.

### **1.8.2. CHAPTER 3: AMPLITUDE AND TEMPORAL DYNAMICS OF MOTION SICKNESS**

Chapter 3 aims to build on the modelling work of Chapter 2. In this chapter, the time evolution of motion sickness was evaluated in a repeated measures design for 17 participants that were subject to 4 levels of single degree-of-freedom horizontal plane accelerations. The aim was to explore the amplitude dynamics of sickness and also verify whether the Oman model generalised for different motion amplitudes and if it did not, to improve it such that it did. The aim of this is twofold. Firstly, it allows for motion sickness prediction in the mixed acceleration environments that are ubiquitous to vehicular travel. Secondly, it allows for adaptive adjustment of motion platform accelerations in motion sickness studies aiming to investigate correlation between motion sickness and dependent variables such as task performance.

The results showed that individuals may show convergent or divergent sickness trajectories, whereby convergent trajectories are modelled better with current tools. The Oman model was validated, and its key parameters were identified: with the fast and slow time constants at a median value of 66.2 and 502.4 s respectively and a median gain of 70.8. Moreover, the results indicated that these time constants were invariant with the amplitude of the motion, making it likely they are idiosyncratic parameters, unique to the individual. It was also found that a non-linear power scaling at the output of the Oman model with an exponent of 0.4 allowed for cross-amplitude generalisability to different stimulus amplitudes.

### **1.8.3. CHAPTER 4: INDIVIDUAL MOTION PERCEPTION PARAMETERS AND MOTION SICKNESS FREQUENCY SENSITIVITY IN FORE-AFT MOTION**

In this chapter, motion sickness was related to motion perception through a combination of experimentation and modelling. In particular, the relationship between tilt-translation ambiguity resolution, as well as the velocity storage mechanism, was empirically studied. For this, 23 participants first underwent two motion perception experiments, from which the time constant of the subjective vertical and the time constant of the velocity storage were derived. In addition to this, an observer-based model of perception evaluated in chapter 5 was used to derive the cross-over frequency of tilt-translation ambiguity resolution. The participants were then subject to 5 sickness sessions whereby they underwent fore-aft oscillations of the same acceleration but varying frequency. In this way, their motion perception parameters could be related to their sickness frequency sensitivities at the individual, rather than the group, level.

The results showed that frequency sensitivity of motion sickness to fore-aft accelerations is an idiosyncratic property of the participant. Some participants were sensitive to low-frequency accelerations, other to mid and higher frequency accelerations. Unlike the individual responses, the group sickness sensitivity curve had a larger bandwidth. This has important consequences for model fitting. Tradition-

ally, sickness models are fitted using singular motion perception parameters on to a group average of sickness sensitivity. This method is inappropriate due to the disconnect between individual and group responses identified in this experiment. This is important for motion, path, and route planning algorithms that usually minimise group averaged sickness response, wherein doing so may be both too limiting to vehicle performance and inadequate for sickness minimisation.

Lastly, even though the relationship between sickness frequency sensitivity and motion perception parameters was in the anticipated direction, the correlations were not significant. However, there was a strong correlation between overall motion sickness sensitivity and the subjective vertical time constant, which supports the importance of verticality perception during exposure to translational sickness stimuli.

### 1.8.4. CHAPTER 5: VALIDATION OF PERCEPTION MODELS FOR MOTION SICKNESS PREDICTION

The most widely used motion sickness model is the SVM. Its operating principle is based on the observer framework, which derives sensory conflict terms from the process used to obtain estimates of true kinematic states. There are, however, a number of observer-based models of motion perception that can likewise be used to derive sensory conflict terms (Bos and Bles, 1998, 2002b; Wada, 2021; Clark et al., 2019; Laurens and Droulez, 2007). The aim of this chapter was to analyse, both analytically and in simulation, the response of three models of motion perception in both motion perception and motion sickness. These were the Subjective Vertical Model (SVM), Multi-Sensory Observer Model (MSOM) and the Particle Filter Model (PFM). In this way, the usefulness of these models for motion sickness prediction was evaluated. Moreover, promising mechanisms of action that might be important for generating correct model predictions could be identified.

The results of this study showed that though the models provided a good match for the motion perception paradigms studied, they did not capture the full range of motion sickness observations. Moreover, two important mechanisms were identified for motion sickness prediction. The first mechanism was an active estimation of the magnitude of gravity, which was found to be the only feasible way of explaining motion sickness caused by vertical accelerations. The second mechanism identified was the somatogravic effect, as mediated by the two-way coupling between the semicircular canals and the otoliths. This was found to be important to model the differences in the frequency sensitivities between vertical and horizontal plane accelerations.

## 1.9. SCOPE

In this introduction, motion sickness has mainly been linked to the observer framework, which was born out of the works of Reason (1978) and Oman (1982). However, there are other theories of motion sickness development. For example, an often cited alternative explanation is the "Postural Instability Theory" (PIT) proposed by Stoffregen and Smart (1998). PIT states that "*animals become sick in situations in which they do not possess (or have not yet learned) strategies that are effective for the maintenance*

of postural stability". The PIT explores motion sickness through the perspective of *ecological psychology*, and is motivated by the work of Gibson ([Shapiro and Spaulding, 2021](#)) on *embodied cognition*. Embodied cognition rejects the methods of internal modelling and sensory conflict as used in this thesis ([Stoffregen et al., 2017](#)). These methods take the *Computational Theory of Mind* (CTM) as their central paradigm, and as discussed in the introduction, are supported by a wide array of empirical findings. Therefore, this thesis approaches the problem of motion sickness through the framework of CTM.

The exact form to model the computational process is open to choice. One can model it at the biophysical level, employing realistic physical modelling of neurons, synapses and their collective interactions. Or indeed, as this thesis has done, at higher levels of abstraction and use classical control theoretic models. These models perform computations on natural units, such as acceleration and angular velocity, contrary to the rate and time coded neural spikes used by the brain. This abstraction comes with advantages and disadvantages. One disadvantage is that certain phenomena, such as the apparent reduction in motion sickness due to bone conducted vibrations (BCVs) ([Bos, 2015](#)), is not an emergent behaviour of the model, but as a consequence of manually changing gains of the model. The advantage, on the other hand, is that control theoretic modelling generally has a smaller number of parameters that can be directly correlated with observations from psychophysical experimental, and thus is more interpretable.

All perception and sickness models in this thesis only include the vestibular system and not the visual, nor the somatosensory system. This is mainly because modelling vestibular perception and motion sickness due to inertial motions only, without the presence of any visual input, is a complex task that has not been solved. Indeed, there were attempts made by the author to include vision in the models evaluated, but it was determined that doing so added complexity without apparent gain. Moreover, experiments have also shown that there is no relationship between the rank order of visual deprivation and susceptibility to motion-induced motion sickness ([Graybiel, 1970](#)). This means that exclusion of vision is not counterproductive to development of usable models. Due to the rarity of complete deafferentation of the somatosensory system, most studies are conducted with one or two participants ([Richardson et al., 2015](#); [Blouin et al., 2007](#); [Hermsdorger et al., 2008](#)). Therefore, a similar statement to [Graybiel \(1970\)](#) on the relationship between motion sickness and somatosensation cannot be made. However, the models we used were able to recreate perceptual observations even without the inclusion of somatosensation. Therefore, as applied in this thesis, simplification is likely suitable for studying motion sickness development in automated driving with internal vision.

Another important point to note is that motion sickness currently does not have a physical unit of measurement. Subjective ratings obtained using the MISC scale was determined to be the most promising way of measuring the increase in sickness as a function of time. The main reason for using the MISC was that it is tied to the specific symptoms experienced by the participants. Using the MISC also makes it easier to relate the symptoms experienced between participants.

# 2

## OBJECTIVE AND SUBJECTIVE QUANTIFICATION OF INDIVIDUAL AND GROUP RESPONSES TO SICKENING STIMULI

---

This chapter has been published as: Tugrul Irmak, Daan M. Pool, Riender Happee, *Objective and subjective responses to motion sickness: the group and the individual*, *Experimental Brain Research*, 239, 515–531 (2021).  
<https://doi.org/10.1007/s00221-020-05986-6>

### 2.1. ABSTRACT

*We investigated and modelled the temporal evolution of motion sickness in a highly dynamic sickening drive. Slalom manoeuvres were performed in a passenger vehicle, resulting in lateral accelerations of 0.4 g at 0.2 Hz, to which participants were subjected as passengers for up to 30 minutes. Subjective motion sickness was recorded throughout the sickening drive using the MISC scale. In addition, physiological and postural responses were evaluated by recording head roll, galvanic skin response (GSR) and electrocardiography (ECG). Experiment 1 compared external vision (normal view through front and side-car windows) to internal vision (obscured view through front and side windows). Experiment 2 tested hypersensitivity with a second exposure a few minutes after the first drive and tested repeatability of individuals' sickness responses by measuring these two exposures three times in three successive sessions. An adapted form of Oman's model of nausea was used to quantify sickness development, repeatability, and motion sickness hypersensitivity at an individual level. Internal vision was more sickening compared to external vision, with a higher mean MISC (4.2 vs. 2.3), a higher MISC rate (0.59 vs. 0.10 min<sup>-1</sup>) and more dropouts (66% vs. 33%) for whom the experiment was terminated due to reaching a MISC level of 7 (moderate nausea). The adapted Oman model successfully captured the development of sickness, with a mean model error, including the decay during rest and hypersensitivity upon further exposure, of 11.3%. Importantly, we note that knowledge of an individuals' previous motion sickness response to sickening stimuli increases individual modelling accuracy by a factor of 2 when compared to group-based modelling, indicating individual repeatability. Head roll did not vary significantly with motion sickness. ECG varied slightly with motion sickness and time. GSR clearly varied with motion sickness, where the tonic and phasic GSR increased 42.5% and 90%, respectively, above baseline at high MISC levels, but GSR also increased in time independent of motion sickness, accompanied by substantial scatter.*

### 2.2. INTRODUCTION

Motion sickness is a maladaptation syndrome where aggravating motions trigger autonomic symptoms such as salivation, dizziness, headaches, panting, hot/cold flushes, stomach awareness, nausea and vomiting. Chronic exposure to sickening motions may lead to the sopite syndrome, which is associated with lethargy, fatigue and drowsiness (Bertolini and Straumann, 2016; Lackner, 2014). Eliminating motion sickness, particularly in ships and trains, has been long sought after, and automated vehicles are another mode of transport added to this list. The public outlook towards automated driving is positive, fuelled by the foreseen freedom automated vehicles can provide. Users wish to be able to engage in activities that do not necessitate road observation. However, as shown in a multitude of previous studies (Turner and Griffin, 1999; Kuiper et al., 2018; Salter et al., 2019), motion sickness becomes a major constraint when taking the eyes off the road. Fortunately, there are conceivable ways of reducing sickness incidence. For instance, route and path planning algorithms as well as smart active suspension controllers installed in future modes of transport may help ease symptoms. However, to be successful, these technologies rely on the accurate modelling of motion sickness, taking into account the motion and the visual viewing conditions.

The modulating effect of viewing condition on sickness has been demonstrated. [Griffin and Newman \(2004a\)](#), driving on Southampton urban roads, observed no significant differences between internal vision, which is when the passenger can only see inside the cabin, and blindfolded vision. However, both conditions showed approximately twice as high subjective sickness ratings as the external vision. Likewise, [Butler and Griffin \(2009\)](#) found internal/blindfolded approximately twice as sickening as external vision in combined fore-aft acceleration and pitch rotation at 0.1 Hz. However, [Butler and Griffin \(2006\)](#) found no differences in sickness between internal, external and blindfolded for pure fore-aft accelerations at 0.1 Hz  $0.89 \text{ ms}^{-2}$  rms. This suggests that the alleviating effect of external vision only occurs when the motions experienced lead to a perception of rotation. One of the aims of this study is therefore to quantify the influence of viewing condition on sickness during complex rotational and translational motions, as present during cornering.

The mathematical modelling of motion sickness thus far focused on population averaged measures of motion sickness. To name two, these may be in the form of motion sickness incidence (MSI) ([O'Hanlon and McCauley, 1974](#)) and motion sickness rating (MSR) ([Griffin and Howarth, 2000](#)). The computation of this averaged illness inherently transforms the data, such as to exhibit a converging sickness response profile, as seen in much of the literature ([Bijveld et al., 2008](#); [Cian et al., 2011](#); [Bos et al., 2005](#)). However, individuals show a range of responses that can broadly be categorized as convergent, i.e., to saturate at a certain level, or divergent, with a rapid increase towards emesis described by [Bock and Oman \(1982\)](#) to be an "avalanche" effect. After exposure to sickening motions, humans need minutes or even hours to recover. Within this recovery period, humans display "hypersensitivity" to new motion stimuli ([Oman, 1990a](#)). The modelling of individual dynamics is used widely in cybernetic research, one example being driver modelling ([Barendswaard et al., 2017](#); [Mars et al., 2011](#); [Van Der El et al., 2017](#)). This study aims to use a similar approach to motion sickness. The use of individual responses for modelling hinges on the assumption that individual responses are repeatable. That is, the response dynamics is a largely deterministic function of the motion stimuli, while the influence of internal psychological factors on the day-to-day response variation, is much smaller than the inter-individual variation. The current study therefore aims to quantify the repeatability of motion sickness responses to sickening stimuli.

Posture is shown to be an important factor in sickness severity. Participants exposed to earth horizontal vibrations when upright reported sickness responses factor four greater than for lying supine ([Golding et al., 1995](#)). The dependency of sickness on posture is in concord with the postural instability theory proposed by [Riccio and Stoffregen \(1991\)](#). They state that animals become sick in situations in which they do not possess adequate control strategies that are required for the maintenance of postural stability, and that postural instability precedes the symptoms of motion sickness, where postural instability is necessary to produce sickness symptoms. Following the postural instability theory, a supine posture is less sickening because it is an inherently more stable configuration. Several experimental studies support the postural instability theory using visual optic flow as a method of inducing sickness

(Stoffregen and Smart, 1998; Villard et al., 2008; Smart et al., 2002; Stoffregen et al., 2014). "Studies using inertial motions have found some postural differences between sick and well groups (Tal et al., 2010; Stoffregen et al., 2013; Varlet et al., 2015). However, these experiments did not measure posture during the build up of sickness, only before and or after. Hence, we studied 3D posture maintenance of the head during our sickening drive experiments."

Models of sickness have predominantly relied on subjective measures of illness or objective vomiting incidence. However, both have their misgivings. For instance, the former is affected by participant uncertainty on how they are feeling, which is an issue in particular at lower sickness levels. The latter, on the other hand, cannot yield any information on individual responses, nor the time history of sickness. Subjective ratings also have a low time and sickness resolution. For instance, the MISC rating scale (Bos et al., 2005) usually ranges from 0-7 from no discomfort to moderate nausea, and reliable estimates may only be given in  $\approx 30$  s intervals. Moreover, querying the MISC may even affect sickness development (due to increased introspection) and performance on other experimental tasks. Accurate modelling, however, ideally requires objective measures with high time and sickness resolution. Physiological measurements such as electrocardiography (ECG) using the low-high frequency ratio (LF/HF), of heart rate variability (HRV), heart rate (HR) and galvanic skin response (GSR) and also postural stability, may be appropriate for this purpose. Many studies have evaluated HR (Cowings and Toscano, 1993; Holmes and Griffin, 2001; Mullen et al., 1998), HRV (Holmes and Griffin, 2001; Himi et al., 2004; Lin et al., 2011; Ohyama et al., 2007; Dahlman et al., 2009) and GSR (Wan and Hu, 2003; Dahlman et al., 2009; Himi et al., 2004) as measures of motion sickness. Under the large range of motion sickness levels encountered by participants in this study, we aim to clarify how these physiological measures correspond to sickness.

Overall, this study aims to 1) quantify the differences for internal and external vision conditions during complex motion experienced in cornering, 2) quantify the repeatability of individual motion sickness responses in time including hypersensitivity, 3) validate Oman's nausea model to describe the individual time evolution of sickness, and 4) relate objective physiological and kinematic variables such as HR, HRV, GSR, and postural stability to subjective sickness rating.

### 2.3. METHODS

The present study comprises two complementary experiments exposing participants to a sickening drive. Experiment 1 aims to quantify the effect of visual view on motion sickness. Experiment 2 aims to quantify individual response repeatability and hypersensitivity.

#### 2.3.1. PARTICIPANTS

In total, 24 participants took part in the first experiment, where 18 participants completed both internal and external visual conditions. Of the 24 that took part, 6 participants were female and 17 were male. Of the 18 participants completing both internal and external vision conditions, 4 were female 14 were male and. 3 of the



18 participants were experimenters themselves. These 18 participants had a median motion sickness susceptibility questionnaire (MSSQ) score of 16 indicating that they were of above average motion sickness susceptibility. The MSSQ was not used in the participant selection process.

For the second experiment, 17 participants took part, of which 13 participants completed all 3 sessions, investigating repeatability. Of these 13 participants, 3 were female and 10 were male. None of the participants were experimenters. The median MSSQ score of these 13 participants was 5 indicating they were of below average susceptibility.

No participants performed both experiments. All participants had normal or corrected to normal vision. None of the participants reported any vestibular disorders. The mean age for the two experiments was 26.1 years (STD = 8.2). Lastly, all participants were asked to refrain from recreational drug consumption, including alcohol and caffeine, from at least 24 hours prior to the experiment.

All participants provided written informed consent prior to participation. The experimental protocols for both Experiments 1 and 2 were approved by the Human Research Ethics Committee of TU Delft under application numbers 420 and 521.

### 2.3.2. APPARATUS

Participants were seated in the middle back seat of a Toyota Prius (2013 model), see Figure 2.1, on top of a friction mat to prevent lateral slippage at the buttocks/seat interface. The vehicle was instrumented with a 6-DoF Inertial Measurement Unit (IMU) mounted at the bottom of the rear middle seat, below the seated participant, recording acceleration, orientation and angular velocity at a frequency of 100 Hz.

In the experiments described in this chapter, we tested sickness development in two visual conditions, i.e., *internal vision* and *external vision*. In the external vision condition, participants had a normal view of the road ahead through the front and side windows of the car. In the internal vision condition, the front view was obscured by a cardboard panel, affixed to the front seats. In addition, the side view was obscured by cardboard templates stuck to the windows. This effectively obstructed all views of the road and the movement of the vehicle.

### 2.3.3. TASK & STIMULI

For both experiments, the vehicle described in Section 2.3.2 was used to drive slalom trajectories. For this purpose, a closed road of length 240 m and width of 10 m was used. The slaloms were of an amplitude of 3.5 m and a frequency of 0.2 Hz. The longitudinal velocity of the vehicle was held approximately constant, via manual control, at 25 km/h. The slalom frequency was maintained with the help of a metronome. The road markings at the road boundary were used as a guide mark for the motion. As a consequence, the participants experienced lateral accelerations with a peak amplitude of 0.4 g. At the end of the available road, a 3-point turn was performed and the slalom restarted. Before each 3-point turn, 8 slaloms were performed. Such a single test stretch was completed in approximately 40 seconds. Each 3-point turn took 8-10 seconds to complete. The relatively large excitation used in both experiments aimed to obtain a robust sickness response and a large distribution



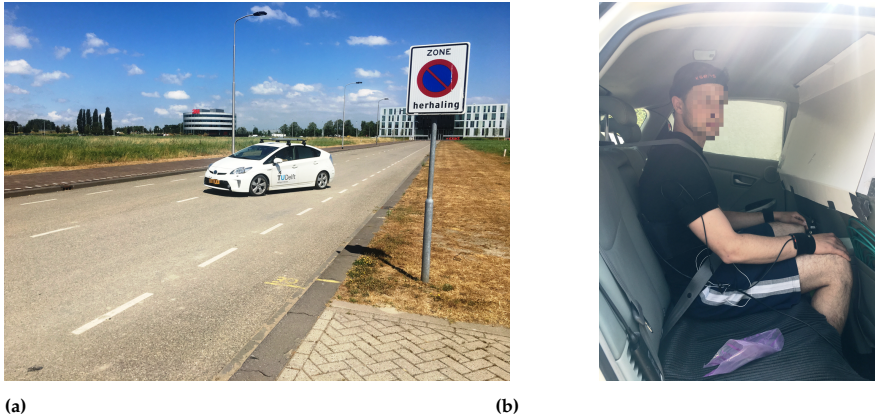


**Fig. 2.1** Experimental setup. **Left** is the Prius 2013 model on the test road used during the experiments in the process of performing a slalom. **Right** shows the internal vision condition where the external view to the sides and front is blocked

of sickness ratings within the population. This supports the analysis and modelling of individual sickness development in time. In both experiments, participants were told to assume a relaxed posture with their feet placed wide apart, their hands on their knees, with a straight back looking directly out of the front wind screen for the external vision condition, or at the cardboard cover occluding the wind screen in the internal vision condition. The air condition regulating the internal temperature of the vehicle was set to 18°C.

In this chapter we define a "session" as an experimental block that starts from the time at which a participant comes in to the experiment staging room on a particular day, until they have completed the experiment and have been debriefed, leaving the staging room. An "exposure" refers to the motion exposure. In the Experiment 1, there is only one motion exposure. In the Experiment 2 there are two: the first motion exposure, followed by a rest, which is followed by a second motion exposure to test for hypersensitivity.

In **Experiment 1**, all participants were tested in the two different visual conditions (external and internal vision) with an average interval of one week between both sessions. In Experiment 1, the sickening drive lasted for a total of 30 minutes, or until the participants reached a MISC rating of 7 or otherwise asked to terminate the experiment. The order of testing for the two visual conditions was balanced between participants.

**Experiment 2** consisted of 3 repeated identical sessions, where participants experienced the sickening drive in the internal vision condition only. A one-week interval was planned between each session, aiming to eliminate effects of habituation. Where Experiment 1 consisted of only a single (maximum 30-minute) motion exposure within each session, in Experiment 2 a second exposure was included in each session to measure hypersensitivity. Each session of Experiment 2 started with the pre-experiment drive to the test road, followed by the first motion exposure (M1).

After a rest period (R1), which brought the participants back down to a MISC rating of 2, they were given the option to proceed with the second motion exposure. This second motion exposure (M2) was terminated after 15 minutes or when participants reached severe motion sickness (MISC of 7) or otherwise requested for the termination of the experiment. After the second exposure, a second rest period (R2) was followed by the post-experiment drive to the staging room.

In both experiments, participants were tasked with reporting their sickness level. For this purpose the MISC scale (Bos et al., 2005) was used as a subjective indicator of motion sickness during the experiment. The MISC scale is a commonly-used symptom based rating system and provides a measure of sickness which is comparable between participants. The participants were first familiarized with the MISC rating at the briefing room, at the start of each session. In Experiment 1 the participants were asked their MISC rating in 1 minute intervals, during and after the sickening drive. The participants' verbal answers, consisting of a single integer MISC rating, were recorded with pen and paper. In Experiment 2, the interval for MISC requests was brought down to 40 seconds. An automated system provided an auditory cue asking "MISC?" and recorded the participants' verbal answers. The recordings were then manually processed, which proved to be more robust than the verbal approach in Experiment 1. In Experiment 2 the MISC was asked from the moment the participant entered the vehicle to the moment they returned to the staging ground for debriefing.

### 2.3.4. INSTRUMENTATION FOR PHYSIOLOGICAL MEASUREMENTS

The kinematics of the participants were measured via the use of the Xsens full body inertial motion capture suit (Xsens, 2020), recording at 240 Hz. The motion capture suit consists of 21 inertial measurement units distributed across relevant body segments. The raw sensor recordings are paired with a bio-mechanical model of the human skeleton. This model is calibrated to the participant upon initialisation. The calibration procedure consists of taking a neutral, N-pose with arms by the side with a straight upright posture for a few seconds before walking for a few paces with a natural gait before turning and returning to assuming the N-pose at the point walking started. The motion capture system processes the raw sensor readings via the use of this biomechanical model before returning joint angular positions and earth referenced orientations, accelerations and angular velocities.

The ECG and the GSR measurements were both sampled at a frequency of 1 kHz via a TMSI Mobita amplifier. The ECG was recorded via 3 leads at the V1, V2 and V3 locations (Rosen et al., 2014). The ground was attached to the participant wrist with a wet electrode wristband. The GSR was recorded via 2 gel electrodes at the index and the middle fingers.

### 2.3.5. DATA PRE-PROCESSING

Head roll was previously reported to relate to motion sickness (Wada et al., 2018). As the lateral vehicle accelerations in our experiments primarily elicit head roll, measured head roll was used as the main indicator of postural instability. We evaluated head roll around the slalom frequency using a 0.15-0.22 Hz band-pass filter. To com-

## 2. INDIVIDUAL AND GROUP RESPONSES TO SICKENING STIMULI

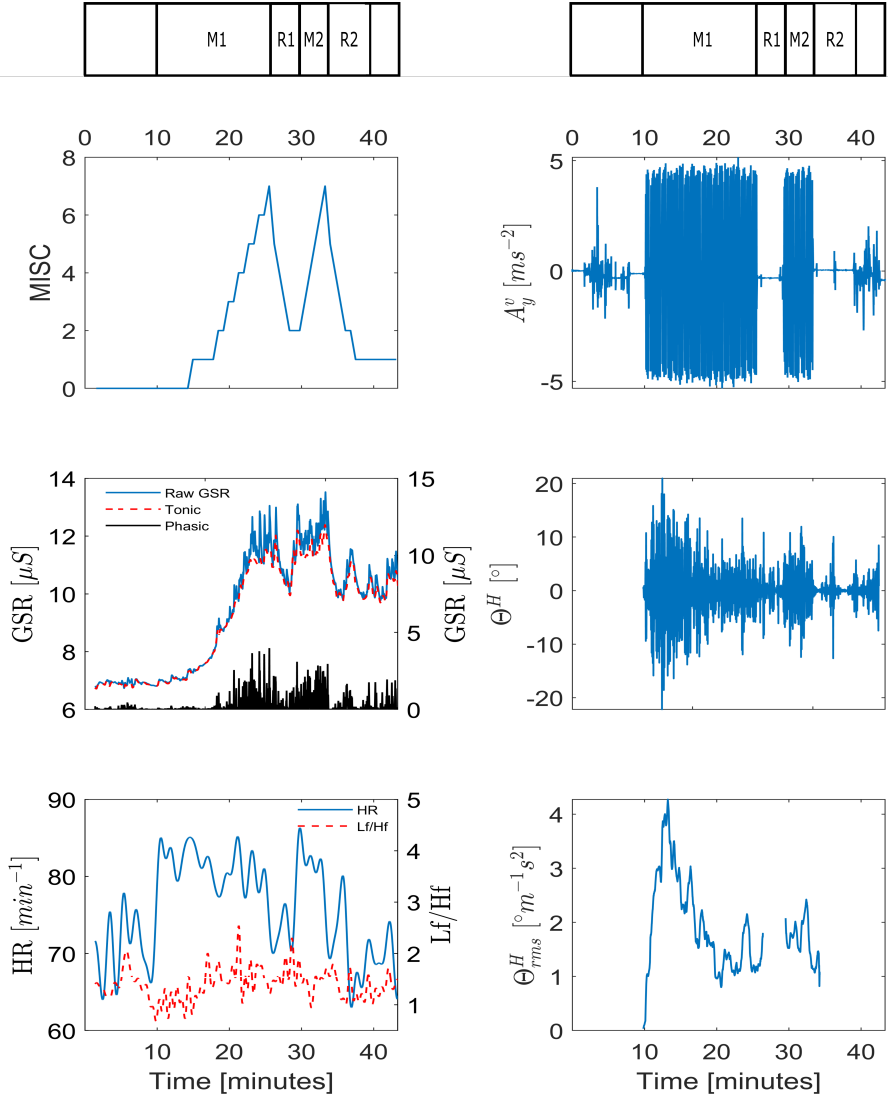


**Fig. 2.2** Example response of participant 11 for session 3 in Experiment 2. MISC level and vehicle acceleration are shown in the top row. The middle row shows the raw, tonic and phasic GSR, as well as the head roll. Likewise, the bottom row, shows the heart rate, LF/HF ratio as well as the ratio of the head roll rms and vehicle lateral acceleration rms

to compensate for variation in vehicle motion, we scaled head roll to the vehicle lateral acceleration. The scaling was done by dividing the moving-average (60 s window) root-mean-square of head roll, with the moving-average root-mean-square of the vehicle lateral acceleration. Due to the scaling by the rms of the vehicle acceleration at

zero acceleration periods, the relative head roll may be very high. These outliers caused by the scaling were removed.

ECG gives information on HR and HRV which may be of use in detecting the development of motion sickness. For this purpose, raw ECG was first recorded and then detrended by fitting a 6th order polynomial. The subsequent trace was then transformed using a sym4 wavelet. The 4th and 5th length scales were taken and an inverse maximal overlap discrete wavelet transform was performed. The resulting output was squared and fed in to a peak detection algorithm. The detected peaks were manually checked and any false positive and false negatives were manually corrected. The HR and HRV were calculated. The latter is the time difference in seconds between adjacent R-R peaks. It was then interpolated using 5th order Lagrange interpolation with a re-sampling frequency of 10 Hz. The heart rate was then filtered with a band pass filter of pass band frequency of 0.01 Hz and stop band frequency of 0.02 Hz. The instantaneous LF/HF was calculated by first computing the Choi-Williams distribution of the HRV, then band pass filtered with a pass band frequency of 0.01 Hz and stop band frequency of 0.02 Hz.

The measurements from the GSR device, which are first given in micro-volts, were first converted to conductance measured in microsiemens ( $\mu\text{S}$ ). The raw GSR files were processed using the batch processing command in Ledalab (Benedek and Kaernbach, 2010b,a). Ledalab is an open source source MATLAB toolbox. It decomposes the GSR signal in to its tonic (low frequency) and phasic, (high frequency) components respectively (Benedek and Kaernbach, 2010b). To quantify the strength of the phasic, GSR its absolute value was integrated over the time span between the MISC prompts by deconvolving the original GSR signal.

Figure 2.2 shows example measurements of the MISC, vehicle lateral acceleration, and physiological data from Experiment 2 for participant 11 in session 3. In this chapter the signals shown for the phasic and the tonic GSR, as well as heart rate and LF/HF ratio of heart rate variability and head roll rms ratio, are analysed to see if they are predictive of the MISC level.

### 2.3.6. DATA ANALYSIS

#### MEAN MISC AND MISC RATE

To answer our research questions on the effects of visual viewing condition, repeatability of sickness response, and hypersensitivity, the severity of sickness must be quantified. While many metrics have been used for this, in this study, we use the *mean MISC* and the *MISC rate* as parameters that quantify sickness.

The **mean MISC** is calculated by averaging all MISC ratings over the intended M1 exposure period. If a given participant finished a motion exposure prematurely (by reaching a MISC rating of 7) then for the remainder of the 30-minute duration a value of 7 is used for this participant in the calculation of the mean MISC. This padding technique has been employed in a number of earlier sickness studies (Webb and Griffin, 2003; Griffin and Newman, 2004b). Figure 2.4a shows the dropout rate in Experiment 1. Figure 2.4c, shows that averaging using a MISC of 7 for missing data creates a MISC as function of time that deviates from individual curves in Figure 2.4d. However, the alternative of omitting missing data, indicated with dashed lines

in Figure 2.4c, is even less appropriate and results in a reduction in mean sickness. Hence, we use the mean MISC as a robust measure per exposure and use MISC rate and Oman’s model to assess MISC development in time for each individual exposure.

The **MISC rate** is calculated as a simple linear measure of how quickly the MISC has increased. It is calculated from the difference in MISC scores between two relevant time points divided by the time interval between these two time points in minutes. Here we report MISC rate from the start towards the end of motion exposures M1 and M2. Both the mean MISC and MISC rate are effective metrics for describing group differences in sickness response.

### OMAN’S MODEL

Literature shows various ways of modelling the time response of motion sickness. In all cases, a sensory conflict term (Oman and Cullen, 2014) is integrated over time (Dai et al., 2010; Bos and Bles, 1998). For the analysis of the repeatability of sickness responses in our Experiment 2, we took the rectified lateral vehicle acceleration as the sensory conflict input. This is appropriate as no visual view of the car motion was available (so all sensed accelerations were conflicting) and because the sickness susceptibility for lateral perturbations shows a plateau from 0.03 to 0.3 Hz (Donohew and Griffin, 2004). The bandwidth of our excitation was within this range, centred narrowly around 0.2 Hz, and as the lateral acceleration was the dominant motion this was deemed a good proxy for internal sensory conflict. Even if the conflict were some scaled factor of the vehicle acceleration, model tuning would scale this appropriately to the output MISC rating. The integration of this conflict term may take the form of a simple integrator as in Dai et al. (2010), or a second-order system as in Bos and Bles (1998). However, these are simple mechanisms which do not explain the observations of hypersensitivity that occurred during this study. Hypersensitivity as a phenomenon was first investigated by Oman (1990a) who developed a model of motion sickness that aimed to account for both the initial rise in sickness and the hypersensitivity that occurred after re-exposure to sickening stimuli.

The model as documented by Oman (1990a) is parametrised to have  $\beta_1 = 60$ ,  $\beta_2 = 600$ ,  $\beta_3 = 2$ . However, these parameters had not been validated in a structured manner, and in (Oman et al., 1986) a potential value for the gain  $K$  was not identified. We therefore leave them as free parameters that are tuned to MISC responses for each individual and session of experiment 2. However, before doing so, we made minor adjustments to the model (Figure 2.3). We set the numerator of the fast path to 1 and removed the constant gain of 5 from the slow path. This allows us to compute a unique gain for  $K$ . We have also set the power term  $\beta_3$  to 1. This is because, when fitting the original model we found the  $\beta_3$  parameter to be redundant for the MISC scale we used. Upon inspecting the results we simplified this model further. There was a strong correlation ( $\rho = 0.69$ ) between the time constants of the slow and fast paths, where  $\beta_2 = 7\beta_1$ . We therefore used this substitution to simplify the original four parameter model in to the two parameter one shown in Figure 2.3. The substitution greatly simplified the model, while inflating the model fit error by only 1%.

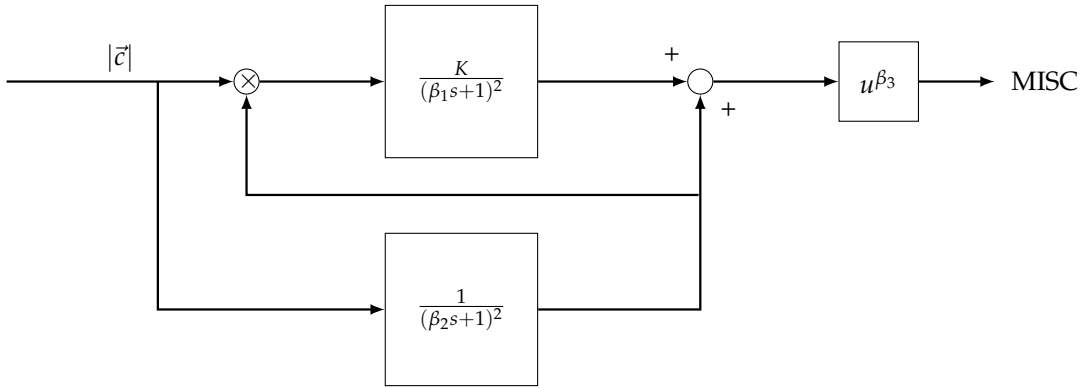


**Fig. 2.3** Adapted Oman's model of motion sickness development in time. The rectified conflict signal  $|c|$  is fed in to the model. There is a fast (upper) path and a slow (lower) path. The slow path multiplies with the conflict as the gain of the fast path. Both systems are 2nd order with repeated poles. The fast and slow path are then summed and the result is raised to a power where  $\beta_3 > 0$

### KINEMATIC AND PHYSIOLOGICAL VARIABLES

In this chapter, we aim to find the relationship between sickness, given by the MISC rating, and head roll, heart rate, LF/HF ratio of heart rate variability, and GSR. To obtain a larger dataset, experiments one and two are combined. Only the first motion exposure of each session is utilized and, because of a potential confound with hypersensitivity and time related effects, M2 in Experiment 2 is not used. Although there are two different visual conditions in the first experiment we show that this makes no significant difference to the head roll response. For the physiological measurements this again is of no importance as we assume that vision does not directly influence these physiological measures.

For the analysis, the MISC rating at a given time is paired with the associated physiological and kinematic variable for the point in time the MISC was recorded. This allows us to perform a regression analysis on these variables and the MISC. As there were some dropouts for whom the experiment was prematurely terminated due to reaching a MISC level of 7 (moderate nausea), and missing or partially missing physiological data due to technical difficulties, all available data were aggregated to paired MISC and physiological responses.

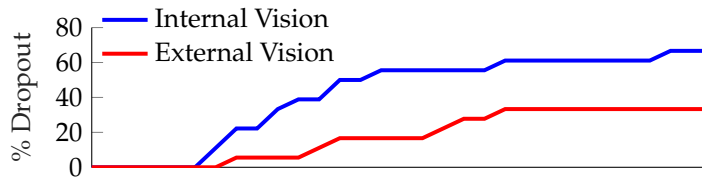
We then built a linear mixed model with random intercepts that relates the chosen kinematic/physiological variable with the associated MISC value. It is seen from the raw data that time since the start of the experiment may also have an influence on these variables. For instance, heart rate is influenced by arousal, which is particularly high at the start of the experiment, likewise, the tonic GSR may increase as the participant sweats due to the exertion required to stabilize posture. To control for this, the effect of time is also modeled. In order to make sure the regression coefficients are not dependent on each other we performed a multicollinearity test before each regression. Indeed, most responses are similar to those seen in Figure 2.2 and are well approximated with a linear model. As the regression residuals have a fat tail and are not normally distributed, we bootstrap the regression, using 4000

iterations of random-x resampling in MATLAB (Fox, 2002). This gives the 2.5% and 97.5% percentile confidence intervals for the regression coefficients.

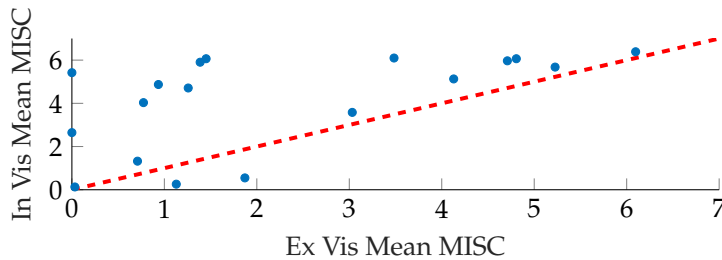
## 2.4. RESULTS

### 2.4.1. EXPERIMENT 1: INTERNAL-EXTERNAL VISION GROUP RESPONSE

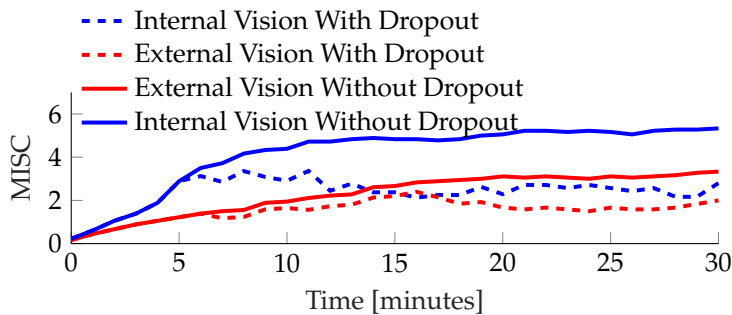
The motion sickness incidence in horizontal motion plateaus between the frequencies 0.03 and 0.3 Hz (Donohew and Griffin, 2004). A two-tailed paired t-test was conducted on the average lateral vehicle acceleration power over this frequency range between the conditions in Experiment 1.



(a) Dropout percentages



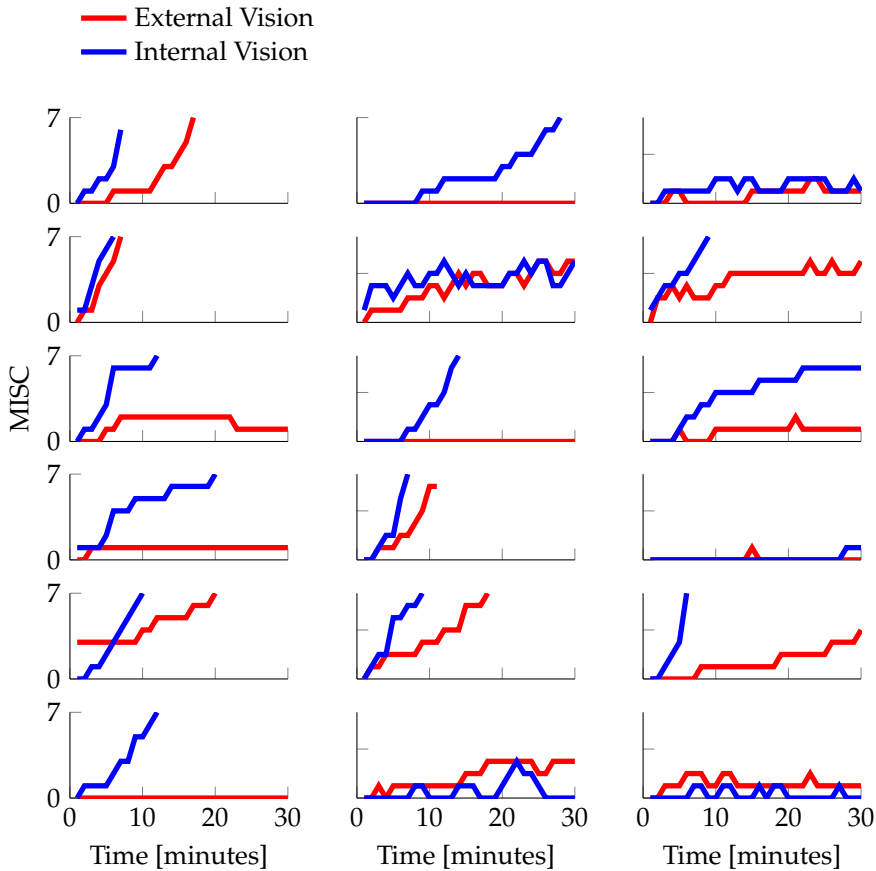
(b) Mean MISC internal vision against mean MISC external vision



(c) Mean MISC group sickness responses

There was no statistically significant difference between the visual conditions ( $t$





(d) Individual sickness responses

**Fig. 2.4** MISC responses for both internal and external vision conditions recorded during the sickening drive in Experiment 1. **a** shows the dropout % as a function of time. **b** shows mean MISC for internal vision against external vision. **c** shows the group-average mean MISC response calculated by omitting the dropouts (dashed lines) and replacing dropouts by MISC 7 (solid lines). **d** shows the individual responses

$= -0.347$ ,  $p = 0.733$ ,  $df = 17$ ). As the applied vehicle motion stimuli are similar, human responses can be compared between the visual conditions. Figure 2.4a shows the dropout rate for the two visual conditions. For internal vision this was 66% and for external vision this was 33%. Figure 2.4c shows the mean MISC for internal and external vision conditions. As can be verified from Figure 2.4d, a large number of participants reached a MISC of 7 within 30-minutes. As explained in Section 2.3.6, for these participants a constant MISC of 7 was taken to compute the mean group MISC up to 30 minutes. Figure 2.4b shows substantial scatter when relating the mean MISC for internal and external vision. Apparently, several participants develop noticeable sickness with internal vision only, while for others the sickness



with internal vision is close to the level reached with external vision.

Effects of visual condition were evaluated at each sample time using a paired Wilcoxon signed rank test since MISC is not normally distributed. The sickness responses for internal and external vision diverge significantly at the 5th minute ( $p = 0.0166$ ,  $SR = 12$ ,  $n = 18$ ). At the end of motion exposure the mean MISC for internal vision is 5.3 (STD = 2.51) and for external vision this is 3.3 (STD = 2.64). The mean MISC across time is 4.2 (STD = 1.5) for internal vision and 2.3 (STD = 0.95) for external vision. Therefore, throughout the duration of this experiment, internal vision is, significantly more sickening than external vision. Due to capping MISC at 7 for those participants that could not complete the 30 minute exposure, the difference is in fact greater than shown here. MISC rate provides a second measure that is not distorted due to the capping of MISC at 7. The median MISC rate for internal vision is 0.59, and for external vision it is 0.1. This is a large and significant (Wilcoxon signed rank test  $p = 0.011$ ) difference. The mean MISC, MISC rate and the dropout rate indicate that, compared to the external vision condition, sickness develops faster and to a greater level in the internal vision condition. However, the effect of visual condition varies strongly across participants.

Figure 2.4d shows the MISC responses of individual participants for the two visual conditions. There is a great variety of responses which, by the averaging in Figure 2.4c, is lost. From visual inspection, the responses seem to follow two categories. One is an exponentially divergent, "hockey stick" type response indicative of an unstable sickness response. The other is an exponentially convergent type response indicative of a stable sickness response. To show this, we fit a function of the form  $at^b$  to these responses. For  $b \geq 1$  the response is divergent and for  $b < 1$  the response is convergent. The  $b$  parameter is distributed over a large range (0-6.2). Moreover, for some participants, due to the coarseness of the subjective ratings in both the temporal and sickness resolution, the parameters cannot be estimated accurately. In addition to this,  $b$  cannot be estimated for the participants that do not get sick. For these participants we set  $a$  and  $b$  to zero. This makes clustering individuals difficult. However, it is likely that  $b$  is a parameter that depends on the magnitude of the sensory conflict. Supporting this, using a paired Wilcoxon signed rank test, we see that the median  $b$  for internal vision (higher sensory conflict) is 0.93 which is significantly greater  $p = 0.0475$  than the 0.39 in external vision (lower sensory conflict). Indeed, the means 1.46 and 0.69, respectively, indicate complex amplitude dependent dynamics for sickness progression. Capturing such richness in response requires models whose parameters can be tuned to fit individual responses.

### 2.4.2. EXPERIMENT 2: MODEL FIT

We first validate the adapted Oman model shown in Figure 2.3 by fitting it to the responses observed from Experiment 2. The fitting was done to the individual session responses of 13 participants. This is because participant 7, 16 and 17 dropped out of session two and/or session three and the vehicle IMU recording of participant 10 was incomplete. To evaluate the model fit we used the Symmetric Mean Absolute Percentage Error (SMAPE):

$$\text{SMAPE} = 100 \frac{\sum_{t=1}^n |F_t - A_t|}{\sum_{t=1}^n |A_t + F_t|}$$

Where  $F_t$  and  $A_t$  are the fitted and the actual value at time  $t$ , respectively. This error metric is well protected against outliers and treats both over- and underestimation in an unbiased manner.

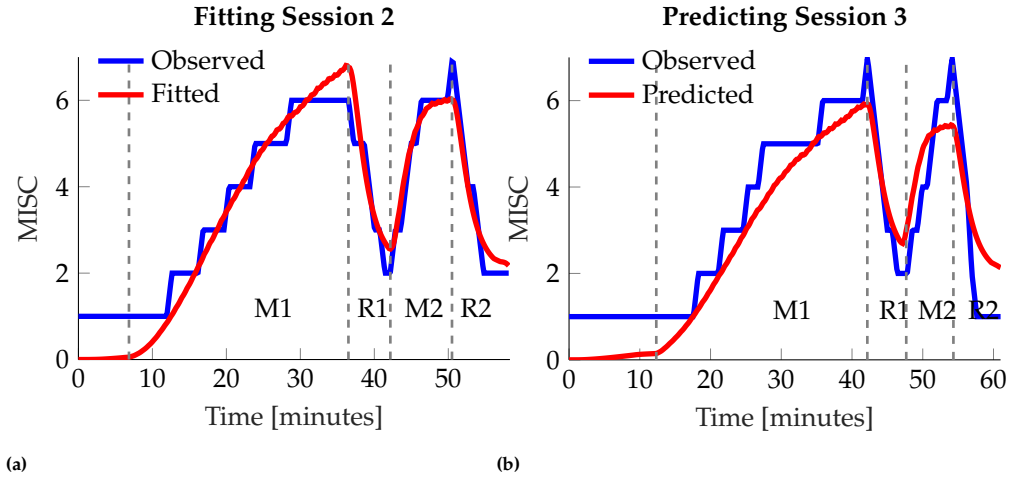


**Fig. 2.5** Example Oman model fit and predictions for the sickening drive data of Participant 6 from Experiment 2. **Left** shows the fitted model to the observed MISC of session 2 (SMAPE of 6.4%). **Right** shows the predicted MISC when the model parameters found for session 2 are used to predict the response of session 3 (SMAPE 11.7%)

The model fit has an average SMAPE of 11.4%. This means that while the model captures most variations, there are certain dynamics that it does not. Looking at the errors per period, the SMAPE for M1, R1, M2 and R2 is 12.3%, 8.8%, 8.3% and 23.4%, respectively. Applying multiple Mann-Whitney U tests between R2 and R1 errors, the  $p$ -values are calculated to be  $p = 0.005$ . Likewise, between M1 and M2  $p = 0.003$ . With a Bonferroni correction the critical value is  $\alpha = 0.025$  confirming significance of both effects. The model has more difficulty capturing the MISC change during R2 compared to R1. This may be because R2 has inherently different dynamics than R1, or more plausibly, because the observation window is larger for R2, which causes the inaccuracy in the modelling of the rest period to become more apparent. For M1 the error is significantly larger than for M2, which could be due to the fact that M2 on average lasts a shorter amount of time.

### 2.4.3. EXPERIMENT 2: REPEATABILITY OF INDIVIDUAL RESPONSES

For motion sickness to be modeled by dynamical equations, repeatability in response is important. Qualitatively, we can see from Figure 2.6 that individuals have a high degree of repeatability between the consecutive sessions.

This individual repeatability can be quantified by using Oman’s model (Figure 2.3). To do this, the model was tuned to fit the sickness response of session 2 in Experiment 2. We verified how well, using accelerations from session 3 as input, the parameters of session 2, could predict the MISC ratings seen for session 3 (here session 2 and 3 were compared to reduce skewing effects of habituation that might be present during session 1 and session 2). An example is shown in Figure 2.5. The SMAPE over the entire duration of the experiment averaged over 13 participants is 23.2% for session 3 using the parameters obtained by fitting the MISC for session 2. This shows responses to be repeatable over consecutive sessions. As a measure of how much more information individual responses gives us, this SMAPE can be compared to the average SMAPE when parameters obtained by tuning for session 2 of a participant is used to predict session 3 of any other participant. In this case the mean SMAPE is 46.6%. This clearly confirms the reduced accuracy of group-based models of sickness: individualized models of motion sickness can reduce the prediction error by a factor of 2.

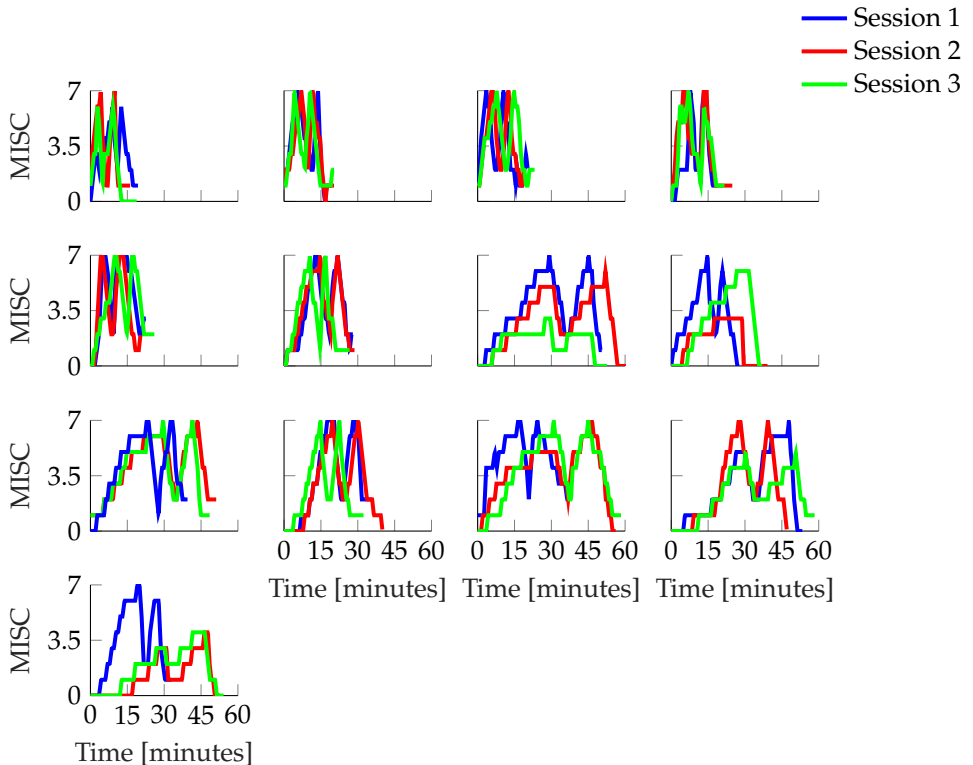


Fig. 2.6 Individual responses to the sickening drive across three repeated sessions in Experiment 2

#### 2.4.4. EXPERIMENT 2: HYPERSENSITIVITY

Hypersensitivity is seen to occur when after a brief rest participants who are exposed to further sickening motions respond in a much faster manner than during their initial exposure. This can clearly be observed in Figure 2.6, with a much quicker rise in M2 than in M1. The median MISC rate was  $1.02 \text{ min}^{-1}$  for M2 and  $0.395 \text{ min}^{-1}$  for M1 and differed significantly ( $p = 0.0421$ , Wilcoxon test). This indicates a much higher sensitivity in the second exposure.

The adapted Oman model was used successfully to model both the initial response (M1) and hypersensitivity (M2), with one set of parameters. Group average parameters are 441 and 2.18 for  $\beta_2$  and  $K$ , respectively. The parameter  $\beta_2$  corresponds to the decay time constant of hypersensitivity. This is, an average value of 441 s, or 7.35 minutes.

#### 2.4.5. EXPERIMENT 2: INFLUENCE OF PARAMETERS

To further support the sickness response modeling results, Figure 2.7 shows the effects of varying the two parameters of the model ( $\beta_2$  and  $K$ ) with respect to their group average values on the model's predicted sickness response. The top figure shows that lowering the time constant  $\beta_2$  leads to a faster sickness development. As, for this chapter, the slow path and fast path time constants are coupled by  $\beta_2 = 7\beta_1$  reducing the value of  $\beta_2$  reduces the value of  $\beta_1$ . Doing so reduces the damping of the sickness response. The lowest  $\beta_2$  and  $\beta_1$  show MISC fluctuations caused by the stop and turn performed after the slalom seen in Figure 2.7. Varying  $K$  on the other hand, has no influence on the time response and  $K$  only acts as the gain on the amplitude of the sickness response. To conclude, the adapted version of the Oman model is seen to successfully characterize the full course of individual sickness response including hypersensitivity and its two parameters cause simple, interpretable changes in the modeled sickness response.

#### 2.4.6. EXPERIMENT 1 & EXPERIMENT 2: KINEMATIC AND PHYSIOLOGICAL VARIABLES

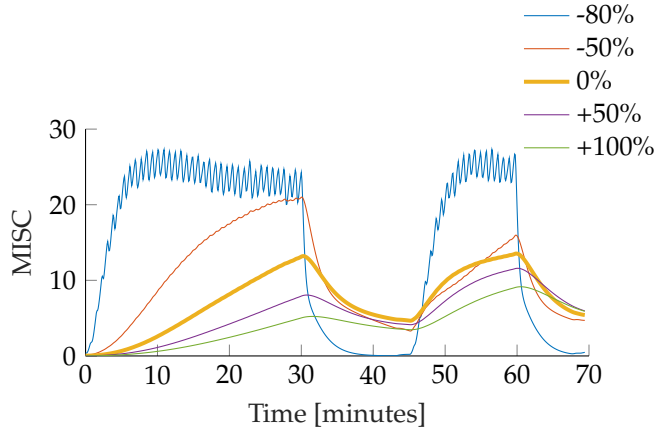
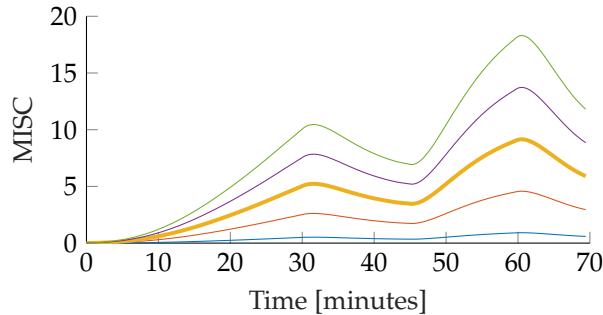
##### GALVANIC SKIN RESPONSE

Motion sickness can cause an increase in both the tonic and phasic GSR, indicative of the fight or flight response (Mackersie L and Calderon-moultrie, 2016). In motion sickness experiments both components may also be a function of time, in addition to sickness. To verify these effects, we use a mixed linear model of the form:

$$\mu S_{tonic} = \alpha_0 + \alpha_1 MISC + \alpha_2 t + u_j + \epsilon_t \quad (2.1)$$

$$\mu S_{phasic} = \gamma_0 + \gamma_1 MISC + \gamma_2 t + v_j + w_t \quad (2.2)$$

Where  $u_j$  and  $v_j$  denote the random intercept for participant  $j$ ,  $\alpha_0$  and  $\gamma_0$  are the intercepts,  $t$  is time and  $\alpha_1/\alpha_2$  and  $\gamma_1/\gamma_2$  are coefficients. The variance inflation factor between MISC and time is found to be 1.46 which is smaller than the value of 4 taken as the point where collinearity starts to become a concern. After fitting the linear mixed model it was seen that the model residuals are not normally distributed,


 (a) Varying  $\beta_2$ 

 (b) Varying  $K$ 

**Fig. 2.7** Effect of varying the group averaged parameters on the average sickness response; **Top** shows the effect of varying the slow path time constant  $\beta_2$ . **Bottom** shows the effect of varying the gain  $K$ .

which reduces confidence in the statistics of the fit. Therefore the model was bootstrapped using 4000 iterations of random-x resampling to derive the 2.5% and 97.5% percentile confidence intervals for the parameters.

For the tonic GSR the effect of MISC is significant, with a mean coefficient 0.485 (CI between 0.379 and 0.586). This means, for an increase of MISC from 0 to 7, a mean rise of the tonic GSR by  $3.4 \mu\text{S}$  over the mean baseline of  $8 \mu\text{S}$ , which is an increase of 42.5%. The time coefficient is also significant with a mean value of  $0.0006 \mu\text{Ss}^{-1}$  (CI between 0.0002 and 0.0010). However, its effect is smaller, resulting in an increase of the tonic GSR by  $1.08 \mu\text{S}$  over the baseline of  $8 \mu\text{S}$  (only 7%).

For the phasic GSR the effect of MISC is also significant. The mean coefficient is  $1.69 \mu\text{S}$  (CI between 1.28 and 2.1). This means for an increase of  $11.83 \mu\text{S}$  over the baseline of  $13.2 \mu\text{S}$ , an increase of 90%. The time coefficient is not significant, as the CI for  $\gamma_2$  (between -0.0019 and 0.0005) crosses zero.

### HEART RATE & HEART RATE VARIABILITY

For the analysis of HR and LF/HF ratio of HRV, we also follow the methodology explained in Section 2.4.6. The variance inflation factor between MISC and time is found to be 1.80, i.e., smaller than the value of 4 taken as the point where collinearity starts to become a concern.

For HR, the effect of MISC is significant, with a mean coefficient of 0.466 (CI between 0.247 and 0.673). This means that for an increase of MISC from 0 to 7, there is a mean rise of HR by 3.3 bpm over the baseline of 87.4 bpm (only 3%). The time coefficient is also significant with a mean of -0.0063 (CI between -0.0070 and -0.0055). This means a reduction of 11.3 bpm (a drop of 12.9%) throughout the 30 minute motion exposure. This drop in time due to relaxation of the participants masks the slight increase due to increased sickness.

For the LF/HF ratio the effect of MISC is also found to be significant. The mean coefficient is -0.0463 (CI between -0.0279 and -0.0647) which is a decrease of 18.52% over the baseline of 1.75 going from MISC 0 to 7. This is contrary to what would be expected based on the traditional view of LF/HF ratio where a decrease is indicative of a more relaxed state. The time coefficient is also significant with a mean of 0.00003 (CI between 0.00036 and 0.00022), a 3.1% increase over baseline. The time effect and the sickness effect are in opposite directions and so the net change in the LF/HF ratio is small.

### HEAD ROLL

Head motion is taken as indicative of postural stability, which may relate to the development of motion sickness over time. Availability of visual cues may help in maintaining head stability and so have an effect on sickness development. The median head roll rms ratio for internal and external vision responses, across 11 participants from Experiment 1 for who valid head roll data was available, were found to be 2.05 and 1.60, respectively. However, this within-participant difference was not significant ( $p = 0.101$ , Wilcoxon test).

With no significant difference between internal and external vision conditions, for the remaining analysis, data from Experiments 1 and 2 are combined for all the participants, leading to data from 33 participants in total.

Within the experiment the MISC level is correlated with time. However, the variance inflation factor between MISC and time is found to be 1.09, i.e., well below the collinearity limit of 4.

For head roll there is a moderate effect of MISC, with a coefficient of 0.0212 (CI between -0.011 and 0.052). However this is not significant. Over a 7-point MISC scale this is a mean increase of head roll rms ratio of 0.15 over the mean head roll rms at the intercept, giving a total head roll rms ratio of 1.85. For a peak lateral vehicle acceleration of  $4 \text{ ms}^{-2}$ , this means an increase of head roll amplitude from 9.6 deg to 10.45 deg, an increase of 8.9%. There is however a significant effect of time. Here the mean coefficient is  $0.000469 \text{ s}^{-1}$  (CI between 0.000577 - 0.000365). Over the course of a 30-minute experiment, starting at a baseline head roll of 9.6 deg, due to the  $4 \text{ ms}^{-2}$  peak lateral vehicle acceleration, the mean increase in rms head roll is 14.4 deg, a 50% increase. From this analysis, it can be concluded that for our data the effect of time on the loss of head stability is stronger than the effect of MISC.

## 2.5. DISCUSSION

In this chapter we took to analyze motion sickness development in the time domain in contrast to the more widely used time averaged/instanced metrics in the literature. The richness of information has therefore allowed for greater insights in to the phenomenology of motion sickness.

### 2.5.1. INTERNAL-EXTERNAL VISION

Internal vision was more sickening with a higher mean MISC (4.2 vs 2.3) compared to external vision, a higher MISC rate (0.59 vs 0.10) and more dropouts (66% vs 33%). Due to the non-linear relationship between MISC and comfort, however, this difference is likely much greater on a subjective comfort scale (such as the fast motion sickness scale [Keshavarz and Hecht \(2011\)](#)). Moreover, due to the mean MISC calculation, which capped those participants who had to prematurely end the experiment at a MISC of 7, the true difference is likely larger than found in this study. These findings concur with [Griffin and Newman \(2004a\)](#), who found a similarly large difference in sickness rating between internal and external vision in natural driving conditions. The effects of visual condition can be due to both an increase in sensory conflict, caused by the removal of external world view, but also the removal of anticipatory information regarding the vehicle trajectory.

The vehicle rotation with respect to earth in both roll and pitch was found to be negligible. Therefore, internal vision provides virtually identical visual cues for orientation with respect to gravity as external vision. The main difference between the information provided by internal and external vision lies in the visual translational and yaw information received. However, [Bos et al. \(2008b\)](#) found in simple motion experiments that the absence of translational or yaw visual information does not impact sickness.

On the other hand, several studies show that the presence of anticipatory cues leads to a substantial reduction of motion sickness. [Feenstra et al. \(2011\)](#) found the mean MISC at the end of motion reduced from 2 to 0.5 when anticipatory information was added to a turbulent flight simulation. Likewise, [Kuiper and Bos \(2019\)](#) found a higher end of motion mean MISC of 3.6 compared to 2.3 when comparing unpredictable motion cues over predictable motion cues in a vestibular only sled experiment. Lastly, [Karjanto et al. \(2018\)](#) observed a major reduction from 10.4 to 1.4 on the motion sickness assessment questionnaire (MSAQ) when anticipatory information was provided to passengers undertaking left and right turns in the absence of external vision, compared to when such cues were not provided. Therefore, even though a number of studies agree on the alleviating effect of anticipatory cues on motion sickness, they do not arrive at the same effect size. The large effect sizes found by [Karjanto et al. \(2018\)](#) or [Feenstra et al. \(2011\)](#) may be due to differences in experimental stimuli or the scale used to measure motion sickness. Some scales such as MSAQ may have larger sensitivity within lower sickness levels than other scales such as the MISC. Therefore, an important consideration is the intensity of the sickening stimuli where [Kuiper and Bos \(2019\)](#) obtained MISC ratings between 2 and 3.5 whereas [Feenstra et al. \(2011\)](#) obtained MISC ratings between 0.5 and 2. The inhibitory effects of mechanisms such as anticipation may not scale proportionally



with motion sickness severity or the magnitude of the sickening stimuli.

The mean MISC level is widely used and is useful in showing clear group responses, but it masks important individual dynamics. Some participants have a convergent MISC response, where the final MISC level seems to exponentially reach a terminal value, where others have a divergent, exponential response (Figure 2.4d). The response dynamics may even be a function of the visual condition, where for instance, Participant 16 has no response for external vision, but an exponential response for internal vision. Likewise, Participant 6 has an exponential response for internal and a convergent response for external. As previously mentioned, current models of motion sickness do not account for this complexity. Instead, they aim to predict the development of sickness at a population level. For instance, [Bos and Bles \(1998\)](#) predict the motion sickness incidence (MSI), defined as the percentage of the population that has vomited. However, we argue that as models of motion sickness are based on hypothesized neurological mechanisms, their predictions must be individual specific and related to the physiological symptoms individuals experience.

### 2.5.2. REPEATABILITY AND OMAN'S MODEL

It is often not feasible to build human models that are capable of individual forecasts. This is due to the number of internal and external factors that may yield to large response variability. Therefore, statistical models based on group metrics are commonly favoured over dynamical system models. However, our results comparing repeated exposures over consecutive sessions show that the time response of motion sickness is largely repeatable. Knowing the response of a participant in the previous sessions allows for the prediction in the next session with a SMAPE of 23.2% for all four stages of the response combined during M1, R1, M2 and R2. If instead, a group average model is used, the average error fitting individual responses is 46.6% which is a factor of 2 greater than the error of the individual based models. This means motion sickness can be modeled on an individual level, where the more historic data available for that individual, the more reliable the model is.

For this repeatability analysis we used an adapted version of the model of nausea developed by [Oman \(1990a\)](#). We performed the first extensive validation of Oman's model to predict the time course of motion sickness on the MISC scale, including hypersensitivity and rest phases of the exposure. We note that for hypersensitivity the sickness rises consistently faster than during the first motion exposure. We estimate the time constant for hypersensitivity,  $\beta_2$ , to be 7.35 minutes. This is similar to the value of 10 minutes reported by [Oman \(1990a\)](#). [Golding and Stottt \(1997\)](#) also measured an "objective" recovery time constant by measuring the loss in tolerable number of head movements during motion re-challenge. They found a decay time constant of 15 minutes. They report that, the decay in sensitivity is not monotonic and that there was a rise 2 hours after stimulation. This rise is not predicted by Oman's model. Indeed the presence of complex slow dynamics matches with our own informal observations. One participant in Experiment 1 withdrew from the study due to sickness persisting after many hours. Likewise two participants in Experiment 2 reported resurgence of nausea in the following hours after the experiment. These were self-reports made by the participants and without the request of



the experimenter, so the real number of those effected by the after motion dynamics, which seem to last in the order of hours to even days may be higher. This is therefore an important topic of future study.

We found that the fast path time constant was a factor 7 smaller than the slow path time constant. Reducing the value of the slow path time constant therefore caused both a reduction in the time to convergence of the sickness response and a reduction in the damping of the system (due to coupling with the fast path time constant). As can be seen from the negative placement of the system poles, the Oman model is stable and convergent. However, this does not stop it from providing good fits to divergent responses up to termination of the experiment. It is important to note that the gain of the fast path is a multiple of the input conflict, the subsequent amplitude of the sickness response is therefore a quadratic function of the conflict signal. This has important implications for mixed acceleration environments, such as traffic, where there may be an under or over estimation of the effect of certain acceleration on the sickness response. Therefore, the relationship between stimulus intensity and individual sickness response dynamics should be investigated further. It may indeed be that there is a bifurcation in the nature of responses depending on the strength of the sensory conflict, which may also relate to the fact that some of our participants showed divergent responses for internal and convergent responses for external vision.

In the current study, we have observed that low time and sickness resolution impedes accurate model identification. That is, given the sparsity of data, multiple model fits may provide equivalent solutions. This was resolved by simplifying the model ( $\beta_2 = 7\beta_1$  &  $\beta_3 = 1$ ). This may compromise model validity in other conditions. For instance, the thresholding included in the original Oman's model (excluded in this study) is indicative of the "functional vestibular reserve" (Graybiel, 1969). This may be of particular importance when considering habituation or when modeling the effect of low amplitude motions that generate sub-threshold sensory conflicts. Future studies should keep the specificity of the current simplified model in mind.

To enhance the resolution in recording motion sickness, verbalized subjective ratings may be collected with a greater sampling frequency. Following an approach similar to (Cleij et al., 2019), sickness ratings may be acquired in a continuous manner via the use of a dial. This approach may increase rating variability, but combined with verbalized ratings as an anchor, this can result in a valuable high-resolution data set for sickness model identification.

### 2.5.3. KINEMATIC AND PHYSIOLOGICAL VARIABLES

For the analysis of the physiological measurements the present study employed a methodology whereby the sample population was not arbitrarily segmented in sick and not-sick groups, as has often been done in the past. Motion sickness occupies a spectrum of severity and clear cut-offs may introduce undesired effects. Linear mixed models with random intercepts were used instead to separate trends in time from effects of motion sickness and to quantify these contributions to MISC.

For the tonic GSR there is a significant increase with both time and sickness. This

is very much expected and likely due to increasing sweating due to the stabilizing action of the muscles when subject to the 0.4 g lateral accelerations. For the phasic GSR there is a significant increase with respect to sickness, but not with time. This is also expected, as the phasic component is more indicative of sympathetic activation [Benedek and Kaernbach \(2010a\)](#). There is a larger effect of sickness on the phasic component, i.e., 90% of the baseline, whereas the increase of the tonic GSR is 42.5% of the baseline.

For the heart rate and the LF/HF ratio the results are found to be more mixed. MISC seems to elevate the heart rate, but this effect is small compared to the general decrease in heart rate due to relaxation from the high state of arousal at the start of the experiment. Thus, the strength of the link between heart rate and motion sickness level likely depends on the nature of the experimental stimulus. Under the extreme scenario tested here, time effects are likely to be larger than in most laboratory experiments. In the present study we observed a small but significant decrease of the LF/HF ratio, which constituted 18.52% of the baseline LF/HF ratio. This measure is traditionally taken as an indicator of sympatho-vagal balance, whereby an increase in the ratio is indicative of increased sympathetic activity. As motion sickness activates the sympathetic nervous system, an increased LF/HF ratio is expected. This activation is evident in the GSR responses. Recently, however, it has come to attention that LF/HF ratio is not a simple linear measure of sympatho-vagal balance, but is instead a much more complex and non-linear metric. For instance, it is now known that LF power of heart rate variability is also modulated by the parasympathetic nervous system, and vice versa for the HF power of heart rate variability [Billman \(2013\)](#). Therefore, LF/HF ratio is a complex measure of sympathetic and parasympathetic activity which on its own, as seen in our results, is not likely to be an effective indicator of motion sickness.

In our experiment we found head roll to increase with exposure to sickening motions. Our regression model showed this to relate significantly only to exposure time. Exposure time relates to fatigue and/or the willingness to go with the motions, rather than opposing them. The nonsignificant relation with sickness does not support the postural instability theory of motion sickness ([Stoffregen and Smart, 1998](#)). However, this may owe to the noisy nature of the experimental data which was collected from sitting participants subject to high accelerations, as well as the filtering process required to obtain the results. Regardless of the outcome, we could have made no statements on whether postural instability preceded sickness, or rather results from sickness. The latter seems more probable in terms of decreased control due to sensory conflict [Bos \(2011\)](#). There is evidence that roll/pitch of the head when combined with linear translational accelerations interact in a non-linear manner to increase sickness to levels higher than would be possible if they were experienced in isolation [Wertheim et al. \(1998\)](#). On the other hand, [Golding et al. \(2003\)](#) observed that the effect of head roll on sickness depended on whether it was active or passive. Here, it was found that active alignment of the head with the direction of the gravito-inertial acceleration would protect against motion sickness whereas active movements against would increase symptoms of motion sickness. For passive motions (created by actuation of the passenger seat), on the other hand, the opposite

was the case. The rotations experienced in the current study cannot be characterized as active or passive. Therefore, whether head roll acts as positive feedback mechanism to increase sickness levels can not be stated.

Of all considered metrics, the phasic GSR correlates most strongly with MISC, increasing 90% above its baseline value at MISC 7. However, the increase only becomes noticeable when averaging over the entire population and after prolonged exposure. It remains to be proven how well this measure can be used as individual (real time) classifier of motion sickness, to complement or even replace subjective assessments such as the MISC.

### 2.5.4. IMPLICATIONS

We confirm that having external vision strongly reduces motion sickness so vehicle manufacturers and also passengers should design and act to maximise world referenced visual information. This can include novel technologies that might increase anticipatory cues, some of which were discussed in section 4.1.

Knowing the dynamics and parameters of hypersensitivity may enable route planning that accounts for motion sickness. For instance, sections of road that provide large sickening stimulus i.e. traffic or mountain road may be scheduled such as to provide adequate reduction in sensitivity in between exposures.

More importantly, by showing that motion sickness is regular and repeatable within individual participants we now have a greater basis for using system-theoretical, model-based approaches for understanding motion sickness.

Lastly, validating the Oman model as an approximate model for sickness dynamics, opens the door for developing robust platform controllers that may allow for the control of sickness levels in individual participants to a desired reference level.

## 2.6. CONCLUSION

From experiments where we measure the development of motion sickness during a highly sickening drive, we find a significant increase in mean MISC, from 2.3 (at the end of exposure) in the external vision condition to 4.2 in the internal vision condition. We believe this is largely due to a reduction of anticipatory cues, rather than removal of visual translational and yaw rotation cues.

We show that individuals exhibit a wide variation in the dynamics of sickness development over time, whose key individual characteristics are masked by group averaged metrics, as often used in previous publications. We for the first time attempt to fit Oman's model of nausea to time-domain data of individual participants. We see that these fits are able to accurately model the full course of individual's sickness development for our experimental data, including the rest and hypersensitivity phases.

Using this model we show that motion sickness is a repeatable phenomenon with individual motion sickness responses showing a high degree of repeatability over consecutive sessions. GSR responses show significant effects of exposure time and of sickness level. These effects are highly significant at the group level with exposure for up to 30 minutes or until a MISC of 7 is reached, but show substantial scatter.

## 2.6. CONCLUSION

---

Due to this natural spread, such objective measures are unlikely to replace subjective sickness measures (e.g., MISC) for real time motion sickness classification.



# 3

## AMPLITUDE AND TEMPORAL DYNAMICS OF MOTION SICKNESS

---

This chapter has been published as: Tugrul Irmak, Varun Kotian, Riender Happee, Ksander N. de Winkel, Daan M. Pool, *Amplitude and Temporal Dynamics of Motion Sickness*, *Frontiers in Systems Neuroscience* (2022)

### 3.1. ABSTRACT

*The relationship between the amplitude of motion and the accumulation of motion sickness in time is unclear. Here, we investigated this relationship at the individual and group level. 17 participants were exposed to four oscillatory motion stimuli, in four separate sessions, separated by at least one week to prevent habituation. Motion amplitude was varied between sessions at either 1, 1.5, 2 or 2.5 ms<sup>-2</sup>. Time evolution was evaluated within sessions applying: an initial motion phase for up to 60 minutes, a 10-minute rest, a second motion phase up to 30 minutes to quantify hypersensitivity and lastly, a 5-minute rest.*

*At both the individual and the group level, motion sickness severity (MISC) increased linearly with respect to acceleration amplitude. To analyse the evolution of sickness over time, we evaluated three variations of the Oman model of nausea. We found that the slow (502 s) and fast (66.2 s) time constants of motion sickness were independent of motion amplitude, but varied considerably between individuals (slow STD=838 s; fast STD=79.4 s). We also found that the Oman model with output scaling following a power law with an exponent of 0.4 described our data much better as compared to the exponent of 2 proposed by Oman. Lastly, we showed that the sickness forecasting accuracy of the Oman model depended significantly on whether the participants had divergent or convergent sickness dynamics. These findings have methodological implications for pre-experiment participant screening, as well as online tuning of automated vehicle algorithms based on sickness susceptibility.*

### 3.2. INTRODUCTION

Motion sickness is a syndrome that arises as a consequence of a wide range of self-motion and orientation cues. It is characterised by symptoms of sweating, headache, dizziness, stomach awareness, where these symptoms usually grow in severity until nausea, retching and ultimately vomiting occurs (Bertolini and Straumann, 2016). The fact that adverse motions may, in a wide range of species (Wang and Chinn, 1956; Hickman et al., 2008; Wassersug et al., 1993; Bauerle et al., 2004), cause a diverse set of symptoms is peculiar.

Therefore, the aetiology of motion sickness remains an active area of scientific inquiry. There are two main theories of motion sickness, these are the "Sensory Conflict" (Reason, 1978; Oman, 1982) theory and the "Postural Instability" theory (Riccio and Stoffregen, 1991). The most developed mathematical models and tools exist for the sensory conflict theory (Wada, 2021; Bos and Bles, 1998; Khalid et al., 2011a). Therefore, this paper will study motion sickness through the concepts of state estimation and sensory conflict, and will not cover the postural instability theory nor attempt to evaluate postural precursors to motion sickness.

The sensory conflict theory (Reason, 1978) argues that motion sickness is mainly due to a conflict between the sensed sensory signals and the sensory signals expected by the brain. These expectations originate from an internal model, which takes the form of a neural store. The conflict leads to adaptation of the internal model. In the formulation of Oman (1982) this conceptual model is likened to a Luenberger Observer (LO). The LO has an internal model of the system (body) and sensor dynamics. Due to the imperfect and noisy nature of the sensory signals, one cannot use the sensor measurements directly. Instead, the true states of the system must

be observed (estimated) by integrating sensory information using an internal model of the system itself. Indeed, there is strong neuronal evidence for the use of internal models for state estimation (Merfeld et al., 1999; Angelaki et al., 2004; Laurens et al., 2013; Oman and Cullen, 2014). To quantify estimation accuracy, the central state estimates are passed through an internal model of sensory dynamics and compared with the actual sensory signals. The resulting error is the estimation error, or the sensory-expectancy conflict. It is hypothesized that the magnitude of the conflict and the duration of exposure then leads to the subsequent symptoms of motion sickness.

There are practical implications that come with a firm understanding of the relationship between the magnitude of sensory conflict and motion sickness accumulation. Firstly, such knowledge allows us to better generalise motion sickness predictions to mixed acceleration environments that are ubiquitous to vehicular transport (Feng et al., 2017). Such predictions may then be used as an objective function to minimise sickening vehicle motions. Secondly, a functional model will allow for the development of control algorithms that can automatically adjust the amplitude of sickening simulator motions such that participants track a desired sickness trajectory. Currently, in experimental studies, researchers must fix their stimulus beforehand and hope that participants do become sick, but do not terminate the experiment prematurely. Active control will allow for setting the desired level and variance of motion sickness, which will increase the statistical quality of data collected. Lastly, a predictive model of sickness accumulation will allow for tuning of automated vehicle algorithms to the susceptibility level of the individual passenger, whilst also allowing prescreening of participants for a desired level of susceptibility. To allow for these novel methods and technologies, the mathematical process that links sensory conflict to the time evolution of motion sickness must be elucidated.

For simple motions, such as single degree-of-freedom vertical or horizontal accelerations, the conflict vector is assumed to be proportional to the acceleration stimulus itself. There is literature on the relationship between the acceleration magnitude (a proxy for the magnitude of the conflict) and group-level responses to sickness. Lawther and Griffin (1988), for instance, show a linear relationship between the amplitude of vertical accelerations on ships and motion sickness incidence (MSI), which is the percentage of people who vomited during the exposure. Likewise, using the more sensitive metric of mean subjective illness score, they also observed a strongly linear relationship between acceleration amplitude and sickness. However, their tested acceleration amplitudes were only in the range of 0-0.7 ms<sup>-2</sup>, which covers a small linearisable part of the complete, possibly nonlinear sickness amplitude dynamics. Indeed, looking at the data of O'Hanlon and McCauley (1973), in the range of 0.25-3.9 ms<sup>-2</sup> there seems to be a sigmoidal relationship between acceleration amplitude and MSI. The subjective vertical model developed by Bos and Bles (1998) captures this sigmoidal relationship by first rectifying the conflict vector, and then input scaling it with a non-linear Hill-function. The resulting scaled conflict is then integrated with a second-order system, to match the MSI observations of O'Hanlon and McCauley (1973).

The approach of combining sensory conflict and accumulation models is unique



because it clearly discriminates between conflict *generation*, which is a by-product of spatial orientation and state estimation, and conflict *integration*, which leads to motion sickness. There are two shortcomings in this approach. Firstly, at the practical level, the motion sickness prediction is made using motion sickness incidence (MSI), defined as the percentage of people that have vomited. This misses the finer increments in symptom development that precedes vomiting, which are more relevant for most practical applications of motion sickness modelling. Secondly, the approach conflates the internal dynamics that lead to sickness at an individual-level with the averaged group-level dynamics. For a physiologically valid model of motion sickness, the final sickness predictions should map to individual ratings, not group-averaged ones.

An individual-level model of the temporal dynamics of motion sickness was developed by Oman (1990a). This model is also uniquely able to describe the phenomenon of ‘hypersensitivity’, which is an essential part of sickness development over time. Hypersensitivity is characterised by the fact that after exposure to sickening motions, any further exposure to sickening motions leads to a more rapid rise in sickness than in the initial exposure (Golding and Stott, 1997). Modelling hypersensitivity is particularly relevant for automated driving, as sickening motions are usually separated by long durations of rest (i.e., at the traffic lights). In our previous work, the Oman model was validated in the context of motion sickness generated by slalom manoeuvres performed by a car at 0.2 Hz with a lateral acceleration of  $4 \text{ ms}^{-2}$ , for up to 30 minutes (Irmak et al., 2020). Here, it was seen that the model provided a good fit to subjective sickness scores as measured on the MIsery rating Scale (MISC) (Bos et al., 2010). Moreover, using the Oman model, parameters governing the trajectory of motion sickness could be used to predict individual responses in re-exposure to the same paradigm. This indicated a high degree of intra-individual repeatability in sickness dynamics. In this previous experiment, we only used an acceleration of a single magnitude. However, in traffic, humans generally encounter mixed acceleration stimuli. The original form of Oman (1990a)’s model predicts the end level of sickness to be a quartic of the input acceleration amplitude. This is because of the model’s ‘slow’ path acting as a gain on its ‘fast’ path and the output power scaling,  $p_o$  shown in Figure 3.2, being set to 2. It is, however, not clear whether this proposed amplitude relationship is correct. Nor is it clear whether the Oman model can generalise to fit sickness for different acceleration inputs, or whether its parameters must be refitted on a case-by-case basis.

In the present study, we assessed the relationship between conflict magnitude, using acceleration stimulus amplitude as a proxy, and the temporal dynamics of motion sickness symptoms at the individual-level. We did this by exposing 17 participants to sinusoidal fore-aft motions of four different acceleration amplitudes. The experiment was performed in the SIMONA Research Simulator at the Aerospace Engineering faculty of TU Delft (Stroosma et al., 2003; Berkouwer et al., 2005). In the subsequent analyses, we first confirm previous literature findings for the relationship between acceleration amplitude and group-level responses. Uniquely, we show that motion sickness at an individual-level for different stimulus amplitudes can be modelled adequately with individually varying Oman model time constants that are

independent of motion amplitude, but using the same group-level averaged power law scaling at the output for all individuals. Moreover, we show that the Oman model in its current form can forecast the future evolution of motion sickness, but the accuracy of the forecasting is dependent on the qualitative form of individuals' sickness dynamics. This has important consequences for prescreening of participants for motion sickness experiments, and tuning of automated driving algorithms to individual passengers.

## 3.3. METHODS

### 3.3.1. ETHICS STATEMENT

All participants provided written informed consent prior to participation. The experimental protocol was approved by the Human Research Ethics Committee of TU Delft under application number 1425.

### 3.3.2. PARTICIPANTS

In total, 17 participants completed this study (mean age: 25.3 years, STD: 2.6 years; 2 female, 15 male). The 17 participants had a mean motion sickness susceptibility questionnaire short form (MSSQ-Short, [Golding \(2006\)](#)) score of 16.2 (STD = 10.1) indicating that they had above average susceptibility, corresponding to the 65<sup>th</sup> percentile.

### 3.3.3. APPARATUS

The experiment was performed in the SIMONA Research Simulator at TU Delft (Figure 3.1). The simulator has a six degree-of-freedom hydraulic hexapod motion system, which can provide a maximum displacement of 1.12 m, a maximum velocity of 0.9 ms<sup>-1</sup> and a maximum acceleration of 13 ms<sup>-2</sup> ([Stroosma et al., 2003](#); [Berkouwer et al., 2005](#)). The participants were placed inside a closed cabin, within which they were seated and secured using a five point harness. To prevent unwanted head movements, their head was supported with a neck restraint. To remove any visual cues, they wore blackened goggles and the cabin lights were turned off (see Figure 3.1). Continuous communication with the experimenter was possible via an intercom system.

### 3.3.4. TASK

Each condition was tested on participants with a rest of at least 1 week (mean: 30.6 days, STD: 20.6 days) in between any two test conditions. In these sessions, participants were subjected to sinusoidal fore-aft motions at a frequency of 0.3 Hz. The amplitude of the accelerations used were; 1, 1.5, 2 and 2.5 ms<sup>-2</sup>. The choice of the highest acceleration was constrained by the maximum possible simulator velocity of 0.9 ms<sup>-1</sup>. The choice of the frequency was based on the highest frequency observed for which the population incidence of sickness does not decrease ([Golding and Markey, 1996](#); [Golding and Stottt, 1997](#); [Irmak et al., 2020](#)).

In each session, participants underwent two motion exposures. The first exposure lasted for 60 minutes, or until the participant reached a MISC of 6. They were

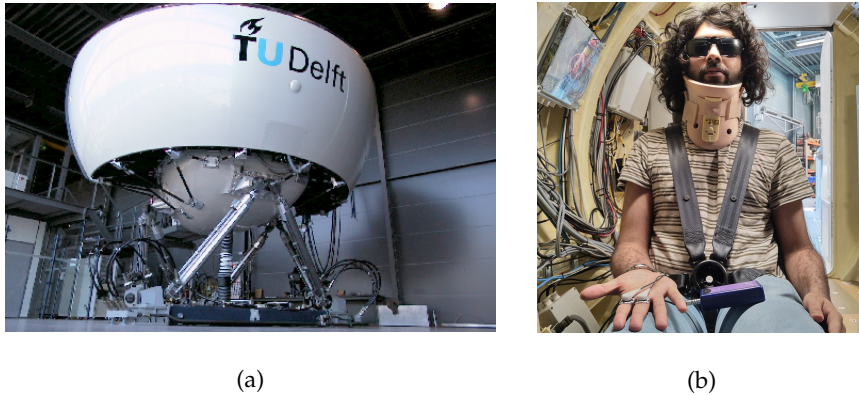


**Fig. 3.1** Experimental setup. (a) is the SIMONA Research Simulator used in the experiment to elicit motion sickness via fore-aft sinusoidal motions of differing amplitudes. (b) shows the second author as a participant in the experiment, wearing a 5-point safety harness, a neck restraint, and blacked-out glasses

then permitted 10 minutes rest, after which the second exposure lasted for 30 minutes, or until they reached a MISC of 6. After this, they first rested for 5 minutes in the simulator, and then for as long as they desired to in the staging room. At the beginning and end of each motion, the motions were faded in and out with a linearly increasing and decreasing amplitude from zero to the level specified over a 10-second period.

Each session only tested one amplitude of the range of acceleration stimuli. Due to time limitations and a desire to sample as broad a range of amplitudes as possible, conditions were not repeated. This is justified by good trial-to-trial repeatability found previously in the measured motion sickness responses (Miller and Graybiel, 1969; Irmak et al., 2020). The order in which each amplitude was experienced was balanced between participants using a Latin square. This prevented confounding effects of habituation between the different amplitudes.

### 3.3.5. QUANTIFYING SICKNESS

Participants were instructed to report their sickness on the 11-point MISC scale (Bos et al., 2010). The MISC scale is anchored to specific motion sickness symptoms: 0 is no symptoms, 1 is uneasiness, 2, 3, 4, 5 represent increasing severity of non-nausea symptoms from vague to severe, 6 is mild nausea, 7 is moderate nausea, 8 is severe nausea with 9 and 10 being retching and vomiting, respectively. The MISC is useful because the ratings are directly linked to symptoms, which is not the case with other scales such as the Fast Motion Sickness Scale (FMS) (Keshavarz and Hecht, 2011) and the Magnitude Estimate scale (Bock and Oman, 1982). Having a non-anchored scale would make the ultimate aim of minimising of sickness predictions with respect to vehicle motions infeasible. It has been reported by Reuten et al. (2021) that there is a clear non-monotonic relationship between a MISC level of 5 and 6 in terms of the feelings of unpleasantness that are often used to characterise the sickness response. However, recently de Winkel et al. (2022) have demonstrated that this ob-

served break from monotonicity was semantic in nature. The discomfort associated with each level of the MISC, as it was used to express motion sickness during exposure to a sickening stimulus, was found to increase monotonously and the MISC could be characterised by a power law of exponent 1.206 (de Winkel et al., 2022). All together, these considerations were deemed sufficient to warrant using the MISC directly for our modelling work.

Every 30 s, a 1 kHz beep was played over the simulator intercom to prompt the participants to verbally state their MISC level. In addition to this prompted response, participants were told that they could voluntarily give a MISC report whenever they thought it changed substantially since the last response was requested. Responses were recorded on audio and transcribed after the experiment session by the experimenter. The audio recordings were voice activated and recorded only for the duration the participant was speaking. Each MISC rating given by the participant was time stamped to the start of the audio sample.

#### DROP-OUT RATE & MISC RATE

To quantify the dynamics of sickness with respect to acceleration amplitude, the severity of sickness must be specified. To this end, we used the MISC rate and the drop-out rate. The MISC rate is defined as the MISC rating at the end of motion exposure, divided by the time in minutes to this end. Whereas, the drop-out rate is simply defined as the percentage of participants that have prematurely terminated a motion exposure.

#### 3.3.6. SICKNESS MODEL

The sickness accumulation model in this study is the Oman (1990a) model shown in Figure 3.2. Here, the input to the model is the magnitude of the rectified sensory-expectancy conflict. In advanced sensory integration models, the sensory conflict is a product of the state estimation/motion perception process (Clark et al., 2019; Wada, 2021). In this experiment, the motions encountered were simple fore-aft accelerations and the sensory conflict was therefore assumed to be proportional to the acceleration stimulus itself.

The output of the model is a generic sickness level, which may be quantified with a sickness rating scale such as the MISC. In the model, there is a 'fast' path and a 'slow' path. The fast path is given by a repeated root second-order system with a time constant  $\beta_1$ . The slow path is given by a repeated root second-order system with a time constant  $\beta_2$ . The slow path controls the gain on the fast path. The existence of the two paths, rather than one standard path as in the subjective vertical model (SVM), enables Oman (1990a)'s model to describe the phenomenon of hypersensitivity.

The original form of the Oman model has an output scaling ( $u^{p_o}$ ), where the sum of the fast and slow paths are raised to the power of 2 ( $p_o = 2$ ), a choice which has, to the best of our knowledge, not been validated. An alternative is an input scaling, which represents a direct sensitivity relationship between sensory-expectancy conflict and motion sickness at the input level, as proposed in Bos and Bles (1998). In this study, both input and output scaling were explored, but as output scaling provided

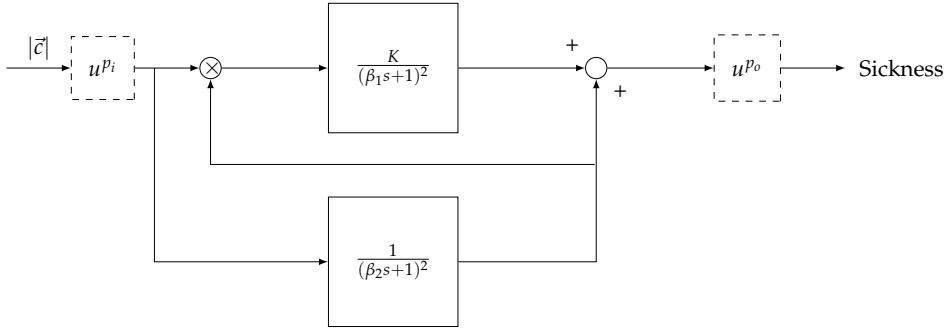


**Fig. 3.2** Oman's model of motion sickness development in time. The rectified conflict signal  $|c|$  is fed in to the model. There is a fast (upper) path and a slow (lower) path. The slow path multiplies with the conflict as the gain of the fast path. Both systems are second order with repeated poles. The fast and slow path are then summed. The model has either an input power scaling or an output power scaling given by  $u^{p_i}$  and  $u^{p_o}$ , respectively

a better fit to the data, this is the model form reported in the results. Nevertheless, we discuss the effect of input and output scaling in the discussion section.

All poles of the Oman model are negative, meaning it has a stable response that eventually converges to a steady-state level of sickness  $MISC_{ss}$ . For a step input of amplitude  $A$ , the effect of output scaling on the model output, is given by the equation

$$MISC_{ss} = (KA^2 + A)^{p_o} \quad (3.1)$$

where  $K$  is the gain of the fast path and  $p_o$  is the output power scaling of the conflict amplitude.

### ERROR METRIC

The formulation of the Oman model considered in this study has four parameters. These are the fast and slow path time constants  $\beta_1$ ,  $\beta_2$ , the gain  $K$  and the output power scaling exponent  $p_o$ .

The error metric used for the optimisation was the mean absolute error (MAE), which is given by the equation:

$$MAE = \frac{\sum_{t=1}^n |F_t - A_t|}{n} \quad (3.2)$$

For each iteration of the optimisation an error is calculated using the predicted MISC ratings  $F_t$  and the measured  $A_t$  ratings. The MAE is not scaled, this means it fits the higher MISC ratings more faithfully than the lower scores. Moreover, it is easy to interpret, as the MAE directly quantifies the average absolute deviation from the observation.

### OPTIMISATION PROCEDURE

Three variations of Oman's model were fitted to the individual participants' data:

1. **Session Fit, Unit Power:** As a baseline for how well the model could feasibly fit the sickness profile, but also to assess how the model parameters may vary between conditions, each session was fitted separately. This means that the time constants  $\beta_1$ ,  $\beta_2$  and the gain  $K$  were fitted for each individual session, and thus stimulus amplitude. The power was assumed to be unity, i.e.,  $p_0 = 1$ , and fixed for all fittings. The optimisation was performed using the MATLAB `fmincon` function. Due to the presence of local minima, this was done using 10 multi-starts.
2. **Joint Fit, Individual-level Power:** The first model does not have a generalisable amplitude relationship from which one can make predictions across acceleration levels. For this reason, the sickness to amplitude relationship is assumed to be an idiosyncratic property of the individual, and so another model was fitted where the power law term was allowed to vary between participants. The fits were done jointly for all conditions for a given individual, meaning that both the time constants ( $\beta_1$  and  $\beta_2$ ), the gain ( $K$ ) and the power law ( $p_0$ ) terms did not vary within an individual between the different conditions, but did vary between individuals. The optimisation was performed using `fmincon` with 10 multi-starts.
3. **Joint Fit, Group-level Power:** To assess whether an individual power law was needed to adequately capture the sickness observations, or whether a group-level power law metric is sufficient, the model was fitted with a power law  $p_0$  term that was fixed between participants. The fits were done jointly for all conditions for a given individual, meaning that both the time constants ( $\beta_1$  and  $\beta_2$ ) and the gain ( $K$ ) did not vary within an individual between the conditions. The optimisation was done using `fmincon` with 10 multi-starts.

#### 3.3.7. STATISTICAL ANALYSIS

##### AICc

Models with more free parameters generally give better fits to experimental data. To assess the significance of such additional model parameters, we used the corrected Akaike Information Criterion (AICc). This is a measure of model fit that is based on the likelihood of the data given the model, whilst including a penalty term for the number of parameters. It is a corrected form of the AIC where the parameter penalty scales quadratically, but approaches the AIC when the number of observations,  $n$  is many times larger than  $k^2$ . [Fabozzi et al. \(2014\)](#) explains how to interpret the absolute value of differences in the AICc between the models, in terms of strength of evidence. According to these rules of thumb, absolute differences in the indices 2, 6, and 10 provide positive, strong, and decisive evidence, respectively, in favour of the model with a lower AICc value.

##### FRIEDMAN TEST

As our metrics do not satisfy the assumptions required for parametric testing, the Friedman test was used for statistical comparisons between different amplitude conditions. The Friedman test is a non-parametric test analogous to the parametric



repeated-measures ANOVA. The significance level is reported in much the same way as in an ANOVA, where a p-value that is less or equal to 0.05 is taken as indication of a statistically significant result.

#### LOGRANK TEST

Logrank test is a hypothesis test used to compare the survival distribution of two samples. In this study, it was used to compute a pairwise comparison between the termination curves of different motion conditions.

## 3.4. RESULTS

### 3.4.1. GROUP-LEVEL OBSERVATIONS

The experiment proved to be very sickening. Figure 4.1 shows the group-level results for all 17 participants over the first 60-minute motion exposure. The dropout rate for all four conditions is shown in Figure 3.3a and was high, whereby the three highest amplitudes – 2.5, 2.0, and 1.5 ms<sup>-2</sup> – had similar dropout rates after 60 minutes of approximately 94%. The lowest amplitude setting had an appreciably lower dropout rate of 64.7%. Using a logrank test between the amplitudes 1 and 1.5 ms<sup>-2</sup>, 1.5 and 2 ms<sup>-2</sup>, and 2 and 2.5 ms<sup>-2</sup>, a significant increase in drop-out was found between the survival curves of 1 and 1.5 ms<sup>-2</sup> (Bonferroni corrected  $p = 0.0047$ ), 1.5 and 2 ms<sup>-2</sup> ( $p = 0.0107$ ), but not between 2 and 2.5 ms<sup>-2</sup> ( $p = 0.473$ ). The hazard ratios were 1.64, 1.56 and 1.25, respectively, indicating a monotonic increase in the probability of dropout with increasing acceleration amplitude.

In this experiment, the most discriminative measure of how sickening a certain stimulus was given by the MISC rate. Figure 3.3b shows a monotonically increasing MISC rate on average across the group of participants (for the individual MISC rates of all participants, see Figure A.1 in Appendix A). This monotonicity is further supported by the fact that a linear model provides a significantly better fit to the MISC rate data than a constant (intercept-only) model (AICc = -1.92 vs AICc = 29.4).

Figure 3.4 shows a more detailed breakdown of time to reach each a certain MISC rating, where the left-most lightest coloured bar graph for each condition is for a MISC of 1 and the right-most darkest colour is 6, for all tested amplitude conditions. Both data for the first (shade of blue) and the second motion exposure (shade of red) are presented. Figure 3.4 again shows that with increasing amplitude, there is a decrease in the time it took to reach a certain MISC level. Furthermore, the presence of motion sickness hypersensitivity is observed during the second motion exposure, shown in the yellow to orange coloured bars, where time to a certain MISC rating is reduced by 61% on average compared to the first exposure.

### 3.4.2. OMAN MODEL

As motivated in Section 3.3.6, three model variations were evaluated: the Session Fit Unit Power, Joint Fit Group-level power and Joint Fit Individual-level Power. The results for these cases are presented separately in this section.

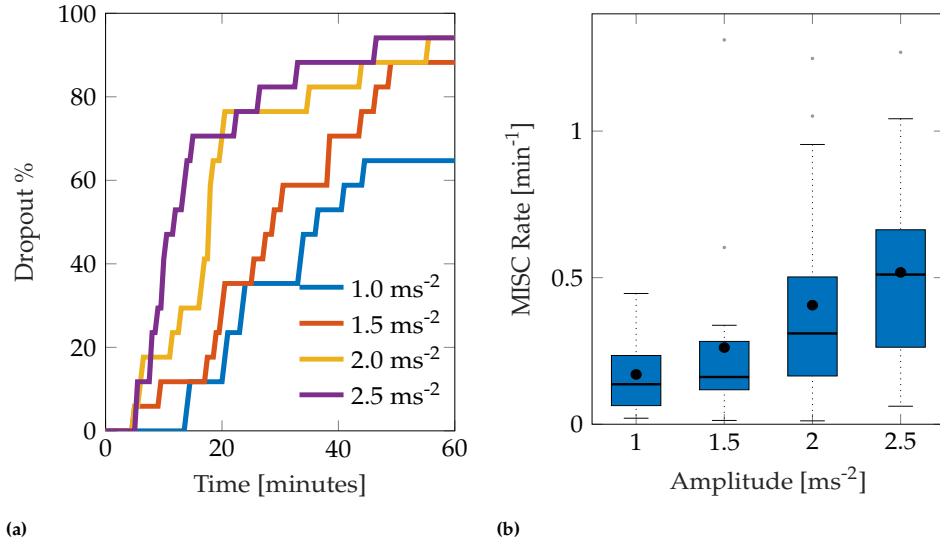


**Fig. 3.3** Main group-averaged results for the first motion exposure. (a) indicates the early termination rate where participants reached a MISC level of 6 prior to the 60-minute mark in first motion exposure. (b) shows the median MISC Rate (as solid black line inside blue shaded box) the mean MISC Rate (black circle) and the 25th and 75th percentiles (bounds of the box)

### SESSION FIT, UNIT POWER

For the Session Fit, Unit Power case, the Oman model is fitted to all amplitude conditions individually for each participant, as also done in [Irmak et al. \(2020\)](#). Figure 3.5 shows Box plots of the fitting errors (MAE), the gains, and the long and short time constants for each amplitude condition.

A Friedman test shows significant differences in the MAE, with an average of 0.54, ( $\chi^2 = 9.15$ ,  $df = 3$ ,  $p = 0.027$ ) across motion amplitude conditions, meaning there is a significant difference between model fitting accuracy across the different amplitude conditions. A post-hoc test, however, shows no significant difference between any set of individual amplitude conditions. On average,  $E_{joint}$  is 0.94 (STD = 0.29).

Figure 3.5 shows a significant downward trend in the gain of the model with increasing amplitude ( $\chi^2 = 12.8$ ,  $df = 3$ ,  $p = 0.005$ ). There were no significant differences in either the fast nor the slow path time constants across the amplitude conditions ( $\chi^2 = 4.05$ ,  $df = 3$ ,  $p = 0.26$  and  $\chi^2 = 1.43$ ,  $df = 3$ ,  $p = 0.7$ , respectively). On average,  $\beta_1$  and  $\beta_2$  had median values of 73.6 s and 510.4 s, respectively. The implication of this is that the fast and slow path time constants are seen to be acceleration amplitude invariant and can thus be considered a constant property of each individual.



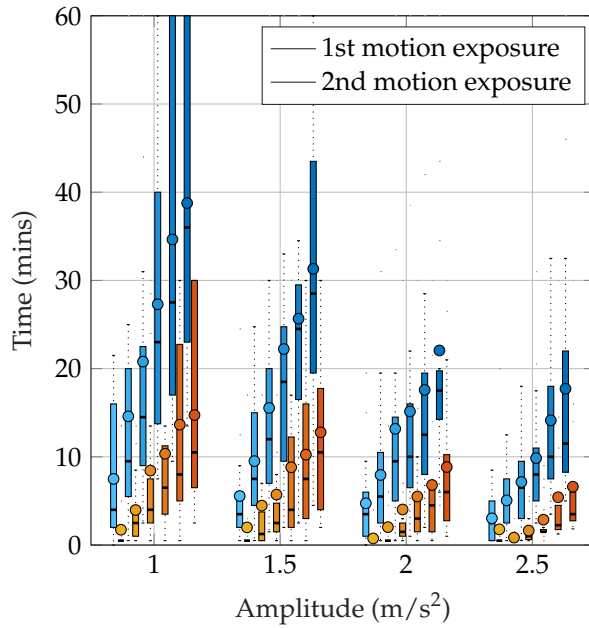


**Fig. 3.4** Time to reach a certain MISC level as a function of amplitude during the first and the second motion exposures, given by the blue and orange-shaded bars, respectively. The darker shades correspond to increasing MISC levels.

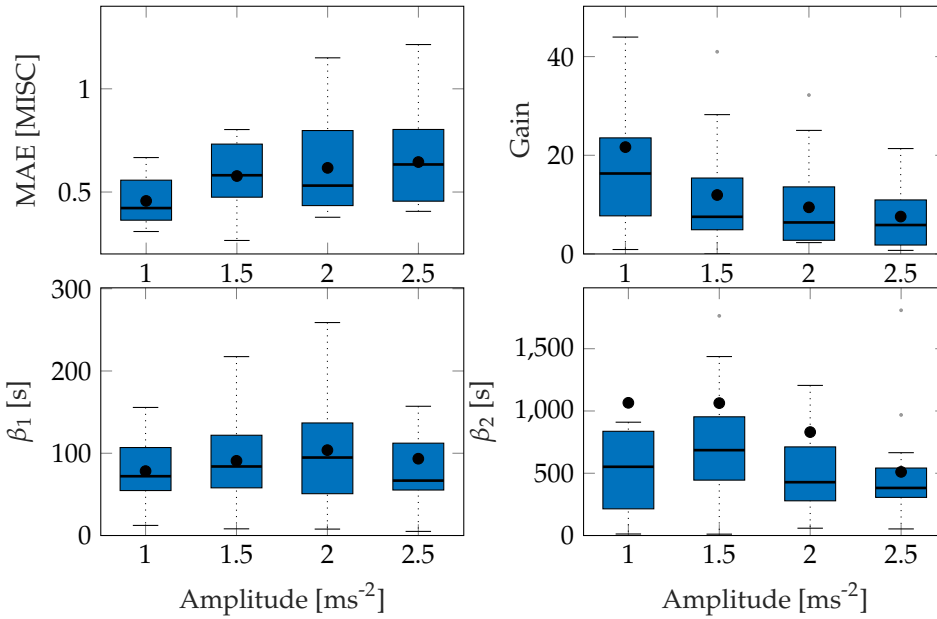


Fig. 3.5 Box plots showing the mean absolute error, the gain and the two time constants of the Session Fit, Unit Power model variation. The Box plot is in standard form, with the centre black line indicating the median and the sides of the box indicating the quartiles

### JOINT FIT, INDIVIDUAL-LEVEL POWER

The Session Fit shows that the gains change as a function of input amplitude, whereas the time constants may be fixed. To get a single set of parameters (rather than amplitude dependent gains) that will predict across all amplitudes, the model requires an *output power-law* scaling. In the Joint Fit, Individual-level Power model variation, the dynamics of sickness with respect to input amplitude are given by allowing this output power scaling  $p_o$ , to freely vary between individuals. This means that the amplitude sensitivity, just like both the gains and the time constants, is modelled as an idiosyncratic property unique to the individual.

For this model variation, the joint error  $E_{joint}$  was 1.01 (STD = 0.23), this is only marginally above the 0.94 of the Session Fit model variation (which is clear from the time domain plots shown in Figure 4.8), indicating that the model simplification from 12 to 4 parameters was successful.

### JOINT FIT, GROUP-LEVEL POWER

In the previous model form, an individual power term was used. This power term can be fixed such that only three individual parameters are required to describe the motion sickness response, rather than four.

Figure 3.6 shows the variation in the joint error term  $E_{joint}$  as a function of the output power scaling, which was fixed for the whole population. It can be seen that

the error term is minimised to 1.028 (STD = 0.23) when the output power scaling  $p_o$  is 0.4. The medians of the other Oman model parameters for output power scaling were 66.2 s and 502.4 s for the fast and the slow path time constants ( $\beta_1$  and  $\beta_2$ ), respectively, and 70.8 for the gain ( $K$ ). Using the output scaling of 2 proposed by Oman (1982) led to an error of 2.54, higher than the minimum we find using an output scaling of 0.4.

Contrary to previous findings by Irmak et al. (2020), there was no correlation between the fast and slow time constants ( $r = 0.074$ ). This may be explained by the fact that we tested multiple amplitudes rather than one in the current study, fitting all concurrently with an associated output-scaling term. This may have reduced any potential correlation between the two time constants. A second factor may be that the previous finding was a spurious correlation, which this study was not able to replicate. This is plausible because the two time constants in fact represent different classes of responses, hormonal and neural (Oman, 1982). These are likely to be independent and uncorrelated processes.

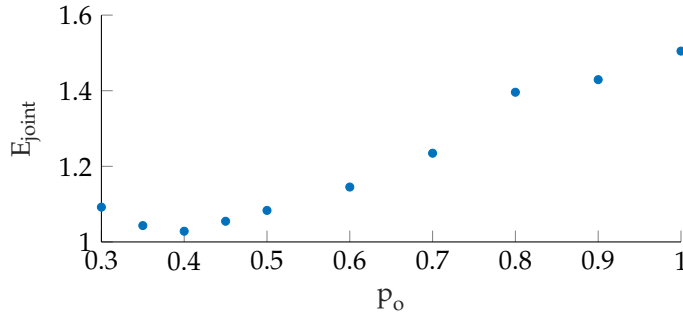


**Fig. 3.6** The error term  $E_{joint}$  with respect to the output power scaling, which is taken to be constant between participants. The lowest  $E_{joint}$  occurs when power is equal to 0.4.

By setting  $p_o = 0.4$  in equation 5.1, the relationship between the conflict magnitude and the predicted sickness output of the model is given by:

$$MISC_{ss} = (KA^2 + A)^{0.4} \quad (3.3)$$

$K$  is the Oman model gain and is usually large with a median value of 70.8. This means that the steady state sickness value predicted by the model has an approximately linear relationship to input motion amplitude  $MISC_{ss} \approx K^{0.4} A^{0.8}$

### FITTING COMPARISON

The three variations of the model evaluated each have a joint error  $E_{joint}$  for each participant. These model errors (shown in Table 3.1) can be compared using the Friedman Test across models to evaluate whether their fit quality differs significantly. Doing so, the three tested models were found to differ significantly from each other ( $\chi^2 = 6.14$ ,  $df = 3$ ,  $p = 0.046$ ) but this difference was marginal and indeed pairwise testing revealed no significant differences.

### 3.4. RESULTS

Figure 4.8 shows a representative sample of fittings for the three model variations for participants 11, 12, 13 and 14 (for the data of all participants, see Figure S2 in the Supplementary Material). It is clear that there is little difference between the three model variations. It can therefore be concluded that individuals have time constants that are invariant of the motion amplitude, and that an output scaling of 0.4 allows the model to fit across multiple amplitude conditions just as well as fitting to a single session. This means that the 3 parameter model with the output power fixed across participants, but the gain and the time constants allowed to vary at the individual level offers a good compromise between fitting performance and model complexity.

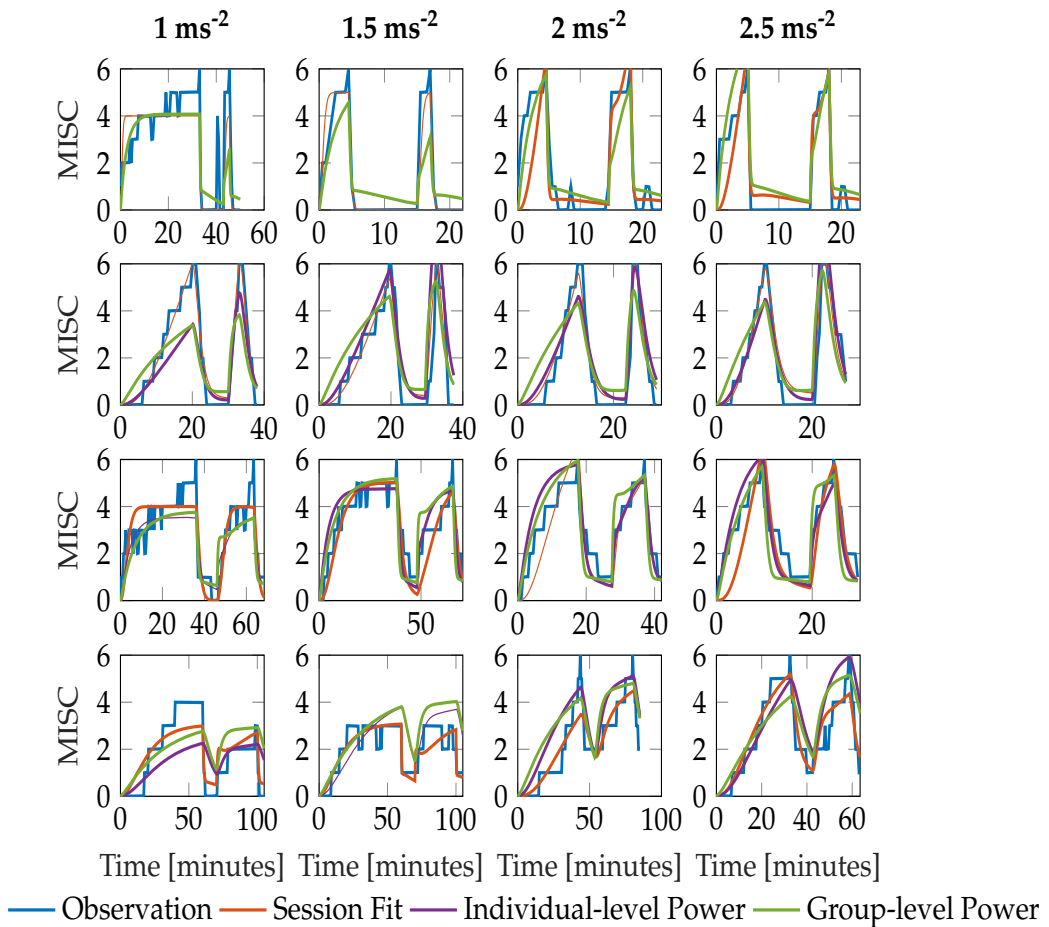


**Fig. 3.7** Representative sample of fittings for the three model variations for participants 11, 12, 13 and 14. The columns show responses for each amplitude condition, increasing in magnitude from left to right. The rows show results for each participant

**Table 3.1** Summary of fitting results, with the error averaged over participants  $E_{joint}$ , the standard deviation over participants in the MAE, and the number of parameters for each model variation

Model Variation	Average $E_{joint}$	STD	# Parameters
Session Fitting, No Power	0.94	0.29	12
Joint Fitting, Individual-level Power	1.01	0.23	4
Joint Fitting, Group-level Power	1.03	0.23	3

### 3.4.3. AMPLITUDE CROSS VALIDATION

Evaluation of model variations so far was with respect to how well they could fit the data. However, for a predictive model, it is also important to identify the capacity for generalising to conditions not explicitly fitted to. We therefore performed cross-validation of the model between the different amplitude conditions. To do this, we looked at the mean MAE when we fitted to one, two and three conditions whilst predicting three, two and one condition. There were 4 combinations for the 1 fitting case, 6 combinations for the 2 fitting case and 4 combinations for the 3 fitting case, leading to 14 cross-validation data sets.

Figure 3.8 shows a Box plot of the mean absolute prediction errors for the procedure described above. Both models with an individual-level and a group-level power term variations show decreasing prediction errors with the number of conditions fitted. The group-level power model with  $p_o = 0.4$  has overall a lower prediction error than the individual-level power model (Friedman test,  $\chi^2 = 12.3$ ,  $p = 0.001$ ,  $df = 1$ ), particularly for when fitting to data from only 1 amplitude condition.

Importantly, the group-level power on average has a fitting MAE of 0.90, which is close to the average prediction error of 1.15 after fitting only one condition. This indicates a high degree of regularity in the amplitude response that can be predicted by a power law of 0.4, and one that cannot be captured by the individual-level power model without larger amounts of data.

### 3.4.4. SICKNESS FORECASTING

One of the properties of an effective predictive model is its ability to forecast future development of the modeled system's states. In this section, we evaluate this forecasting ability of the Oman model.

Figure 3.9 shows the first motion phase responses of participants 11-14, where the rows represent the different participants and the columns the different amplitude conditions (for the data of all participants, see Figure S3 in the Supplementary Material). In our experiment, participants 10, 11, 14 and 17 vomited or retched (MISC 10 and 9, respectively) very shortly after (<30 s) reaching a MISC level of 6. Because this occurred very shortly after reaching 6, in Sections 3.4.2 and 3.4.3, a MISC of 6 was taken as the end point of the experiment data used for fitting. In Figure 3.9 the full MISC trajectories are shown (blue lines), which for participants 11, 12, and 14 show a region of stable growth until a MISC of 6, then a blow-up to vomiting, as similarly reported in the results of Graybiel (1969).

This phenomenon cannot be captured by the Oman model, which, as noted before in section 3.3.6, converges in a stable manner to a final sickness level that may

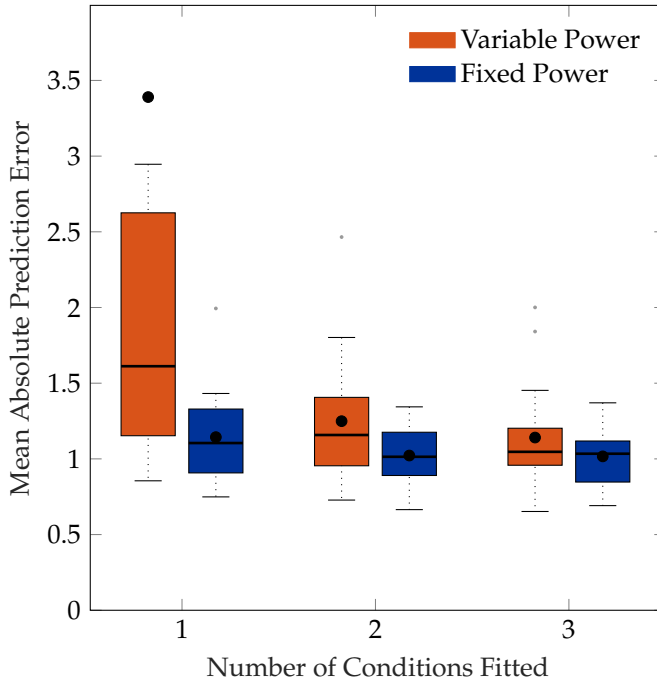


Fig. 3.8 Box plot showing the mean absolute prediction errors for when 1, 2 and 3 cases are fitted to predict 3, 2 and 1 other conditions, respectively. The orange Box plots show prediction errors for the individual-level power law, and the blue Box plots show the prediction errors for the power law fixed to 0.4.

be higher than 10. Predicting such high levels of sickness may not be a concern for most practical applications, for which the aim generally is to keep sickness at the lower MISC levels. Figure 3.9 shows Oman model predictions (in orange) when the model is fitted to all data up to a MISC value of 3 (blue shaded ranges) and sickness is then forecasted until the end of the experiment. It can be seen that this extrapolation from lower MISC levels in to the future for some participants suffers from premature convergence (e.g., participant 11 in Figure 3.9), where the model captures an initial seeming convergence of the MISC data to a final rating. This effect is explained by the small amount of data provided (only up to and including MISC 3) and the inherently convergent nature of the Oman model.

Overall, it is the diverging sickness trajectories that show the largest forecasting errors, e.g., participants 12 and 14 in Figure 3.9. This can be shown statistically, by fitting a model of the form

$$\text{MISC} = at^b \quad (3.4)$$

as proposed in Irmak et al. (2020), where  $t$  is time since the start of exposure and  $a$ ,  $b$  are model coefficients. The responses that can be described by  $b \geq 1$  have a diverging sickness response with respect to time, whereas those with  $b < 1$  have a converging response. The fitted model had an average coefficient  $b$  of 1.085 (25–75th

percentiles: 1.043–1.448). This means that the MISC is approximately linear with respect to time. When fitting the Oman model using a long fitting window, it can describe both converging and diverging responses equally well. This is despite its natural tendency to converge. This is because for divergent cases, the model estimates a very large steady-state value, meaning that the initial rising part of the response is able to approximate the divergent cases quite well. However, when forecasting from lower MISC levels, using a shorter observation window, it is seen that forecasting performance for divergent cases is significantly worse than forecasting for convergent cases. This can be seen by comparing a constant (intercept-only) and a linear mixed-effect model, relating the power term to the mean absolute error in the forecast region (AICc = 149.0 and 136.9, respectively). With a difference between AICc values 10 [Fabozzi et al. \(2014\)](#), it can be seen that the linear model is significantly better, meaning that the forecasting error increases with increasing divergence of the sickness response. The cause of the suboptimal forecasting is partly due to the model form, which is always stable, but also due to the limited data used for fitting and extrapolating from.

At the individual level, 15 out of 17 participants had MISC responses that were in at least 3 out of 4 conditions either consistently divergent or consistently convergent. The remaining 2 participants showed convergent MISC responses in half of the conditions and divergent responses in the other half. This means that, on average, individuals show a propensity towards one type of motion sickness trajectory. This supports the existence of idiosyncratic differences in the qualitative form of sickness dynamics. We did not find a difference in the power term between the motion conditions ( $\chi^2 = 1.2$ ,  $df = 3$ ,  $p = 0.75$ ). This indicates that the divergent/convergent dynamics is not modulated by differences in the motion amplitude in the range explored in this study.

In our study, the MSSQ was correlated marginally significantly with overall sickness susceptibility ( $\rho = 0.50$   $p = 0.05$ ). The overall sickness susceptibility was quantified by averaging the MISC rates during the first motion exposure of an individual for all amplitude conditions. This finding indicates the usability of the MSSQ for predicting sickness susceptibility and hence as a tool for participant selection. However, a better selection could be made by first perturbing the participants at  $2.5 \text{ ms}^{-2}$  until they reached a MISC of 3 which would on average take 8 minutes. The Oman model may then be used to estimate participants' susceptibility directly. Doing this on the data from the experiment, there is a very strong correlation between the Oman model estimation of susceptibility and the overall sickness susceptibility as computed from the average MISC rate for a participant ( $\rho = 0.72$   $p = 0.002$ ). This level of predictability with respect to actual sickness susceptibility is directly useful in candidate participant screening. A better predictive model would have higher susceptibility discrimination, at even lower MISC levels, requiring less simulator time. Indeed, the correlation between the Oman model forecasting and overall susceptibility is not significant  $\rho = 0.15$  ( $p = 0.58$ ) when data to only MISC of 2 is considered.

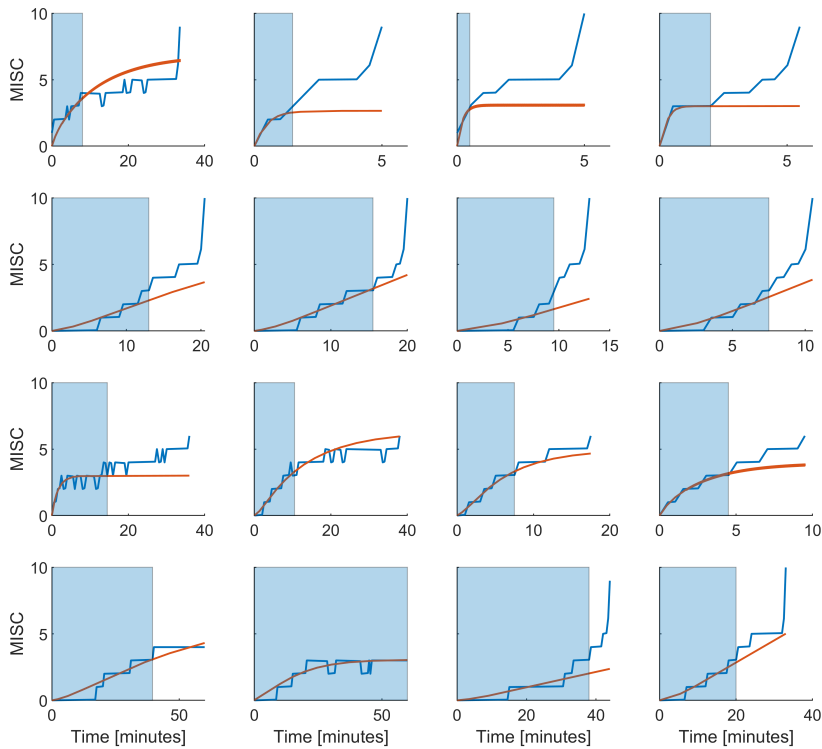


**Fig. 3.9** Representative sample of extrapolations from MISC 3 to the end of the first motion phase, for the Oman model. The columns show responses for each amplitude condition, increasing in magnitude from left to right. The rows show results for participants 11, 12, 13 and 14. The blue shaded area gives the observations the model uses to make forecasts.

### 3.5. DISCUSSION

This study investigated the amplitude and temporal dynamics of motion sickness at both the group and the individual levels. Participants underwent fore-aft sickening motions at four different acceleration amplitudes. Motion sickness development over time was reported using the MISC scale. First, using the dropout percentage and the MISC rate, the group-level response to varying amplitudes was evaluated. Also, three variations of the Oman model of nausea were used to characterize the dynamics of motion sickness at the individual-level. This was done by both fitting observed sickness at different amplitudes, but also by assessing the cross-amplitude validity of the model. Lastly, we investigated how well the Oman model can forecast future sickness based on a shortened measurement of initial sickness development.



### 3.5.1. GROUP-LEVEL OBSERVATIONS

For the group-level response to increasing acceleration amplitudes, *we found a significant increase in sickness severity with increasing acceleration amplitude*, and hence sensory conflict magnitude, on the development of motion sickness. As seen in Figure 4.1, not only was this effect monotonous with respect to the acceleration amplitude, it could also be accurately characterised by a linear relationship, which was shown by comparing a constant mixed-effect model of MISC rate with a linear mixed-effect model (AICc = -1.92 vs. AICc = 29.4).

Previous studies by Griffin and Mills (2002); O'Hanlon and McCauley (1973); Alexander and Wendt (1947) also reported a monotonic increase in sickness with respect to acceleration amplitude. In the study of Griffin and Mills (2002) only low-amplitude motions in the range of 0.4-1.56 ms<sup>-2</sup> were used, and only the last two conditions were significantly higher in sickness severity from the baseline case of no motion. Therefore, a functional relationship between motion amplitude and sickness could not be formulated. The studies by O'Hanlon and McCauley (1973) and Alexander and Wendt (1947) assessed vomiting incidence at the end of their experiments (MSI) and found a log-normal relationship between MSI and acceleration amplitude. However, it would be incorrect to say sickness itself exhibits log-normal behaviour for the range of accelerations used in these studies. Indeed, in our study, we report both the dropout rate and the rate of sickness development. For the dropout rate, which is a similar metric to the MSI, dropout percentages for 2.5 and 2 ms<sup>-2</sup> are not significantly different, whereas MISC rate indicates a linear, rather than a log-normal, relationship between sickness and acceleration amplitude. The data of Lawther and Griffin (1988) suggest that this linear relationship may continue down to the range of 0.1-0.7 ms<sup>-2</sup>, i.e., to lower amplitudes than tested in our experiment. At the lowest acceleration magnitudes, i.e., below 0.1 ms<sup>-2</sup>, experienced sickness did not differ from the stationary case. This apparent 'sickness threshold' is equivalent to reported translational acceleration perception thresholds (Gianna et al., 1996; Heerspink et al., 2005). As remarked previously, acceleration is often used as a proxy for sensory conflict for experiments lacking visual stimuli, and in our current experiment set up the two are assumed to be proportional to each other. Very sickening stimuli, such as the cross-coupled coriolis, which can elicit vomiting in minutes as opposed to 10 minutes as in this study, likely produce much higher sensory conflicts, which may be translated to an equivalent acceleration, indicating that the monotonic amplitude relationship likely holds at even higher accelerations than 2.5 ms<sup>-2</sup>. Approximately 95% of all vehicle accelerations are within the maximum acceleration used in this study (Feng et al., 2017). Therefore, we can conclude that linearity in the sickness response can be an adequate modelling assumption at the group-level for automated vehicles.

With respect to the metrics used to quantify group-level responses, we chose the drop-out rate and MISC rate. The drop-out rate provides an easy to interpret measure of sickness, whilst also allowing us to perform survival analysis. For our experiment, the MISC rate is less directly dependent on our selected termination criteria. It is defined as the MISC rating at the end of motion exposure, divided by the time in minutes to this final value. In the current study, we fitted the model

$at^b$  to all MISC responses; the resulting average value for  $b$  is 1.085 (25–75th percentiles: 1.043–1.448). This means that the MISC is approximately linear with respect to time, increasing monotonously with respect to time, with no long-duration decreases. Therefore, computing the average gradient of the MISC curve, i.e., our MISC rate, is an appropriate parametrisation of the response.

In cases such as naturalistic driving where such monotony is not observed, a model-based approach may be more appropriate. The kind of model used for this purpose is a formal accumulation model, such as the Oman model. This is because in such a scenario, the sickness response will be complex and time-varying, depending on the accelerations encountered. Using traditional ways of parametrising the sickness response will make both within- and between-participant comparison difficult, requiring, in the least, many sessions to average across a representative sample of acceleration exposures. With a model-based approach, the parameters of the fitted model will be invariant with respect to the motions encountered and easier to compare.

#### 3.5.2. INDIVIDUAL-LEVEL MODELLING

In this study, we showed that motion sickness development over time could be accurately modelled at the individual level, for the different tested amplitude conditions separately, with a modified version of Oman's sickness model. We found that the time constants of sickness development were approximately motion amplitude independent, with median time constants of 66.2 s and 502.4 s for the model's 'fast' and 'slow' time constants, respectively. One concern of automotive engineers in utilising the findings of motion sickness studies could be the fact that usually the motions encountered in these studies are aggressive, with the intent of quickly making participants motion sick, whereas motions that lead to motion sickness in vehicles tend to be more gradual and accumulate over the span of up to an hour. In this study, we tested both aggressive motions ( $2.5 \text{ ms}^{-2}$ ) and gentle motions ( $1 \text{ ms}^{-2}$ ). The fact that no difference in the time constants was found implies that the temporal dynamics of motion sickness are amplitude-independent, with only varying scaling factors affecting the final level of sickness. This suggests that the findings of sickness studies, all else equal, can be directly applied to automotive control and design.

In this study, we report only on nonlinear output scaling in Oman's model. However, we also investigated the use of input scaling, see Figure 3.2. The original Oman model has the conflict vector as an input, which is processed by the two paths, whose outputs are then summed. This summed output is the *latent* sickness. The output power scaling transforms this latent sickness into a subjective magnitude estimate, via an exponential term corresponding to Steven's power law (Stevens, 1946), which maps stimulus intensity to perceived intensity. As employed by Bos and Bles (1998), the reasoning for input scaling is different. Here, the conflict signal itself is assumed to be remapped with a nonlinear scaling (sigmoid), where small sensory conflicts remap to zero and large conflicts are saturated. We approximate this through an input power law. We found that the output power law provided a much better fit to our data, with a mean joint error ( $E_{joint}$ ) of 1.03 compared to 1.4 for the input scaling. As Figure 3.6 shows that with output scaling for all powers up to 0.8 the joint fitting

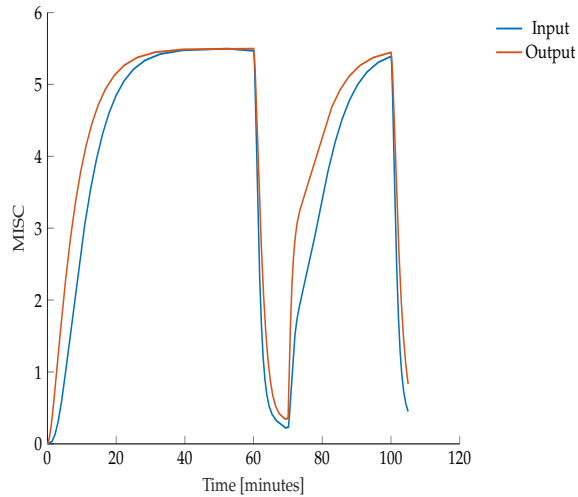


**Fig. 3.10** Example showing the effect of input (blue line) and output (orange line) power scaling on the predictions of the Oman model for constant amplitude input

error is below this optimum result for input scaling, we conclude that output scaling on the modelled latent sickness metric is superior for our experiment data.

While both with input and with output scaling Oman’s model can model convergence to an identical final steady-state sickness level (with adapted gain and power law exponent), see Figure 3.10, this will always result in differences in the temporal dynamics. In these example model responses, the input and output power scaling, as well as the short and long time constants, are all the same, while the model gain is adjusted such that both modelled responses converge to the same steady-state sickness. Regardless, it can be seen that for constant amplitude stimuli, the output scaling responds faster to the input, particularly in the hypersensitivity phase. This is because the output of the slow and fast paths accumulate more slowly when the input signal strength is reduced by an input scaling, than when it is not. The reason why this steeper increase may better represent our data is that the MISC is on an ordinal scale. Participants are likely to spend less time at the lower ends of the MISC scale, which represent smaller increments on a scale of subjective discomfort (de Winkel et al., 2022), than the higher end of the MISC scale. This is particularly relevant for the hypersensitivity phase.

As shown in Figure 3.6, an output scaling of 0.4 provided the best fit to our dataset. The power of 0.4 approximately linearises the conflict to sickness relationship, where for large values of  $K$ , equation 5.5 reduces to  $MISC_{ss} \approx K^{0.4} A^{0.8}$ . Likewise, for the input scaling this optimal power was found to be similar, i.e., 0.5. This value fully linearises the conflict to sickness relationship. This means that irrespective of the scale used to measure sickness the Oman model, or any other model of sickness accumulation, should have a power-law relationship that enforces linearity, whereby only the gain of the system is expected to change depending on the rat-

ing scale used. Finding the system gain for the different rating scales would greatly contribute to comparing and generalising the findings of different motion sickness experiments.

For the first time, this study evaluated forecasting/predicting sickness at the level of the individual, based on a short duration of initial sickness data (MISC3). The development of sickness over time in the first motion exposure could be predicted accurately, with a MAE of 0.93. In our previous work (Irmak et al., 2020), we identified two groups of participants by fitting a power law to measured MISC as a function of time (see equation 5.6). The participants for whom the exponent  $b \geq 1$  were classified as *divergent* and those with  $b < 1$  were classified as *convergent*. In that study, the Oman model was able to fit both groups equally well, which cast doubt on whether these two groups were indeed qualitatively different. However, in the present study we found that the Oman model had significantly higher accuracy when *predicting* convergent, as compared to divergent cases, thus supporting the notion that MISC trajectories are indeed qualitatively different between individuals.

One notable property of the Oman model that affects forecasting of future motion sickness is that it is always stably convergent. That is, there is a steady-state sickness value  $MISC_{ss}$  that it will converge to as time tends to infinity. This means that if the participant has converging dynamics, and sickness is observed until a MISC of 3, the model will predict a convergence to approximately a MISC of 3. However, it is known from the data that this is not the case, and that participants likely continue to become more sick, especially if they have reached moderate sickness relatively quickly. A striking example of this issue is shown in Figure 3.9 for the first participant. Here, the observations indicate convergent dynamics, even though the participant reaches a MISC of 4 in under 4 minutes. This participant will inevitably vomit in finite time. The model, however, cannot account for this. Moreover, some participants (such as the first participant of Figure 3.9) show convergent sickness behaviour at first, followed by a sudden increase towards vomiting. There can be multiple reasons for this. One explanation is that the participants use the MISC scale as a subjective discomfort scale, and that for these participants, a MISC of 6, which was the termination criterion in this study, was seen as the point after which they could not continue because they would otherwise vomit. Alternatively, it can also be that these participants experienced an unstable "avalanche" of symptoms. Such an effect has been reported in literature (Graybiel, 1969; Bock and Oman, 1982). To account for both the stable and unstable behaviour seen in motion sickness responses, the next step should be to model the dynamics of sickness as a *bistable* system. In this, participants may have two equilibrium points. One that is at a level of sickness below 10, depending on motion amplitude, and the other at a MISC level of 10. Modeling this requires higher degree non-linear differential equations than included in Oman's model.

Sickness forecasting as demonstrated in this paper is not only a theoretical exercise, but has methodological implications for both motion sickness studies and applications such as the individualisation of automated driving algorithms. In this study, we showed that using the Oman model and a short duration perturbation at the highest amplitude, one can reliably predict the overall motion sickness sus-

ceptibility of an individual. Such a paradigm can be used as a screening method for ensuring participants of similar sickness susceptibilities are enrolled in to motion sickness studies. This would for instance increase the power of studies comparing different mitigation methods. Moreover, such a method provides a basis for individualised and online sickness-mitigating adaptive tuning of automated driving algorithms.

Well-known models of motion sickness development contain two components, being 1) Conflict models predicting conflicts resulting from sensory integration, and 2) Accumulation models predicting motion sickness development in time. One example of a motion sickness model is the subjective vertical conflict (SVC) model (Bos and Bles, 1998; Wada, 2021). The conflict generation part of the model is based on the difference between the sensed vertical and the subjective vertical, which is thought to drive motion sickness. It is a specific implementation of the idea of sensory-expectancy conflict put forth by Oman (1982). Conflict models are needed to capture sensitivity towards complex motion stimuli, including multiple motion directions and frequencies. The conflict derived in the SVC is then accumulated using a simple second order filter. This accumulation model is less sophisticated than the Oman model used in this study, which is able to describe hypersensitivity.

Our study focuses on motion sickness accumulation in time for a single degree-of-freedom motion stimulus, i.e., a 0.3 Hz sinusoidal fore-aft seat motion. For such a simple stimulus, conflict models degrade to a simple gain, where the exact gain (proportion of fore-aft acceleration that is attributed to the subjective vertical) is dependent on the stimulus frequency and the subjective vertical time constant.

In our approach, this gain is (implicitly) identified in our fitting of Oman's model. Therefore, if the actual sensory conflict would be only 50% of the input motion, then the gain of our fitted model would simply be 50% larger. Thus, our method of using acceleration as the input to Oman's model is, for our specific stimulus, equivalent to the conflict between the sensed and the expected vertical that can be derived from the SVC model.

One important application of this work is that now that the relationship between conflict and the subsequent sickness is known, the system that maps motion inputs to sensory-conflict can be identified by using closed-loop system identification techniques (Qian et al., 2016; Rojas et al., 2007).

#### 3.5.3. LIMITATIONS

As discussed previously, particularly at the lower amplitudes, there might be an amplitude threshold below which people do not experience motion sickness. In this study, the range of the amplitudes studied was between 1 and 2.5 ms<sup>-2</sup>. In future studies, it is essential to also include lower amplitudes to also gain an improved quantitative understanding of motion sickness severity and temporal dynamics for low-amplitude stimuli. In addition to increasing the range of accelerations for which our motion sickness models are effective, experiments that include a high number of different motion amplitudes measured within the same experimental session, as representative of real vehicular transportation, would further help to strengthen motion sickness model validation.

### 3.6. CONCLUSION

---

In the present study, the model successfully described hypersensitivity after a 10-minute break. In a previous study by [Irmak et al. \(2020\)](#) the break duration was until the participant reached a MISC of 2, which only very rarely exceeded 10 minutes. This means that the model can describe hypersensitivity observed after break durations up to 10 minutes. One limitation is therefore the lack of data to verify whether the same modelling accuracy is retained for longer rest durations. Being able to model these longer rest durations may not be relevant for short distance journeys, however, it may be useful for predicting motion sickness during multi-stage long distance travel.

Lastly, it is likely that the amplitude and temporal dynamics found in this study do not depend on the direction of motion. Therefore, pure vertical and lateral motions will likely have similar time constants, gains and output power. This is given by the fact that the severity of sickness in different directions is similar to each other ([Donohew and Griffin, 2004](#)). However, if a coupling exists between different degrees-of-freedom, such that the resultant stimulus has a complex frequency spectrum, this may cause currently unknown interactions in the conflict signal due to differing frequency sensitivities ([Irmak et al., 2021a](#)). Similarly, with reduced motion predictability ([Kuiper et al., 2020](#)) compared to our current sinusoidal acceleration stimuli, a greater sickness response is expected. In these cases, particularly the gains of the accumulation model may need to be calibrated.

### 3.6. CONCLUSION

This study investigated the individual amplitude sensitivity in motion sickness caused by sensory conflicts induced by fore-aft accelerations. At the group-level, we found that sickness severity increases linearly with acceleration amplitude between 1-2.5  $\text{ms}^{-2}$  and argue that it does so for all relevant acceleration amplitudes in vehicular transport. From fitting a modified version of Oman's model of sickness progression, we found that, at the individual-level, sickness on average increased linearly with acceleration amplitude, even though some participants exhibit higher or lower order amplitude sensitivities. Importantly, we note that the time constants governing motion sickness development vary between individuals, but are independent of the acceleration amplitude. Furthermore, our data shows that a group-level fixed output scaling with an exponent of 0.4 enables Oman's model to inherently account for stimulus amplitude variations, as considered in our tested amplitude conditions. Lastly, we showed that the Oman model can be used to forecast the temporal evolution of sickness beyond a brief observed initial exposure. In this we found that forecasting works better for convergent, rather than divergent responses, this is largely due to the inherently convergent dynamics of the model. Overall, these findings enable improved modelling of motion sickness accumulation in mixed acceleration environments, such as traffic, and better participant prescreening for motion sickness experiments, as well as tuning of automated driving algorithms for individual passengers.



# 4

## INDIVIDUAL MOTION PERCEPTION PARAMETERS AND MOTION SICKNESS FREQUENCY SENSITIVITY IN FORE-AFT MOTION

---

This chapter has been published as: Tugrul Irmak, Ksander N. de Winkel, Daan M. Pool, Heinrich H. Bühlhoff, Riender Happee, *Individual motion perception parameters and motion sickness frequency sensitivity in fore-aft motion*, *Experimental Brain Research*, 239, 1727–1745 (2021). <https://doi.org/10.1007/s00221-021-06093-w>



## 4.1. ABSTRACT

*Previous literature suggests a relationship between individual characteristics of motion perception and the peak frequency of motion sickness sensitivity. Here, we used well-established paradigms to relate motion perception and motion sickness on an individual level.*

*We recruited 23 participants to complete a two-part experiment. In the first part, we determined individual velocity storage time constants from perceived rotation in response to Earth Vertical Axis Rotation (EVAR) and subjective vertical time constants from perceived tilt in response to centrifugation. The cross-over frequency for resolution of the gravito-inertial ambiguity was derived from our data using the Multi Sensory Observer Model (MSOM). In the second part of the experiment, we determined individual motion sickness frequency responses. Participants were exposed to 30-minute sinusoidal fore-aft motions at frequencies of 0.15, 0.2, 0.3, 0.4 and 0.5 Hz, with a peak amplitude of 2 m/s<sup>2</sup> in five separate sessions, approximately one week apart. Sickness responses were recorded using both the MIsery SCALE (MISC) with 30 s intervals, and the Motion Sickness Assessment Questionnaire (MSAQ) at the end of the motion exposure.*

*The average velocity storage and subjective vertical time constants were 17.2 s (STD = 6.8 s) and 9.2 s (STD = 7.17 s). The average cross-over frequency was 0.21 Hz (STD = 0.10 Hz). At the group level, there was no significant effect of frequency on motion sickness. However, considerable individual variability was observed in frequency sensitivities, with some participants being particularly sensitive to the lowest frequencies, whereas others were most sensitive to intermediate or higher frequencies. The frequency of peak sensitivity did not correlate with the velocity storage time constant ( $r = 0.32$ ,  $p = 0.26$ ) or the subjective vertical time constant ( $r = -0.37$ ,  $p = 0.29$ ). Our prediction of a significant correlation between cross-over frequency and frequency sensitivity was not confirmed ( $r = 0.26$ ,  $p = 0.44$ ). However, we did observe a strong positive correlation between the subjective vertical time constant and general motion sickness sensitivity ( $r = 0.74$ ,  $p = 0.0006$ ).*

*We conclude that frequency sensitivity is best considered a property unique to the individual. This has important consequences for existing models of motion sickness, which were fitted to group averaged sensitivities. The correlation between the subjective vertical time constant and motion sickness sensitivity supports the importance of verticality perception during exposure to translational sickness stimuli.*

## 4.2. INTRODUCTION

Motion sickness is a syndrome whereby aggravating body motions trigger autonomic symptoms such as salivation, dizziness, headaches, panting, hot/cold flushes, stomach awareness, nausea and vomiting (Bertolini and Straumann, 2016). Chronic exposure to sickening motions may lead to the sopite syndrome, which is associated with lethargy, fatigue and drowsiness (Matsangas and Mccauley, 2014).

Riccio and Stoffregen (1991) argue that motion sickness is caused by postural instability (known as postural instability theory of motion sickness). Others argue that sickness occurs due to a mismatch between sensed sensory signals and the sensory signals expected by the brain (Bos, 2011) (Sensory Conflict Theory), and that postural instability is a consequence of such mismatch.

[Reason \(1978\)](#) was the first to promote the sensory conflict theory. Here, the predicted sensory signals were hypothesized to originate from an internal model, which takes the form of a neural store. He hypothesised that this conflict leads to adaptation of the internal model and consequently, habituation to the sickening stimuli. [Oman \(1982\)](#) likened this conceptual model to the manner by which a Luenberger Observer (LO) operates. The LO has an internal model of the system (which is composed of both body and environment dynamics) and sensor dynamics. Due to the imperfect and noisy nature of the sensory signals ([Faisal et al., 2008](#); [Nouri and Kar-mali, 2018](#); [Jamali et al., 2013](#)) one cannot use the sensor measurements directly. Instead, the true states of the system must be observed (estimated) by integrating sensory information using an internal model of the system itself. Indeed, there is strong neuronal evidence for the use of internal modelling for state estimation ([Merfeld et al., 1999](#); [Angelaki et al., 2004](#); [Laurens et al., 2013](#); [Oman and Cullen E. Kathleen, 2015](#)). These estimated states are then used for task planning and execution. To quantify estimation accuracy, the central state estimates are passed through the internal model of sensory dynamics and compared with the actual sensory signals. The resulting error is the estimation error, or the sensory-expectancy conflict. This conflict is used to drive the estimated body motions towards the true state, and to adapt the parameters of the internal model, such that it provides better estimates. It is hypothesized that the conflict is integrated and the subsequent symptoms of motion sickness are due to its accumulation ([Dai et al., 2010](#)).

Therefore, based on the strong neuronal support for internal modelling, the scope of this chapter will not cover postural instability theory nor attempt to evaluate postural precursors to motion sickness, instead, we aim to build on the concepts of state estimation and sensory conflict.

The form this state estimation model needs to take to make accurate predictions of motion sickness is not clear. If the human state estimation process is indeed linked to motion sickness, one would expect to see a clear relationship between certain parameters of state estimation and motion sickness. State estimation is a latent process and cannot be directly measured. Instead, one may measure its correlates in reflexive actions, such as eye movements elicited by the vestibular-ocular reflex (VOR) or through perceived motions such as angular velocity, linear displacement and orientation, as reported subjectively by human participants ([Merfeld et al., 2005a](#)). From such correlates, simple individual-specific parameters can be derived such as the velocity storage time constant and the subjective vertical time constant. These parameters characterize motion perception and reveal key aspects of an individual's state estimation process. Here, the velocity storage time constant is indicative of how the individual computes ego-angular velocity ([Bertolini et al., 2011a](#)) and the subjective vertical time constant provides a measure of the frequency characteristics of tilt and translation perception.

Several studies investigated the relationship between individual motion perception parameters and motion sickness susceptibility. [Dai et al. \(2003, 2007\)](#) used a cross-coupled motion paradigm where participants were requested to roll their head about the naso-occipital axis whilst being rotated in yaw. The number of head rotations a participant could tolerate was negatively correlated with the velocity storage

time constant ( $r = -0.94$ ). In addition, as the participants followed a habituation protocol, there was a significant reduction in the velocity storage time constant, in tandem with an increase in the number of tolerable head movements (Dai et al., 2003).

Relatedly, Clément et al. (2001) used the cross-coupled motion paradigm, this time with pitching motion about the interaural axis of the head. They found that during habituation to the sickening motion, there was again a significant decrease in the duration of the post-rotary nystagmus (and consequently in the velocity storage time constant), as well as in motion sickness. In a similar experiment, Clément et al. (2007) found that the velocity storage time constant reduced by 22.7% with habituation. Likewise, Bos et al. (2002) found that subjects highly susceptible to motion sickness showed a slower decay of nystagmus, thus a longer velocity storage time constant, with a larger peak velocity than less susceptible subjects.

Though there seems to be converging evidence of a strong relationship between the velocity storage time constant and motion sickness sensitivity, Quarck et al. (2000) found no significant differences between the velocity storage time constant of sickness susceptible and non-susceptible participants. Likewise, Tanguy et al. (2008) found no difference in the velocity storage time constant between figure skaters (who were significantly less susceptible to motion sickness) and controls.

It is important to note that the nauseogenic stimulus in both Quarck et al. (2000) and Tanguy et al. (2008) was off-vertical axis rotation (OVAR), which is different from the cross-coupled stimulation employed in the former studies. Here, as during constant rotation about the body axis, the semi-circular canal stimulation reduces to zero. The effect of angular velocity perception on sickness sensitivity should therefore be much lower in this motion paradigm.

The potential cause of sickness in OVAR was investigated by Wood (2002). Here, it was noted that the modulation of the torsional and horizontal components of eye velocity, indicative of tilt and translation, respectively, crossed over at approximately the region where Denise et al. (1996) measured peak sickness during OVAR, which was approximately at 0.3 Hz for their group of participants. Following on from this study, Wood et al. (2007) measured tilt and translation perception above and below the previously identified cross-over frequency. The cross-over frequency characterises how the central nervous system performs gravito-inertial ambiguity resolution (referred to in some literature as tilt-translation ambiguity resolution). The ambiguity resolution is necessary because the otoliths do not measure inertial acceleration separately from gravity. Instead, due to Einstein's equivalence principle, these are sensed in the form of a combined vector named gravito-inertial acceleration (or specific force). For appropriate actuation of an organisms' effectors, this combined vector must be decomposed into acceleration and gravity. For the OVAR motion paradigm, the central nervous system attempts gravito-inertial ambiguity resolution by employing an internal model which can be effectively seen as high (for translation) and low-pass (for tilt) filtering of the otolith signal. The time constant for tilt perception (referred to as the subjective vertical time constant), determines the cross-over frequency and has been hypothesized to correlate with the peak frequency of sickness (Wood, 2002).

Correlating a single parameter with sickness sensitivity for a single motion paradigm, as in the angular vestibular-ocular reflex (aVOR) time constant studies, may provide misleading conclusions of a general sensitivity effect of this parameter, rather than for example the frequency effect that was found by [Wood \(2002\)](#); [Dai et al. \(2007\)](#); [Denise et al. \(1996\)](#) for OVAR.

From a system identification perspective, the mechanistic relationship between motion perception parameters and sickness, such as through the observer framework as used by [Oman \(1982\)](#) and [Bos and Bles \(1998\)](#), only becomes identifiable when the frequency sensitivity of sickness is measured and correlated with the parameters. [Bos and Bles \(1998\)](#) and [Khalid et al. \(2011a\)](#) attempt to identify such a model of motion sickness by fitting mean perception parameters from literature to group level frequency sensitivity data collected for vertical ([O'Hanlon and McCauley, 1974](#)) and lateral accelerations ([Donohew and Griffin, 2004](#)), respectively. Individuals, however, differ largely from each other in their motion sickness sensitivity ([Lackner, 2014](#)) and likely also differ in their frequency sensitivity to sickness. If this is the case, group average frequency sensitivity may not be the same as individual frequency sensitivity, which may vary substantially between individuals, therefore using group average sensitivity to fit these models may not be correct.

In the present study, we will assess individual variability in the frequency response of motion sickness sensitivity and evaluate the relation with motion perception parameters. We will do this by having participants perform a two-part experiment. In the first part, we will determine the time constant of velocity storage and the subjective vertical for each individual. The former parameter will be evaluated by using an Earth Vertical Axis Rotation (EVAR) motion paradigm. The latter will be evaluated both by computing the time constant of subjective tilt change during centrifugation (not taking into account the effect of yaw present during centrifugation), as well as in a more nuanced manner, by computing the cross-over frequency using the Multi Sensory Observer Model (MSOM) ([Newman, 2009](#); [Newman et al., 2012](#); [Clark et al., 2019](#)). The motions will be generated using the Cyber Motion Simulator at the Max Planck Institute for Biological Cybernetics in Tübingen ([Barnett-Cowan et al., 2012](#)). In the second part of the experiment, we will determine frequency sensitivity to horizontal plane accelerations, just as in [Donohew and Griffin \(2004\)](#), [Golding and Markey \(1996\)](#) and [Golding and Stottt \(1997\)](#), but specifically evaluating the response at the individual level. This will be done on the Max Planck CableRobot simulator ([Miermeister et al., 2016](#)). In subsequent analyses, we will relate the perception parameters obtained in the first part of the experiment to the sickness response observed in the second part of the experiment. Based on the literature, we hypothesize that:

1. Group sensitivity of sickness due to fore-aft acceleration is frequency dependent.
2. Frequency-dependent sickness sensitivity varies substantially between individuals.
3. Individual motion perception parameters are indicators of motion sickness sensitivity:

- a The peak frequency of sickness is expected to increase with lower subjective vertical time constant and higher cross-over frequency;
- b The peak frequency of sickness is expected to correlate with the velocity storage time constant;
- c Overall motion sickness sensitivity is expected to correlate with the subjective vertical time constant, cross-over frequency and the velocity storage time constant.

### 4.3. METHODS

The study was designed to assess whether a relation exists between parameters that describe perception of passive self-motion from vestibular stimulation and motion sickness sensitivity. To this end, we performed a combined set of two experiments, on 1) motion perception and 2) motion sickness sensitivity as a function of frequency.

#### 4.3.1. ETHICS STATEMENT

All participants provided written informed consent prior to participation. The experimental protocol was approved by the ethical committee of the Human Research Ethics Committee of TU Delft, The Netherlands, under application number 1030.

#### 4.3.2. PARTICIPANTS

In total, 23 participants took part in this study (mean age: 26.7 years, STD: 4.1 years, 15 female, 8 male). Participants were compensated for their time at a rate of 10 €/hr, with a 30€ bonus upon completion of all 6 sessions. Due to the incipience of the COVID-19 pandemic (2020), we were forced to stop data collection abruptly. As a consequence, 12 participants completed all 5 sickness sessions; 6 completed 4; 3 completed 3; and 1 completed only 2 sessions. The 23 participants had a mean motion sickness susceptibility questionnaire short form (MSSQ-Short [Golding \(2006\)](#)) score of 16.6 (STD = 10.5), indicating an above average sensitivity, corresponding to the 67<sup>th</sup> percentile. The MSSQ-Short scores were not used in the participant selection process.

#### 4.3.3. APPARATUS

For both experiments a neck-brace was used to limit unwanted head rotations. Participants were also blindfolded by the placement of a hollowed out VR headset over their eyes. A Tobii Pro glasses eye-tracker (Tobii Pro AB, Danderyd, Stockholm, Sweden) was placed within the VR headset.

### PERCEPTION EXPERIMENT

This experiment was performed using the Max Planck Institute's CyberMotion Simulator (CMS, see Figure 4.1a) ([Barnett-Cowan et al., 2012](#)). The CMS is an anthropomorphic robot arm (KUKA Roboter GmbH, Augsburg, Germany, model Robocoaster) at the end of which is a closed cabin within which the participant is seated and secured using a five point harness. During the experiment, participants wore

ear-enclosing headphones that attenuated the rumble noise of the simulator. Continuous communication with the experimenter could be made via the integrated microphone. Perceptual responses were provided by the participant using a custom made pointer device. The pointer device (see Figure 4.1c) consists of a stainless steel rod of approximately 20 cm that is connected through the middle to a rotary potentiometer. The potentiometer is housed in a plastic box that was placed above the right leg of the participant such that it may be actuated by the right hand. The rod could be rotated in the vertical sagittal plane.

### SICKNESS EXPERIMENT

Motion sickness was elicited by fore-aft motions performed on the Max Planck Institute's CableRobot Simulator (CRS, see Figure 4.1b) (Miermeister et al., 2016). The CRS is a cable driven simulator: the cables are attached to a central cabin and actuated by electric motors controlling the extension of the cables. The allowable work space of the cabin is 8 m×4 m×4 m (longitudinal, lateral and vertical in the seating direction). The participant was seated in a racing chair and secured via a five-point harness. An additional safety belt was placed across the lap of the participant. During the experiment, participants wore ear-enclosing headphones with an embedded microphone, which allowed continuous communication. Sickness ratings were queried in 30 s intervals with a 1 kHz beep, and verbal responses were recorded automatically to a computer connected to the microphone.

### 4.3.4. TASK & STIMULI

#### PERCEPTION EXPERIMENT

All participants first took part in the perception experiments. The CMS was used to provide stimuli to estimate motion perception parameters of the velocity storage time constant and the subjective vertical time constant.

Centrifugation was used to determine the subjective vertical time constant. The centrifuge arm was rotated with an angular acceleration as a function of time,  $t$  of the form:  $47.5(-\cos(2\pi ft) + 1)$  deg/s<sup>2</sup>, where  $f = 0.709$ . This lasted for 1.41 s, at which point the centrifuge reached a constant earth vertical rotation velocity of 67 deg/s. Participants were placed with a radial offset of 3.11 m from the centre of centrifuge rotation. They were oriented facing out from the direction of centripetal acceleration. Participants were instructed to align the orientation of the rod to (the pitch of) their perceived vertical (Correia Grácio et al., 2013). As the participants were blindfolded, this was done based on the sense of touch only.

Velocity storage time constants were determined in conditions where the CMS was used to rotate participants around an Earth-vertical axis (EVAR) at 57 deg/s. The angular acceleration was a function of time,  $t$  of the form:  $47.5(-\cos(2\pi ft) + 1)$  deg/s<sup>2</sup>, where  $f = 0.833$ . This lasted for 1.2 s, at which point the rotation reached a velocity of 57 deg/s. Here, participants were instructed to indicate their perceived angular velocity by rotating the rod away from or towards their body, in proportion to the subjectively experienced speed and the direction of their perceived rotation, the displacement of the rod from the vertical for EVAR indicated the speed of the perceived angular velocity, with the anchoring point being the upright position, in-



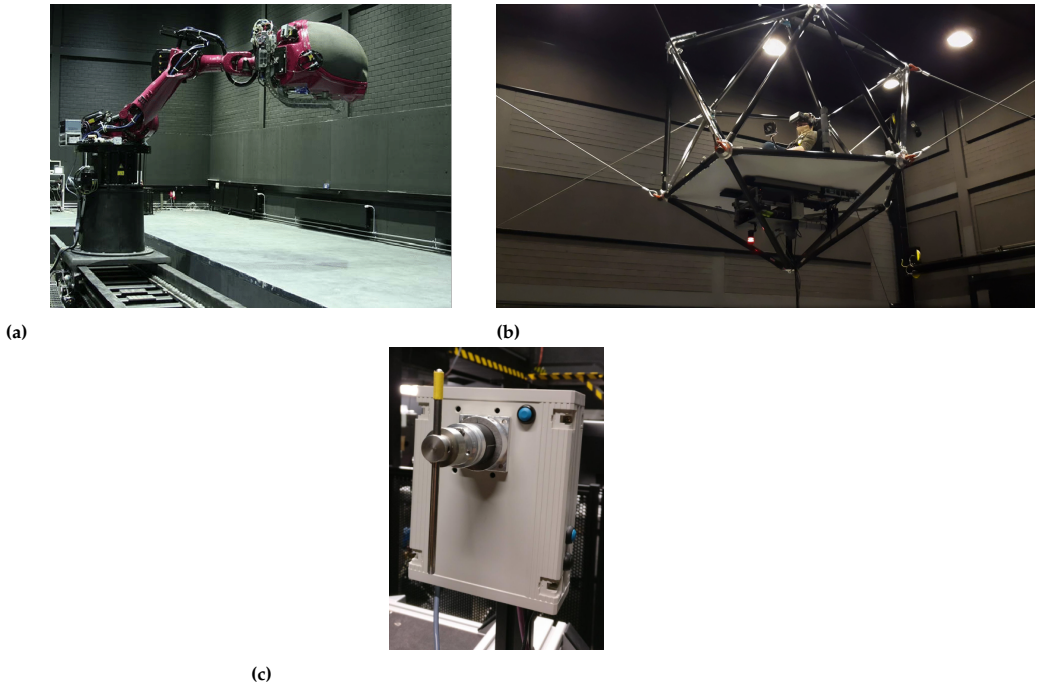


**Fig. 4.1** Experimental setup. *a* is the CMS used to measure motion perception in centrifugation mode. *b* shows the CRS used to measure frequency sensitivity in motion sickness development. *c* shows the pointer device, participants were instructed to align the orientation of the rod to (the pitch of) their perceived vertical

dicating standstill (the rod was reset to this position for every new motion trial). This psychophysical task is similar to the one used by Bertolini et al. (2011a), who instructed their participants to match their perceived speed with the speed of rotation of a similar rod. In our experiment, participants were instead asked to do the easier control task of matching their perceived speed, with the position of the rod. The mapping of rod deflection to spin rate is arbitrary, so we cannot know what the actual perceived speed of the participant was. However, the responses do indicate how the perceived speed decayed with respect to time, which is the only requirement for determining the velocity storage time constant. Therefore, just as in Bertolini et al. (2011a), the amplitude of rod deflection was normalized. The normalization was done with respect to the maximum rod position during the initial 60 s rotation.

The two motion paradigms were each repeated 4 times for a total of 8 trials. The motion paradigms from the 8 trials were presented in random order. Including the fade-in/fade-out periods, the motions for each trial lasted for 60 s. After this, the platform was stopped and remained stationary for another 60 s. Participants were instructed to report their perceptions also during the stationary phase. After the stationary phase, the platform was re-orientated for the next trial.

Vertical and horizontal eye movements were recorded using the Tobii Pro glasses and processed, but not analysed further as the data was of poor quality in approximately 50% of the participants.

#### SICKNESS EXPERIMENT

The week after the perception experiments on the CMS, participants began their first motion sickness session. Each participant underwent five motion sickness sessions, separated by a minimum of 4 days to minimise habituation. Participants were seated on the CRS platform and subjected to (maximum) 30-minute sinusoidal fore-aft motions with peak accelerations of  $2 \text{ m/s}^2$  and frequencies of 0.15, 0.2, 0.3, 0.4 and 0.5 Hz, with a 10-second smoothed start and end. The fade-in function for time  $t$  was:  $(t/10) - (1/2\pi)\sin(2\pi(t/10))$ . For the fade-out, the value of this function was subtracted from 1.

Each session only tested one frequency of the acceleration stimulus. Due to time limitations and a desire to sample as broad a range of frequencies as possible, conditions were not repeated. This is justified by good trial-to-trial repeatability found in motion sickness response (Miller and Graybiel, 1969; Irmak et al., 2020). The choice of the lowest frequency was imposed by the maximum possible stroke at  $2 \text{ m/s}^2$ . The choice for the highest frequency was based on the observed frequency at which sickness was approximately one tenth of that at lower frequencies (Donohew and Griffin, 2004). The order in which each frequency was experienced was randomized for all the participants. This prevented confounding effects of habituation between the different frequencies.

The participants were instructed to report their sickness on the 11-point subjective Misery Scale (MISC) (Bos et al., 2010). Although MISC may probe multiple symptom clusters, MISC is still monotone with respect to subjective severity of sickness. This is supported by the fact that in our study mild nausea (MISC 6) was never seen prior to build up of the other symptoms (as shown in Figure B.4), an observation that has also been reported in previous literature (Bos et al., 2005). Therefore, the scores recorded are on an ordinal scale with respect to sickness severity. The MISC was queried every 30 seconds. Each sickness session lasted up to a maximum of 30 minutes, or until the participant reached a MISC level of 6. A MISC level of 6 corresponds to slight nausea and was deemed an appropriate threshold both in order to prevent participant dropout from further sessions but also due to ethical concerns. After each session, participants were asked to complete the Motion Sickness Assessment Questionnaire (MSAQ) (Gianaros et al., 2001). The MSAQ is a 16-item questionnaire composed of 4 sub-components querying various types of sickness. The types of symptoms are: gastrointestinal symptoms such as stomach awareness, central symptoms such as feeling light headed, peripheral symptoms such as feeling sweaty, and sopite symptoms such as fatigue. Each item was rated on a scale from 1 to 9, providing Likert-type ordinal data. The MSAQ gave a more detailed breakdown of participant symptoms at the worst point of their sickness, which was almost always at the end of the experimental session.



#### 4.3.5. DATA REDUCTION

A large amount of data was collected in both parts of the experiment. To evaluate our hypotheses, we summarized the perception data to a simple set of parameters that characterized each participants' response. Likewise, for each sickness session we calculated a single robust metric that represented the amplitude of the sickness experienced.

#### VELOCITY STORAGE AND SUBJECTIVE VERTICAL TIME CONSTANTS

The subjective vertical and velocity storage time constants for perception were identified by first pooling the normalized responses of each motion paradigm per participant and averaging across the repetitions. The time constants of the perceived subjective vertical and the angular velocity were estimated as the time it took for the perceived quantity to converge 63.2% of the way to steady state. For the subjective vertical this was estimated by fitting an exponential function of the following form  $y = b_1(1 - \exp(-b_2t))$  using the *fitnlm* function in MATLAB. The average  $R^2$  value across individuals was 0.96, indicating a good fit of the model (individual fitting shown in B.1a). For velocity storage, the time constant was estimated non-parametrically by simply finding the point at which the perceived angular velocity passed 63.2% of the way to steady state (individual responses, as shown in B.1a). A different method than fitting an exponential was chosen here because of plateauing behaviour. This is discussed in the results.

#### CROSS-OVER FREQUENCY

The subjective vertical time constant derived from the centrifugation is specific to the experimental paradigm used. If a variable arm centrifugation would have been used, or a faster yaw velocity, the time constant of the subjective tilt would likely be different. This is due to the presence of the perceived yaw signal (Merfeld et al., 2000), which is influenced by the velocity storage time constant. The fore-aft acceleration that was used to induce sickness does not have this angular component. For this perturbation, just as in OVAR, it is likely that the cross-over frequency of gravito-inertial perception is the underlying parameter of most importance. The perception paradigms used do not allow for a direct measurement of this value. However, the results from the paradigms studied can be used with models of sensory integration to estimate the cross-over frequency of gravito-inertial perception. For this purpose we use the Multi Sensory Observer Model (MSOM) (Newman, 2009; Newman et al., 2012; Clark et al., 2019). The MSOM was chosen because it has been validated across a wide range of motion paradigms and belongs to the observer class of spatial orientation models linked by Oman (1982) to motion sickness development.

The MSOM, shown in Figure 4.2, was implemented in Simulink. The aim of the MSOM is to predict perceived angular velocity, inertial acceleration and orientation of the human participant given the inputs of head referenced head angular velocity  $\omega_h$  and head referenced gravito-inertial force  $f_h$ . In this model perceived orientation and so the the rod orientation set by the participant is assumed to be inline with the gravitational vector. This assumption for passive centrifugation matches experimental observations (Panic et al., 2015; de Winkel et al., 2020), such as in this study, but may not hold for active motion and control of orientation, where the upright

may be defined with the direction of balance instead (Ricci *et al.*, 1992). In its current formulation the MSOM has five parameters,  $K_\omega$ ,  $K_{f\omega}$ ,  $K_f$  and  $K_a$  and  $K_1$ . The parameter  $K_\omega$  is the feedback gain of the angular velocity perception path. For a given time constant of the semi-circular canals (SSC) and the internal model of the semi-circular canals ( $\overline{SSC}$ ) its value determines the velocity storage time constant of angular velocity perception. The otoliths (OTO) and the internal model of the otoliths ( $\overline{OTO}$ ) is given as a unity transfer function. The parameter  $K_{f\omega}$  determines the contribution of a change in the orientation of the gravito-inertial force on the perceived angular velocity. Parameter  $K_f$  sets the change in perceived orientation given a change in the orientation of the gravito-inertial force. Parameter  $K_a$  is the translational acceleration feedback gain, determining the gain of the perceived acceleration through the otolith organs. Lastly,  $K_1$  is the angular velocity gain to the gravity estimator. This is actually a function of  $K_\omega$  of the form  $K_\omega / (1 + K_\omega)$

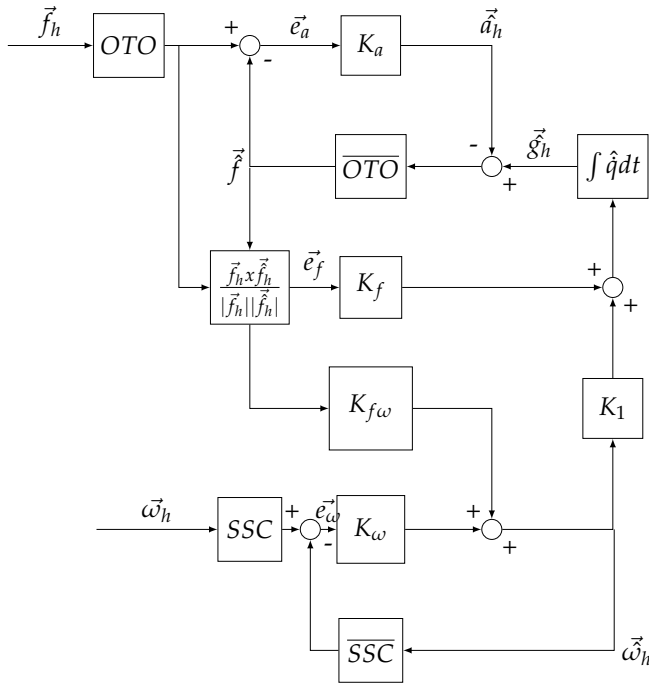


Fig. 4.2 Multi Sensory Observer Model used to compute the cross-over frequency between acceleration and gravity perception

For our implementation, the gain  $K_{f\omega}$  was set to zero because it was found that during OVAR perception of angular velocity tended to zero, which would not be the case for a finite  $K_{f\omega}$  (Vingerhoets *et al.*, 2005). Moreover, the semi-circular canals SSC and the internal model of the semi-circular canals  $\overline{SSC}$  were both represented as first-order high-pass systems, with a time constant fixed at 5.7 s for all participants based on Merfeld *et al.* (1993). Setting this as a free variable would have created an

underdetermined model. The reference data for model fitting was the rod setting for the centrifugation and the EVAR motion paradigms. Because the model is not able to predict biases, such as an overshoot of the subjective vertical or miscalibration in the internal representation of rod orientation, as may have been the case for some of the participants, the rod data was first filtered through a median filter of window 1 s, it was then normalised and scaled to the theoretically expected maximal tilt and angular velocity percepts. This operation did not affect the predicted cross-over frequency, as even though amplitude information was lost, the temporal dynamics were maintained.

For reference, Figure B.2 shows the fits for the 14 participants for which both centrifugation and EVAR data was available. The fits were performed using a genetic algorithm with a group size of 100 for each generation. The fitting was then further refined using the interior-point method. This process was repeated 5 times from different initial conditions. The cross-over frequencies found were approximately the same between different iterations and were therefore averaged across iterations per participant. The error function used for the fitting was The Symmetric Mean Absolute Percentage Error (SMAPE):

$$\text{SMAPE} = 100 \frac{\sum_{t=1}^n |F_t - A_t|}{\sum_{t=1}^n (|A_t| + |F_t|)}$$

This error metric is well protected against outliers and treats both over and underestimation in an unbiased manner. For each iteration, the SMAPE between the fitted,  $F_t$  and the actual  $A_t$  perceived angular velocity and subjective vertical were calculated. The average of the two errors was then minimised by the optimisation.

The solution for  $K_\omega$  was unique for each individual. The parameters  $K_a$  and  $K_f$ , however, could not be uniquely estimated from the current data. However, the ratio between the  $K_a$  and  $K_f$  values found was unique. It is this ratio that determines the cross-over frequency, which is given by the intersection of acceleration and gravity perception gains, as shown in Figure 4.3 (and Figure B.3 for all participants). Figure 4.3 was generated by plotting the magnitude response of the linearised simulink model (obtained using bode response option native to Simulink). This subsequent linearisation gave as outputs gravity and acceleration for a small horizontal acceleration input perturbation. The factor by which this small horizontal acceleration becomes gravity and acceleration respectively is given as the gain. In this case Figure 4.3 shows the small acceleration perturbation at lower frequencies is perceived as change in gravity, i.e. tilt and at higher frequencies as acceleration. Therefore, it was possible to use our two motion perception paradigms to determine a unique cross-over frequency as per the MSOM.

### SICKNESS MAGNITUDE

In this study, motion sickness was measured using two methods: the MISC ratings that were taken during a session, and the MSAQ that was filled out at the end of a session. MISC ratings were obtained for the duration of each sickness-session, with intervals of 30 s (Figure B.4 shows MISC trajectories for all participants and conditions). Sickness intensity can be quantified in different ways, for example, using the

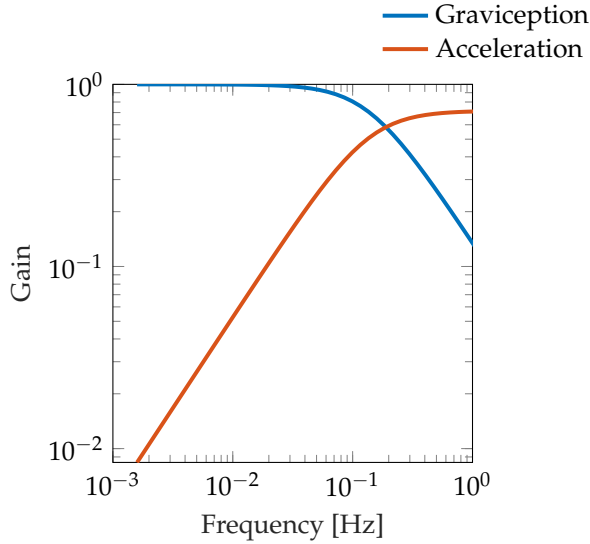


Fig. 4.3 Example of one participant showing a cross-over frequency of 0.18 Hz

mean MISC, which is the average MISC rating across the entire period of the run, or the MISC rate, which is the maximum MISC rating divided by the time taken to reach it. Likewise, for the MSAQ, either the total score or the various sub-scores can be used to quantify the frequency sensitivity. Each measure can transform the frequency sensitivity curves seen, with no guarantee that the chosen measure is the best measure.

Therefore, instead of choosing a single sickness metric among the different choices in an arbitrary manner, we performed factor analysis to ascertain the latent factor structure. With the factor loadings we then established an aggregated measure that best correlated to the underlying sickness experienced by the participants. This has the added advantage of reducing measurement noise. Here, there are 7 metrics to quantify sickness: the mean MISC ( $M_\mu$ ), MISC rate ( $\dot{M}$ ), maximum MISC ( $M_{max}$ ), MSAQ Gastro ( $MS_g$ ), MSAQ Central ( $MS_c$ ), MSAQ Peripheral ( $MS_p$ ) and MSAQ Sopite ( $MS_s$ ). These are strongly correlated with each other, but also to a number of latent factors. In our experiment we had a within-participant design where the same participant was exposed to 5 conditions in terms of motion frequencies. Hence variance is influenced by both within and between participant sources.

These metrics were first standardized with respect to their group mean and standard deviation such that they were unitless. To account for dependency in the metrics, factor analysis on the averaged within-participant correlation matrix (Reise et al., 2005) was performed. As the data is ordinal Spearman's rank correlation matrix was used (Klinke and Wagner, 2008).

Factor 1 explained 41.1% of the variance and mainly related to the overall level of sickness, as is seen from the high loadings on the mean and maximum MISC, as well

**Table 4.1** Table of factor loadings of different subjective sickness scores; mean MISC, MISC rate, maximum MISC, MSAQ gastrointestinal, MSAQ central, MSAQ peripheral and MSAQ sopite, on to three latent factors. Bold numbers indicate high factor loadings.

Item	Factor 1	Factor 2	Factor 3
$M_\mu$	<b>0.8984</b>	0.2000	0.1160
$M$	0.1306	<b>0.9884</b>	0.0318
$M_{max}$	<b>0.8816</b>	0.0174	0.2572
$MS_g$	<b>0.7897</b>	0.0083	0.2329
$MS_c$	0.4338	0.0444	0.4029
$MS_p$	<b>0.6631</b>	0.1257	0.0912
$MS_s$	0.1516	0.0194	<b>0.8512</b>

as the gastric component of the MSAQ. Factor 2 explained an additional 14.8% of the variance and mainly related to the duration of symptom development, with the highest loading for the MISC rate. Lastly, Factor 3 explained an additional 14.7% of the variance and primarily captured other sources of discomfort, such as drowsiness and irritation. This was indicated by the high loading on the sopite component of the MSAQ. As we are interested in sickness, Factor 1 is the most important. Here, the loadings on the mean MISC, maximum MISC and MSAQ Gastro and MSAQ Peripheral were greater than the loadings on the other metrics. Moreover, unlike the other items loaded on Factor 1, they did not cross-load onto the other factors. Therefore, using these metrics, a joint Sickness Index (SI) was constructed (Wieland et al., 2017). The SI is given in the form

$$SI = \frac{F_{11}}{4\sigma_1} M_\mu + \frac{F_{13}}{4\sigma_3} M_{max} + \frac{F_{14}}{4\sigma_4} MS_g + \frac{F_{16}}{4\sigma_6}$$

where  $F_{11}$  is the factor loading of the first factor on the first metric  $M_\mu$ ,  $F_{13}$  is the factor loading of the first factor on the third metric  $M_{max}$  and  $F_{14}$  is the factor loading of the first factor on the fourth metric  $MS_g$  and lastly  $F_{16}$  is the factor loading of the first factor on the sixth metric  $MS_p$ . Likewise,  $\sigma_1$  is the standard deviation in the scores of the first item rating  $M_\mu$ ,  $\sigma_3$  is the standard deviation in the scores of the third item rating  $M_{max}$ ,  $\sigma_4$  is the standard deviation in the scores of the fourth item rating  $MS_g$  and lastly  $\sigma_6$  is the standard deviation in the scores of the sixth item rating  $MS_p$ . The coefficients of both  $M_\mu$ ,  $M_{max}$ ,  $MS_g$  and  $MS_p$  are all standardized with respect to their respective standard deviations (Fernando et al., 2012).

#### 4.3.6. PEAK FREQUENCY OF SICKNESS

Due to being a more robust measure than the unprocessed peak or the one estimated in the statistical model, the spectral centroid was taken as the point of peak sickness. This was given by the equation

$$\frac{\sum_1^N f(n)SI(n)}{\sum_1^N SI(n)}$$

where  $N$  is the  $n$ th condition for a given participant,  $f$  is the frequency of this condition and  $SI$  is the sickness index seen at this condition.

### GENERAL MOTION SICKNESS SENSITIVITY

The estimated frequency sensitivities may be affected by noise in individuals' responses, for instance due to difficulty distinguishing between low levels of sickness, or due to day-to-day variability in sensitivity between sessions. A more robust measure of overall sensitivity to sickening stimuli was obtained by averaging the responses for different frequencies. To evaluate overall sensitivity, we calculated a mean  $SI$  across all frequency conditions available for each individual participant.

## 4.4. RESULTS

### 4.4.1. PERCEPTION EXPERIMENT

The centripetal force of  $4.2 \text{ m/s}^2$  should change the direction of the gravito-inertial force (GIF) to be  $23.2 \text{ deg}$  from the direction of gravity. Figure 4.4a shows the average response pooled across all repetitions for all participants. Here, there was an over-estimation (when compared to the GIF) of the final tilt angle, at  $31.3 \text{ deg}$ . The mean time constant of this tilt percept was  $9.2 \text{ s}$  (STD =  $7.17 \text{ s}$ ). As shown in Figure 4.5a, this time constant was similar to reported values in literature (Graybiel and Brown, 1951; Merfeld et al., 2000; Curthoys, 1996; De Graaf et al., 1996). Figure B.1 shows the development of the tilt percept for all 17 participants that data could be collected for. Eight of the participants converged to within  $2 \text{ deg}$  of the GIF, another 8 showed a higher tilt angle with only one noting a lower tilt angle.

In the first  $60 \text{ s}$  of EVAR, participants reported a constant perception of rotation (shown in B.1). This is contrary to the expectation of a steadily decaying perception of angular velocity. This retention of perceived angular velocity was likely due to noise and rumble of the simulator. For this reason, the decay in the perceived angular velocity following a period of  $60 \text{ s}$  after the complete cessation of the simulator was used instead to quantify the velocity storage time constant. Figure 4.4b shows this perception after-effect for EVAR, averaged across all participants, for all repetitions. Here, the mean time constant for the decay was  $17.2 \text{ s}$  (STD =  $6.8 \text{ s}$ ). As shown in Figure 4.5b, this was similar to the values reported in literature (Guedry, 1974; Okada et al., 1999; Vingerhoets et al., 2005). Once at the maximal value, the mean response showed a plateau of approximately  $4 \text{ s}$ . Looking at the individual responses in Figure B.1, it can be seen that for 11 participants the duration for which participants stayed at 90% of maximum tilt sensation was more than  $5 \text{ s}$ . For the remaining 7, perceived velocity decreased faster, i.e., 90% within  $5 \text{ s}$ .

### 4.4.2. SICKNESS EXPERIMENT

#### GROUP FREQUENCY SENSITIVITY

In our study only 7 out of 23 participants reached mild nausea (MISC of 6 at one or more frequencies). This indicates a mild level of sickness was reached in this study. The Sickness Index (SI) between participants does not show a clear frequency dependency (Figure 4.6). However, individual participants do show a marked frequency

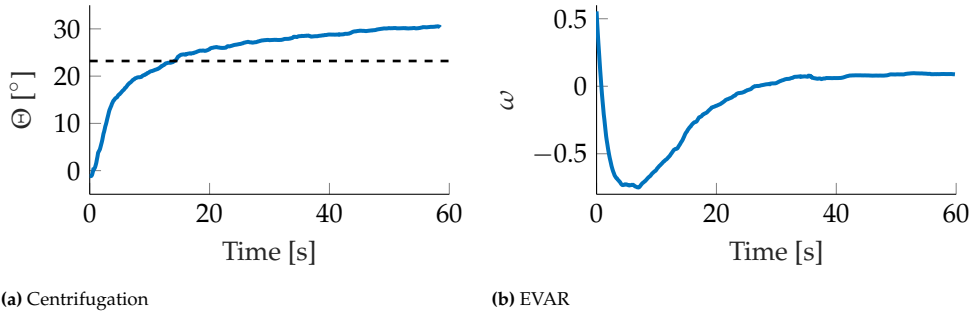


**Fig. 4.4** Mean perceptual responses of all participants.  $a$  is the mean subjective vertical tilt. The y-axis indicates the orientation of the pointer device which was taken as proxy for subjective vertical tilt. The black dashed line signifies the expected tilt.  $b$  shows the mean subjective angular velocity after rotation, where the y-axis indicates the normalized perceived angular velocity

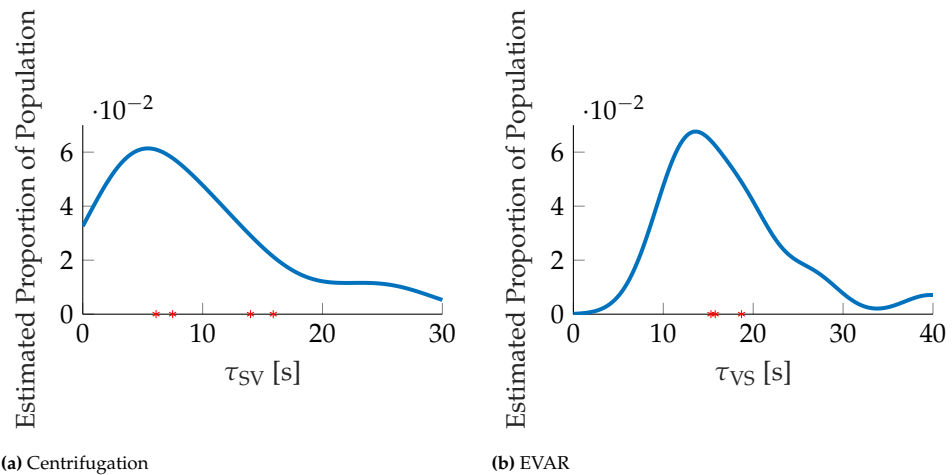


**Fig. 4.5** Estimated distribution of perception parameters using kernel density estimation, as well as the mean parameters findings in the literature indicated by asterisks on the x-axis.  $a$  estimated distribution for the time constant of the subjective vertical. The stars going from left to right are [Curthoys \(1996\)](#), [De Graaf et al. \(1996\)](#), [Merfeld et al. \(2000\)](#) and [Graybiel and Brown \(1951\)](#).  $b$  estimated distribution for the time constant of velocity storage. The stars going from left to right are [Guedry \(1974\)](#), [Okada et al. \(1999\)](#) and [Vingerhoets et al. \(2005\)](#)

dependency (Figure 4.7).

As per [Donohew and Griffin \(2004\)](#), we expected (H1), *Group sensitivity of sickness due to fore-aft acceleration to be frequency dependent*), where the relation between frequency and motion sickness reported previously can be approximated by an upside down parabola. Consequently, we assumed the sickness index to be described by a quadratic function of the form:

$$SI = b_1 - b_2(f - b_3)^2$$

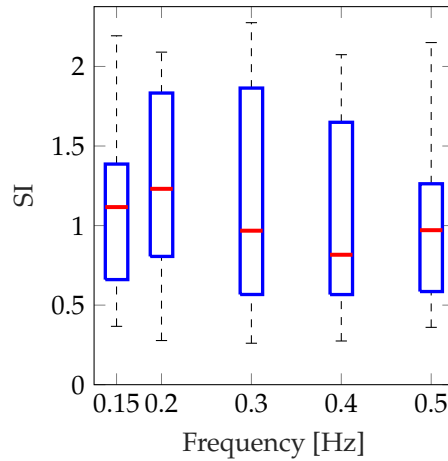


Fig. 4.6 Sickness Index for different frequencies. The bars show the median, the 25th and 75th percentiles, and the full range

where  $b_1$  is the intercept,  $b_2$  is the strength of the quadratic effect and  $b_3$  is the frequency of maximum sickness. The coefficients  $b_2$  and  $b_3$  were bounded such that they were both greater than or equal to zero.

The hypothesis that there is such a quadratic relation can be tested statistically by comparing AIC and BIC scores for this model to those metrics for an intercept-only model. AIC and BIC scores are measures of model fit which are based on the likelihood of the data given the model, whilst including a penalty term for the number of parameters. This penalty term has a constant scaling with the number of parameters for the AIC, but has a logarithmic scaling with the number of observations for the BIC. This means that for a large number of observations, the BIC is more conservative in its selection of more complex models. [Fabozzi et al. \(2014\)](#) specifies how to interpret the absolute value of differences in the AIC and BIC scores between the models, in terms of strength of evidence. According to these rules of thumb, absolute differences in the indices 2, 6, and 10 provide positive, strong, and decisive evidence (respectively) in favor of the model with the lower value.

As a benchmark, we first fitted a Fixed Effect Intercept only model,  $SI = b_1$ . The observed AIC and BIC values were 173.5 and 176.0, respectively. For the full Fixed Effect Quadratic model,  $SI = b_1 - b_2(f - b_3)^2$ , the observed AIC and BIC were 174.0 and 181.6, respectively. This suggested that there was no common frequency effect in the group. Indeed, a visual inspection of the box plot in Figure 4.6 is consistent with this assessment. However, when the error between model predictions and the observations made for each individual participant was evaluated, it was seen that the errors were not evenly distributed around zero, but instead, these were offset in either direction of zero (shown in Figure B.5). This suggests that accounting for individual variability could improve the model fit. We attempted to account for this variability between individuals by using a mixed-effects intercept and quadratic



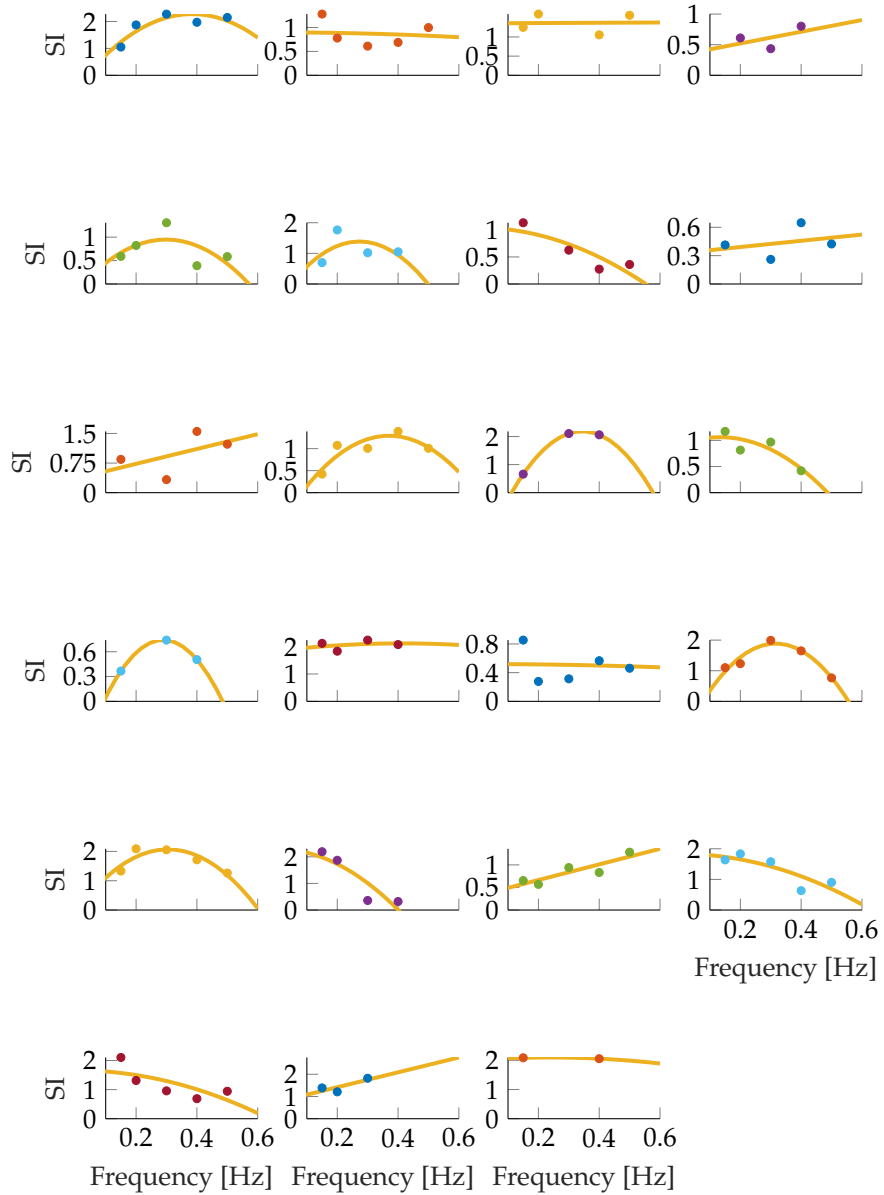


Fig. 4.7 Participant sickness index as a function of frequency, with individual quadratic fits

models. However, these did not provide successful fits to the data and so for the sake of brevity this is not shown.

### INDIVIDUAL SENSITIVITY

The reason behind the frequency-invariant group-level response could be the aggregation of individual differences in frequency group sensitivity. As shown in Figure 4.7 individuals show markedly different sensitivity variations with frequency: for some, there appears to be a peak at intermediate frequencies (i.e., going from left to right, participants 5, 10, 13, 16 and 17), whereas others appear to experience more sickness at low frequencies (i.e., participants 7, 12, 18, 20 and 21) or at higher frequencies (i.e., participants 1, 10, 11 and 19). Also, for some participants the range of frequencies tested might not be wide enough to reveal a peak sickness response.

We tested whether individuals on average had different frequency sensitivities by fitting the model to each individual's data separately. However, individual participants contributed at most five data points, and the model has three parameters, this left few degrees of freedom. The model could not be fitted for participants who had less than four data points, and hence, the five individuals for whom this was the case were excluded from this analysis.

Because participants are independent, we can sum model likelihoods, the number of parameters, and the number of observations to calculate overall model fit indices for the intercept-only and the quadratic models. For the intercept-only model, the AIC and BIC scores were 82.4 and 125.7, respectively, with 31.0 and 160.9 for the quadratic model. In this analysis, the AIC thus favors the quadratic model, whereas the BIC favors the intercept-only model due to a larger penalty on the number of parameters. Likelihood ratio test between the Individual Intercept and Individual Quadratic model gave  $p < 0.001$ , this indicates that the Individual Quadratic model is a better fit to the data.

Because this analysis excluded some participants, new joint fixed intercept and quadratic models were fitted as benchmarks to assess the evidence for individual differences. These models were fitted to the joint data of all participants included in the individual fits. The scores obtained were AIC: 144.2 and BIC: 146.6 for the intercept model and AIC: 144.0 and BIC: 151.2 for the quadratic model. The conclusions thus differ depending on the choice of criterion.

Taking the more conservative BIC, the joint intercept-only model is preferred compared to the individual quadratic model (BIC: 146.6 vs BIC: 160.9). This means that taking the BIC the hypothesis (H.2) of a frequency dependent variation in sickness sensitivity which also varies across different individuals is rejected. Based on the AIC however, the individual quadratic model is preferred over the fixed intercept and fixed quadratic models (AIC:31.0 vs 144.2 and 144.0). This is confirmed using a likelihood-ratio test where  $p < 0.001$ . Therefore, the hypothesis (H.2) of a frequency dependent variation in sickness sensitivity which also varies across different individuals is accepted.

### 4.4.3. SICKNESS AND PERCEPTION

#### VELOCITY STORAGE & SUBJECTIVE VERTICAL TIME CONSTANT

As per H.3, we expected there to be a negative correlation between the frequency sensitivity of sickness and (H.3a) the subjective vertical time constant (as computed simply from the centrifugation results), and (H.3b) the velocity storage time constant. The spectral centroid

**Table 4.2** Table showing both individual and group fits for 18 participants. Bold elements indicate the best fitting model.

Fit type	SSE	Log-likelihood	AIC	BIC
Individual Intercept	12.0	-23.2	82.4	125.7
<b>Individual Quadratic</b>	5.0	38.5	<b>31.0</b>	160.9
Joint Intercept	27.5	-71.1	144.2	146.6
Joint Quadratic	26.8	-69.0	144.0	151.2

was taken as the point of peak sickness. The correlations between this frequency and the perception parameters were computed for those subjects for which both the appropriate perception data and at least four sickness runs existed.

The correlation coefficients between the spectral centroid and the velocity storage (shown in Figure 4.8a) and subjective vertical time constants (shown in Figure 4.8b) were  $r(14) = 0.32$  ( $p = 0.26$ ) and  $r(13) = -0.37$  ( $p = 0.29$ ), respectively. *Therefore, the evidence does not support the hypothesis of a correlation between the subjective vertical and the velocity storage time constants and the frequency of peak sickness (our H.3a and H.3b).*

### CROSS-OVER FREQUENCY

The mean cross-over frequency of the 14 participants was 0.21 Hz, this ranged from 0.04 Hz to 0.42 Hz. This approximately matched the frequency range where sickness is seen for horizontal accelerations.

For 11 participants both the quadratic function describing the peak sickness frequency and the MSOM fits was estimated. The correlation coefficient between the spectral centroid and the cross-over frequency was  $r(11) = 0.26$  ( $p = 0.44$ ). *Therefore, the evidence does not support a correlation between the cross-over frequency and the frequency of peak sickness (H.3a).*

### AVERAGE SICKNESS SENSITIVITY AND PERCEPTION

In line with earlier literature (Dai et al., 2003, 2007, 2010), motion sickness sensitivity may be correlated with perception parameters. To evaluate this, a mean SI was computed by averaging across all frequency conditions available for each individual participant.

The correlation coefficients between the mean SI and the velocity storage and the subjective vertical time constants were  $r(18) = 0.31$  ( $p = 0.21$ ) and  $r(17) = 0.74$  ( $p = 0.0006$ ), respectively (the latter is shown in Figure 4.8c). For the cross-over frequency this was  $r(14) = -0.54$  ( $p = 0.047$ ). *Thus, our data provides evidence for a relationship between individuals' overall sickness sensitivity and their subjective vertical time constant (H.3c).*

## 4.5. DISCUSSION

For the first time, this study investigated individual frequency sensitivity of motion sickness to fore-aft accelerations. Moreover, it analyzes the relationship between

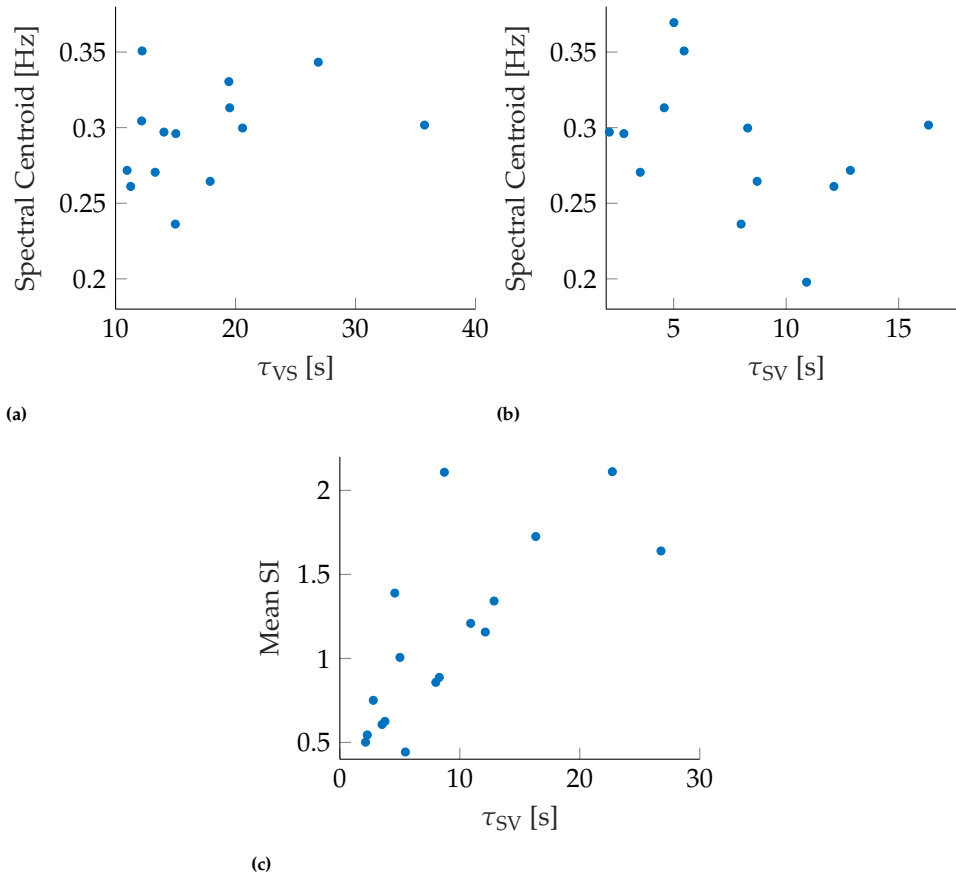


**Fig. 4.8** (a) shows the spectral centroid against the velocity storage time constant. (b) shows the spectral centroid against the subjective vertical time constant. (c) Mean sickness sensitivity against the subjective vertical time constant

individual sensitivity to motion sickness and motion perception. Participants underwent centrifugation and EVAR motions such that perception parameters could be obtained. After this, each participant experienced sickening translational accelerations of varying frequencies in the fore-aft direction. Sickness was quantified for each individual at five different frequencies using an aggregate metric obtained using factor analysis. We then attempted to correlate the obtained individual frequency-sensitivity curves to the perception parameters of the participants. In the following we discuss our findings in relation to the hypotheses and consider methodological issues with quantifying motion sickness and perception.

### 4.5.1. QUANTIFYING SICKNESS

Literature shows many ways of quantifying sickness: O'Hanlon and McCauley (1974) use the motion sickness incidence (MSI), which is the proportion of experiment participants that have vomited before the motion end point. In a similar manner, Donohew and Griffin (2004) use the proportion of those that developed at least mild nausea as a metric and Golding and Markey (1996); Golding and Stottt (1997) use sickness ratings at motion end point, but also the time taken to reach a particular sickness rating.

The choice of the scale to use is heavily dependent on the experimental design and the aim of the experiment, with each choice presenting advantages and disadvantages. For instance, the MSI is an objective measure of sickness. However, it is only feasible if one wishes to explore the end point of sickness. Using the proportion of the sample to reach a certain level of sickness is good for summarizing group-level sensitivity, but cannot capture individual responses. Moreover, it is only a good measure if a large number of people do reach a certain level of sickness, which is also the case for "time to" measures of sickness sensitivity. In our study only 7 out of 23 unique individuals reached mild nausea, i.e., about a third, compared to over half in the most sickening conditions of Donohew and Griffin (2004). This means that in our experiment not enough people got sufficiently sick for the differences in the percentages to be a meaningful measure. Time-to-sickness rating measures suffer from a similar need of having a large proportion of participants reaching a certain level of sickness. For those participants that do not reach the sickness threshold, the maximum experiment time is set artificially as the time to sickness. This operation distorts the data. Moreover, with the aim of measuring individual frequency sensitivity, there is no way of ensuring an individual will get to the same level of sickness within the available period of time across the frequency spectrum. In an attempt to overcome the limitations of individual metrics, this study uniquely used a joint Sickness Index (SI). The novelty is that the SI is a combination of the MISC, which is a generalized uni-dimensional sickness score that can be obtained quickly and regularly, with parts of the MSAQ, which is more elaborate and can only be completed after an experimental session. By combining these metrics, a more accurate representation of the latent sickness construct may be obtained than when using either metric in isolation.

### 4.5.2. GROUP SICKNESS SENSITIVITY

Looking at the group sensitivity in our study, we found *no significant variation in the SI between the frequency conditions studied, meaning a plateau in the group sensitivity to sickness up to 0.5 Hz*. This finding contrasts with our Hypothesis 1 and earlier literature: for example, Golding and Markey (1996); Golding and Stottt (1997) found no significant difference in the sickness end point ratings from 0.205-0.5 Hz. However, they did find a significant difference in the time-to-sickness rating within this range. However, as discussed above, such a metric could not be sensibly computed for our study. Golding overall argues for a slight decrease in motion sickness sensitivity of -3 to -4 dB per octave from 0.2-0.4 Hz. This is in disagreement with Donohew and Griffin (2004), who finds a very sharp decrease of -12 db per octave from 0.25-0.8 Hz.

Therefore, the evidence combined over studies seems to indicate a small decrease in group sensitivity from 0.4 Hz to 0.5 Hz, after which there is a sharper decrease. The variability within these studies may be influenced by a large set of factors. One of these is the sickness metric used. For instance, [Donohew and Griffin \(2004\)](#) normalized the percentage reaching mild nausea with the root mean square (RMS) acceleration of their platform, assuming a linear relationship between mild nausea and RMS acceleration magnitude. Another cause can be the large scatter in individual sensitivities. For instance, in [Golding and Markey \(1996\)](#) 8/12 participants reached a sickness rating of 4 for the 0.5 Hz condition, whereas in [Golding and Stottt \(1997\)](#) only 3/12 did so. This large individual variability is also supported directly by our observations.

### 4.5.3. INDIVIDUAL SICKNESS SENSITIVITY

The present study is the first investigation of individual frequency sensitivity of motion sickness to fore-aft accelerations. We find that although the group sensitivity is flat, individual sensitivities vary steeply, with some participants more susceptible to low-frequency oscillations, and others more susceptible to mid- and high-frequency accelerations. To test for individual variability in the frequency sensitivities, we compared the fit of quadratic models to the fit of intercept-only models on the basis of the AIC and BIC model fit scores. The AIC values supported the conclusion that there is frequency sensitivity in motion sickness responses and that the peak sensitivity varies between individuals, and this was confirmed using the likelihood-ratio test ( $p < 0.001$ ). The BIC values supported a conclusion that there is individual variability, but only with respect to the overall sensitivity; using this score, there was no evidence for frequency sensitivity. A reason for the disagreement between the BIC and AIC scores is that the BIC is much more conservative. Here, the penalisation of model complexity scales with the logarithm of the number of observations, which for our case was 82. Moreover, a likely cause for the favorability of the intercept-only model according to the BIC score is that some participants did not get sick (due to the low acceleration amplitude) and so had a flatter frequency sensitivity. Likewise, for some that did get sick, the range of frequencies we observed may not have been large enough to measure the attenuation of their sickness sensitivity. Moreover, as motion sickness is not experienced at very low (i.e.  $\leq 0.03$  Hz, [Donohew and Griffin \(2004\)](#)) or high (i.e.,  $\geq 0.5$  Hz frequencies, [Donohew and Griffin \(2004\)](#); [Cheung and Nakashima \(2006\)](#)), the BIC favored intercept-only model will not be tenable when a larger frequency range is considered. Therefore, the AIC-favored Individual Quadratic model is more credible, supporting that there are indeed differences in the motion sickness frequency sensitivity of our participants. Literature ([Miller and Graybiel, 1969](#); [Irmak et al., 2020](#)) shows that individuals exhibit repeatable sickness response when subject to the same motion stimuli over consecutive motion trials, while our results show large individual variation, indicating an effect of frequency sensitivity. Consequently, we accept the hypothesis that (H.2) *The frequency-dependent sickness sensitivity varies across different individuals*. This also means that individual sickness frequency sensitivities are not represented well by the group-level frequency sensitivity.

#### 4.5.4. PERCEPTION AND SICKNESS

As summarised in the introduction, there have been several studies linking motion perception parameters to motion sickness. However, to the authors' knowledge, none have taken the frequency-domain approach usually employed in engineering disciplines to resolve the problem of how the two may be mechanistically related. Based on our review of the literature, we hypothesized that motion sickness frequency sensitivity may be related to three motion perception parameters: the velocity storage time constant, the subjective vertical time constant (from simple centrifugation) and the cross-over frequency as per the MSOM.

The subjective vertical time constant that was computed was similar to values reported in the literature (see Figure 4.5a). We note that the end value of the perceived tilt angle with respect to the GIF could be different had the participants been facing towards the centre of rotation. Here, the added utricular shear in the hyper-gravity environment of the centrifuge would have caused an over-estimation of roll tilt and a larger difference with the GIF (Clark et al., 2015). However, this is not likely to affect the time dynamics. The velocity storage time constant was also similar to values reported in the literature (see Figure 4.5b). For the subjective angular velocity perception we report plateauing of the perceived velocity for 11 participants. This is in line with Bertolini et al. (2011a), who found the same plateau for 10 of their participants and a faster decay for the remaining 6.

Overall, both the recorded tilt perception and angular velocity perception results match previous literature findings and are therefore valid correlates of the internal state estimates. Moreover, they display substantial variation between participants (Figure B.1) indicating a positive perspective to explain individual motion sickness sensitivity.

Our results showed that *the subjective vertical time constant was negatively correlated with peak sickness frequency whereas the cross-over frequency (H.3a) and the velocity storage time constant were positively correlated (H.3b)*. However, the correlations were weak, and did not reach statistical significance. It is possible that this was due to a lack of statistical power. Due to the corona virus pandemic human-subject experiments were restricted during the course of our study, which unfortunately led to some missing frequencies in some of our participants. Despite the correlations not reaching significance, we can argue their implications. For instance, the positive correlation between the cross-over frequency and the frequency sensitivity is in line with the hypothesis that sickness occurs at the point of most perceptual ambiguity. The subjective vertical time constant as determined from centrifugation is inversely proportional to this cross-over frequency, which explains its negative correlation with sickness sensitivity. Moreover, the range of cross-over frequencies obtained from MSOM fits are within the range where we find maximum sickness to occur. Although our findings do not provide irrefutable proof, they are consistent with a relation between gravito-inertial ambiguity resolution and motion sickness induced by translational accelerations.

A key finding is the *(H.3c) strong correlation ( $r = 0.74$ ) between an individual's average motion sickness sensitivity and their subjective vertical time constant*. To confirm this wasn't just due to the complex determination of the overall sickness using the



mean SI we also computed the correlation between mean MISC and the subjective vertical time constant, this was  $r(17) = 0.8$  ( $p = 0.0001$ ). To the authors' knowledge, such a correlation has not been reported in the literature. Literature does, however, report on the importance of the velocity storage time constant as a marker for sensitivity (Dai et al., 2003, 2007). In our experiment this correlation was not evident ( $r = 0.32$ ). The likely reason for this is the absence of any rotational stimuli in our experimental paradigm that would contribute to sickness. In studies that did find a correlation with the velocity storage time constant, rotational motions were used to induce sickness, namely, the cross-coupled coriolis stimulation. Our results thus suggest that for purely translational stimuli, the subjective vertical time constant is a major determinant of sensitivity.

To summarize, the time constant of the subjective vertical is positively correlated with the overall sickness sensitivity. It is also known from literature that the subjective vertical time constant is determined by the frequency properties of gravito-inertial ambiguity resolution (Laurens and Angelaki, 2011). Moreover, we know from our study that individuals have substantial variance in their frequency sensitivities. However, contrary to our initial expectation, we did not find a correlation between the subjective vertical time constant and the frequency sensitivity of individuals that might explain this variance. Given what is known about the relevance of the subjective vertical time to spatial orientation and, (as this study also finds) to general sickness sensitivity, this is surprising. Hence, further investigations should be devoted to the subjective vertical time constant and the cross-over frequency. One way to do this is, just as Dai et al. (2003) had done for the velocity storage time constant, is by studying the effect of motion sickness habituation on the subjective vertical time constant. Another way is by explicitly attempting to measure the cross-over frequency and comparing the sickness seen here with adjacent frequencies.

### 4.5.5. LIMITATIONS

The statistical analyses in this study provided limited support for conclusions on frequency sensitivity. The reason for this is twofold. As discussed above, one part of the issue is the choice of a statistical criterion (AIC vs BIC). Since there is no single true or correct way to resolve this, we must rely on theoretical considerations (Dziak et al., 2019). A second issue, which arguably affects any study on motion sickness, is that there was only a limited number of observations available and that these observations are to some extent corrupted by noise, i.e., the signal-to-noise ratio. The range of frequencies tested may not have been large enough to capture the peak sensitivity for all individuals. The thresholding at 0.15 Hz means that the spectral centroid can never be less than 0.15 Hz. This has important implications for the correlations between the spectral centroid and the self-motion parameters. Participants who were sensitive to lower frequencies and likely had even lower spectral-centroids were biased towards higher values, therefore, potentially reducing the significance of the correlation we found between the spectral centroid and the self-motion parameters.

The choice of frequencies was a compromise between, on the one hand, the range of frequencies where motion sickness may peak according to the literature and the minimum amplitude required to induce sickness, and on the other hand the limi-



tations of the simulator. To increase the signal-to-noise ratio as well as reduce bias, future studies may test a broader range of frequencies and/or increase the motion amplitude.

Statistical power can be enhanced increasing the number of repetitions. However, this presents logistical and dropout related difficulties associated with getting the same participant to become sick on a weekly basis for multiple months. To illustrate, in the present experiment, it took more than a month of continuous testing to obtain a single data point for five frequencies for a sample of 23 participants. Each of these participants was required to return to the experimental facility six times (including the experimental session for collection of perception data). Simply collecting one additional repetition for each experimental condition requires nearly twice that amount of time for data collection and the number of visits for each participant.

In future studies, it may also be possible to increase the signal-to-noise ratio by collecting and merging different kinds of data. In the present study, we did this by combining the MISC and MSAQ data into a Sickness Index. Similarly, we recorded eye-movements with the intent to combine this data with the perception data to improve the state-estimation, but these recordings unfortunately were not of sufficient quality for further analysis. Finally, the cross-over frequency was not directly measured but inferred from the MSOM. There may be inaccuracies introduced by fitting the model; measuring the cross-over frequency directly by adopting a different experimental paradigm may also contribute to our understanding of its relation to motion sickness.

This study was designed to relate motion sickness to motion perception and did not investigate postural instability (Riccio and Stoffregen, 1991). Future studies could in particular relate the subjective vertical time constant to postural stabilisation through experiments and models of sensory integration, postural stabilisation and motion sickness development.

#### 4.6. CONCLUSION

This study investigated individual frequency sensitivity of motion sickness to fore-aft accelerations and its relationship to individual parameters of motion perception. We found that at a group level, sickness sensitivity was frequency invariant from 0.15-0.5 Hz. Importantly we found support for differing frequency sensitivity to motion sickness between individuals, with some being susceptible to low-frequency motions, others to intermediate and others to high-frequency accelerations. Therefore, group sensitivity does not represent individual sensitivities. We observed no significant correlations between the velocity storage time constant, the subjective vertical time constant and cross-over frequency and motion sickness frequency sensitivity. This may be due to the limited number of observations. The direction of the effects, however, does support the notion that the cross-over frequency, which is the point of maximum perceptual ambiguity between acceleration and gravity perception, is indicative of the frequency at which the sickness response has its maximum. Moreover, we observed a strong correlation ( $r = 0.74$ ) between the subjective vertical time constant and overall sickness sensitivity. This may be indicative of the importance of verticality perception to sickness development during exposure to

## 4.6. CONCLUSION

---

translational sickness stimuli.

These findings are of particular significance to motion sickness modelling and indicate that aetiologically valid models should fit individual, rather than group-level, frequency sensitivities. Additionally, our results indicate that future models should take into account the apparent relationship between the subjective vertical time constant and the overall motion sickness sensitivity. Lastly, the results are of particular significance to the automotive community, as they highlight the individual nature of motion sickness and the need for caution when using group sickness sensitivities to tune vehicle controllers for the reduction of motion sickness.



# 5

## VALIDATION OF PERCEPTION MODELS FOR MOTION SICKNESS PREDICTION

---

This chapter is to be submitted to Biological Cybernetics, as: Tugrul Irmak, Daan M. Pool, Ksander N. de Winkel, Riender Happee, Validation of Perception Models for Motion Sickness Prediction

## 5.1. ABSTRACT

*The human motion perception system has long been linked to motion sickness through state estimation conflict terms. However, to date, the extent to which available perception models are able to predict motion sickness, or which of the employed perceptual mechanisms are of most relevance to sickness prediction, has not been studied. In this study, the Subjective Vertical model, the Multi-Sensory Observer model and the probabilistic Particle Filter model were all validated for their ability to predict motion perception and sickness, across a large set of motion paradigms of varying complexity from literature. It was found that even though the models provided a good match for the perception paradigms studied, they could not be made to capture the full range of motion sickness observations. The resolution of the gravito-inertial ambiguity has been identified to require further attention, as key model parameters selected to match perception data did not optimally match motion sickness data. Two additional mechanisms that may enable better future predictive models of sickness have, however, been identified. Firstly, active estimation of the magnitude of gravity appears to be instrumental for predicting motion sickness induced by vertical accelerations. Secondly, the model analysis showed that the influence of the semicircular canals on the somatogravic effect may explain the differences in the dynamics observed for motion sickness induced by vertical and horizontal plane accelerations.*

## 5.2. INTRODUCTION

Motion sickness is a syndrome whereby aggravating body motions trigger autonomic symptoms such as salivating, dizziness, headaches, panting, hot/cold flushes, stomach awareness, nausea and vomiting (Bertolini and Straumann, 2016; Bos et al., 2005). Chronic exposure to sickening motions may lead to the sopite syndrome, which is associated with lethargy, fatigue and drowsiness (Matsangas and Mccauley, 2014). The exact mechanisms of motion sickness and its time evolution are still poorly understood. Many experimental motion paradigms are, however, known to illicit sickness and sickness is encountered in common modes of transport. Sickness dynamics can be very different from paradigm to paradigm. For instance, humans seem to have a wide band-pass sickness sensitivity to pure lateral acceleration, achieving maximum sickness over a frequency band from 0.03-0.3 Hz (Donohew and Griffin, 2004). For pure vertical acceleration, the sensitivity is narrower, peaking at a distinct centre frequency of approximately 0.2 Hz (O'Hanlon and McCauley, 1974). Moreover, while translational accelerations may lead to sickness in minutes, Earth-vertical yaw rotation (which on its own is not sickening) when coupled with roll leads to vomiting within tens of seconds. Sickness thus exhibits a complex dependency on the frequency, amplitude and direction of motion stimuli.

Reason (1978) argued that sickness was due to sensory conflict. This conflict is the difference between sensed sensory signals and the sensory signals predicted by the brain. The predictions originate from an internal model, which takes the form of a neural store. The neural store can be interpreted as a memory for concurrent patterns of efferent signals (e.g. motor commands) and re-afferent signals (i.e. sensory signals) (Held, 1961). Oman (1982) likened this conceptual model to the manner by which a Luenberger Observer (LO) operates. The LO uses an internal model of

the system (body) and sensor dynamics to estimate the state of the system. Due to the imperfect and noisy nature of the sensory signals, one cannot use the sensor measurements directly. Instead, the true states of the system must be observed (estimated) by using sensory information together with an internal model of the system itself. These estimated states are then used for task planning and execution. To quantify estimation accuracy, the central state estimates are passed through the internal model of sensory dynamics and compared with the actual sensory signals. The resulting error is the estimation error, or the sensory-expectancy conflict. This conflict is used to drive the state estimation towards the true state, and to adapt the parameters of the internal model, such that they make better predictions. It is hypothesized that the conflict accumulates over time in a process that resembles leaky integration, resulting in motion sickness.

A more specific example of this general principle was used in Merfeld et al. (1993) to model the phenomenon of velocity storage. When subject to constant velocity earth vertical yaw rotations, the rate of neural spikes originating from the hair cells of the semicircular canals decay toward baseline in 4-5 s. This is because, due to viscous forces, the relative velocity between the endolymph fluid and the hair cells is a transient phenomenon. Velocity storage is the apparent extension in the time constants of angular velocity perception and the angular vestibular-ocular reflex, compared to the raw semicircular canal signal. In Merfeld et al. (1993) it was hypothesized that the velocity storage manifested itself due to the actions of the central nervous system (CNS) similar to the LO shown in Figure 5.1.

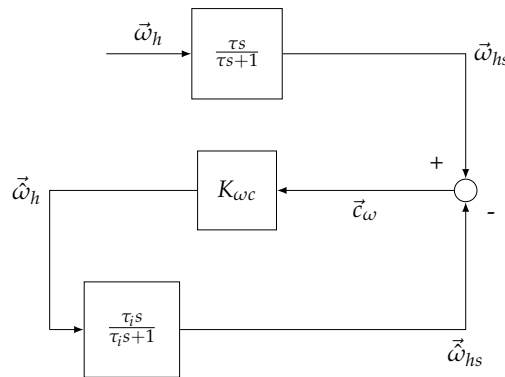


**Fig. 5.1** The hypothesised mechanism of velocity storage. The real angular velocity of the head  $\vec{\omega}_h$  is measured by the semicircular canals. This measurement is imperfect and results in the high-pass filtering of the head angular velocity into  $\vec{\omega}_{hs}$ . This is compared with the output of the internally predicted semicircular canal output,  $\vec{\omega}_{hs}$ . The difference between the two is the conflict and is passed through the gain  $K_{\omega c}$  to give an estimate of the real head angular velocity,  $\vec{\omega}_h$ .

Here, the semicircular canals sense the head angular velocity  $\omega_h$  with first-order high-pass dynamics with a time constant of approximately 4-5 s (Merfeld et al., 1999), resulting in  $\omega_{hs}$ . The CNS wishes to observe the real head angular velocity. For this, it compares the output of the internal model, which is the expected sensed head angular velocity  $\hat{\omega}_{hs}$ , with the actual sensed head angular velocity  $\omega_{hs}$ .

It uses the conflict between the two to drive the observed angular velocity  $\hat{\omega}_h$ , until the actual sensed and internally estimated velocities match.

In a Spatial Orientation Model (SOM), which Figure 5.1 shown above is an example of, the concept of the LO is generally simplified to consider only the sensors and their internal representations; disregarding internal models of the body. The main purpose of these models is to develop an understanding of the systems governing motion perception and reflexive actions in humans. Here, for example, motion perception may be measured by asking for participant reports of their subjective vertical, or their angular velocity by turning a hand dial (Bertolini et al., 2011b; Correia Gracio et al., 2013; de Winkel et al., 2018). Reflexive actions may be measured by electro-oculography for eye movements and IMUs for posture. As such, SOMs have seen use in a wide range of contexts: from studying how erroneous motion perception may lead to air traffic accidents (Newman et al., 2012; Borah et al., 1988), to the underlying causes of vestibular disorders and courses of diagnosis and treatment (Holly and Harmon, 2013).

The SOM framework (as shown in Figure 5.1) naturally results in conflict terms. Although there are qualitative differences between motion perception and reflexive actions, motion sickness per se appears to be mainly related to low-frequency movements, where perception and action are often in agreement (Merfeld et al., 2005b). Moreover, Merfeld et al. (2005c) find that perception is best modelled by the internal model framework. This framework has also been the basis of various motion sickness models. For instance, Zupan et al. (1994) and Denise (1993) extended their perception and action sensory weighting model (SWM) to predict motion sickness experienced during OVAR. Here the conflict was generated between the central state estimate and a *coherence copy* of the head angular velocity, which is the same signal, but computed from other centrally coded variables (for example, the primary organs measuring head angular velocity are the semicircular canals, but head rotation with respect to the gravity vector may also be computed from otolith information). Likewise, Bos and Bles (1998) independently extended their SOM to predict the frequency response of sickness to vertical translational accelerations (VTA). Unlike the SWM, this model hypothesised that the only conflict of importance was the conflict between the sensed vertical and the estimated vertical, and was thus named the Subjective Vertical Model (SVM). Predictions made by this model provided an accurate match to empirical sickness data collected by O'Hanlon and McCauley (1974), and has recently been extended to model the effect of learning exogenous motion dynamics on motion sickness development (Wada, 2021).

Although SOMs all have the purpose of enhancing our understanding of the systems governing motion perception and reflexive actions, the proposed models have very different structures. Most models focus on vestibular-only perception, reflecting darkness or eyes-closed conditions or conditions where visual motion perception is less relevant. Likewise, this paper focuses on vestibular-only perception. Here, structural differences between SOMs are mainly related to the various mechanisms employed to perform gravito-inertial ambiguity resolution. This ambiguity resolution is necessary because the otoliths do not report inertial acceleration separately from gravity acceleration. Instead, due to Einstein's equivalence principle, these are

reported in the form of a combined vector named the gravito-inertial acceleration or specific force. For appropriate actuation of effectors, this combined vector must be decomposed into acceleration and gravity.

For instance, the SVM performs gravito-inertial ambiguity resolution by first pre-filtering the input gravito-inertial acceleration. The low-pass filter output is the sensed gravity and the high-pass filter output is the sensed acceleration; this is known as frequency segregation. Other models do not include such an explicit frequency segregation. Such differences lead to different conflict dynamics, and to different sickness predictions.

In the present study, we aim to identify pathways and underlying dynamics that predict motion sickness. To do so, we compare structurally different vestibular-only SOMs, taking into consideration the accumulated body of motion perception and motion sickness data. The work will not be limited to specific conflicts or degrees of freedom, but will explore the relationship between the conflict magnitude of the different sensory channels in various well-known motion paradigms. Ultimately, this study should contribute to models that can serve to prevent motion sickness when used to design technology. This is particularly relevant in the context of self-driving car sickness (Salter et al., 2019; Diels and Bos, 2016).

We will compare three structurally distinct SOMs: the Subjective Vertical Model (SVM) (Bles et al., 1998; Bos and Bles, 1998, 2002b) where the final model implementation is based on Kamiji et al. (2007), the Multi-Sensory Observer Model (MSOM) (Newman, 2009) and the Particle Filter Model (PFM) (Laurens and Droulez, 2007, 2008). The choice of these models is motivated by a number of considerations. The SVM has been used extensively as the basis of a number of motion sickness studies in ships and cars (Kamiji et al., 2007; Wada et al., 2015; Turan et al., 2009; Khalid et al., 2011a; Wada, 2021). The MSOM model was developed principally to evaluate disorientation in the context of aircraft operation (Newman et al., 2012; Kravets et al., 2021). The choice of the PFM is aimed at including probabilistic modelling to study motion perception and sickness. The particle filter is an optimal estimator used for highly non-linear state estimation without the assumption of Gaussian noise. This is contrary to the other two methods. Filtering performance may yield novel insights, particularly for highly non-linear motions experienced during, for instance, the cross-coupled coriolis motion paradigm. Overall, comparing model performance allows for the identification of responsible mechanisms.

It should be noted that there are other models, such as the previously mentioned SWM. However, the key mechanisms within these models overlap with the chosen three. Inclusion of these models would therefore increase the volume of work, but is unlikely to provide additional insights. Where possible, we linearised the SOMs and performed an analytical evaluation of their conflict dynamics. We then performed simulations of the full model responses to various well-known perception and sickness motion paradigms. In this chapter, the models were tuned independently to fit both the sickness and the perception data available in the literature. The models, along with the two tunings, were then validated against a second sickness dataset using a range of data from the literature (Dai et al., 2003; Howarth and Griffin, 2003; Donohew and Griffin, 2004; O’Hanlon and McCauley, 1974; Bijveld et al., 2008; Cian



et al., 2011).

### 5.3. MODELS & METHODS

In this chapter, we followed a three-step methodology:

1. We linearised the models and performed an analytical analysis of the sensory-expectancy conflict terms. This was done for translational acceleration inputs.
2. Model parameters were tuned to literature datasets for both motion perception and sickness. This allowed us to further quantify the validity of the models and evaluate the relationship between perception and motion sickness.
3. Numerical simulations were then run using the full models, for both the simple motion input cases and the more complex input cases. The simulated sensory conflicts were then fed through a motion sickness accumulation model. The sickness predictions resulting from this were compared with experimental sickness observations from a validation dataset.

#### 5.3.1. MODELS

We selected three structurally distinct SOMs as a representative sample of the variety of models available in the literature. These models are the SVM, the MSOM, and the PFM. The vestibular inputs to the models are head gravito-inertial force ( $\vec{f}_h$ ) and head angular velocity ( $\vec{\omega}_h$ ). Head gravito-inertial force is measured by the otolith vestibular organ and is a sum of the inertial force and gravity. Head angular velocity is measured by the semicircular canals. The inputs are all in the head frame of reference. The model outputs are estimates of: head referenced gravity ( $\vec{g}_h$ ), head referenced translational acceleration ( $\vec{a}_h$ ), head referenced velocity ( $\vec{v}_h$ ), head referenced angular velocity ( $\vec{\omega}_h$ ) and an estimate of the orientation ( $\vec{\theta}$ ) of the head with respect to earth. All models assume passive motion. Body dynamics and self-motion control inputs are not considered.

The vestibular inputs required for the numerical simulations are computed by modelling a hypothetical motion simulator used to generate the motions (e.g. OVAR) as a kinematic chain. Here, a three-joint system is formulated using standard Denavit-Hartenberg notation and the experienced motions are computed in a feed-forward manner. The motion implementation is documented in detail in Appendix C.1. All motion paradigms are simulated in darkness, using the vestibular-only models. All simulations were run with a time step of 0.01 s using the Runge-Kutta method for the MSOM and SVM, and the Euler-method for the PFM. The computational time requirements were much larger for the PFM, which was simulated with 800 particles. In the following, we describe each model in detail.

#### SUBJECTIVE VERTICAL MODEL (SVM)

The SVM, shown in Figure 5.2, is composed of three main parts: **A** the sensing module, **B** the feedback gain module and **C** the internal model module. The head referenced gravito-inertial force and angular velocity is input through **A** to create sensed

gravity, acceleration and angular velocity. To do this it is assumed that the central nervous system first conducts preprocessing in the form of frequency segregation on the gravito-inertial force, by high- and low-pass filtering it into accelerations and gravity components, respectively. The sensed gravity from this operation is then summed with the change in the orientation of the gravity vector as sensed by the semicircular canals. Both operations can be expressed with the so-called Mayne equation (Mayne, 1974):

$$\frac{d\vec{g}_{hs}}{dt} = \frac{1}{\tau_{lp}}(\vec{f}_h - \vec{g}_{hs}) - \vec{\omega}_{hs} \times \vec{g}_{hs} \quad (5.1)$$

Here,  $\vec{g}_{hs}$  is the sensed estimated gravity vector,  $\tau_{lp}$  is the time constant of the low-pass filter and  $\vec{\omega}_{hs}$  is the head angular velocity sensed by the semicircular canals.

The sensed states of acceleration, gravity and head angular velocity are then compared to the internal estimates of these states. The difference between the sensed and the internal state estimates is called the *sensory conflict*. The sensory conflict terms are given as: angular velocity conflict  $\vec{c}_\omega$ , gravity conflict  $\vec{c}_g$  and acceleration conflict  $\vec{c}_a$ . The conflicts are then fed back into the internal model via the gain module **B**.

In the feedback gain module, the gravity and acceleration conflicts are passed through the integral gains,  $\frac{K_{gc}}{s}$  and  $\frac{K_{ac}}{s}$ , while the angular velocity conflict is passed through a proportional gain,  $K_{\omega c}$ . These outputs are summed to create the estimated gravito-inertial force. This is passed to the internal model module **C**, which has the same structure as the sensing module **A**. The human perceives and reports the subsequent estimates,  $\vec{g}_h$ ,  $\vec{a}_h$  and  $\vec{\omega}_h$  during perception investigations. The purpose of the internal model **C** is to track the sensed quantities. Bos and Bles (1998) argue that it is the error in the tracking, which is caused by a frequency-dependent phase lag, that leads to sickness.

For translational acceleration inputs, the conflict terms of the model shown in Figure 5.2 are derived in Appendix C.3. This results in the following transfer functions:

$$\frac{\vec{c}_g(s)}{\vec{f}_h(s)} = \frac{s}{\tau_{lp}s^2 + (1 + K_a\tau_{lp})s + K_g} \quad (5.2)$$

$$\frac{\vec{c}_a(s)}{\vec{f}_h(s)} = \frac{s^2\tau_{lp}}{\tau_{lp}s^2 + (1 + K_a\tau_{lp})s + K_g} \quad (5.3)$$

In equation 5.3 the acceleration conflict  $\vec{c}_a$  has high-pass dynamics. As stated in the Section 5.2, sickness due to horizontal accelerations has band-pass behaviour. Therefore,  $\vec{c}_a$  is inappropriate for sickness modelling. The gravity conflict  $\vec{c}_g$  has the desired band-pass dynamics. As seen in equations 5.2 and 5.3, the semicircular canal dynamics do not influence the conflicts due to perceived horizontal and vertical accelerations. This also means that the only way to create a difference in the dynamics of the sickness response between vertical and horizontal accelerations is by having a different set of values for the parameters  $\tau_{lp}$ ,  $K_g$  and  $K_a$  for the different motion

directions. Note that due to a lack of a coupling between acceleration input and angular velocity perception, an angular velocity conflict is absent without a rotational input  $\omega_h$  in the SVM.

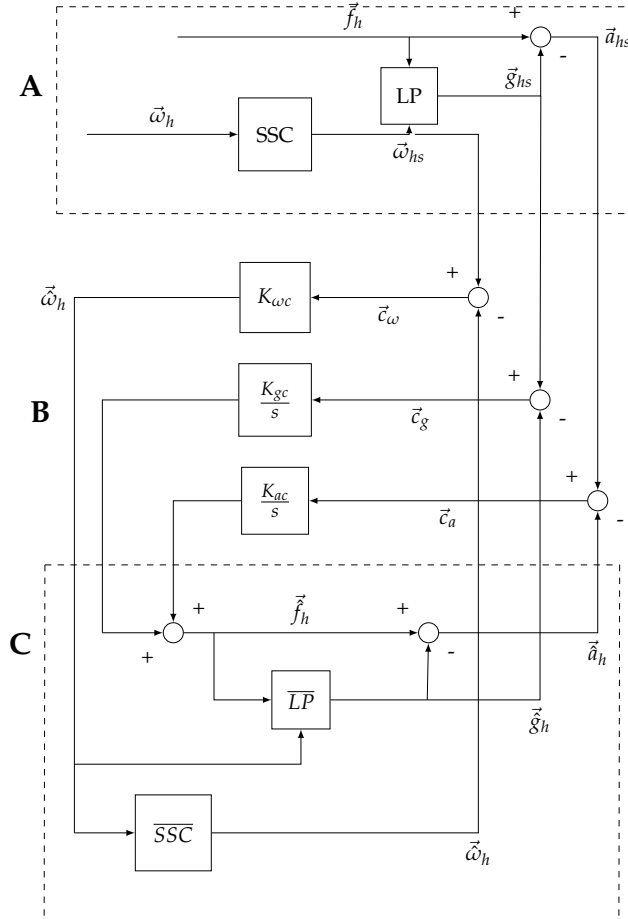


**Fig. 5.2** The Subjective Vertical model. It is parameterized by:  $K_{ac}$  is the acceleration feedback gain into the internal model in the form of an integral feedback  $\frac{K_{ac}}{s}$ ,  $K_{gc}$  is the gravity feedback gain into the internal model in the form of an integral feedback  $\frac{K_{gc}}{s}$ ,  $K_{\omega c}$  is the angular velocity conflict feedback gain into the internal model in the form of a proportional feedback  $SSC$  and  $\overline{SSC}$  are first-order high-pass filters representing sensor dynamics of the semicircular canals,  $LP$  and  $\vec{LP}$  are first-order low-pass filters capturing gravity estimation according to the Mayne equation.

### MULTI-SENSORY OBSERVER MODEL

The MSOM (Figure 5.3) functions as a classical observer model, whereby the sensory afferent signals are directly used by the internal model, which contains an internal representation of sensor dynamics coupled to the physical relationships be-

tween different states. It has a more integrated structure than the SVM and cannot be easily segmented into different modules. Here, the inputs to the model are the gravito-inertial force  $\vec{f}_h$  and the head angular velocity  $\vec{\omega}_h$ , both in the head frame of reference. These inputs are measured by otoliths (OTO) and the semicircular canals (SSC), respectively, to produce afferent sensory signals. These sensory signals are compared to an internally expected gravito-inertial force  $\vec{f}_h^{\tilde{}}$  and angular velocity  $\vec{\omega}_h^{\tilde{}}$ . These lead to the otolith magnitude and angular velocity sensory conflict terms,  $\vec{c}_o$  and  $\vec{c}_\omega$ . The angular velocity conflict is multiplied by a gain  $K_\omega$  and then added to the angular velocity calculated from the otoliths to create the estimated head angular velocity  $\vec{\omega}_h^{\tilde{}}$ . This angular velocity is multiplied by a gain  $K_1$  (where  $K_1 = \frac{K_{\omega f} + 1}{K_\omega}$ ) and added again to the head angular velocity estimated from the otoliths. This is then used to rotate the gravity vector toward the internally expected angular position of the head. In this, as it has implications for model dynamics, it is important to note (as discussed below) that the magnitude of the estimated gravity  $\vec{g}_h^{\tilde{}}$  is always  $-9.81 \text{ ms}^{-2}$ . Only the vector components of this estimation change when rotated by angular signals from the otolith and the semicircular canal path. The newly computed gravity is summed with the acceleration estimate to create the internally expected gravito-inertial force  $\vec{f}_h^{\tilde{}}$ . The angular signal from the otoliths is derived by computing the angular difference between the expected and the sensed gravito-inertial force. This is the third sensory conflict, called otolith angle conflict,  $\vec{c}_{oa}$ . This is obtained by taking the cross-product of  $\vec{f}_h^{\tilde{}}$  and  $\vec{f}_h$ .

In the MSOM, the estimated gravity vector only changes due to a rotation signal from the otolith angle conflict or the semicircular canals. Unlike the SVM, the magnitude of the estimated gravity  $\hat{g}_h$  is always assumed to be constant of  $-9.81 \text{ ms}^{-2}$ . This causes important differences in the dynamics of the MSOM compared to the dynamics of the SVM. For instance, for vertical acceleration inputs there is no rotation signal, so the estimated gravity remains constant and the remaining gravito-inertial force is attributed to acceleration. Therefore, the only conflict that occurs during vertical acceleration is the otolith magnitude conflict, for which the frequency response takes the form:

$$\frac{c_{oz}(j\omega)}{f_{hz}(j\omega)} = \frac{1}{1 - K_a} \quad (5.4)$$

Irrespective of the value of  $K_a$ , equation 5.4 shows that the conflict response will be independent of acceleration frequency. As stated in Section 5.2 vertical sickness sensitivity in humans is narrow band-pass, with a centre frequency of approximately 0.2 Hz. Therefore, this is inappropriate for sickness prediction. One can change the gain  $K_a$  to integral or differential, which will result in high-pass or low-pass dynamics, respectively, but this would not resolve the fundamental issue. Even though more complex feedback gain combinations may be employed to correct this, any changes in the conflict dynamics would also change the dynamics of the acceleration estimate from high-pass to a more complex frequency response, due to

$$\hat{a}_{hz}(j\omega) = K_a c_{oz}(j\omega) . \quad (5.5)$$

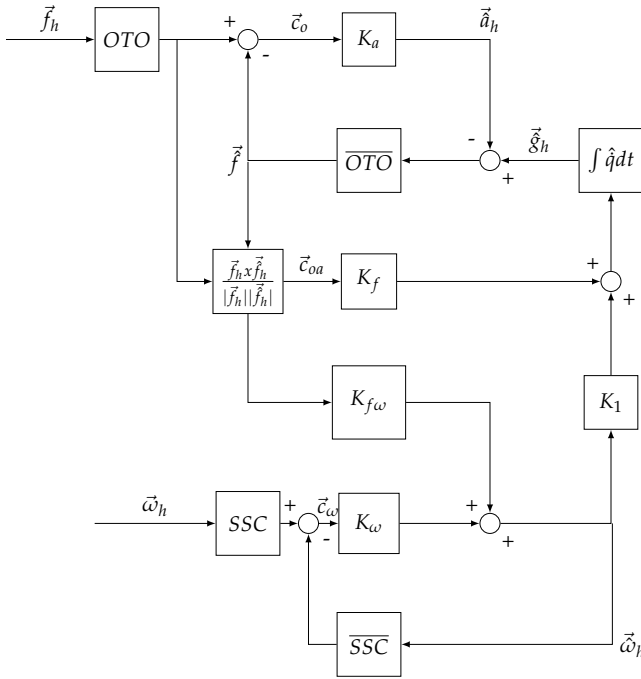


**Fig. 5.3** The Multisensory Observer model. It is parameterized by:  $K_a$ , which multiplies the otolith magnitude conflict to create the internally estimated acceleration  $\vec{a}_h$ ,  $K_f$ , which multiplies the otolith angle conflict to create the angular velocity computed from the angular difference between the internally estimated and sensed gravito-inertial force  $\vec{f}_h$  and  $\vec{f}_h$ ,  $K_{f\omega}$ , which has the same function but instead of being used to compute a new gravity estimate it is summed to create an internal estimate of angular velocity  $\vec{\omega}_h$ , and  $K_{\omega}$ , which multiplies the angular velocity conflict. The subsequent signal is summed with the estimate of angular velocity coming from  $K_{f\omega}$ . SSC and  $\overline{SSC}$  are first-order high-pass filters denoting the semicircular canals and the internal model of the semicircular canals, respectively, and lastly, OTO and  $\overline{OTO}$  are unit transfer functions denoting the otoliths and the internal model of the otoliths, respectively

Experiments thus far have not, however, shown such complex acceleration perception responses (Merfeld et al., 2005b). For lateral acceleration inputs, if one assumes no cross-talk between otolith computed angle and the integrated semicircular canal output by setting  $K_{f\omega}$  to zero (as derived in Appendix C.4), the frequency response of the conflict terms take the form:

$$\frac{c_{oy}(s)}{f_{hy}(s)} = \frac{s}{s(1 - K_a) + K_f} \quad (5.6)$$

$$\frac{c_{oay}(s)}{f_{hy}(s)} = -\frac{c_{oy}}{|g|} \quad (5.7)$$

In equation 5.6 it can be seen that indeed the otolith magnitude error response is high-pass. Likewise, the otolith angle error is just a factor of  $g_z$  smaller in magnitude. Just as for vertical inputs, the gains can be set in such a way that the resulting conflict frequency response approximates the observed lateral sickness response. However, doing so will also affect the high-pass dynamics of the acceleration estimate.

### PARTICLE FILTER MODEL

As shown in Figure 5.4, the PFM works on a distinctly different principle than the SVM and MSOM. It is composed of two major parts: the forward propagation, which consists of the prior distribution and the likelihood weighting and the subsequent re-sampling, which determines the final posterior distribution. The posterior distribution is propagated solely from the semicircular canal signal. Using the notation used by [Laurens and Droulez \(2007\)](#), for any given particle,  $i$  Gaussian noise  $w_t^i$  is added to the average sensed canal signal (at the previous time step)  $\vec{V}_{t-1}$  creating  $\vec{C}_t^i$ . From this the angular velocity of the particle,  $\Omega_t^i$  is computed by directly inverting the canal equation:

$$\omega_t^i = \omega_{t-1}^i - T_{can}^{-1} \frac{\vec{C}_t^i \delta t}{T_c} - T_{can}^{-1} (\vec{C}_t^i - \vec{C}_{t-1}^i) \quad (5.8)$$

This angular velocity integrated over time gives the rotation of the particle  $i$  from time  $t - 1$  to  $t$ :  $R(\Omega_t^i \delta t)$ . This, when multiplied with particle orientation from  $t = 0$  to  $t - 1$  gives the orientation of each particle at  $t$  specified by  $\Theta_t^i$ . This is the particle-to-earth transformation matrix, from which the earth referenced acceleration  $\vec{A}_t^i$  can be computed. Note that the magnitude of gravity  $|G|$  (Figure 5.4) is earth referenced and assumed, just like in the MSOM, to be constant at  $-9.81 \text{ ms}^{-2}$ . Collecting all the states gives the prior distribution. Each particle is then weighted with respect to the state transition probabilities. The assumption is that the brain assigns the greatest probability to stationary states. Thus, the particles that are closest to zero acceleration and angular velocity are weighted the highest. This weighing factor is given by  $P(\vec{A}_t)P(\Omega_t)$ , which is defined to have a Gaussian distribution. Thus, the further down the tails of the distribution the particle acceleration or angular velocity is, the lower its weight. After the weighing, the particles are sampled with a probability proportional to their weight.

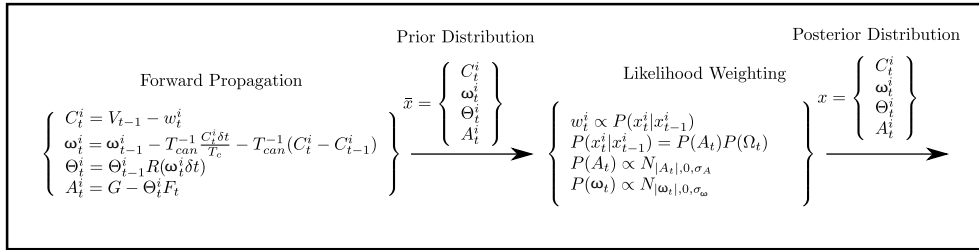


**Fig. 5.4** The Particle Filter model. It is parameterized by: the weighting factor  $w_t^i$  given by a multiplication of Gaussian priors (of mean zero and variance  $\sigma_A$  and  $\sigma_\omega$ ) on the inertial acceleration  $P(\vec{A}_t)$  and angular velocity  $P(\omega_t)$ , the head-to-canal transformation matrix  $T_{can}^{-1}$ , the integration time step  $\delta t$  and the canal time constant  $T_c$

For the PFM, no conflict terms are explicitly present, but an angular velocity conflict can be calculated in the form

$$\vec{c}_\omega(t) = SSC(\vec{\omega}_h(t)) - \overline{SSC}(\vec{\omega}_h(t)) \quad (5.9)$$

Here  $SSC$  is the function giving the output of the semicircular canals,  $\vec{\omega}_h$  is the angular velocity of the head and  $\vec{\omega}_h^i$  is the internally estimated angular velocity of the head. There are, however, no otolith or acceleration/gravity conflict terms. This is because inverting the otolith equation to estimate acceleration and gravity requires the sensed gravito-inertial force. Summing the gravity estimate and acceleration estimate gives back the same sensed gravito-inertial force, meaning an otolith conflict cannot be calculated for the PFM.

### 5.3.2. MOTION SICKNESS ACCUMULATION MODEL

An example of how the conflict terms are mapped to the accumulation of a sickness metric is given for the SVM (Bos and Bles, 1998). Here, the gravity conflict,  $\vec{c}_g$  is taken, and its magnitude is computed and scaled according to a Hill function of the form

$$h = \frac{(|\vec{c}_g|/b)^n}{1 + (|\vec{c}_g|/b)^n} \quad (5.10)$$

where  $h$  is the scaled conflict and  $n$  and  $b$  are the parameters of the chosen Hill function. After this scaling, a second-order system of the form

$$MSI = \frac{P}{(\mu s + 1)^2} h \quad (5.11)$$

integrates the conflict over time to predict motion sickness incidence (MSI), which is the percentage of people that have vomited from time zero to time current. Where  $P$  and  $\mu$  are the parameters dictating how the conflict is accumulated. Thus, the SVM includes four additional parameters ( $b$ ,  $n$ ,  $P$  and  $\mu$ ) to describe motion sickness accumulation.

Khalid et al. (2011a) tried to extend the SVM to describe horizontal motion sickness. Here they note that the subjective horizontal conflict is like a high-pass filter "*which should be adjusted (by low-pass filtering) before being translated into the MSI*". However, with such a filter, any experimentally observed frequency dependency of motion sickness susceptibility could be matched, reducing model uniqueness. This would also mean the need for at least two extra parameters to obtain band-pass characteristics, and these would not have any physiological basis.

Therefore, in the current study, the absolute value of each conflict term is computed. The consequent terms are then scaled and integrated over time. These two operations do influence the predicted sickness frequency response. However, they are applied to the absolute value of the conflict signal, which has most of its power in its DC bias term (0 Hz), as shown in the Appendix C.2. Such operations therefore have a negligible effect on the frequency response characteristics within the range of frequencies where sickness is observed.

Because the rest of our analysis will evaluate multiple motion paradigms, it is of greater utility to use a simpler system that does not have the free parameters used in Bos and Bles (1998) for sickness accumulation. A simple integrator on the absolute conflict is sufficient. Each conflict term likely has a different importance weighting

$W_i$  for motion sickness. This weighting is found by optimizing the sickness predictions compared to measured sickness data. This means the sickness proxy, MS, used for this study is defined as

$$MS = \int_0^t \vec{W} \cdot |\vec{c}(t)| dt, \quad (5.12)$$

This MS is different but correlated to MSI, which was explicitly fitted to vomiting. Here,  $|\vec{c}(t)|$  is a vector whose elements are the magnitude of individual conflict types (i.e., angular velocity conflict and gravity conflict). For a given conflict type this magnitude is computed by assuming unit weight for all the components of this vector, i.e., the first element of  $|\vec{c}(t)|$  is

$$\sqrt{c_{gx}^2 + c_{gy}^2 + c_{gz}^2}.$$

Lastly, the current study utilises all available internal conflict terms. For the SVM these are the gravity conflict  $\vec{c}_g$ , acceleration conflict  $\vec{c}_a$  and angular velocity conflict  $\vec{c}_\omega$ . For the MSOM these are the magnitude of the conflict between the otolith signal and predicted otolith signal  $\vec{c}_o$ , angular velocity conflict  $\vec{c}_\omega$ , and otolith signal orientation and predicted signal orientation  $\vec{c}_{oa}$ . For the PFM, this is the angular velocity conflict  $\vec{c}_\omega(t)$ .

### 5.3.3. MODEL TUNING

In this chapter, the time-domain perception predictions of the models are first given for the parameter values reported in the literature where these, so called "untuned" parameters are based on [Bos and Bles \(2002a\)](#), [Bos and Bles \(1998\)](#) and [Kamiji et al. \(2007\)](#) for the SVM, [Newman \(2009\)](#) for the MSOM and [Laurens and Droulez \(2007\)](#), [Laurens and Droulez \(2008\)](#) for the PFM.

We then tuned the models to a number of data sets on empirical observations on motion perception and on motion sickness. Under the SOM framework, there is a coupling of perception and motion sickness dynamics. Therefore, a *perception tuning* is important for comparing structural, rather than parameter dependent differences between the models. The additional *sickness tuning* allows for the evaluation of how closely the models can fit experimentally observed sickness data, independent of perception. Evaluating both perception-tuned and sickness-tuned results together helps identify whether the SOM framework is effective for explaining motion sickness.

### PERCEPTION TUNING

Models were fitted to perception data for centrifugation, earth vertical axis rotation (EVAR) and off vertical axis rotation (OVAR). Data for centrifugation were obtained for eccentric rotations at  $36^\circ\text{s}^{-1}$  and  $60^\circ\text{s}^{-1}$ , associated with centripetal accelerations of  $2.41$  and  $6.7$   $\text{ms}^{-2}$ , respectively ([Graybiel and Brown, 1951](#));  $200^\circ\text{s}^{-1}/12.2$   $\text{ms}^{-2}$  ([Curthoys, 1996](#)); and  $250^\circ\text{s}^{-1}/10.3$   $\text{ms}^{-2}$  ([Merfeld et al., 2000](#)). In these studies, perceived orientations were measured by asking participants to report perceived roll by adjusting a bar to be in line with either the subjective horizontal or the subjective vertical. The angular displacement of the bar is a measure of the perceived tilt. Data for EVAR and OVAR were obtained from [Vingerhoets et al. \(2005\)](#). Seated



participants were tilted to  $\{0, 15, 30\}^\circ$  relative to Earth-vertical. In the  $0^\circ$  and  $30^\circ$  tilt conditions, participants were rotated at  $30^\circ\text{s}^{-1}$ ; in the  $15^\circ$  tilt condition, participants were rotated at  $\{20, 30, 40, 50\}^\circ\text{s}^{-1}$ . Participants were presented with a laser-projected dot moving across a screen. Using a toggle switch, subjects indicated how the speed of the dot had to be adjusted (faster or slower) in order for it to be perceived as space fixed. Hence, the adjustment of the dot speed was a measure of the perceived rotation velocity.

These conditions were simulated by feeding the corresponding motion signals to the perception models. Centrifugation was simulated for a participant sitting Earth vertically upright at a radius of 6.1 m, 1 m and 0.54 m from the centre of rotation. EVAR was simulated by rotating an earth vertically upright participant about the Earth vertical axis. OVAR was simulated tilting the participant off-vertical such that the long axis of the body makes an angle with the Earth vertical and rotating the participant about the long body axis. To ensure sufficient convergence, all simulations were run for 200 s of simulated time.

The perception models were fitted to the data by minimizing the symmetric mean absolute error (SMAE) between model and empirical data for time-domain signals of rotation perception during EVAR, roll perception during centrifugation, as well as translation and rotation perception during OVAR. In the process of optimizing the model parameters to fit the perception data, the models were first tuned to match an EVAR perception decay time constant of 18.7 s, as reported by [Vingerhoets et al. \(2005\)](#). This time constant reflects the 'velocity storage' mechanism, which is a neural mechanism that extends the perception of rotational velocity to persist for a period of time even when the semicircular canals have assumed a zero output during constant velocity rotation. This time constant is thought to be of particular importance to motion sickness because it correlates strongly with individual motion sickness sensitivity ([Dai et al., 2003, 2007](#); [Young et al., 2003](#)).

The EVAR paradigm was used for perception tuning because it is a pure rotation, which allows a direct estimation of this time constant. The consequence of fixing the EVAR time constant is that it reduces the dimensionality of the final optimization and so allows faster and better convergence. After fitting the models to match this time constant, the other internal model parameters were estimated.

The considered models are overparametrised, which causes many local minima in parameter estimation. Therefore, Simulated Annealing (SA) was used to estimate the global minimum. SA is a probabilistic technique used to approximate the solution to global optimization problems ([Henderson et al., 2006](#)) such as the one encountered here. Ten SA runs of 100 iterations were performed about the literature referenced parameter values. Model parameters belonging to the 10th percentile for lowest prediction error were identified. This resulted in up to 30 candidate parameter sets.

Subsequently, k-means clustering was used to cluster the candidate points to three regions. K-means was deemed appropriate, as parameter sets were grouped closely to each other. The validity of the identified regions was then verified by inspection. Local optimization using the interior-point algorithm was run on the three centroids. This tuning ensured that the final parameters result in representa-

tive modelling of perceptual phenomena across a wide domain.

#### SICKNESS TUNING

For the sickness tuning, the perception-tuned models were taken as the initial starting point. The models were then further tuned to available motion sickness data from literature. We used experimentally obtained frequency sensitivities for lateral translational accelerations (LTA) (Donohew and Griffin, 2004) and VTA (O’Hanlon and McCauley, 1974). These datasets are the only sickness paradigms with reliable data that could be used for optimization. Fitting on frequency sensitivities to sickness is common in motion sickness literature and has been done before for VTA and LTA by Bos and Bles (1998) and Khalid et al. (2011a), respectively, to tune the SVM.

#### 5.3.4. MODEL VALIDATION FOR SICKNESS

To judge the generalizability of the models, it is important for the validation dataset to be independent of the fitting datasets. For this purpose the three models were validated with respect to the predicted and experimentally observed motion sickness magnitude across five frequently used motion paradigms in motion sickness: cross-coupled coriolis perturbation (CCCP) (Dai et al., 2003), pure roll perturbation (PRP) (Howarth and Griffin, 2003), LTA (Donohew and Griffin, 2004), VTA (O’Hanlon and McCauley, 1974), and OVAR (Bijveld et al., 2008; Cian et al., 2011). Here, CCCP is performed by rotating participants earth vertically whilst rolling them in discrete steps about the naso-occipital axis. For CCCP, the waiting duration between each head roll was 10 s and each head roll took 2 s to perform. For PRP, LTA and VTA, the perturbation frequency was 0.2 Hz.

Unfortunately, there are no experiments that investigate motion sickness for all these paradigms over the same duration and using the same sickness rating scale. Therefore, the relative differences in sickness magnitude between these paradigms had to be inferred. Fortunately, however, the associated experiments have all based their rating system on motion sickness symptoms. Still, the termination points of these experiments are not consistent. For instance, experiments on PRP may not provoke nausea at all, or the number of participants that experience it may be too small for a reliable sickness proxy. For this reason, a commonly shared point of “mild symptoms with no nausea” is taken for this model comparison. The mean duration to reach this rating is used to characterize sickness intensity. Experimental studies on motion sickness led by Griffin (Howarth and Griffin, 2003; Donohew and Griffin, 2004) report a mean duration of 15 minutes for LTA and greater than 30 minutes for PRP. So, for the motion stimuli used by Griffin, LTA should be at least twice as provocative as PRP. The relative magnitude of VTA compared to LTA is a contentious topic. For example, unpublished observations by Mills and Griffin referred to in Donohew and Griffin (2004) report similar sickness ratings for both VTA and LTA. Golding et al. (1995), however, maintains that the sickness response is actually coupled to posture. Horizontal perturbations, when the participant is earth horizontal (lying down), are about half as provocative as vertical perturbations for an earth vertical participant (upright). On the other hand, horizontal perturbations for an upright participant are 2.5 to 1.8 times as provocative as upright vertical per-

turbations (Golding et al., 1995). Current models do not account for this possible posture dependency. Hence, in the present study, the tuned models were evaluated for upright seating. OVAR experiments in the dark (Bijveld et al., 2008; Cian et al., 2011) show that the duration for mean sickness to reach mild symptoms with no nausea is 2.1 minutes. This is a factor of 7 smaller than that reported for LTA. Lastly, for CCCP, there are no experiments which map the slow rise in sickness over time. This is mostly because sickness induced by CCCP is intense and quick (Dai et al., 2003). Investigators mainly focus on the number of head movements tolerated. In most cases, participants reach mild symptoms after 10-20 head turns. Therefore, the mean duration to reach mild symptoms with nausea can be said to be in the order of tens of seconds and so CCCP is estimated to be 100 times as sickening as the LTA paradigm used by Donohew and Griffin (2004). To summarise, the inferred relative sickness magnitudes are: CCCP 1, OVAR 0.07, LTA 0.01, VTA 0.005-0.02, PRP 0.005.

For validation in the frequency-domain, the motion paradigms of LTA from Donohew and Griffin (2004) and VTA from ISO 2631 (1997) were used, because these are the only sickness paradigms with reliable frequency-domain data that provides adequate information to perform an optimization. The frequency-domain data for Donohew and Griffin (2004) is based on the proportion of participants developing mild nausea when subject to horizontal accelerations for up to 30 minutes, whereas for ISO 2631 (1997) it is based on the proportion of participants vomiting when subject to vertical accelerations for up to 2 hours. In the experiments from which the data were obtained, the participants' heads were not constrained, but as head motion measurements are not available, seat motion was used as input to the perception models.

## 5.4. MODEL TUNING RESULTS

Following the procedure outlined in the [Model Tuning](#) section, the three models were tuned to data from perception and sickness experiments. Tuning reduces the parameter-dependent variability between the models, highlights the consequences of the structural differences identified in the previous sections, and allows us to evaluate whether perception predictions are consistent with sickness predictions and vice versa.

### 5.4.1. FIT TO EMPIRICAL PERCEPTION TIME-DOMAIN DATA

In the following, we evaluate how well models tuned to either perception time-domain data or sickness frequency-sensitivity data predict empirical time-domain perception data. The left column of [Figure 5.5](#) shows how the models perform using parameters reported in the literature; the centre and right columns, respectively, show the tuning to aggregated perception and sickness datasets obtained in the present study.

For EVAR ([Figure 5.5a](#)), the PFM and the SVM behave similarly: both converge exponentially to zero. In agreement with experimental data, the perceived rotational velocity fades in steady-state motion. The MSOM, however, eventually undershoots, indicating perception of counter-rotation to the initial direction of motion. The un-

ershoot here owes to the second-order nature of the semicircular canal dynamics employed by the original paper (Newman, 2009). For the perception tuning, the second-order semicircular dynamics used in Newman (2009) are simplified to a first-order system. After tuning, the EVAR time constant is set to 18.7 s for all the perception-tuned models (as shown in Figure 5.5b). The lower gain of the PFM for EVAR is due to the canal noise required for the model to function (Figure 5.5b). When the models are tuned to sickness (right column in Figure 5.5) it is seen that the time constant for the MSOM increases to substantially above experimental observations. The time constant for the SVM is not adapted, because the velocity storage in the SVM plays no role in sickness development due to lateral or vertical translational accelerations.

The second row of Figure 5.5 shows roll perception for centrifugation in the dark. The red line indicates the experimental observations by Merfeld et al. (2000). From fitting an exponential model of the form  $\Theta_x = A(1 - e^{-bt})$  to the perceived roll, the time constant  $b$  is 26.3 s. Oscillations are observed at the beginning of the simulation for the PFM in Figure 5.5d from  $t = 20$  s until  $t = 80$  s. These oscillations are due to the time step used. A large time step means that the estimate of orientation is different from the actual orientation, causing a misestimation of acceleration when the otolith equation is inverted. This phenomenon is proportional to the angular velocity at the point in time and the noise about this point in time. Therefore, under certain motion conditions, the particle filter is underdamped. The MSOM was initially tuned to the data from Graybiel and Brown (1951), for which the authors used a lower yaw rate of  $60 \text{ }^\circ\text{s}^{-1}$  than Merfeld's yaw rate of  $250 \text{ }^\circ\text{s}^{-1}$ . This higher yaw velocity perturbs the system such that the response overshoots and the estimation requires a longer time to converge. After perception tuning (Figure 5.5e), the predicted roll percept by the MSOM no longer has this overshoot. Likewise, the SVM also responds much faster to the stimuli. Lastly, there is a decrease in the time constant of the PFM from 52 s to 27 s, which is closer to the experimentally observed value of 22 s (Merfeld et al., 2000). It can be seen that tuning these results to sickness (Figure 5.5f) creates responses that do not match the perceptual data. The MSOM now has a very large time constant meaning slow convergence, likewise, SVM is slower also to converge than before.

The final modelled perceptual phenomenon is OVAR. The participant in this case first has a sense of rotation, which transitions into a sense of translation around a conic or cylindrical trajectory. Vingerhoets et al. (2005) evaluated motion perception for two components, rotation and translation. The untuned results for the two components are shown in Figures 5.5g and 5.5j. In Figure 5.5g, the MSOM and the PFM show a steady-state rotation bias. This rotation bias should create the perception of changing heading, which in experiments is only rarely observed (Wood et al., 2007; Vingerhoets et al., 2005). With the perception tuning, as shown on Figure 5.5k, this bias is removed for the MSOM. However, removing the bias is not feasible for the PFM without compromising its centrifugation fits. For all models, the sickness tuning (Figures 5.5l and 5.5i) yields a poorer match with the measured perception results for OVAR.

**Table 5.1** SVM parameters untuned, perception-tuned and sickness-tuned; untuned parameters are based on Bos and Bles (2002a), Bos and Bles (1998) and Kamiji et al. (2007). MSOM parameters; untuned parameters are published in Newman (2009). PFM parameters; untuned parameters published in Laurens and Droulez (2007) and Laurens and Droulez (2008).

	SVM				MSOM				PFM		
	Untuned	Percept	Sick		Untuned	Percept	Sick		Untuned	Percept	Sick
$\tau_{ssc}$ [s]	5.7	5.7	5.7	$\tau_{ssc}$ [s]	5.7	5.7	5.7	$\tau_{ssc}$ [s]	4	5.7	5.7
$\tau_{lp_{xy}}$ [s]	5	1.23	15.0	$K_a$	-4	-3.2	-7.2	$\sigma_c$ [ $^\circ s^{-1}$ ]	10	10	10
$\tau_{lp_z}$ [s]	5	1.23	5.13	$K_f$	4	15.4	0.004	$\sigma_a$ [ $ms^{-2}$ ]	5	0.5	1.5
$K_{ac_{xy}}$	1	0.005	1.2	$K_{f\omega}$	8	0	8.4	$\sigma_\Omega$ [ $^\circ s^{-1}$ ]	30	26	26
$K_{ac_z}$	1	0.005	0.78	$K_\omega$	8	2.28	11.2				
$K_{gc_{xy}}$	5	1.88	3.26	$K_{\omega f}$	1	1	1				
$K_{gc_z}$	5	1.88	5.88								
$K_{\omega c}$	2.28	2.28	2.28								

**Table 5.2** Symmetric mean absolute error between the predicted and experimental perception results shown for the untuned, perception-tuned and sickness-tuned models.

Models	Motion Paradigm			
	EVAR	OVAR Trans	OVAR Rot	Centrifugation
MSOM Untuned	0.634	0.215	0.471	0.282
MSOM Perception	0.088	0.210	0.324	0.069
MSOM Sickness	0.699	0.243	0.616	0.640
SVM Untuned	0.088	0.260	0.324	0.297
SVM Perception	0.088	0.237	0.324	0.094
SVM Sickness	0.088	0.333	0.324	0.474
PFM Untuned	0.615	0.303	0.441	0.320
PFM Perception	0.559	0.257	0.564	0.106
PFM Sickness	0.564	0.278	0.552	0.211

The perception and sickness-tuned, as well as the original untuned, parameter values are listed in Table 5.1. Table 5.2 shows the overall goodness of fit for all tunings. Here, the perception tuning procedure is overall successful in reducing the error between the perception dataset and the model predictions. The most accurate overall perception results are provided by the MSOM, whereas for centrifugation the SVM is of greater accuracy. Sickness-tuned parameters performed poorer in per-

ception than both perception-tuned and untuned, indicating that the models cannot account accurately for both perception and sickness at the same time.

### 5.4.2. PERCEPTION FREQUENCY RESPONSES

To further illustrate between-model differences, the perception dynamics of the perception and sickness-tuned perception models are estimated in the frequency-domain for all relevant inputs and outputs. These results illustrate how the SOMs resolve the gravito-inertial ambiguity. Figure 5.6 shows Bode magnitude responses for small input accelerations for both the perception-tuned and sickness-tuned models. Each subplot of the figure is referred to by its row and column number in the form  $R_yC_x$ .

In Figure 5.6a,  $R_1C_1$  and  $R_1C_2$  show the horizontal plane translational acceleration estimates for the perception-tuned model as having high-pass dynamics for both the PFM and the MSOM, whereas for the SVM, this response is band-pass. For vertical acceleration inputs (as shown in  $R_3C_1$ ), the PFM and the MSOM have a frequency-invariant constant gain for the estimated vertical acceleration. This is contrary to the SVM, which again shows a band-pass response. In the three models, the acceleration and the gravity estimates are coupled. Horizontal-plane translational accelerations (shown in  $R_2C_1$  and  $R_2C_2$ ) lead, in all three models, to a low-pass response in the gravity estimate. This means that in all three models, sustained horizontal acceleration is perceived as sustained rotation. Here, the higher the perturbation frequency, the less it disturbs the perceived gravity vector. The low-pass behaviour is stronger for the SVM with a slope decreasing at a factor of 100 per decade; the PFM and MSOM are next with a slope decreasing at an approximate factor of 10 per decade. The SVM and the PFM both have their break frequency at 0.2 Hz; the MSOM has its break frequency at 0.6 Hz. Vertical accelerations do not cause a change in the vertical estimate of gravity for the MSOM and PFM (hence they cannot be shown in  $R_3C_2$ ). The dynamics of this estimated vertical component of gravity differ for the SVM, where the SVM predicts the same low-pass response as in the horizontal plane. Horizontal plane accelerations lead to a high-pass angular velocity estimate for the PFM only. The other perception-tuned models do not include such a cross estimate of angular velocity.

Figure 5.6b shows the sickness-tuned responses. The acceleration estimate is of higher gain, with a larger plateau, for all the models. Likewise, the break frequencies for the gravity gain with respect to horizontal plane accelerations have shifted to lower frequencies than for the perception-tuned case. Just as in the perception-tuned case, both the MSOM and PFM are frequency-invariant for vertical acceleration perception. Interestingly, there is a qualitative difference in the frequency response for the MSOM across all responses. This takes the form of a peak in the response at approximately 0.02 Hz. This peak is most pronounced for the angular velocity estimation (shown in  $R_4C_1$  and  $R_4C_2$ ). A similar peak is also observed for the sickness-tuned PFM. Here there is band-pass behaviour with a maximum at  $\approx 0.1$  Hz.

### 5.4.3. FIT TO EMPIRICAL SICKNESS FREQUENCY SENSITIVITIES

Figure 5.7 shows both the perception- and sickness-tuned frequency sensitivity of motion sickness. For the MSOM and the SVM, the weights for the available conflict

terms were found by fitting the empirical sickness frequency sensitivities for vertical and lateral accelerations, see Section 5.4.2. These weights are listed in Table 5.3 where both for the MSOM and SVM only one conflict term was selected.

**Table 5.3** Weights on the different conflict terms found by fitting the empirical sickness frequency sensitivities.

Models	Conflicts				
	$c_\omega$	$c_g$	$c_a$	$c_o$	$c_{oa}$
MSOM	0	n/a	n/a	1	0
SVM	0	1	0	n/a	n/a
PFM	1	n/a	n/a	n/a	n/a

Figure 5.7a shows the perception-tuned frequency sensitivities to lateral accelerations. Here, none of the models are seen to capture the band-pass nature of the experimental response. For Figure 5.7b, only the SVM is able to fit the experimentally observed frequency sensitivity to vertical accelerations, albeit with a shift in its maximum to 0.2 Hz rather than 0.16 Hz. The MSOM shows a unit gain throughout, confirming the analytical findings in Section 5.3.1. Due to the absence of any angular velocity estimation, the PFM does not produce a conflict for vertical sickness and hence no sickness is predicted.

The sickness-tuned result in Figure 5.7c shows that the SVM provides the closest fit to the experimental results, forming a band-pass response similar to the experimentally observed response to lateral accelerations. Likewise, the PFM and MSOM also show band-pass responses. However, unlike the SVM, the peak conflict occurs briefly at 0.06 Hz and 0.02 Hz, respectively. Lastly, Figure 5.7d shows the sickness-tuned frequency sensitivity to vertical accelerations. Here, the SVM's response is now centred on 0.16 Hz. Just as before, the MSOM has a unit gain. Lastly, as there is no angular velocity estimate induced by vertical oscillations, the PFM does not predict any sickness.



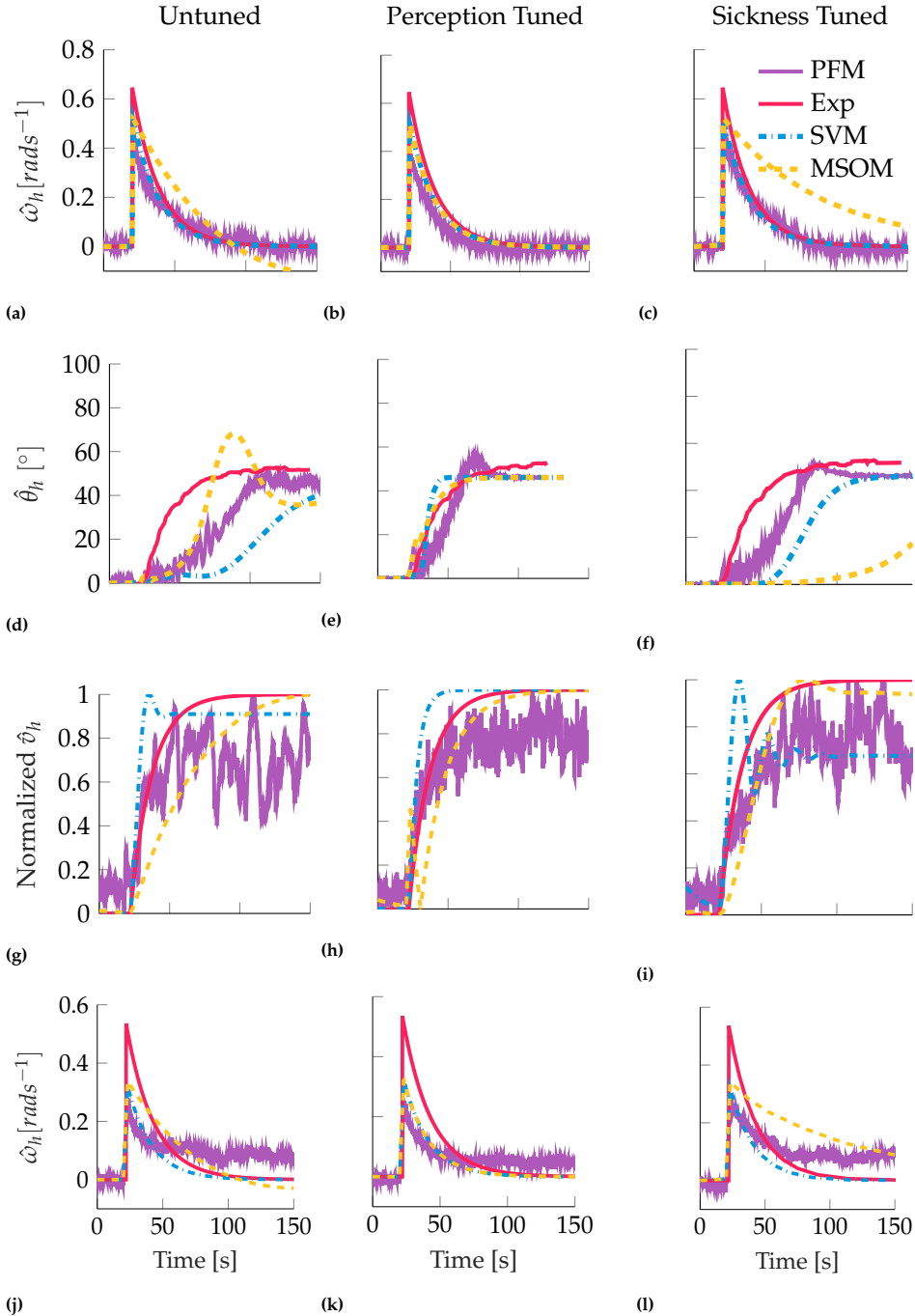
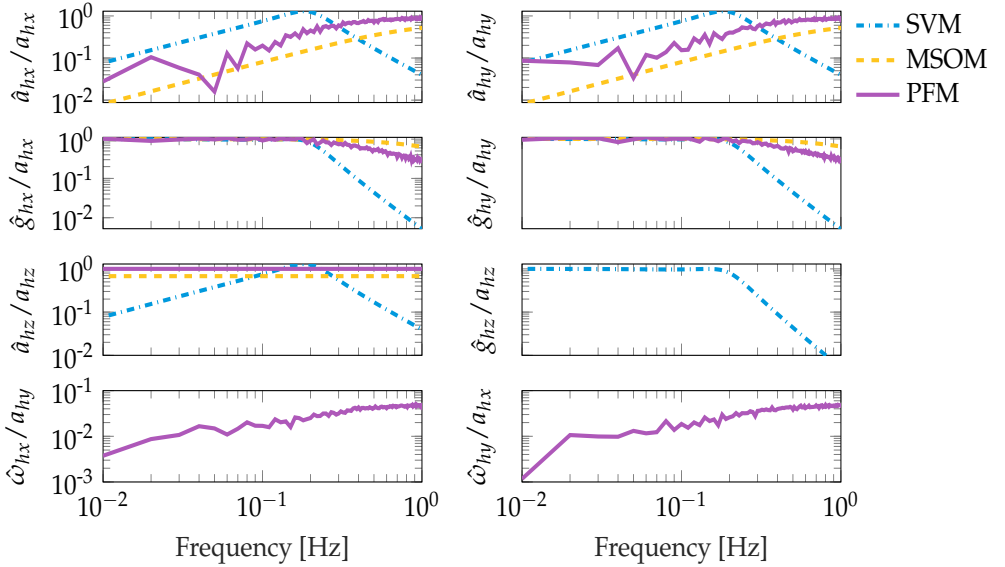
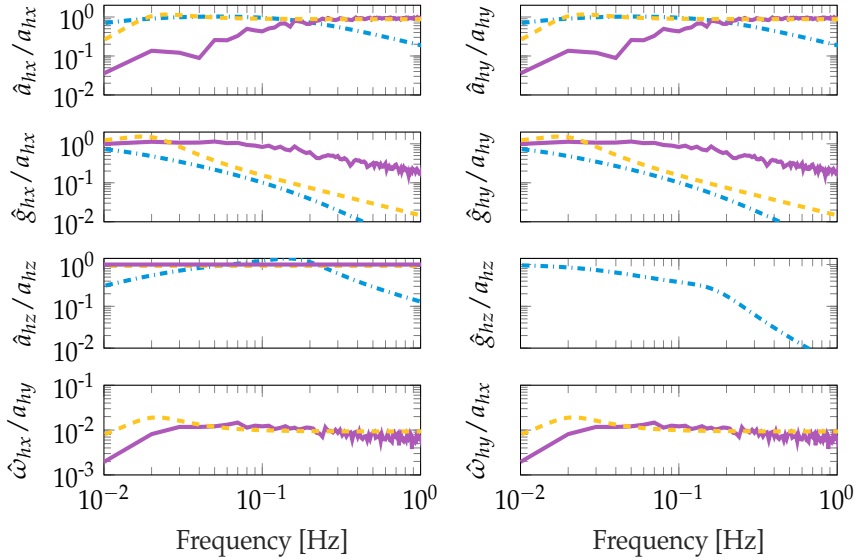


**Fig. 5.5** Perception predictions for EVAR, centrifugation and OVAR, according to the PFM (purple lines), SVM (dashed blue) and MSOM (dashed yellow), plotted against experimental data (red lines). The first row shows yaw velocity perception for EVAR. The second row shows roll perception during centrifugation. In the third and fourth rows, the normalized translation velocity perception (obtained by integrating translational acceleration) and rotation perception are shown for OVAR, respectively. The left column shows fits based on parameters obtained from the literature; the centre column perception-tuned fits; the right column sickness-tuned fits. All motion paradigms are performed in darkness.





(a) Perception Tuned



(b) Sickness Tuned

**Fig. 5.6** Frequency-domain model responses of perceived motion. **(a)** responses of the perception-tuned model state estimates in response to small acceleration input whilst earth vertically orientated in darkness. The three lines represent SVM (blue), MSOM (yellow) and PFM (magenta). Input head acceleration is  $a_h$ , estimated head acceleration is  $\hat{a}_h$ , estimated gravity is  $\hat{g}_h$  the units for both are  $\text{ms}^{-2}$ . **(b)** responses of the sickness-tuned model state estimates.

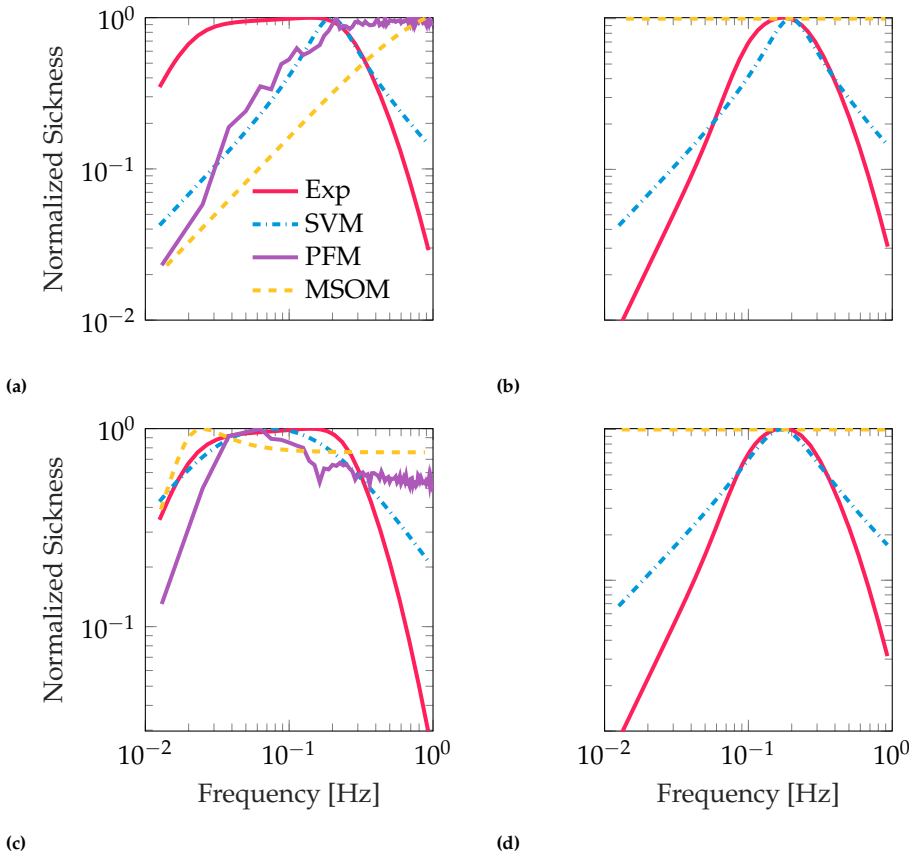


**Fig. 5.7** Frequency sensitivity of motion sickness to sickening stimuli. **(a)** Perception-tuned frequency sensitivity to horizontal plane accelerations. **(b)** Perception-tuned frequency sensitivity to vertical plane accelerations. **(c)** Sickness-tuned frequency sensitivity to horizontal plane accelerations. **(d)** Sickness-tuned frequency sensitivity to vertical accelerations. The red line is experimentally observed frequency sensitivity, blue line is SVM, yellow line is MSOM and magenta line is PFM. The PFM is absent in **(b)** and **(d)** because it does not have any conflicts in the vertical direction

## 5.5. SICKNESS VALIDATION

After the tuning process, the three perception models were validated for the magnitude of sickness they predict for five frequently used motion paradigms in sickness research. The selected paradigms are VTA, LTA, PRP, OVAR, and CCCP. This validation was done for both the perception tuning and the sickness tuning.

Figure 5.9 shows the predicted sickness for these motion paradigms for each model, alongside experimental observations. Conflicts with zero weights as found in the sickness fitting procedure are not shown. Figure 5.9a shows the perception-tuned sickness predictions; Figure 5.9b shows sickness-tuned sickness predictions. Model performance can be evaluated by comparing the predicted sickness with the

empirical data (see section 5.3.4), which is plotted in the form of red diamonds in each panel of Figure 5.9.

### 5.5.1. SUBJECTIVE VERTICAL MODEL

The conflict used by Bos and Bles (1998) to characterise motion sickness in the SVM was the gravity conflict. Indeed, from our sickness fitting, we confirm it to take the greatest weighting. In Figure 5.9a, OVAR dominates this conflict and is 2.6 times greater than CCCP. The PRP is also seen to be of the same order as LTA and VTA, this is also a higher sickness prediction than the relative differences inferred in section 5.3.4.

The sickness-tuned SVM follows the empirical observations more closely (see Figure 5.9b). Here, unlike for the perception-tuned case, the relative magnitudes of CCCP, OVAR and LTA approximately match the expectations. One difference again is the greater strength of PRP. The reason for this consistent over-estimation is due to the role of the angular velocity feedback. In the SVM, the gain  $K_\omega$  works to track the sensed signal. A weak angular velocity feedback means that there is a greater difference between the sensed and the internally estimated angular velocity. As the angular velocity is used in the form of the Mayne equation (Mayne, 1974) to rotate the gravity vector, there is a greater difference between the sensed gravity and internally estimated gravity, i.e., the gravity conflict. Increasing the angular velocity feedback gain reduces this conflict. Figure 5.8 shows this variation in gravity conflict with respect to both PRP and LTA as a function of  $K_\omega$ .

As there is no connection between the perceived rotational velocity and linear acceleration estimates for the SVM, for LTA it is unresponsive to changes in  $K_\omega$ . Interestingly, for PRP the conflict asymptotically converges to around  $68 \text{ ms}^{-2}/\text{rad}$ , which is only marginally smaller than the value found for LTA and so does not match the experimental findings (Figure 5.8). Moreover, for  $K_\omega \geq 4$  the EVAR time constant is 28 s, meaning that even if the conflict is reduced, the velocity storage time constant leaves the bounds of experimentally observed angular velocity perception values.

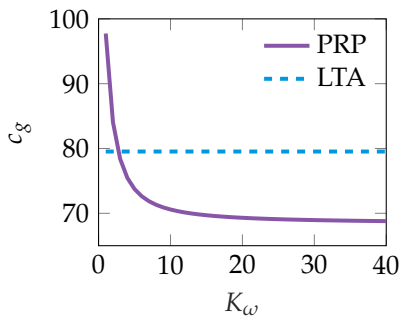
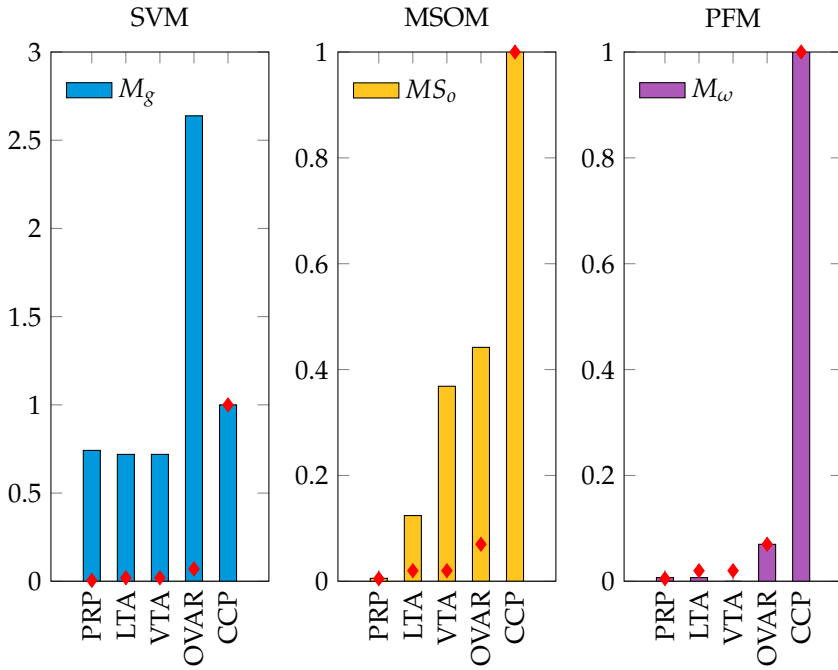
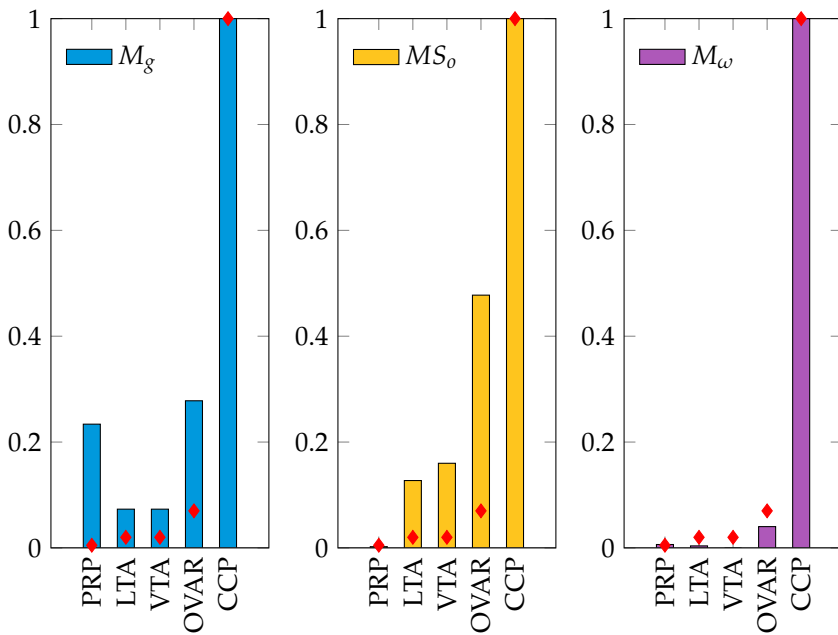


Fig. 5.8 SVM gravity conflict  $\bar{c}_g$  for PRP (purple line) and LTA (dashed blue line) with respect to angular velocity feedback gain  $K_\omega$ .



(a) Perception Tuned



(b) Sickness Tuned

**Fig. 5.9** Magnitude of cumulative conflict for five motion paradigms when normalized against CCCP for the three perception models. The left column shows results for the SVM (in blue); the middle columns show results for the MSOM (yellow); and the right column shows the results for the PFM (magenta). The top row (a) shows predicted sickness for perception-tuned models; the bottom row (b) shows the predicted sickness for sickness-tuned models. Red diamonds mark experimental results.

### 5.5.2. MULTI-SENSORY OBSERVER MODEL

For the MSOM, the perception-tuned otolith magnitude error in Figure 5.9a shows that CCCP, OVAR and LTA follow a reasonable ranking of sickness intensity. There is, however, a large difference between the predicted sickness magnitude for VTA and LTA, which is contradicted by experimental data. The reason for this is the flat nature of the frequency response (Figure 5.7b) for VTA compared to the LTA (Figure 5.7a), which attenuates the sickness due to lateral accelerations. The predicted sickness for PRP is close to experimental findings. This is because the MSOM is able to easily discriminate the roll signal from acceleration, leading to only a small sensory conflict.

The sickness-tuned MSOM makes similar predictions to the prediction-tuned MSOM. Here, the CCCP is again confirmed to be the most sickening, followed by OVAR. Still, the magnitude of the difference between CCCP and OVAR is not similar to experimental findings. The sickness-tuned responses for VTA and LTA are of similar amplitude. This is because the frequency responses to vertical and lateral accelerations as shown in Figure 5.7b and 5.7c are more similar to each other at the frequency of 0.2 Hz, which was the input perturbation frequency for the validation. Likewise, similar to the perception-tuning, the sickness-tuned model is able to discriminate the roll signal from acceleration, leading to a negligible roll-induced sensory conflict.

### 5.5.3. PARTICLE FILTER MODEL

Due to lack of otolith or other acceleration conflict, the PFM predicts no motion sickness for the vertical motion paradigm. For the rotational motion paradigms, however, both the perception-tuned and the sickness-tuned PFM perform well. OVAR and PRP are found to be a factor of 27 and 170 times smaller in sickness magnitude than CCCP, which matches well with the experimental values (of 14 and 200 times, respectively). The reason why the angular conflict is larger in OVAR than in PRP for the PFM is the existence of a strong oscillation in the estimated angular velocity in both fore-aft and lateral directions. This effect is not present in the SVM due to the lack of a bidirectional influence between the otoliths and the semicircular canals, and it is attenuated in the MSOM due to the gain  $K_{f\omega}$  being set to zero to optimize perception predictions.

## 5.6. DISCUSSION

Motion sickness has long been linked to state estimation conflicts in motion perception. In this study, we evaluated different perception models for their ability to reproduce both empirical motion perception and motion sickness data. The models were tuned to time-domain perception data, as well as frequency-domain sickness data. Evaluating both the perception-tuning and sickness-tuning results together helped identify whether the SOM framework is effective for predicting motion sickness.

The perception-tuned SVM, MSOM and PFM could all adequately approximate most selected perceptual phenomena, but for each there were also important devia-

tions from measured data from literature. The sickness-tuned models on the whole did not adequately fit the perception data. Likewise, the success of fitting to sickness frequency sensitivities was limited (Figure 5.7), with only the SVM providing reasonable fits. In the following, we first discuss the ability of the different models to reproduce human motion perception, and then discuss their ability to reproduce observations on motion sickness. In the latter discussion, we specifically evaluate the role of sensory conflict, and identify two key mechanisms that may be required in any model of motion sickness.

### 5.6.1. PERCEPTION

Overall, the perception-tuned models described empirical perception data better than the original untuned models (SMAE of 0.243 compared to 0.354, indicative of smaller residual variance in the former). This is expected because the tuning was done with respect to a different collection of paradigms than the disparate paradigms each individual model was tuned on in their original publications. The sickness-tuned models on average had an SMAE of 0.418, indicating that both sickness and perception phenomena could not be captured by the same set of parameters. The implication of this is that current models of perception are not directly suitable for predicting motion sickness.

#### SUBJECTIVE VERTICAL MODEL

For the perception tuning, the time-domain perception predictions of the SVM were found to be accurate. The model was able to satisfactorily match the empirical EVAR, OVAR and centrifugation responses. Interestingly, for centrifugation, the yaw rate of the centrifuge had a profound impact on the model predictions. However, there is no clear effect of yaw velocity in the experiments evaluated. For instance, in [Curthoys \(1996\)](#) the time constant of the subjective vertical was 6.1 s at  $200^\circ\text{s}^{-1}$ , whereas this was 14.0 s for [Merfeld et al. \(2000\)](#) at  $250^\circ\text{s}^{-1}$  and 15.9 s for [Graybiel and Brown \(1951\)](#) at  $60^\circ\text{s}^{-1}$ . To match the experimental data, the observer gains of the SVM need to be dependent on the yaw rate. This means that there were many parameter sets that approximately satisfied the error minimisation criterion when all centrifugation conditions were optimized together. Therefore, the model in its current form is over-parametrized with respect to the perception predictions for the data broad range of data analysed in this study. Moreover, in the frequency-domain, the estimated acceleration for all directions has band-pass dynamics. However, it is known from literature that the dynamics should be high-pass ([Merfeld et al., 2005b,c](#)).

#### MULTI-SENSORY OBSERVER MODEL

As it has the smallest overall error, the time-domain perception-tuned perception predictions of the MSOM are the most accurate. It is important to mention that the gain  $K_{f\omega}$ , responsible for the coupling between the semicircular canals and the otoliths, was set to 0 in the perception-tuned MSOM, compared to the value of 8 in the original model. This is due to the reports of zero angular velocity perception in the experiments of [Vingerhoets et al. \(2005\)](#) on OVAR. Moreover, just like the SVM, there is no unique set of parameters that describes all centrifugation results.

In the frequency domain, the acceleration and gravity estimates of the MSOM for horizontal plane acceleration input match literature findings. Interestingly, the vertical acceleration percept is a unit gain. This means the vertical acceleration estimate is frequency invariant. Studies indeed suggest that there is anisotropy in our perception of travelled distance, with vertical translations being worse than horizontal plane translations (Hinterecker et al., 2018). It is not clear from literature, however, whether this anisotropy is caused by differences in the frequency response of our perception to vertical acceleration or indeed due to the differences in the integration of acceleration into travelled distances by the central nervous system. Experiments on the frequency response of vertical displacement perception may help validate the model for this degree of freedom.

#### PARTICLE FILTER MODEL

In the PFM, there is a trade-off between fitting the OVAR and centrifugation responses. Decreasing the standard deviation of the acceleration prior,  $\sigma_a$ , led to more accurate centrifugation responses, but also increased the yaw angular velocity bias-term on the OVAR responses. The bias in the OVAR is present in the PFM because reducing the standard deviation of the prior on acceleration makes perceiving a translation along a cylindrical trajectory during OVAR less likely than rotating in yaw whilst tilting, whereas experiments (Angelaki et al., 2009a) show that during long exposure to OVAR only a translational percept remains and heading is perceived to be constant. In the frequency-domain, the responses of the PFM and the MSOM are, despite employing fundamentally different methods, very similar. This is because both models make the key assumption that the magnitude of the gravity vector is constant and, unlike the SVM, perform no pre-filtering.

#### 5.6.2. SICKNESS

For all three models, the sickness tuning provided a better fit to motion-sickness data, as expected. Out of the compared models, the SVM, with a combined SMAE of 0.074, provided the closest fit to both the lateral and vertical sickness frequency responses reported in the literature. In comparison, the SMAE was 0.259 for the MSOM and 0.343 for the PFM, respectively.

The validation data-set was used to evaluate the predicted relative sickness magnitude across a broader range of motion conditions. In this, the validation results for the different models were more mixed. Although the PFM gave the best performance for the rotational degrees of freedom, it did not predict any vertical sickness. In comparison, both the SVM and the MSOM made better predictions for motion sickness due to inertial accelerations. For the SVM there was an over estimation of the sickness resulting from roll rotations, whereas for the MSOM roll rotation did not lead to any sickness. With respect to the difference between OVAR and CCCP, both sickness tuned models performed similarly.

#### SUBJECTIVE VERTICAL MODEL

Out of the models compared, the best match between the empirical frequency-sensitivity data for sickness and model predictions was obtained for the SVM model. Inspection of the fitting results revealed that the model when tuned to sickness-fitted VTA

responses remarkably well, better than the other models. The underlying reason for why the SVM is the only model capable of frequency-variant VTA-induced sickness predictions is that the magnitude of the estimated gravity is permitted to vary. Here, there is a leakage from the gravito-inertial force to the magnitude of the estimated gravity term. For both the MSOM and the PFM, the magnitude of gravity is fixed to  $9.81 \text{ ms}^{-2}$ . In hypergravity experiments involving centrifugation such a fixed magnitude of gravity predicts a perceived sense of translation, however, this is not observed (Clark et al., 2015). This supports the notion that the internally expected magnitude of gravity is variable, as allowed in the SVM.

Despite its success, one drawback of the SVM is that it is a partial-observer. Specifically, head angular velocity is observed, but acceleration and gravity are not. Instead, the gravito-inertial force is first low-pass and then high-pass filtered. The output of the filters are the sensed gravity and acceleration, respectively, which are tracked by the internal model. This direct filtering of the gravito-inertial force has the most pronounced influence on the model's output. The resulting tracking error directly leads to the conflict terms. This mechanism is an important theoretical deviation from the general observer framework outlined by Oman (1982). This explains the reduced accuracy for predicting motion sickness for rotational motions, (see Figure 5.9b) as is evident by the SVM's high sickness predictions for PRP, which contradict experimental data (shown in Figure 5.8).

### MULTI-SENSORY OBSERVER MODEL

When tuned for sickness, the MSOM has the band-pass dynamics that are associated with motion sickness caused by horizontal plane accelerations (see Figure 5.7c). It is notable that the relevant conflict is generated only for the somatogravic effect. The somatogravic effect is a striking demonstration of a perceptual conflict and occurs when there is an ambiguity in the sensation of tilt and translation during low-frequency horizontal accelerations. Previous research, including our own, has supported it being a possible contributor to motion sickness (Wood, 2002; Wood et al., 2007; Irmak et al., 2021b). It is a positive outcome that there is a direct perceptual correlate of this conflict term in the MSOM. Though the SVM does model the somatogravic effect, due to the absence of an explicit two-way coupling between the semicircular canals and the otoliths, there is no difference in the frequency sensitivities between vertical and horizontal, unless parameters are tuned explicitly for the different directions. Moreover, because unlike the SVM it is a full observer, the MSOM is able to accurately discriminate roll rotation, which makes the predicted motion sickness from roll closer to the experimentally observed values (Figure 5.9b).

The main disadvantage of the MSOM is that the peak predicted frequency of sickness for LTA is at 0.02 Hz. It is, however, known from experiments (Donohew and Griffin, 2004) that that sickness occurs over a broader range of frequencies for LTA and peaks at a higher frequency (0.03 - 0.3 Hz). Moreover, the MSOM results in frequency-invariant vertical motion sickness predictions (see Figure 5.7d). This is mostly not observed in previous experiments (Zaichik et al., 1999) and is due to the nature of the acceleration estimation process, which assumes a constant magnitude for the gravity vector.



### PARTICLE FILTER MODEL

Similar to the MSOM, the PFM includes/provides band-pass sickness predictions through the somatogravic effect mediated by the two-way coupling between the semicircular canals and the otoliths, thus providing a perceptual correlate for its conflict term. Interestingly, the PFM provides the most accurate fit to motion sickness due to rotations (see Figure 5.9b). This may be due to the fact that it can account for the non-linear dynamics introduced by them. Moreover, unlike the other two models, it is a probabilistic model that performs Bayesian inference on vestibular stimuli. This is advantageous because it automatically accounts for the presence of noise at the input, which the other models do not. Not only are probabilistic models a more faithful representation of reality, but they may also explain non-classical behaviour. For instance, it is known that noisy galvanic vestibular stimulation (GVS) as well as bone conducted vibrations (BCV) retard the development of motion sickness (Weech et al., 2018). Probabilistic approaches may help explain this behaviour in an emergent fashion, as a consequence of performing inference on more noisy sensory afferents. In contrast, deterministic models such as the SVM and the MSOM may only be fitted to the data manually and provide no deeper explanatory power.

The key disadvantage of the PFM is that it does not predict any VTA-induced sickness. This is because, unlike the MSOM, there is no internal estimate for the gravito-inertial force. Moreover, the model performs inversion of the semicircular canal signal  $C_t$  to obtain an estimate of the head velocity  $\omega_t$ . Inverse models are affected more by noise than forward models, and for some problems the solution space may even be infinite. This makes employing forward models more appealing.

### IMPLICATIONS FOR SICKNESS MODELLING

The current study shows that SOM parameters fitted to perception data do not accurately predict motion sickness and vice versa. A combined fitting may of course yield a compromise, but will not address the fundamental limitations identified in this study. Firstly, the MSOM and PFM have a contradictory or even an absent prediction of sickness for vertical acceleration stimuli. Moreover, the SVM predicts a higher magnitude of motion sickness for roll than is observed empirically, whilst deviating substantially from the theoretical framework developed by Oman (1982).

We propose that a more complete model of motion sickness would contain the following two mechanisms identified in this study. Firstly, models should include an explicit two-way coupling between the semicircular canals and the otoliths (Lim et al., 2017). This is crucial for capturing the somatogravic effect, a phenomenon many experiments have shown to have a striking association with motion sickness induced by horizontal plane accelerations (Wood, 2002; Wood et al., 2007; Irmak et al., 2021a). Secondly, models should have a variable estimate for the magnitude of gravity. Without allowing variability in the magnitude estimate, it is impossible to capture how vertical motion, as it does not result in any perceived rotations, can lead to motion sickness.

Furthermore, the underlying framework in which these two mechanisms are implemented should be probabilistic. For this, a reformulation of the PFM is needed whereby only forward models of sensory processing are used. Moreover, the PFM

has frequency-invariant likelihoods, whereas humans are known to have frequency-dependent likelihoods (Angelaki et al., 2009b). Specifically, low-frequency stimulation of the otoliths is more likely to be due to tilt, while high-frequency stimulation is more likely to be due to translation. Angelaki et al. (2009b) state that the system “*knows*” what these likelihoods should be. The system can indeed *learn* the frequency-dependent likelihoods by matching vestibular stimulation patterns to a ground truth. In experimental settings, this ground truth would be defined by the researcher, but in reality it would likely become implicitly evident to the organism via the visual and proprioceptive cues. The likelihoods would be used to estimate the real states of the organism and the expected sensory stimulation, which would then be compared with actual sensory stimulation to drive sensory conflict terms. The sensory conflict terms would be used concurrently to both update the internal model and also to drive motion sickness. The probabilistic nature of the conflict generation process would not only allow for the modelling of the small but evident variance in intra-individual sickness trajectories seen in our previous work (Irmak et al., 2020), but could also account for other emergent phenomena such as the effect of increased sensory noise via GVS, BVC or even ageing (Nestmann et al., 2020).

Despite presenting vestibular-only data in this chapter, the authors also attempted to include vision in the models evaluated. For the SVM, the model proposed by Bos et al. (2008a) was taken. For the MSOM the full visual-vestibular formulation by Newman (2009) was used. Lastly, the form of the PFM formulated in Laurens and Droulez (2008) was used. Visual inputs accounted for in the SVM and MSOM include angular and linear velocity, as well as orientation, whereas for the PFM only angular velocity is included. As observed in experiments (Irmak et al., 2020), including vision decreases sensory conflict and consequently, motion sickness. Regardless, vision was ultimately omitted in this study. This was primarily because the benefits of including vision were outweighed by the complexity introduced by the increased number of parameters and the lack of sufficient experimental results in the literature to define and validate models of visual contributions to motion perception. Nonetheless, the effect of vision remains a crucial focus for future work and is currently being pursued by researchers (Bos et al., 2008b; Wada et al., 2020).

In this study, a simple integrator was used to model the accumulation of motion sickness over time. In reality, this accumulation is more complex, with both time and amplitude non-linearities. For instance, it is known that as humans become sick, their sensitivity to further sickness increases (Oman et al., 1986; Golding and Markey, 1996; Irmak et al., 2020). Furthermore, motions below a certain amplitude may often fail to elicit any sickness (Lawther and Griffin, 1988). These effects have been explored in previous chapters of this thesis and should be accounted in a complete model of motion sickness.

### 5.6.3. FUTURE WORK

To bring clarity to motion sickness modelling via the sensory conflict approach, additional experimental data regarding perceived acceleration (or translation, as the more easily measured correlate) and gravity (or tilt) frequency responses as analysed in this chapter should be obtained. These should be directly related to the sickness

frequency responses observed under the same motion paradigms. This would help to identify the nature of the relationship between the somatogravic effect and motion sickness.

Recent experiments also show major differences between participants in both perception and motion sickness (Irmak et al., 2021a). As these two are coupled per the sensory-conflict approach, we can use SOMs to quantify individual variations in sickness sensitivity through observer parameters (e.g., feedback gains). For instance, Dai et al. (2010) used their SOM to relate eye-velocities and motion sickness observed during OVAR. Here individualisation is important, as per the "Ecological Fallacy" averaging over an entire group may mask important relationships between sickness and perception that occur at the individual level. Indeed, our previous work (Irmak et al., 2021a) has shown that individuals have differing frequency sensitivities and so fits to population averaged sensitivities are not always appropriate.

Finally, for validation of future and current models, investigation of sickness across a wide range of sickening phenomena is needed. This study attempted such a validation in Section 5.5, but in the absence of experiments employing a consistent sickness scale such as the MIserY SScale (Bos et al., 2005) and a consistent perturbation duration and magnitude, unfortunately, only approximate comparisons could be performed. Having extensive combined perception/sickness data would allow us to better discriminate between competing models and allow identification of causal mechanisms.

## 5.7. CONCLUSION

The results indicate that all models are able to provide good perception fits to the selected motion paradigms. Despite this, there are large differences in the frequency response of the acceleration and gravity perception between the SVM, the MSOM and the PFM. This is attributed to the different assumptions made for resolving the gravito-inertial ambiguity in each model. Under the observer framework for sickness prediction, these assumptions are found to directly influence the sickness predictions.

Overall, none of the models can capture the full range of empirical motion sickness observations considered in this chapter, including lateral and vertical translational acceleration, pure roll, off-vertical axis rotation and cross-coupled coriolis perturbations.

Based on our model comparisons, we identified two critical components that may resolve this. The first mechanism is the coupling of the semicircular canal with the output of the otoliths to compute a more reliable gravity (i.e., orientation) and acceleration estimate. This is necessary to capture the differences in the dynamics between motion sickness induced by horizontal and vertical accelerations. The second mechanism is that the models should have a variable estimate for the magnitude of gravity. Without a slowly varying magnitude estimate, models cannot predict the well-known motion sickness due to vertical accelerations. In addition, we propose that these mechanisms are best implemented within in a probabilistic framework similar to the particle filter evaluated in this study. Adoption of such a framework will better account for individual differences in sickness susceptibility, as well as

## 5.7. CONCLUSION

---

emergent phenomena such as variations in sickness sensitivity caused by changes in sensory noise induced by GVS/BCV of the mastoids. This makes the approach the most promising research direction towards key applications for mitigating motion sickness in automated vehicles.



# 6

## DISCUSSION & RECOMMENDATIONS

*As discussed in the Introduction chapter of this thesis, its various chapters have three underlying threads of reasoning that motivate their respective research questions. This chapter aims to recapitulate the main findings of each individual thread and weave them in to a singular cogent form, whilst making explicit both the societal, and the scientific impact of this thesis. Furthermore, a number of both practical and future research related recommendations are given.*

The fact that adverse motions may, in a very wide range of species, cause a diverse set of symptoms is peculiar. Yet reality is clear and attempts to explain this phenomenon date back to ancient Greek and Chinese texts. Our modern understanding of motion sickness is undoubtedly more refined than these earliest of attempts. However, the more we understand, the more we have left to learn. Key unknowns pertain to the sensory processes underlying motion sickness development, the relationship between motion sickness and motion perception, and the differences in individual sickness dynamics and susceptibilities. To be able to design comfortable controllers for future automated vehicles, these questions must be resolved. The objective of this thesis was therefore to

### Thesis Objective

Understand and model motion sickness accumulation and its individual differences for the comfortable control of automated vehicles.

## 6.1. DISCUSSION

### 6.1.1. PART I: QUANTITATIVE ANALYSIS OF INDIVIDUAL DIFFERENCES

Motion sickness has high individual variability in all its facets. Individuals have differing symptoms, time evolution of motion sickness, and sensitivities to the same motion. Motion sickness research has thus far mainly been concerned with studying how motion sickness manifests in the population, rather than the individual. For highly variable phenomena, population relationships may not hold at the individual level; asserting that they do so is an *ecological fallacy* (Freedman, 1999). Part I of the thesis, therefore, set out to provide a quantitative analysis of individual differences in motion sickness.

Chapter 2 evaluated the repeatability of individual sickness trajectories when individuals were subject to the same motion condition, week-after-week, for three weeks. The answer to this question determines whether there is any merit in attempting to model and characterise differences in sickness development at the individual level. It was found that participants had a high degree of repeatability in their time evolution of sickness over consecutive sessions. This is in accordance with the findings of Graybiel (1969), who found that that end sickness in a session was highly correlated with end sickness in a subsequent session. The results in chapter 2 demonstrate that it is not only the end point of sickness that is repeatable, but the entire time history of sickness. This means that individuals display consistent sickness susceptibility. This has a number of important implications. It suggests that day-to-day variations in physiological and psychological state have limited effects on motion sickness susceptibility. Personality 'trait' variables such as extraversion and neuroticism have not been found to correlate significantly with motion sickness susceptibility (Golding, 2006). Of course, these studies investigate between-participant

correlations, and it may be that differing levels of anxiety within an individual can lead to different motion sickness trajectories. However, experiments with complex psychological manipulations, such as motivation, as experienced in previous studies ([Irmak et al., 2021b](#)), are difficult to manage ([Crano, 1991](#)) and often times participants are unresponsive to the manipulation.

Another implication of repeatability is that one can study motion sickness using system identification techniques ubiquitous in control theoretic modelling. In this direction, chapter 4 investigated individual frequency sensitivities to fore-aft accelerations. This was done using the Cable Robot Simulator (CRS) and the Cyber Motion Simulator (CMS) at the Max-Planck Institute for Biological Cybernetics in Tübingen. In this experiment, participants were subject to 30-minute experiment sessions with sinusoidal fore-aft accelerations week-after-week for five weeks. The aim of the experiment was to measure the effect of motion frequency at both the group and the individual-level. The results show a flat sickness response with respect to acceleration frequency for the group, but a highly variable one for the individual, with some individuals being susceptible to low, some to medium and others to higher frequencies. This means that the assumption of the group sickness response being representative of the individual is not correct. The individual frequency sensitivity curves were then correlated to motion perception parameters. Doing this at the individual level allows for a better evaluation of candidate models, this is because the probability of a model fitting one frequency response with one set of perception parameters, as is done in the literature ([Wada, 2021](#); [Khalid et al., 2011a](#); [Bos and Bles, 1998](#)), is much greater than a model fitting many frequency responses concurrently.

The derivation of individual frequency sensitivity curves and their subsequent use to ascertain the causal mechanism that leads to motion sickness rest on the assumption that these curves are proportional to the actual internal sensory conflict that occurred in individual participants. Indeed, the findings of chapter 3 largely confirm this assumption. This study was conducted using the SIMONA Research Simulator at the Aerospace Engineering faculty of TU Delft. Participants were exposed to four different motion amplitudes (1, 1.5, 2 and 2.5 ms<sup>-2</sup>) in four separate sessions. The Oman model of nausea accumulation was fitted to the subjective sickness ratings. [Oman \(1982\)](#) had already reported an output power scaling of 2, but this was not validated well, chapter 3 therefore provides the first experimentally founded result. In this, we found that the non-linear output scaling term of 0.4 can be used to model the effects of stimulus amplitude variations on sickness accumulation. This non-linear scaling approximately linearises the amplitude relationship, meaning that the level of sickness quantified using the MISC scale is indeed linearly proportional to the scaled internal sensory conflict. This also means that in this case, the assumption of a group-level amplitude response to sickness being representative of the individual is indeed ecologically valid. The main findings from the quantitative analysis of individual differences were therefore



## Main Findings of Part I

- Individuals have repeatable motion sickness responses
- Group frequency sensitivity is not representative of the individual sensitivity
- At both the individual and the group levels, the acceleration amplitude is linearly related to the measured sickness intensity

### 6.1.2. PART II: MODELLING THE TEMPORAL DYNAMICS OF MOTION SICKNESS

The accumulation of motion sickness in time has primarily been studied with respect to the group. For this, it is usual for population-averaged metrics, such as mean sickness rating and motion sickness index (percentage of people vomiting), to be used. Indeed, most modelling studies have aimed at matching their predictions to these group averages.

Therefore, in addition to the individual variation in frequency and amplitude dynamics, there are also variations in the temporal dynamics, i.e., the accumulation of sickness with respect to time. chapter 3 studied the temporal dynamics in detail and found that in addition to quantitative differences between participants in the time constants of sickness accumulation, there were also qualitative differences in their response profile. This difference manifests itself in the form of convergent or divergent sickness trajectories. It was found that for those participants with a disposition to a convergent trajectory, the exposure required to get more sick increases as sickness level increases. This is contrary to those participants with a divergent sickness trajectory. Here, we find that as sickness level increases, it was easier for the participant to get even more sick with continued exposure. These findings confirm the results reported in chapter 2 about idiosyncratic differences in the qualitative form of sickness accumulation.

The Oman model of nausea is the only model developed to capture the temporal dynamics of motion sickness at the individual level. Therefore, it offers more insights into the physiological processes that govern motion sickness evolution, an insight that is obscured when evaluating groups. Moreover, the Oman model is able to account for hypersensitivity, which occurs when individuals who have been recently made sick are sensitised to further motions, such as to become sick much quicker than during their initial exposure. This is particularly relevant for automated driving which consists of sickening motions separated by relatively large durations of rest (e.g. going in to a highway then on to a mountain road). In chapters 2 and 3, the input to the Oman model was assumed to be proportional to the sensory conflict. In Part III, this assumption is replaced by models of motion perception, which aim to derive the sensory conflict terms by using the observer framework.

One problem associated with the Oman model was that, prior to the work de-

scribed in this thesis, it was not rigorously validated. Furthermore, parameters such as the time constants and the output power scaling were not estimated from experiment data, while a value for the gain parameter was not defined at all. Chapter 2 attempted to resolve this issue by fitting an adapted form of the model to the sickening drive data, which included hypersensitivity in a second motion exposure. Here, the fast and slow time constants of the system were identified as 63 s and 441 s, respectively, with a fast path gain of 2.18. One limitation of the data gathered in chapter 2 is that it is from a single condition and therefore provided no information on if, and how, these parameters may vary with the magnitude of the sensory conflict.

Chapter 3 addressed this limitation by providing within-participant sickness data when participants were exposed to four acceleration amplitude conditions. Here, it was found that the values of the fast and slow time constants were stimulus amplitude invariant. Furthermore, confirming the parameter estimates of chapter 2, the median parameter estimates found in chapter 3 were 66.2 s and 502.4 s for the fast and slow paths, respectively. This indicates that the physiological process underlying sickness accumulation seems invariant for the individual and is an idiosyncratic property. This finding, paired with the fact that habituation to sickening stimuli is often stimulus specific, and does not transfer well to other sickening stimuli (Golding, 2006), provides support for these time constants being a fixed property of the system driving motion sickness.

As discussed previously, chapter 2 and 3 also found that there was qualitative variation in the temporal dynamics of motion sickness between participants. This difference manifested in convergent and divergent sickness trajectories. It was found in chapter 3 that divergent trajectories were modelled less well by the Oman model of nausea. This was primarily due to the convergent nature of the model, which, due to negative system poles, converged to a final sickness value in a stable manner. In a number of participants studied in chapter 3 bistable behaviour could be observed. These participants converged to a specific value of sickness, after which, in the span of seconds, their sickness scores 'blow-up' to vomiting. There can be a number of reasons for this. One is a possible misinterpretation of the MISC scale, whereby participants do not rate based on perceived symptoms, but based on the level they can tolerate with the maximum being the experiments' set termination criteria (in this instance a MISC of 6). Previous literature (Graybiel, 1969; Bock and Oman, 1982), however, indicates that symptoms can indeed 'avalanche', or blow-up, as also found in this thesis. The main findings from modelling the temporal dynamics of motion sickness were therefore

## Main Findings of Part II

- Individuals may show convergent or divergent sickness trajectories, whereby convergent trajectories are modelled better with current tools
- Validation of the Oman model and estimates of its key parameters: fast and slow time constants at a median value of 66.2 and 502.4 s, with a median gain of 70.8
- Power scaling the output of the Oman model with an exponent of 0.4 allows cross-amplitude generalisability of the Oman model to different stimulus amplitude conditions
- Individuals may exhibit bistable behaviour, where their sickness, after converging to a specific value, is seen to 'blow-up' to vomiting

### 6.1.3. PART III: MODELLING THE DYNAMICS OF SENSORY CONFLICT

Sensory conflict is a concept that has not been empirically verified, yet most theories of motion sickness assert its existence and posit its origins in the state estimation and motion perception framework used by the brain. In chapter 5 of this thesis, three motion perception models were evaluated, both for their perception predictions and their sickness predictions. These were the Subjective Vertical Model (SVM) (Bos and Bles, 1998; Kamiji et al., 2007), the Multi-Sensory Observer Model (MSOM) (Clark et al., 2019) and the Particle Filter Model (PFM) (Laurens and Droulez, 2007). It was found that, overall, the perception models did not generalise well to describe observed motion sickness across the range of motion paradigms evaluated. However, when specifically tuned for the empirical group-level sickness observations of O'Hanlon and McCauley (1974); Donohew and Griffin (2004), the SVM provided the best fit for sickness caused by translational accelerations. The underlying reason for this is the fact that SVM was the only model able to make frequency-variant fits for vertical motion sickness. The PFM has no vertical conflict and the MSOM has no frequency-variant vertical conflict. The reason why the SVM can be fitted, and the other two models could not, is because there is a leakage from the gravito-inertial force to the magnitude of the estimated gravity term, i.e. both the direction and the magnitude of gravity is actively estimated in the SVM. For both the MSOM and the PFM, the magnitude of gravity is fixed to  $9.81 \text{ ms}^{-2}$ . This means that overall, the SVM produced better fits to experimental sickness data.

Despite this fact, the SVM has certain drawbacks. As discussed in the introduction, the observer framework is used to model motion sickness. Here, the actual kinematic states of the organism are observed from noisy and ambiguous sensory signals. Indeed, both the MSOM and the PFM function in this manner. The SVM, however, is a partial observer, whereby only the angular velocity is strictly observed,

but acceleration and gravity are not. Instead, the 'perceived' variables that result from the initial filtering are tracked by the 'subjective' outputs of the internal model, whereby this tracking is facilitated by a feedback mechanism. This mechanism, which deviates from the theoretical framework set by [Oman \(1982\)](#), also explains, as shown in chapter 5 of this thesis, why the SVM overestimates sickness due to roll compared to the other models. Lastly, it is also not clear what the perceptual correlates of either the 'perceived' nor the 'subjective' variables in the SVM are.

For both the PFM and the MSOM the conflict term with the closest dynamics to the observed sickness is only generated for horizontal plane accelerations. This is interesting because it has a direct perceptual correlate in the well-known somatogravic effect. The somatogravic effect is an example of a perceptual conflict that occurs when there is an ambiguity in the perception of tilt and translation, usually induced by low-frequency horizontal plane accelerations. The difference between these two models and the SVM is that the somatogravic effect is mediated by the two-way coupling between the semicircular canals and the otoliths. This creates an emergent difference in the frequency sensitivities between vertical and horizontal accelerations. This is a characteristic that the SVM can only match by directional tuning of its parameters.

The somatogravic effect can be studied by investigating the time constant of the subjective vertical ([Correia Grácio et al., 2013](#)). This time constant determines the dynamics by which translation is inferred as tilt and vice versa. Indeed, the experiments in chapter 4 show the importance of the subjective vertical time constant, which was seen to be strongly correlated with overall sickness susceptibility ( $r = 0.74$ ). Interestingly, the time constant was not found to be correlated with the frequency of peak sickness. This could be because the experiment in chapter 4 was affected by multiple sources of uncertainty in determining both the perception parameters and the sickness responses, which may explain the lack of an observable effect. The results did not show a correlation between the velocity storage time constant and neither general motion sickness susceptibility, nor the peak sickness frequency. This is contrary to studies by [Dai et al. \(2003, 2007, 2010\)](#) and is likely due to the nature of the perturbation, which did not employ any rotational movement.

It is argued in chapter 5 that probabilistic models of sensory integration may represent a promising way of building on the current deterministic control-theoretic methods. Firstly, probabilistic models are able to capture the tilt-translation ambiguity as a bimodal distribution over most likely kinematic states for the organism, where the state uncertainty may be correlated with motion sickness. Secondly, as discussed previously, one characteristic of the SVM that allows for it to make frequency-variant sickness predictions for vertical accelerations is the fact that the magnitude of the gravity is free to vary. Probabilistic models have been shown to capture variations in the magnitude of gravity, whereby variations in the specific force cause dispersion in the distribution of the gravity estimates ([Kravets et al., 2021](#)). Such uncertainty may indeed help to better explain motion and model sickness due to vertical accelerations. The main findings from modelling the dynamics of sensory conflict were therefore

### Main Findings of Part III

- Perception-tuned sensory integration models adequately matched the perception data. Sickness tuning provided a reasonable sickness fits in the frequency domain.
- Current models do not generalise well across multiple motion paradigms to describe relative differences in observed motion sickness magnitudes
- The Subjective Vertical Model provides the best match to empirically observed group-level frequency sensitivities to horizontal and vertical plane motions
- An important mechanism to predict motion sickness induced by vertical accelerations is the active estimation of the magnitude of gravity
- The somatogravic effect, as mediated by the two-way coupling between semicircular canal and otolith sensory data, explains the differences in frequency sensitivity between vertical and horizontal acceleration stimuli
- The time constant of the subjective vertical, and hence the somatogravic effect, correlates strongly with individuals' motion sickness susceptibility

#### 6.1.4. IMPLICATIONS & RECOMMENDATIONS

In the following sections, the societal and scientific implications of this thesis are identified and recommendations for further research are given.

##### ONE SIZE DOES NOT FIT ALL

It is clear from the findings of this thesis that individuals vary considerably in how external motions affect them. With the removal of the driver, automated vehicles themselves will have complete control over their movements. Engineers have so far attempted to reduce motion sickness by penalising the most sickening frequencies, as identified in the experiments of [O'Hanlon and McCauley \(1974\)](#); [Donohew and Griffin \(2004\)](#), in their cost functions. However, as shown in chapter 4 of this thesis, individuals have widely varying frequency sensitivities, and group-level frequency sensitivities usually have a much wider bandwidth than individual sensitivities. This means that optimising with respect to group-level response likely leads to more motion sickness than optimising with respect to the individual.

Individualisation of trajectory planning and control algorithms is, however, not trivial. The experimentation required to obtain individual sensitivities took 6 weeks to complete; such a testing protocol is impractical for any applications. To do this in a commercial setting, a multi-stage research undertaking is first recommended.

Using the version of the Oman model in chapter 3, the individual frequency responses of chapter 4 could be matched by having an input transfer function weighing the different frequency accelerations to the Oman model. As said before, an estimation requiring prolonged exposure to single motion stimuli likely provides redundant information and, as shown in chapter 3, even an exposure to a MISC of 3 yields adequate information about individual susceptibility to a specific motion paradigm. Therefore, closed-loop system identification can be used in conjunction with a motion platform to perturb the participant individual in such a manner as to extract maximum information about their motion sickness dynamics. Such closed-loop identification methods have been successfully used in other engineering applications (Qian et al., 2016). The next step is to perform open-loop identification in the vehicular setting using continuous MISC data. If these techniques prove effective, one can aim to do open-loop identification based on sparse end-of-ride ratings given by passengers, whereby the parameters of the individual model are slowly tuned as the vehicle is used over the course of months. Such a strategy can enable reduced incidence of motion sickness without requiring complex sensory integration models.

Closed-loop identification in this manner is not only important for practical purposes, but also for progress in motion sickness research. Currently, a major hurdle is the 'data bottleneck'. Motion sickness data can generally only be gathered from a small number of participants for a small number of conditions, as larger experiments are both too time-consuming and costly. This thesis has shown that individuals have repeatable and regular responses, where these responses are well characterisable by a control theoretic model of motion sickness accumulation. Therefore, as discussed, model-based identification is likely the most promising way of alleviating this bottleneck.

### CONTEMPORARY MOTION SICKNESS MODELLING

John von Neumann famously said, *"With four parameters I can fit an elephant, and with five I can make him wiggle his trunk."* Indeed, we now know you only need four (complex) parameters (Mayer et al., 2010). This amusing quote underlies the important fact that it is not surprising for a complex model with many parameters to fit any dataset well. Motion perception models aim to emulate the complex behaviour of the brain and therefore tend to have a very large number of parameters. It is therefore easy to overfit the sensory conflict terms derived from these models to sickness data. In chapter 5 of this thesis, motion sickness models were also *validated* against a broad range of motion paradigms to which they were not fitted. Moreover, parameters obtained from motion sickness fitting were evaluated for their perception predictions. This validation of models in both sickness and perception is a methodological improvement that provides a way to avoid the pitfall of overfitting, which plagues models with many parameters.

As a consequence of this thorough validation, a number of practical recommendations are formulated here. Using data-driven models based on motion sickness dosage value (MSDV) (ISO 2631, 1997) are just as suitable as spatial orientation models to predict motion sickness. This is because models are fitted to the same empirical group-level sickness sensitivities derived from O'Hanlon and McCauley (1974); Donohew and Griffin (2004). Moreover, control theoretic models of motion sickness do

not generalise well to the motion paradigms they were not fitted to. In this sense, one advantage data based models have is that they are simpler to implement and are faster models to run, meaning they can be incorporated in real-time inside a control framework. These considerations are of particular concern to engineers who aim to mitigate motion sickness via various vehicle control strategies. On the other-hand, some researchers may want to preemptively explore the use of these mathematical models of motion sickness in a control framework (Buchheit et al., 2021), even though they are currently incomplete.

At a theoretical level, probabilistic modelling of perception, and thus motion sickness as its hypothesised derivative, seems to be the most promising future research direction to expand current deterministic approaches with. In a probabilistic framework, the aim would be to model uncertain sensory states that are often encountered during exposure to sickening motions. As discussed before, the tilt-translation ambiguity caused by low-frequency horizontal plane accelerations and off-vertical axis rotations, causes motion sickness. Evidence put forth in this thesis with respect to the importance of the subjective vertical time constant, and other cited literature, affirm the relevance of modelling these ambiguous sensory states. The two deterministic models (the SVM and MSOM) studied in this thesis, however, cannot model sensory ambiguity. On the other hand, the PFM is a fully probabilistic model, which is also inadequate because it is unable to model the frequency dependent nature of the posterior distribution of state variables. Recent works have indeed started to explore this direction, (Kravets et al., 2021) and it is the recommendation of this thesis that further effort be devoted to this topic. The manner by which these models are implemented can be very diverse. For instance, Kravets et al. (2021) uses a brute-force Monte Carlo method, which requires large amount of computational resources and has low biological plausibility. It may be prudent to use predictive coding as a strategy for implementing probabilistic inference (Friston et al., 2006; Friston, 2008). This is because, as discussed in the Introduction of this thesis, perception is a hierarchical operation organised up from the sensory periphery, to the simple integration of various sensory modalities, to higher level cognition. All layers are likely connected in a recurrent manner, which is best suited for a predictive coding framework.

### MEASURING MOTION SICKNESS

Motion sickness is not a physical quantity that can be measured directly, like a pressure, temperature or voltage. It is embodied within human perception, and therefore is subject to a number of biases. Moreover, humans cannot provide an absolute indication of their motion sickness level at a fine time or sickness resolution. This has led researchers to search for physiological signals such as ECG, GSR, EGG and EEG to objectively quantify the level of experienced motion sickness. In chapter 2 of this thesis, it was shown that although the galvanic skin response (GSR) in particular, was highly correlated with motion sickness, there was substantial individual scatter. Moreover, the specificity of any physiological signal remained an issue. For instance, GSR and ECG are both known to be correlated with other factors aside from motion sickness (Shi et al., 2017; Wang et al., 2018). Therefore, to study the dynamics and characteristics of motion sickness in a laboratory setting, these signals are, in general,



not useful. One specific way they may be used is to study the temporal evolution of specific symptoms, in which case these symptoms should be directly relatable to the chosen physiological signal and subjective ratings of that symptom should be collected continuously, in tandem.

Physiological measurement methods usually require skin contact with electrodes, and so are not yet appropriate for commercial use. In a vehicular setting, non-invasive passenger observations through methods such as facial expression and posture detection may be more straightforwardly realised. We know that researchers have already used certain behavioural markers such as yawning, signing and burping to visually observe sickness in their participants (Leung and Hon, 2019; Matsangas and Mccauley, 2014). Passive passenger observation via cameras may be used similarly, like a watchful chauffeur, to adapt vehicle behaviour to signs of passenger discomfort.

Whether passive observation is a feasible way of inferring motion sickness can be verified with an experiment where the participants are placed on a motion simulator and moved as they would be inside a vehicle. All participants ideally follow the same sickness trajectory, getting slowly to the same end-level of sickness. To enable this, a closed-loop control strategy, similar to the one discussed in section 6.1.4 can be used. To ensure natural behaviour, participants would be given freedom to do anything they would also do in an automated vehicle. Subjective sickness scores would be collected and compared to both behavioural markers (such as emotions, yawning, burping, seating adjustments). If passengers can indeed be passively monitored, the approach would translate readily to technology that can be utilised in automated passenger vehicles.

## 6.2. GENERAL CONCLUSION

In conclusion, this thesis provided crucial additional insights into the nature of motion sickness, elaborating on three aspects which were: quantitative analysis of individual differences, modelling temporal dynamics of perceived sickness and modelling the dynamics of sensory conflict. Where possible to do so, these insights were derived in a quantitative manner, through a control-theoretic modelling approach.

Before writing this thesis, the focus of motion sickness research was primarily on its average across the population. In the various chapters of this thesis, it was shown that individuals have repeatable motion sickness responses and that they generally show motion sickness dynamics that differ from the group. It was also shown that these dynamics could be correlated to motion perception parameters, thus providing a richer data-set for model development and validation. The individual was therefore shown to be a feasible unit to study, and doing so will provide further insights into the physiological processes that underlie sickness development.

Likewise, the temporal dynamics of motion sickness were studied in scenarios relevant for automated vehicles. For this, within-subject experiments with continuous sickness ratings were used to rigorously validate the Oman model and identify the time constants and gains that characterize the modelled sickness accumulation. For the first time, the Oman model was validated for multiple motion amplitude conditions and its non-linear power scaling at the output was found to effectively



capture the amplitude dependency in our experimental data. Moreover, important qualitative differences in sickness response were found, with people exhibiting convergent or divergent dynamics, whereby the former could be modelled more reliably by the Oman model.

Finally, existing models of motion perception were thoroughly validated for their ability to provide sickness predictions based on modelled perceptual conflicts. Important mechanisms for motion sickness modelling in the form of active estimation of the magnitude of gravity and the somatogravic effect, as mediated by the two-way coupling between the semicircular canals and the otoliths. Moreover, for the first time, we observed a strong correlation between the subjective vertical time constant, which influences the somatogravic effect, and overall motion sickness susceptibility.

The introductory paragraphs of this thesis mapped out the future terrain, whereby a key obstacle in utilisation of any autonomous driving technology is motion sickness. Overall, the research described in this thesis has increased both our understanding of motion sickness and also the availability of tools to ultimately mitigate it.

# REFERENCES

- Alexander CMKJB S J, Wendt GR (1947) Studies of motion sickness: [xvi]. the effects upon sickness rates of waves of various frequencies but identical acceleration. *Journal of Experimental Psychology* 37:440–448
- Angelaki DE, Shaikh AG, Green AM, Dickman JD (2004) Neurons compute internal models of the physical laws of motion. *Nature* 430(July):560–564, URL <https://doi.org/10.1038/nature02754>
- Angelaki DE, Klier EM, Snyder LH (2009a) A vestibular sensation: probabilistic approaches to spatial perception. *Neuron* 64(4):448–461, DOI <https://doi.org/10.1016/j.neuron.2009.11.010.A>
- Angelaki DE, Klier EM, Snyder LH (2009b) A vestibular sensation: probabilistic approaches to spatial perception. *Neuron* 64(4):448–461
- Barendswaard S, Pool DM, Abbink DA (2017) A Method to Assess Individualized Driver Models: Descriptiveness, Identifiability and Realism Driver Model used for Assessment. In: *Driving Simulation Conference*, URL <https://doi.org/10.1016/j.trf.2018.02.014>
- Barlow HB, Levick WR (1971) Responses to Single Quanta of Light in Retinal Ganglion Cells of the Cat. *Vision Research* (3):87–101, URL [https://doi.org/10.1016/0042-6989\(71\)90033-2](https://doi.org/10.1016/0042-6989(71)90033-2)
- Barnett-Cowan M, Meilinger T, Vidal M, Teufel H, Bühlhoff HH (2012) MPI cybermotion simulator: Implementation of a novel motion simulator to investigate multi-sensory path integration in three dimensions. *Journal of Visualized Experiments* (63):1–6, URL <https://doi.org/10.3791/3436>
- Bauerle A, Anken RH, Hilbig R, Baumhauer N, Rahmann H (2004) Size and cell number of the utricle in kinetically swimming fish : a parabolic aircraft flight study. *Advances in Space Research* 34:1598–1601, DOI 10.1016/j.asr.2004.01.024
- Benedek M, Kaernbach C (2010a) A continuous measure of phasic electrodermal activity. *Journal of Neuroscience Methods* 190(1):80–91, URL <http://dx.doi.org/10.1016/j.jneumeth.2010.04.028>
- Benedek M, Kaernbach C (2010b) Decomposition of skin conductance data by means of nonnegative deconvolution. *Psychophysiology* 47:647–658, URL <https://doi.org/10.1111/j.1469-8986.2009.00972.x>

- Berkouwer WR, Stroosma O, Van Paassen MM, Mulder M, Mulder JA (2005) Measuring the performance of the SIMONA Research Simulator's motion system. Collection of Technical Papers - AIAA Modeling and Simulation Technologies Conference 2005 2(August):1258–1269, DOI 10.2514/6.2005-6504
- Bertolini G, Straumann D (2016) Moving in a Moving world: A Review on vestibular Motion Sickness. *Frontiers in neurology* 7(14):1–11, URL <https://doi.org/10.3389/fneur.2016.00014>
- Bertolini G, Ramat S, Laurens J, Bockisch CJ, Marti S, Straumann D, Palla A (2011a) Velocity Storage Contribution to Vestibular Self-Motion Perception in Healthy Human Subjects. *Journal of Neurophysiology* 105(1):209–223, URL <https://doi.org/10.1152/jn.00154.2010>.
- Bertolini G, Ramat S, Laurens J, Bockisch CJ, Marti S, Straumann D, Palla A (2011b) Velocity Storage Contribution to Vestibular Self-Motion Perception in Healthy Human Subjects. *Journal of Neurophysiology* 105(1):209–223, URL <https://doi.org/10.1152/jn.00154.2010>.
- Bijveld MM, Bronstein AM, Golding JF, Gresty MA (2008) Nauseogenicity of off-vertical axis rotation vs. equivalent visual motion. *Aviation, space, and environmental medicine* 79(7):661–665, URL <https://doi.org/10.3357/ASEM.2241.2008>
- Billman GE (2013) The LF/HF ratio does not accurately measure cardiac sympathovagal balance. *Frontiers in Physiology* 4(February):1–5, URL <https://doi.org/10.3389/fphys.2013.00026>
- Bles W, Bos JE, Graaf B, Groen E, Wertheim AH (1998) Motion sickness: Only one provocative conflict. *Brain Research Bulletin* 47(5):481–487, DOI [https://doi.org/10.1016/S0361-9230\(98\)00115-4](https://doi.org/10.1016/S0361-9230(98)00115-4)
- Blouin J, Teasdale N, Mouchnino L (2007) Vestibular signal processing in a subject with somatosensory deafferentation : The case of sitting posture. *BMC Neurology* 7(25):1–8, DOI 10.1186/1471-2377-7-25
- Bock OL, Oman CM (1982) Dynamics of Subjective Discomfort in Motion Sickness as Measured with a Magnitude Estimation Method. *Aviation, space, and environmental medicine* 53(8):773–777
- Borah J, Young LR, Curry RE (1988) Optimal Estimator Model for Human Spatial Orientation. *Annals of the New York Academy of Science* 545(1), DOI <https://doi.org/10.1111/j.1749-6632.1988.tb19555.x>
- Bos J, Valk P, Hogervorst M (2008a) TNO Contribution to the Quest 303 Trial-Human Performance Assessed by a Vigilance and Tracking Test, a Multi-Attribute Task, and by Dynamic Visual Acuity (TNO (November 2015), URL <http://oai.dtic.mil/oai/oai?verb=getRecord{%&}metadataPrefix=html{%&}identifier=ADA485753>

## REFERENCES

---

- Bos JE (2011) Nuancing the relationship between motion sickness and postural stability. *Displays* 32(4):189–193, URL <http://dx.doi.org/10.1016/j.displa.2010.09.005>
- Bos JE (2015) Less sickness with more motion and/or mental distraction. *Journal of Vestibular Research: Equilibrium and Orientation* 25(1):23–33, DOI 10.3233/VES-150541
- Bos JE, Bles W (1998) Modelling motion sickness and subjective vertical mismatch detailed for vertical motions. *Brain Research Bulletin* 47(5):537–542, URL [https://doi.org/10.1016/S0361-9230\(98\)00088-4](https://doi.org/10.1016/S0361-9230(98)00088-4)
- Bos JE, Bles W (2002a) TM-02-C009 Visual-vestibular interactions and spatial (dis)orientation in flight and flight simulation. Tech. rep., TNO
- Bos JE, Bles W (2002b) Visual-vestibular interactions and spatial (dis)orientation in flight and flight simulation. Tech. rep., TNO
- Bos JE, Bles W, de Graaf B (2002) Eye movements to yaw, pitch, and roll about vertical and horizontal axes: adaptation and motion sickness. *Aviation, space, and environmental medicine* 73 5:436–44
- Bos JE, Mackinnon SN, Patterson A (2005) Motion Sickness Symptoms in a Ship Motion Simulator : Effects of Inside , Outside , and No View. *Aviat Space Environ Med* 76(12):1111–1118
- Bos JE, Bles W, Groen EL (2008b) A theory on visually induced motion sickness. *Displays* 29:47–57, URL <https://doi.org/10.1016/j.displa.2007.09.002>
- Bos JE, de Vries SC, van Emmerik ML, Groen EL (2010) The effect of internal and external fields of view on visually induced motion sickness. *Applied Ergonomics* 41(4):516–521, URL <http://dx.doi.org/10.1016/j.apergo.2009.11.007>
- Bowins B (2010) Motion sickness : A negative reinforcement model. *Brain Research Bulletin* 81:7–11, DOI 10.1016/j.brainresbull.2009.09.017
- Buchheit B, Schneider EN, Alayan M, Dauth F, Strauss DJ (2021) Motion sickness prediction in self-driving cars using the 6dof-svc model. *IEEE Transactions on Intelligent Transportation Systems* pp 1–10, DOI 10.1109/TITS.2021.3125802
- Butler C, Griffin MJ (2009) Motion Sickness with Combined Fore-Aft and Pitch Oscillation: Effect of Phase and the Visual Scene. *Aviation, space, and environmental medicine* 80(11):946–954, URL <https://doi.org/10.3357/ASEM.2490.2009>
- Butler CA, Griffin MJ (2006) Motion sickness during fore-and-aft oscillation: effect of the visual scene. *Aviation, space, and environmental medicine* 77(12):1236–43
- Cheung B, Nakashima A (2006) A review on the effects of frequency of oscillation on motion sickness p 29

- Cian C, Ohlmann T, Ceyte H, Gresty MA, Golding JF (2011) Off vertical axis rotation motion sickness and field dependence. *Aviation, space, and environmental medicine* 82(10):959–963, URL <https://doi.org/10.3357/ASEM.3049.2011>
- Clark TK, Newman MC, Oman CM, Merfeld DM, Young LR (2015) Human perceptual overestimation of whole body roll tilt in hypergravity. *Journal of Neurophysiology* 113(7):2062–2077, URL <https://doi.org/10.1152/jn.00095.2014>
- Clark TK, Newman MC, Karmali F, Oman CM, Merfeld DM (2019) *Mathematical models for dynamic, multisensory spatial orientation perception*, vol 248, 1st edn. Elsevier B.V., URL <http://dx.doi.org/10.1016/bs.pbr.2019.04.014>
- Cleij D, Venrooij J, Pretto P, Katliar M, Bühlhoff HH, Steffen D, Hoffmeyer FW, Schöner H (2019) Comparison between filter- and optimization-based motion cueing algorithms for driving simulation. *Transportation Research Part F: Psychology and Behaviour* 61:53–68, URL <https://doi.org/10.1016/j.trf.2017.04.005>
- Clément G, Deguine O, Vasseur-clausen McCsP, Pavy-letraon A (2001) Effects of cosmonaut vestibular training on vestibular function prior to space flight. *Eur J Appl Physiol* 85:539–545, URL <https://doi.org/10.1007/s004210100494>
- Clément G, Deguine O, Bourg M, Pavy-letraon A (2007) Effects of vestibular training on motion sickness, nystagmus, and subjective vertical. *Journal of Vestibular Research* 17(February 2007), URL <https://pubmed.ncbi.nlm.nih.gov/18626134/>
- Correia Grácio BJ, de Winkel KN, Groen EL, Wentink M, Bos JE (2013) The time constant of the somatogravic illusion. *Exp Brain Res* 224(3):313–321, URL <https://doi.org/10.1007/s00221-012-3313-3>
- Correia Gracio BJ, de Winkel KN, Groen EL, Wentink M, Bos JE (2013) The time constant of the somatogravic illusion. *Exp Brain Res* 224(3):313–321
- Cowings PS, Toscano WB (1993) *Autogenic-Feedback Training (AFT) as a Preventive Method for Space Motion Sickness: Background and Experimental Design*. Tech. rep., NASA, URL <https://ntrs.nasa.gov/archive/nasa/casi.ntrs.nasa.gov/19940011064.pdf>
- Crano WD (1991) Pitfalls associated with the use of financial incentives (and other complex manipulations) in human social research. *Basic and Applied Social Psychology* 12(4):369–390
- Cullen KE (2018) *Multisensory Integration and the Perception of Self-Motion*. September, Oxford University Press, DOI <https://doi.org/10.1093/acrefore/9780190264086.013.91>
- Curthoys IS (1996) The delay of the oculogravic illusion. *Brain Research Bulletin* 40(5):407–410, URL [https://doi.org/10.1016/0361-9230\(96\)00134-7](https://doi.org/10.1016/0361-9230(96)00134-7)

## REFERENCES

---

- Dahlman J, Sjörs A, Lindström J, Ledin T (2009) Performance and Autonomic Responses During Motion Sickness. *Human Factors* 51(1):56–66, URL <https://doi.org/10.1177/0018720809332848>
- Dai M, Kunin M, Raphan T, Cohen B (2003) The relation of motion sickness to the spatial-temporal properties of velocity storage. *Exp Brain Res* 151(2):173–189, URL <https://doi.org/10.1007/s00221-003-1479-4>
- Dai M, Raphan T, Cohen B (2007) Labyrinthine lesions and motion sickness susceptibility. *Exp Brain Res* 178(4):477–487, URL <https://doi.org/10.1007/s00221-006-0759-1>
- Dai M, Sofroniou S, Kunin M, Raphan T, Cohen B (2010) Motion sickness induced by off-vertical axis rotation (OVAR). *Exp Brain Res* pp 207–222, URL <https://doi.org/10.1007/s00221-010-2305-4>
- De Graaf B, Bos J, Tielemans W, Rameckers F, Rupert A, Guedry F (1996) Otolith contribution to ocular torsion and spatial orientation during acceleration. Tech. rep., Naval Aerospace Medical Research Laboratory
- de Winkel KN, Katliar M, Diers D, Bühlhoff HH (2018) Causal inference in the perception of verticality. *Scientific reports* 8(1):1–12
- de Winkel KN, Edel E, Happee R, Bühlhoff HH (2020) Multisensory interactions in head and body centered perception of verticality. *Front Neurosci* URL <https://doi.org/10.3389/fnins.2020.599226>
- de Winkel KN, Irmak T, Kotian V, Pool DM, Happee R (2022) Relating individual motion sickness levels to subjective discomfort ratings. *Experimental Brain Research* pp 1–10
- Denise P (1993) The cerebellum as a predictor of neural messages—II. Role in motor control and motion sickness. *Neuroscience* 56(3):647–655, DOI [https://doi.org/10.1016/0306-4522\(93\)90362-J](https://doi.org/10.1016/0306-4522(93)90362-J)
- Denise P, Etard O, Zupan LH, Darlot C (1996) Motion sickness during off-vertical axis rotation prediction by a model of sensory interactions and correlation with other forms of motion sickness. *Neuroscience Letters* 203(3):183–186, URL [https://doi.org/10.1016/0304-3940\(96\)12303-X](https://doi.org/10.1016/0304-3940(96)12303-X)
- Diels C, Bos JE (2016) Self-driving carsickness. *Applied Ergonomics* 53:374–382, URL <http://dx.doi.org/10.1016/j.apergo.2015.09.009>
- Donohew BE, Griffin MJ (2004) Motion sickness: effect of the frequency of lateral oscillation. *Aviation, space, and environmental medicine* 75(8):649–56
- Dziak JJ, Coffman DL, Lanza ST, Li R, Jermini LS (2019) Sensitivity and specificity of information criteria. *Briefings in Bioinformatics* 21(2):553–565, DOI [10.1093/bib/bbz016](https://doi.org/10.1093/bib/bbz016), URL <https://doi.org/10.1093/bib/bbz016>, <https://academic.oup.com/bib/article-pdf/21/2/553/33583256/bbz016.pdf>

- Fabozzi FJ, Focardi SM, Rachev ST, Arshanapalli BG (2014) Appendix E: Model Selection Criterion: AIC and BIC, John Wiley & Sons, Ltd, pp 399–403. URL <https://doi.org/10.1002/9781118856406.app5>
- Faisal AA, Selen LPJ, Wolpert DM (2008) Noise in the nervous system. *Nature Reviews Neuroscience* 9(april):292–303, URL <https://doi.org/10.1038/nrn2258>
- Feenstra PJ, Bos JE, Gent RNHWV (2011) A visual display enhancing comfort by counteracting airsickness. *Displays* 32(4):194–200, URL <http://dx.doi.org/10.1016/j.displa.2010.11.002>
- Feng F, Bao S, Sayer JR, Flanagan C, Manser M, Wunderlich R (2017) Can vehicle longitudinal jerk be used to identify aggressive drivers? An examination using naturalistic driving data. *Accident Analysis and Prevention* 104(May):125–136, DOI 10.1016/j.aap.2017.04.012, URL <http://dx.doi.org/10.1016/j.aap.2017.04.012>
- Fernando M, Samita S, Abeynayake R (2012) Modified Factor Analysis to Construct Composite Indices: Illustration on Urbanization Index. *Tropical Agricultural Research* 23(4):327
- Fiorello D, Martino A, Zani L, Christidis P, Navajas-cawood E (2016) Mobility data across the EU 28 member states : results from an extensive CAWI survey. *Transportation Research Procedia* 14:1104–1113, DOI 10.1016/j.trpro.2016.05.181, URL <http://dx.doi.org/10.1016/j.trpro.2016.05.181>
- Fox J (2002) Bootstrapping Regression Models. URL <https://socialsciences.mcmaster.ca/jfox/Books/Companion-1E/appendix.html>
- Freedman DA (1999) Ecological Inference. *International Encyclopedia of the Social & Behavioral Sciences: Second Edition* pp 868–870, DOI 10.1016/B978-0-08-097086-8.42117-3
- Friston K (2005) A theory of cortical responses. *Philos Trans R Soc Lond B Biol Sci* 360(April):815–836, DOI 10.1098/rstb.2005.1622
- Friston K (2008) Hierarchical Models in the Brain. *PLOS Computational Biology* 4(11), DOI 10.1371/journal.pcbi.1000211
- Friston K, Kilner J, Harrison L (2006) A free energy principle for the brain. *Journal of Physiology* 100:70–87, DOI 10.1016/j.jphysparis.2006.10.001
- Gianaros PJ, Muth ER, Mordkoff TJ, Levine ME (2001) A Questionnaire for the Assessment of the Multiple Dimensions of Motion Sickness. *Aviation, space, and environmental medicine* 72(2):115–119
- Gianna C, Heimbrand S, Gresty M (1996) Thresholds for detection of motion direction during passive lateral whole-body acceleration in normal subjects and patients with bilateral loss of labyrinthine function. *Brain Research Bulletin* 40(5):443–447, DOI [https://doi.org/10.1016/0361-9230\(96\)00140-2](https://doi.org/10.1016/0361-9230(96)00140-2), spatial Orientation

## REFERENCES

---

- Golding F, Stott JRR (1997) Objective and subjective time courses of recovery from motion sickness assessed by repeated motion challenges j. *Journal of vestibular research : equilibrium & orientation* 7(6):421–428
- Golding JF (2006) Motion sickness susceptibility. *Autonomic Neuroscience: Basic and Clinical* 129:67–76, DOI 10.1016/j.autneu.2006.07.019
- Golding JF, Markey HM (1996) Effect of frequency of horizontal linear oscillation on motion sickness and somatogravic illusion. *Aviation Space and Environmental Medicine* 67(January):121–126, URL <https://pubmed.ncbi.nlm.nih.gov/8834936/>
- Golding JF, Phil D, Markey HM, Stott JRR (1995) The effects of motion direction, body axis, and posture on motion sickness induced by low frequency linear oscillation. *Aviation, space, and environmental medicine* 66(11):1046–1051
- Golding JF, Bles W, Bos JE, Haynes T, Gresty MA (2003) Motion Sickness and Tilts of the Inertial Force Environment: Active Suspension Systems vs Active Passengers. *Aviation, space, and environmental medicine* 74(3):220–227
- Graybiel A (1969) Structural elements in the concept of motion sickness. *Aerospace medicine* 40(4):351–367
- Graybiel A (1970) Susceptibility to acute motion sickness in blind persons. *Aerospace medicine* 41(6)
- Graybiel A, Brown RH (1951) The delay in visual reorientation following exposure to a change in direction of resultant force on a human centrifuge. *Journal of General Psychology* 45(2):143–150, DOI <https://doi.org/10.1080/00221309.1951.9918275>
- Griffin MJ, Howarth HVC (2000) Motion Sickness History Questionnaire M.J. Griffin and H.V.C. Howarth ISVR Technical Report No. 283 May 2000. Tech. Rep. 283, ISVR University of Southampton, URL <https://eprints.soton.ac.uk/10465/1/Pub1228.pdf>
- Griffin MJ, Mills KL (2002) Effect of frequency and direction of horizontal oscillation on motion sickness. *Aviation, space, and environmental medicine* 73(6):537–543, URL <http://europepmc.org/abstract/MED/12056668>
- Griffin MJ, Newman MM (2004a) Visual Field Effects on Motion Sickness in Cars. *Aviation, space, and environmental medicine* 75(9):739–748
- Griffin MJ, Newman MM (2004b) Visual Field Effects on Motion Sickness in Cars. *Aviat Space Environ Med* 75(9):739–748
- Guedry FE (1974) Psychophysics of Vestibular Sensation BT - Vestibular System Part 2: Psychophysics, Applied Aspects and General Interpretations. Springer Berlin Heidelberg, Berlin, Heidelberg, pp 3–154, URL [https://doi.org/10.1007/978-3-642-65920-1\\_1](https://doi.org/10.1007/978-3-642-65920-1_1)



- Guedry Jr FE (1970) Conflicting sensory orientation cues as a factor in motion. In: Fourth Symposium on the Role of the Vestibular Organs in Space Exploration..., Scientific and Technical Information Division, National Aeronautics and ... , vol 187, p 45
- Heerspink H, Berkouwer W, Stroosma O, Van Paassen MM, Mulder M, Mulder B (2005) Evaluation of vestibular thresholds for motion detection in the simona research simulator. In: AIAA modeling and simulation technologies conference and exhibit, p 6502, DOI 10.2514/6.2005-6502
- Held R (1961) Sensory deprivation: Facts in search of a theory. exposure-history as a factor in maintaining stability of perception and coordination. *Journal of Nervous and Mental disease*
- Henderson D, Jacobson S, Johnson A (2006) The Theory and Practice of Simulated Annealing, pp 287–319. DOI 10.1007/0-306-48056-5\_10
- Hermesdorger J, Elias Z, Cole D, Quaney BM, Nowak DA (2008) Preserved and Impaired Aspects of Feed-Forward Grip Force Control After Chronic Somatosensory Deafferentation. *Neurorehabil Neural Repair* 22:374–384, DOI 10.1177/1545968307311103
- Hickman MA, Cox SR, Mahabir S, Miskell C, Lin J, Bungeer A, Call RBMC (2008) Safety , pharmacokinetics and use of the novel NK-1 receptor antagonist maropitant ( Cerenia TM ) for the prevention of emesis and motion sickness in cats. *J vet Pharmacol Therap* 31:220–229, DOI 10.1111/j.1365-2885.2008.00952.x.Safety
- Himi N, Koga T, Nakamura E, Kobashi M (2004) Differences in autonomic responses between subjects with and without nausea while watching an irregularly oscillating video. *Auton Neurosci* 116:46–53, URL <https://doi.org/10.1016/j.autneu.2004.08.008>
- Hinterecker T, Pretto P, de Winkel KN, Karnath HO, Bühlhoff HH, Meilinger T (2018) Body-relative horizontal–vertical anisotropy in human representations of traveled distances. *Exp Brain Res* 236, DOI 10.1007/s00221-018-5337-9
- Holly JE, Harmon SM (2013) NIH Public Access. *Journal of vestibular research : equilibrium & orientation* 22(2):81–94, DOI 10.3233/VES-2012-0441, URL <https://doi.org/10.3233/VES-2012-0441>
- Holmes SR, Griffin MJ (2001) Correlation Between Heart Rate and the Severity of Motion Sickness Caused by Optokinetic Stimulation. *Journal of Psychophysiology* 15:35–42, URL <https://doi.org/10.1027//0269-8803.15.1.35>
- Howarth HVC, Griffin MJ (2003) Effect of roll oscillation frequency on motion sickness. *Aviation, space, and environmental medicine* 74(4):326–31, URL <http://www.ncbi.nlm.nih.gov/pubmed/12688450>

## REFERENCES

---

- Htike Z, Papaioannou G, Velenis E, Longo S (2020) Motion Planning of Self-driving Vehicles for Motion Sickness Minimisation. European Control Conference 2020, ECC 2020 pp 1719–1724, DOI 10.23919/ecc51009.2020.9143789
- Huang Y, Rao RPN (2011) Predictive coding. *WIREs Cognitive Science* 2(5), DOI 10.1002/wcs.142
- Huppert D, Benson J, Brandt T (2017) A historical view of motion sickness-A plague at sea and on land, also with military impact. *Frontiers in Neurology* 8(APR):1–15, DOI 10.3389/fneur.2017.00114
- Irmak T, Pool DM, Happee R (2020) Objective and Subjective Responses to Motion Sickness: The Group and The Individual. *Exp Brain Res* URL <https://doi.org/10.1007/s00221-020-05986-6>
- Irmak T, de Winkel KD, Pool D, Bühlhoff H, Happee R (2021a) Individual motion perception parameters and motion sickness frequency sensitivity in fore-aft motion. *Experimental Brain Research* 239:1727 – 1745
- Irmak T, de Winkel KN, Pattanayak A, Happee R (2021b) Motion Sickness , Motivation , Workload and Task Performance in Automated Vehicles. In: *Comfort Congress*
- ISO 2631 (1997) Mechanical vibration and shock — Evaluation of human exposure to whole-body vibration — Part 1: General requirements. Standard, International Organization for Standardization, Geneva, CH
- Jamali M, Carriot J, Chacron MJ, Cullen KE (2013) Strong Correlations between Sensitivity and Variability Give Rise to Constant Discrimination Thresholds across the Otolith Afferent Population. *Journal of Neuroscience* 33(27):11302–11313, URL <https://doi.org/10.1523/JNEUROSCI.0459-13.2013>
- Johnson WH, Sunahara FA (1999) Importance of the vestibular system in visually induced nausea and self-vection. *Journal of Vestibular Research* 9:83–87
- Kamiji N, Kurata Y, Wada T, Doi S (2007) Modeling and validation of carsickness mechanism. In: *SICE Annual Conference 2007*, pp 1138–1143, DOI <https://doi.org/10.1109/SICE.2007.4421156>
- Karjanto J, Yusof N, Wang C, Terken J, Delbressine F, Rauterberg M (2018) The effect of peripheral visual feedforward system in enhancing situation awareness and mitigating motion sickness in fully automated driving. *Transportation Research Part F: Psychology and Behaviour* 58:678–692, URL <https://doi.org/10.1016/j.trf.2018.06.046>
- Kennedy RS, Tolhurst GC, Graybiel A (1965) The Effects of Visual Deprivation on Adaptation to a Rotating Environment. *Tech. rep.*, DOI 10.1136/bmj.1.3971.358

- Keshavarz B, Hecht H (2011) Validating an efficient method to quantify motion sickness. *Human Factors* 53(4):415–426, URL <https://doi.org/10.1177/0018720811403736>
- Khalid H, Turan O, Bos JE (2011a) Theory of a subjective vertical-horizontal conflict physiological motion sickness model for contemporary ships. *Journal of Marine Science and Technology* 16(2):214–225, URL <https://doi.org/10.1007/s00773-010-0113-y>
- Khalid H, Turan O, Bos JE, Incecik A (2011b) Application of the subjective vertical – horizontal-conflict physiological motion sickness model to the field trials of contemporary vessels. *Ocean Engineering* 38(1):22–33, DOI 10.1016/j.oceaneng.2010.09.008, URL <http://dx.doi.org/10.1016/j.oceaneng.2010.09.008>
- Klinke S, Wagner C (2008) Visualizing exploratory factor analysis models. Tech. rep., Humboldt-Universität zu Berlin, Berlin
- Klosterhalfen S, Kellermann S, Pan F, Stockhorst U, Hall G, Enck P (2005) Effects of Ethnicity and Gender on Motion Sickness Susceptibility. *Aviat Space Environ Med* 76(11):1051–1057
- Kornmeier J, Maira C, Bach M (2009) Brain and Cognition Multistable perception : When bottom-up and top-down coincide. *Brain and Cognition* 69(1):138–147, DOI 10.1016/j.bandc.2008.06.005, URL <http://dx.doi.org/10.1016/j.bandc.2008.06.005>
- Koslucher F, Haaland E, Malsch A, Webeler J (2015) Sex Differences in the Incidence of Motion Sickness Induced by Linear Visual Oscillation. *AEROSPACE MEDICINE AND HUMAN PERFORMANCE* 86(9):787–793, DOI 10.3357/AMHP.4243.2015
- Kravets VG, Dixon JB, Ahmed NR, Clark TK (2021) Compass: Computations for orientation and motion perception in altered sensorimotor states. *Frontiers in Neural Circuits* 15:113, DOI 10.3389/fncir.2021.757817, URL <https://www.frontiersin.org/article/10.3389/fncir.2021.757817>
- Kuiper OX, Bos JE (2019) Knowing What’s Coming : Unpredictable Motion Causes More Motion Sickness. *Human Factors and Ergonomics Society* URL <https://doi.org/10.1177/0018720819876139>
- Kuiper OX, Bos JE, Diels C (2018) Looking forward : In-vehicle auxiliary display positioning affects carsickness. *Applied Ergonomics* 68(April):169–175, URL <https://doi.org/10.1016/j.apergo.2017.11.002>
- Kuiper OX, Bos JE, Schmidt EA, Diels C, Wolter S (2020) knowing what’s coming: unpredictable motion causes more motion sickness. *Human factors* 62(8):1339–1348

## REFERENCES

---

- Kyriakidis M, Happee R, Winter JCFD (2015) Public opinion on automated driving : Results of an international questionnaire among 5000 respondents. *Transportation Research Part F: Psychology and Behaviour* 32:127–140, DOI 10.1016/j.trf.2015.04.014, URL <http://dx.doi.org/10.1016/j.trf.2015.04.014>
- Lackner JR (2014) Motion sickness : more than nausea and vomiting. *Exp Brain Res* 232:2493–2510, URL <https://doi.org/10.1007/s00221-014-4008-8>
- Laurens J, Angelaki DE (2011) The functional significance of velocity storage and its dependence on gravity. *Experimental Brain Research* 210(3-4):407–422, URL <https://doi.org/10.1007/s00221-011-2568-4>
- Laurens J, Angelaki DE (2017) A unified internal model theory to resolve the paradox of active versus passive self- motion sensation. *Elife* (18 Oct):1–45, URL <https://doi.org/10.7554/eLife.28074.001>
- Laurens J, Droulez J (2007) Bayesian processing of vestibular information. *Biological Cybernetics* 96(4):389–404, DOI <https://doi.org/10.1007/s00422-006-0133-1>
- Laurens J, Droulez J (2008) Bayesian Modelling of Visuo-Vestibular Interactions. In: *Probabilistic Reasoning and Decision Making in Sensory-Motor Systems*, pp 279–300, DOI [https://doi.org/10.1007/978-3-540-79007-5\\_12](https://doi.org/10.1007/978-3-540-79007-5_12)
- Laurens J, Meng H, Angelaki DE (2013) Computation of linear acceleration through an internal model in the macaque cerebellum. *Nat Neurosci* 16(11), URL <https://doi.org/10.1038/nn.3530>
- Lawther A, Griffin MJ (1988) Motion sickness and motion characteristics of vessels at sea. *Ergonomics* 31(10):1373–1394, DOI 10.1080/00140138808966783
- Leung A, Hon K (2019) Motion sickness: an overview. *Drugs in Context* 8, DOI 10.7573/dic.2019-9-4
- Li D, Hu J (2021) Mitigating Motion Sickness in Automated Vehicles With Frequency-Shaping Approach to 6(4):7714–7720
- Lillywhite PG, Laughlin SB (1979) Transducer noise in photoreceptor. *Nature* 277(February):569–572
- Lim K, Karmali F, Nicoucar K, Merfeld DM (2017) Perceptual precision of passive body tilt is consistent with statistically optimal cue integration. *Journal of neurophysiology* 117(5):2037–2052
- Lin Ct, Lin Cl, Chiu Tw, Member S, Duann Jr (2011) Effect of respiratory modulation on relationship between heart rate variability and motion sickness. In: *2011 Annual International Conference of the IEEE Engineering in Medicine and Biology Society*, pp 1921–1924, URL <https://doi.org/10.1109/IEMBS.2011.6090543>

- Mackersie L C, Calderon-moultrie N (2016) Autonomic Nervous System Reactivity During Speech Repetition Tasks : Heart Rate Variability and Skin Conductance. *Ear and Hearing* 37:118–125, URL <https://doi.org/10.1097/AUD.0000000000000305>
- Mackrous I, Carriot J, Jamali M, Cullen KE (2019) Cerebellar prediction of the dynamic sensory consequences of gravity. *Current Biology* 29(16):2698–2710
- Manley GA (2012) Evolutionary paths to mammalian cochleae. *JARO - Journal of the Association for Research in Otolaryngology* 13(6):733–743, DOI 10.1007/s10162-012-0349-9
- Mars F, Saleh L, Chevrel P, Claveau F, Lafay Jf (2011) Modeling the Visual and Motor Control of Steering With an Eye to Shared-Control Automation. In: *Proceedings of the Human Factors and Ergonomics Society Annual Meeting*, 55, URL <http://dx.doi.org/10.1177/1071181311551296>
- Matsangas P, McCauley ME (2014) Sopite Syndrome : A Revised Definition. *Aviation, space, and environmental medicine* URL <https://doi.org/10.3357/ASEM.3891.2014>
- Mayer J, Khairy K, Howard J (2010) Drawing an elephant with four complex parameters. *Am J Phys* 78, DOI 10.1119/1.3254017
- Mayne R (1974) A systems concept of the vestibular organs. In: *Vestibular system part 2: psychophysics, applied aspects and general interpretations*, Springer, pp 493–580
- McCauley ME, O’Hanlon JF, Royal JM, Wackie RR, Wylie CD (1976) Motion Sickness Incidence Exploratory Studies of Habituation, Pitch and Roll, and the Refinement of a Mathematical Model. Tech. Rep. April
- Merfeld DM, Young LR, Oman CM, Shelhamer MJ (1993) A multidimensional model of the effect of gravity on the spatial orientation of the monkey. *Journal of vestibular research : equilibrium & orientation* 3(2):141–61, URL <http://www.ncbi.nlm.nih.gov/pubmed/8275250>
- Merfeld DM, Zupan L, Peterka RJ (1999) Humans use internal models to estimate gravity and linear acceleration. *Nature* 398(April):615–618
- Merfeld DM, Zupan LH, Gifford CA (2000) Neural Processing of Gravito-Inertial Cues in Humans. II. Influence of the Semicircular Canals During Eccentric Rotation. *Journal of Neurophysiology* 85(4):1648–1660, URL <https://doi.org/10.1152/jn.2001.85.4.1648>
- Merfeld DM, Park S, Gianna-Poulin C, Black FO, Wood S (2005a) Vestibular perception and action employ qualitatively different mechanisms. I. Frequency response of VOR and perceptual responses during Translation and Tilt. *Journal of Neurophysiology* 94(1):186–198, URL <https://doi.org/10.1152/jn.00904.2004>

## REFERENCES

---

- Merfeld DM, Park S, Gianna-Poulin C, Black FO, Wood S (2005b) Vestibular perception and action employ qualitatively different mechanisms. I. Frequency response of VOR and perceptual responses during Translation and Tilt. *Journal of Neurophysiology* 94(1):186–98, DOI <https://doi.org/10.1152/jn.00904.2004>
- Merfeld DM, Park S, Gianna-Poulin C, Black FO, Wood S (2005c) Vestibular Perception and Action Employ Qualitatively Different Mechanisms. II. VOR and Perceptual Responses During Combined Tilt&Translation. *Journal of Neurophysiology* 94(1):199–205, DOI <https://doi.org/10.1152/jn.00905.2004>
- Miermeister P, Lächele M, Boss R, Masone C, Schenk C, Tesch J, Kerger M, Teufel H, Pott A, Bühlhoff HH (2016) The CableRobot simulator large scale motion platform based on Cable Robot technology. *IEEE International Conference on Intelligent Robots and Systems 2016-Novem*:3024–3029, URL <https://doi.org/10.1109/IRoS.2016.7759468>
- Miller EF, Graybiel A (1969) A Standardized Laboratory Means of Determining Susceptibility to Coriolis (Motion) Sickness. Tech. rep., NASA
- Mitchell D, Krusemark ML, Hafner E (1977) Pica: A species relevant behavioral assay of motion sickness in the rat. *Physiology & Behavior* 18:125–130
- Mullen TJ, Berger RD, Oman CM, Cohen RJ (1998) Human Heart Rate Variability Relation Is Unchanged During Motion Sickness. *Journal of Vestibular Research* 8(I):95–105
- Naitoh T, Wassersug RJ, Yamashita M (2001) Factors influencing the susceptibility of anurans to motion sickness. *Journal of Comparative Physiology - A Sensory, Neural, and Behavioral Physiology* 187(2):105–113, DOI 10.1007/s003590100181
- Nam Jh (2017) An operating principle of the turtle utricle to detect wide dynamic range. *Hearing Research* pp 1–9, DOI 10.1016/j.heares.2017.09.015, URL <https://doi.org/10.1016/j.heares.2017.09.015>
- Nestmann S, Karnath HO, Bühlhoff HH, Nikolas de Winkel KN (2020) Changes in the perception of upright body orientation with age. *PloS one* 15(5):e0233160
- Newman MC (2009) A Multisensory Observer Model for Human Spatial Orientation Perception. PhD thesis, Massachusetts Institute Of Technology, URL <https://core.ac.uk/download/pdf/4416187.pdf>
- Newman MC, Lawson BD, Rupert AH, Mcgrath BJ (2012) The Role of Perceptual Modeling in the Understanding of Spatial Disorientation During Flight and Ground-based Simulator Training. In: *AIAA Modeling and Simulation Technologies Conference*, URL <https://doi.org/10.2514/6.2012-5009>
- Nouri S, Karmali F (2018) Variability in the Vestibulo-Ocular Reflex and Vestibular Perception. *Neuroscience* 393:350–365, URL <https://doi.org/10.1016/j.neuroscience.2018.08.025>

- O'Hanlon JF, McCauley ME (1973) Motion sickness indices as a function of the frequency and accelerations of vertical sinusoidal motion. Tech. Rep. September, Human Factors Research, Incorporated
- O'Hanlon JF, McCauley ME (1974) Motion sickness incidence as a function of the frequency and acceleration of vertical sinusoidal motion. *Aerospace medicine* 45(4):366–9, URL <http://www.ncbi.nlm.nih.gov/pubmed/4821729>
- Ohyama S, Nishiike S, Watanabe H, Matsuoka K (2007) Autonomic responses during motion sickness induced by virtual reality. *Auris Nasus Larynx* 34(3):303–306, URL <http://dx.doi.org/10.1016/j.anl.2007.01.002>
- Okada T, Grunfeld E, Shallo-Hoffmann J, Bronstein AM (1999) Vestibular perception of angular velocity in normal subjects and in patients with congenital nystagmus. *Brain* 122(7):1293–1303, URL <https://doi.org/10.1093/brain/122.7.1293>
- Oman CM (1982) A heuristic mathematical model for the dynamics of sensory conflict and motion sickness. *Acta Oto-Laryngologica* 94(sup392):4–44, URL <https://doi.org/10.3109/00016488209108197>
- Oman CM (1990a) Motion sickness : a synthesis and evaluation of the sensory conflict theory. *Canadian Journal of Physiology and Pharmacology* 68(2):294–303, URL <https://doi.org/10.1139/y90-044>
- Oman CM (1991) Sensory conflict in motion sickness: an observer theory approach. *Pictorial communication in virtual and real environments* pp 362–376
- Oman CM (2012) Are evolutionary hypotheses for motion sickness “ just-so ” stories ? 1. *Journal of Vestibular Research* 22:117–127, DOI 10.3233/VES-2011-0432
- Oman CM, Cullen KE (2014) Brainstem processing of vestibular sensory exafference : implications for motion sickness etiology. *Exp Brain Res* pp 2483–2492, URL <https://doi.org/10.1007/s00221-014-3973-2>
- Oman CM, Cullen E Kathleen (2015) Brainstem processing of vestibular sensory exafference: implications for motion sickness etiology. *Exp Brain Res* 232(8):2483–2492, URL <https://doi.org/10.1007/s00221-014-3973-2.Brainstem>
- Oman CM, Lichtenberg BK, Money KE, Mccoy RK (1986) M.I.T./Canadian vestibular experiments on the Spacelab-1 mission 4. Space motion sickness: symptoms, stimuli and predictability. *Exp Brain Res* 65:316–334, URL [https://doi.org/10.1016/0022-460X\(90\)90652-G](https://doi.org/10.1016/0022-460X(90)90652-G)
- Oman M (1990b) Motion sickness : a synthesis and evaluation of the sensory conflict theory. *Can J Physiol Pharmacol*
- Östh J, Eliasson E, Happee R, Brolin K (2014) A method to model anticipatory postural control in driver braking events. *Gait and Posture* 40(4):664–669, DOI 10.1016/j.gaitpost.2014.07.021



## REFERENCES

---

- Otto B, Riepl RL, Otto C, Klose J, Enck P, Klosterhalfen S (2005)  $\mu$ -Opiate receptor agonists – a new pharmacological approach to prevent motion sickness ? *British Journal of Clinical Pharmacology* 61:27–30, DOI 10.1111/j.1365-2125.2005.02505.x
- Panic H, Panic AS, Dizio P, Lackner JR (2015) Direction of balance and perception of the upright are perceptually dissociable. *J Neurophysiol* (June 1):3600–3609, URL <https://doi.org/10.1152/jn.00737.2014>
- Parker LA (2014) Conditioned flavor avoidance and conditioned gaping : Rat models of conditioned nausea. *European Journal of Pharmacology* 722:122–133, DOI 10.1016/j.ejphar.2013.09.070, URL <http://dx.doi.org/10.1016/j.ejphar.2013.09.070>
- Paulin XMG, Hoffman LF (2019) Models of vestibular semicircular canal afferent neuron firing activity. *J Neurophysiol* 122:2548–2567, DOI 10.1152/jn.00087.2019
- Qian J, Nadri M, Dufour P (2016) Optimal input design for parameter estimation of nonlinear systems: case study of an unstable delta wing. *International Journal of Control* 90:1–15, DOI 10.1080/00207179.2016.1225990
- Quarck G, Etard O, Oreel M, Denise P (2000) Motion sickness occurrence does not correlate with nystagmus characteristics. *Neuroscience Letters* 287:49–52, URL [https://doi.org/10.1016/S0304-3940\(00\)01140-X](https://doi.org/10.1016/S0304-3940(00)01140-X)
- Rao RPN, Ballard DH (1999) Hierarchical Predictive Coding Model Hierarchical Predictive Coding of Natural Images. *Nature neuroscience* 2(1):79–87, URL <http://neurosci.nature.com>
- Reason JT (1978) Motion sickness adaptation: a neural mismatch model. *Journal of the Royal Society of Medicine* 71(11):819–29, URL <http://www.ncbi.nlm.nih.gov/pubmed/731645%0Ahttp://www.pubmedcentral.nih.gov/articlerender.fcgi?artid=PMC1436193>
- Reise SP, Ventura J, Nuechterlein KH, Kim KH, Reise SP, Ventura J, Kim KH (2005) An illustration of multilevel factor analysis. *Journal of Personality Assessment* (October 2014):37–41, URL [http://dx.doi.org/10.1207/s15327752jpa8402{}\\_02](http://dx.doi.org/10.1207/s15327752jpa8402{}_02)
- Reuten A, Nooij S, Bos JE, Smeets J (2021) How feelings of unpleasantness develop during the progression of motion sickness symptoms. *Experimental brain research* 239(12):3615–3624
- Riccio GE, Stoffregen TA (1991) An ecological Theory of Motion Sickness and Postural Instability. *Ecological Psychology* 3(3):195–240, URL [http://dx.doi.org/10.1207/s15326969eco0303{}\\_2](http://dx.doi.org/10.1207/s15326969eco0303{}_2)
- Riccio GE, Martin EJ, Stoffregen TA (1992) The Role of Balance Dynamics in the Active Perception of Orientation. *Journal of Experimental Psychology: Human Perception and Performance* 18(3):624–644, DOI 10.1037/0096-1523.18.3.624



- Richardson AG, Attiah MA, Berman JI, Chen HI, Liu X, Zhang M, Spiegel JVD, Lucas TH (2015) ScienceDirect The effects of acute cortical somatosensory deafferentation on grip force control. *CORTEX* 74:1–8, DOI 10.1016/j.cortex.2015.10.007, URL <http://dx.doi.org/10.1016/j.cortex.2015.10.007>
- Rojas CR, Welsh JS, Goodwin GC, Feuer A (2007) Robust optimal experiment design for system identification. *Automatica* 43(6):993–1008, DOI <https://doi.org/10.1016/j.automatica.2006.12.013>, URL <https://www.sciencedirect.com/science/article/pii/S0005109807000696>
- Rolnick A, Lubow RE (2007) Why is the driver rarely motion sick ? The role of controllability in motion sickness. *Ergonomics* 34:7(May):867–879, DOI 10.1080/00140139108964831
- Roodman D (2020) On the probability distribution of long-term changes in the growth rate of the global economy: an outside view. Tech. rep., Open Philanthropy, URL <https://www.openphilanthropy.org/sites/default/files/Modeling-the-human-trajectory.pdf>
- Rosen AV, Koppikar S, Shaw C, Baranchuk A (2014) Common ECG Lead Placement Errors. Part II : Precordial Misplacements 2(3):99–103
- Rusakov DA, Savtchenko LP, Latham PE (2020) Noisy synaptic conductance: bug or a feature? *Trends in Neurosciences* 43(6):363–372
- Salter S, Diels C, Herriotts P, Kanarachos S, Thake D (2019) Motion sickness in automated vehicles with forward and rearward facing seating orientations. *Applied Ergonomics* 78(December 2018):54–61, URL <https://doi.org/10.1016/j.apergo.2017.11.002>
- Saunders DG (1976) A case of motion sickness treated by systematic desensitization and in vivo relaxation. *Journal of Behavior Therapy and Experimental Psychiatry* 7(4):381–382
- Schmidt EA, Kuiper OX, Wolter S, Diels C, Bos JE (2020) An international survey on the incidence and modulating factors of carsickness. *Transportation Research Part F: Psychology and Behaviour* 71:76–87, DOI 10.1016/j.trf.2020.03.012, URL <https://doi.org/10.1016/j.trf.2020.03.012>
- Schwartz JL, Grimault N, Hupe Jm, Moore BCJ, Pressnitzer D, Fourier J (2012) Multistability in perception : binding sensory modalities , an overview. *Philos Trans R Soc Lond B Biol Sci* 367:896–905, DOI 10.1098/rstb.2011.0254
- Shapiro L, Spaulding S (2021) Embodied Cognition. In: Zalta EN (ed) *The Stanford Encyclopedia of Philosophy*, Winter 2021 edn, Metaphysics Research Lab, Stanford University
- Shi H, Yang L, Zhao L, Su Z, Mao X, Zhang L, Liu C (2017) Differences of heart rate variability between happiness and sadness emotion states: a pilot study. *Journal of Medical and Biological Engineering* 37(4):527–539

## REFERENCES

---

- Smart LJ, Stoffregen TA, Benoît GB (2002) Visually Induced Motion Sickness Predicted by Postural Instability. *Human Factors* 44(3):451–465, URL <https://doi.org/10.1518/0018720024497745>
- Steele JE (1961) Motion Sickness and Spatial Perception. Tech. rep., DOI 10.1007/bf00471870
- Sterzer P, Kleinschmidt A, Rees G (2009) The neural bases of multistable perception. *Trends in Cognitive Sciences* 13(7):310–318, DOI 10.1016/j.tics.2009.04.006
- Stevens SS (1946) On the theory of scales of measurement. *Science* 103(2684):677–680
- Stoffregen TA, Smart LJ (1998) Postural instability precedes motion sickness. *Brain Research Bulletin* 47(5), URL [https://doi.org/10.1016/S0361-9230\(98\)00102-6](https://doi.org/10.1016/S0361-9230(98)00102-6)
- Stoffregen TA, Chen Fc, Varlet M, Alcantara C (2013) Getting Your Sea Legs. *PLOS ONE* 8(6), URL <https://doi.org/10.1371/journal.pone.0066949>
- Stoffregen TA, Chou Y, Koslucher FC (2014) Motion control, motion sickness, and the postural dynamics of mobile devices. *Exp Brain Res* 232:1389–1397, URL <https://doi.org/10.1007/s00221-014-3859-3>
- Stoffregen TA, Chang Ch, Chen Fc, Zeng Wj (2017) Effects of decades of physical driving on body movement and motion sickness during virtual driving. *PLOS ONE* pp 1–22, URL <https://doi.org/10.1371/journal.pone.0187120>
- Stroosma O, van Paassen R, Mulder M (2003) Using the simona research simulator for human-machine interaction research. *AIAA Modeling and Simulation Technologies Conference and Exhibit (August)*:1–8, DOI 10.2514/6.2003-5525
- Tal D, Bar R, Nachum Z, Gil A, Shupak A (2010) Neuroscience Letters Postural dynamics and habituation to seasickness. *Neuroscience Letters* 479(2):134–137, URL <http://dx.doi.org/10.1016/j.neulet.2010.05.044>
- Tanguy S, Quarck G, Etard O, Gauthier A, Denise P (2008) Vestibulo-ocular reflex and motion sickness in figure skaters. *Eur J Appl Physiol* 104:1031–1037, DOI 10.1007/s00421-008-0859-7
- Treisman M (1977) Motion Sickness : An Evolutionary Hypothesis. *Science* 197:493–496
- Turan O, Verveniotis C, Khalid H (2009) Motion sickness onboard ships: Subjective vertical theory and its application to full-scale trials. *Journal of Marine Science and Technology* 14(4):409–416, DOI <https://doi.org/10.1007/s00773-009-0064-3>
- Turner M, Griffin MJ (1999) Motion sickness in public road transport: passenger behaviour and susceptibility. *Ergonomics* 42(November 2014):444–461, URL <https://doi.org/10.1080/001401399185586>

- Van Der El K, Pool DM, Mulder M (2017) Measuring and modeling driver steering behavior: From compensatory tracking to curve driving. *Transportation Research Part F: Psychology and Behaviour* URL <https://doi.org/10.1016/j.trf.2017.09.011>
- Varlet M, Bardy BG, Chen F, Alcantara C, Stoffregen TA (2015) Coupling of postural activity with motion of a ship at sea. *Exp Brain Res* 233:1607–1616, URL <http://dx.doi.org/10.1007/s00221-015-4235-7>
- Villard SJ, Flanagan MB, Albanese GM, Stoffregen TA (2008) Postural Instability and Motion Sickness in a Virtual Moving Room. *Human Factors* 50(2):332–345, URL <https://doi.org/10.1518/001872008X250728>. Copyright
- Vingerhoets R, Medendorp WP, Van Gisbergen J (2005) Time Course and Magnitude of Illusory Translation Perception During Off-Vertical Axis Rotation. *Journal of Neurophysiology* 95(3):1571–1587, URL <https://doi.org/10.1152/jn.00613.2005>
- Wada T (2021) Computational Model of Motion Sickness Describing the Effects of Learning Exogenous Motion Dynamics Model of Sensory Conflict Theory Based. *Frontiers in Systems Neuroscience* 15(February):1–11, DOI 10.3389/fnsys.2021.634604
- Wada T, Kamij N, Doi S (2015) A Mathematical Model of Motion Sickness in 6DOF Motion and Its Application to Vehicle Passengers. In: 2nd International Conference on Digital Human Modelling, URL <http://arxiv.org/abs/1504.05261>, 1504.05261
- Wada T, Fujisawa S, Doi S (2018) International Journal of Industrial Ergonomics Analysis of driver's head tilt using a mathematical model of motion sickness. *International Journal of Industrial Ergonomics* 63:89–97, URL <https://doi.org/10.1016/j.ergon.2016.11.003>
- Wada T, Kawano J, Okafuji Y, Takamatsu A, Makita M (2020) A computational model of motion sickness considering visual and vestibular information. In: 2020 IEEE International Conference on Systems, Man, and Cybernetics (SMC), IEEE, pp 1758–1763
- Wadud Z, Mackenzie D, Leiby P (2016) Help or hindrance ? The travel, energy and carbon impacts of highly automated vehicles. *Transportation Research Part A* 86:1–18, DOI 10.1016/j.tra.2015.12.001, URL <http://dx.doi.org/10.1016/j.tra.2015.12.001>
- Wan H, Hu S (2003) Correlation of phasic and tonic skin-conductance responses with severity. *Percept Mot Skills* 97:1051–1057, URL <https://doi.org/10.2466/pms.2003.97.3f.1051>
- Wang CA, Baird T, Huang J, Coutinho JD, Brien DC, Munoz DP (2018) Arousal effects on pupil size, heart rate, and skin conductance in an emotional face task. *Frontiers in Neurology* 9:1029

## REFERENCES

---

- Wang M, Arteaga D, He BJ (2013) Brain mechanisms for simple perception and bistable perception. *Proceedings of the National Academy of Sciences* 2(5), DOI 10.1073/pnas.1221945110/-/DCSupplemental.www.pnas.org/cgi/doi/10.1073/pnas.1221945110
- Wang S, Chinn HI (1956) Experimental Motion Sickness in Dogs Importance of Labyrinth and Vestibular Cerebellum. *American Journal of Physiology-Legacy Content* 185:617–623
- Wassersug RJ, Izumi-kurotani A, Yamashita M, Naitoh T (1993) Motion sickness in amphibians. *Behavioral and Neural Biology* 60(1):42–51, DOI 10.1016/0163-1047(93)90703-K
- Webb NA, Griffin MJ (2003) Eye movement, vection, and motion sickness with foveal and peripheral vision. *Aviation Space and Environmental Medicine* 74(6):622–625
- Weech S, Moon J, Troje NF (2018) Influence of bone-conducted vibration on simulator sickness in virtual reality. *PLOS ONE* 13(3):1–21, DOI 10.1371/journal.pone.0194137, URL <https://doi.org/10.1371/journal.pone.0194137>
- Wertheim AH, Bos JE, Bles W (1998) Contributions of roll and pitch to sea sickness. *Brain Research Bulletin* 47(5):517–524, URL [https://doi.org/10.1016/S0361-9230\(98\)00098-7](https://doi.org/10.1016/S0361-9230(98)00098-7)
- Wertheim AH, Mesland BS, Bles W (2001) Cognitive suppression of tilt sensations during linear horizontal self-motion in the dark. *Perception* 30(6):733–741, DOI 10.1068/p3092
- Wieland A, Durach CF, Kembro J, Treiblmaier H (2017) Statistical and judgmental criteria for scale purification. *Supply Chain Management* 22(4):321–328, URL <https://doi.org/10.1108/SCM-07-2016-0230>
- Wood J, Mims E, Wood D, Struve A, Patrick Y, Stewart J (1994) D. Wood., *J Clin Pharmacol* 34:628–634
- Wood SJ (2002) Human otolith-ocular reflexes during off-vertical axis rotation: Effect of frequency on tilt-translation ambiguity and motion sickness. *Neuroscience Letters* 323(1):41–44, URL [https://doi.org/10.1016/S0304-3940\(02\)00118-0](https://doi.org/10.1016/S0304-3940(02)00118-0)
- Wood SJ, Reschke MF, Clément G (2007) Tilt and Translation Motion Perception During Off Vertical Axis Rotation. *Exp Brain Res* 182(3):365–377, URL <https://doi.org/10.1007/s00221-007-0994-0>
- Xsens (2020) MVN User Manual. Tech. rep.
- Young LR, Sienko KH, Lyne LE, Hecht H, Natapoff A (2003) Adaptation of the vestibulo-ocular reflex, subjective tilt, and motion sickness to head movements during short-radius centrifugation. *Journal of Vestibular Research* 13:65–77

Zaichik L, Rodchenko V, Rufov I, Yashin Y, White A (1999) Acceleration perception. In: Modeling and Simulation Technologies Conference and Exhibit, p 4334

Zupan L, Droulez J, Darlot C, Denise P, Maruani A (1994) Modelization of Vestibulo-Ocular Reflex (VOR) and Motion Sickness Prediction. In: ICANN '94, pp 106–109, URL [https://doi.org/10.1007/978-1-4471-2097-1\\_25](https://doi.org/10.1007/978-1-4471-2097-1_25)

# A

## APPENDIX OF CHAPTER 3

### A.1. INDIVIDUAL NORMALISED MISC RATE

Figure A.1 shows the normalised MISC rate in the first motion exposure as a scatter plot with respect to the amplitude condition for all individuals that took part in the amplitude study. The MISC rate is normalised against the maximum MISC rate observed for a participant across all of their conditions. This gives a better representation of the amplitude sensitivity of the participants.

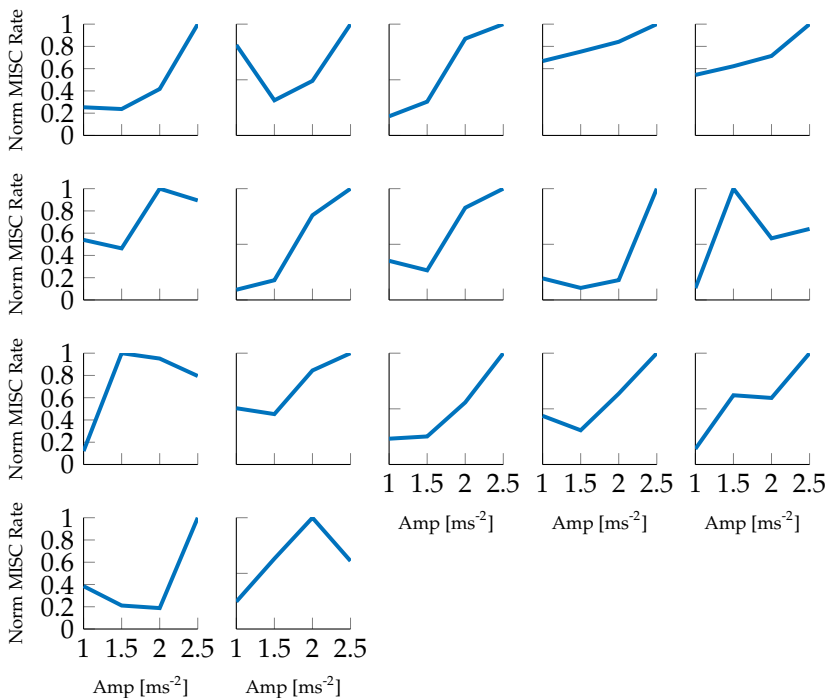


**Fig. A.1** Normalised MISC rate obtained from dividing the MISC at the end of the session with the time to the end of the session, shown for all individuals. The MISC rate is normalised against the maximum MISC rate observed for a participant across all of their conditions.

## A.2. MODEL FITS TO ALL INDIVIDUAL RESPONSES

Figure A.2 shows the fits of the three model variations for all participants and all conditions.

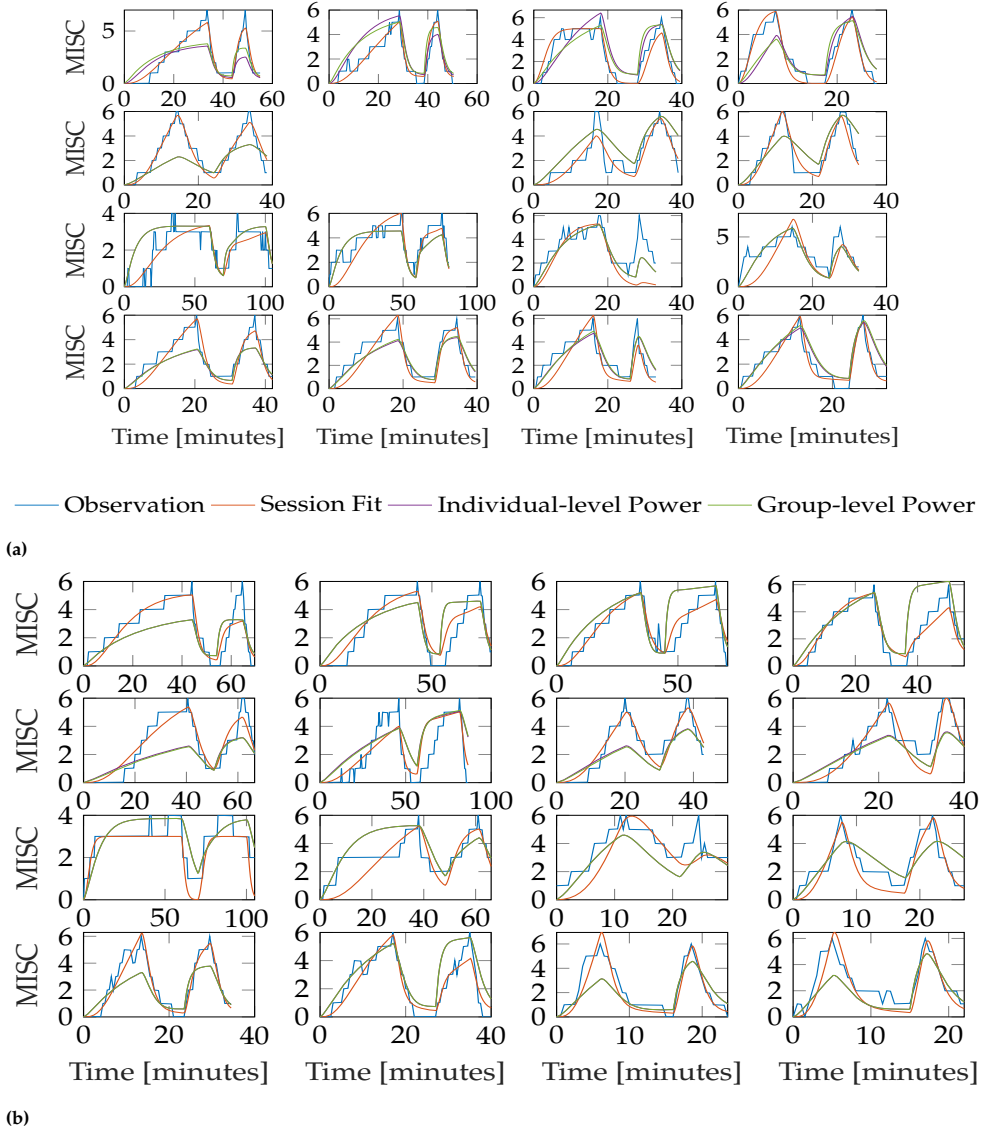


Fig. A.2

### A.3. SICKNESS FORECASTING

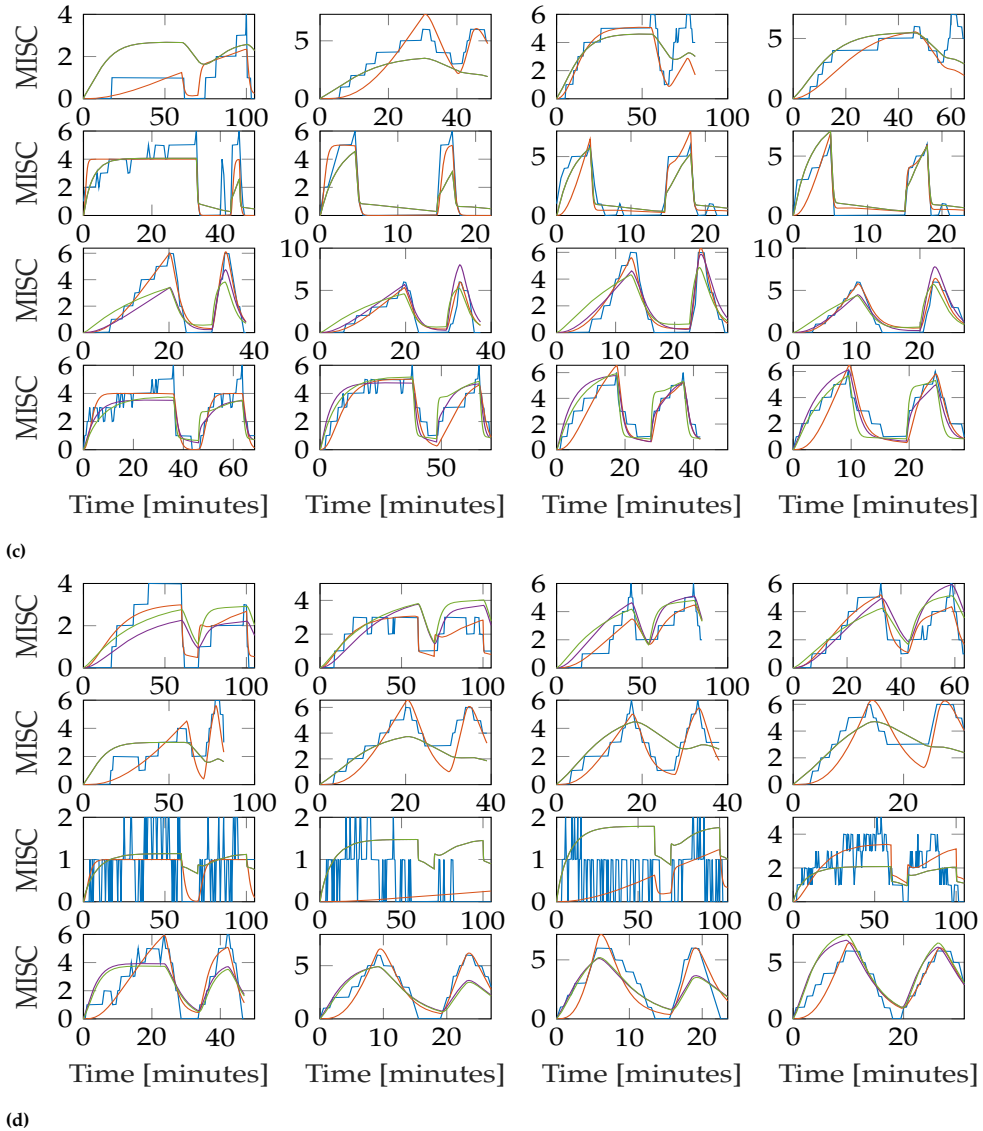
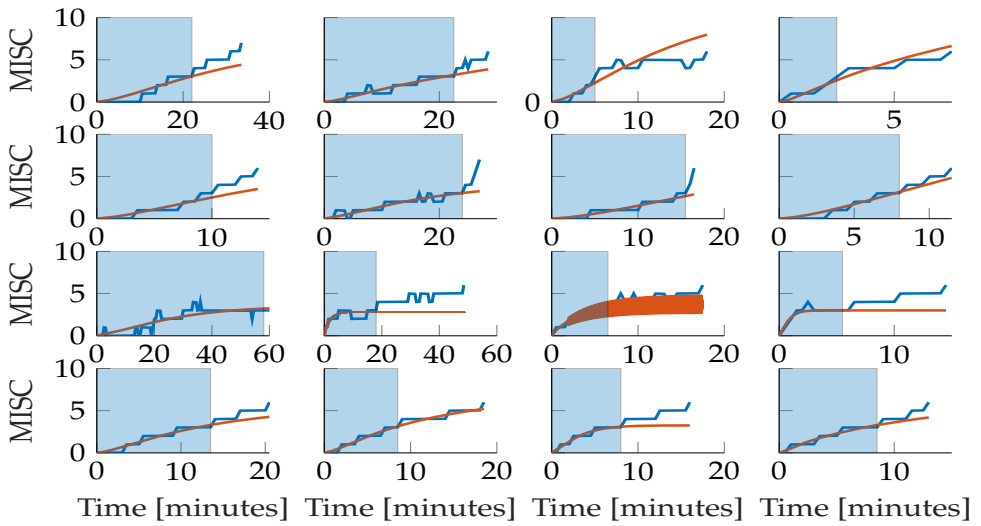


Fig. A.2 Three variations of the Oman model; Session Fit, Variable Power and Fixed Power. Fitted to all sessions of all individuals. Each row is an individual participant, and each column is a motion condition, with increasing fore-aft acceleration amplitudes of 1, 1.5, 2 and 2.5 going from left to right

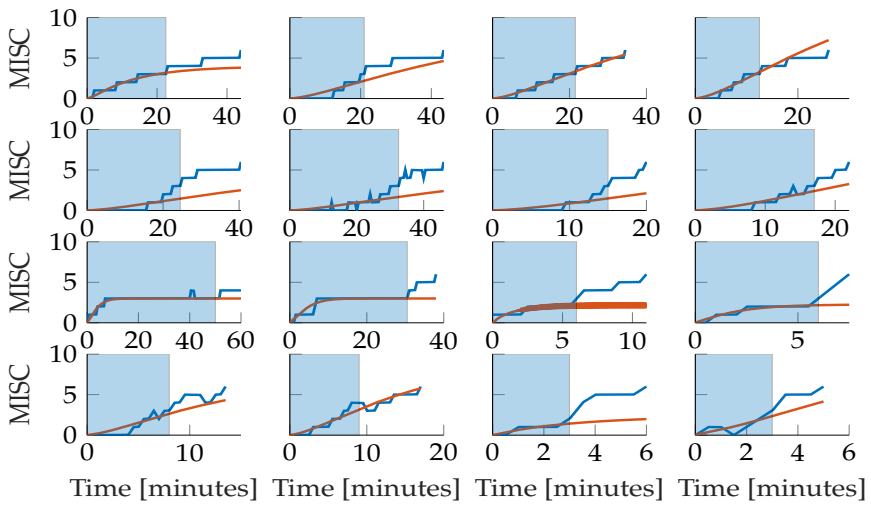
### A.3. SICKNESS FORECASTING

Figure A.3 shows extrapolations from MISC 3 to the end of the first motion phase, for the Oman model (in orange) and real observation (in blue) for all participants.





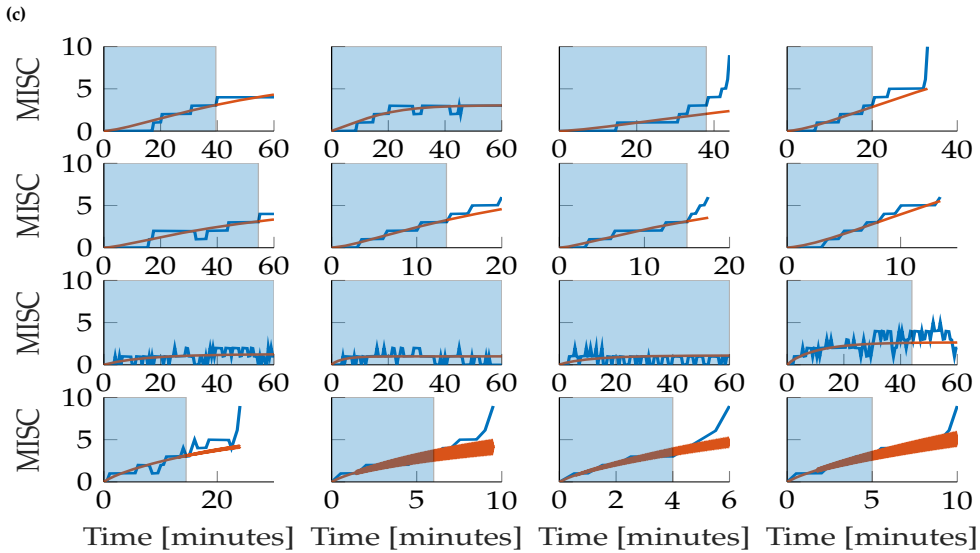
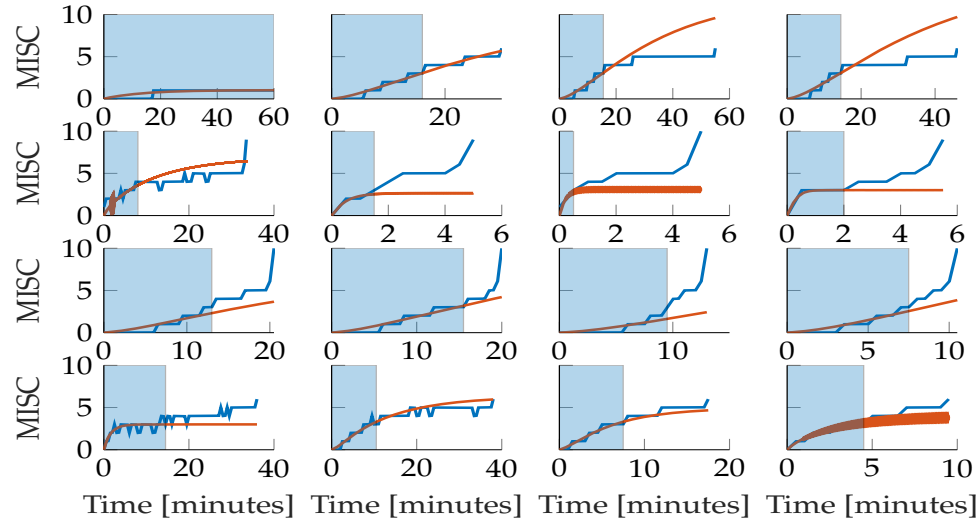
(a)



(b)

Fig. A.3

### A.3. SICKNESS FORECASTING



(d)

Fig. A.3 Extrapolations from MISC 3 to the end of the first motion phase, for the Oman model (in orange) and real observation (in blue) for all participants. The columns show responses for each amplitude condition, increasing in magnitude from left to right. The rows show results for each participant. The blue shaded area gives the observations the model has access to make forecasts

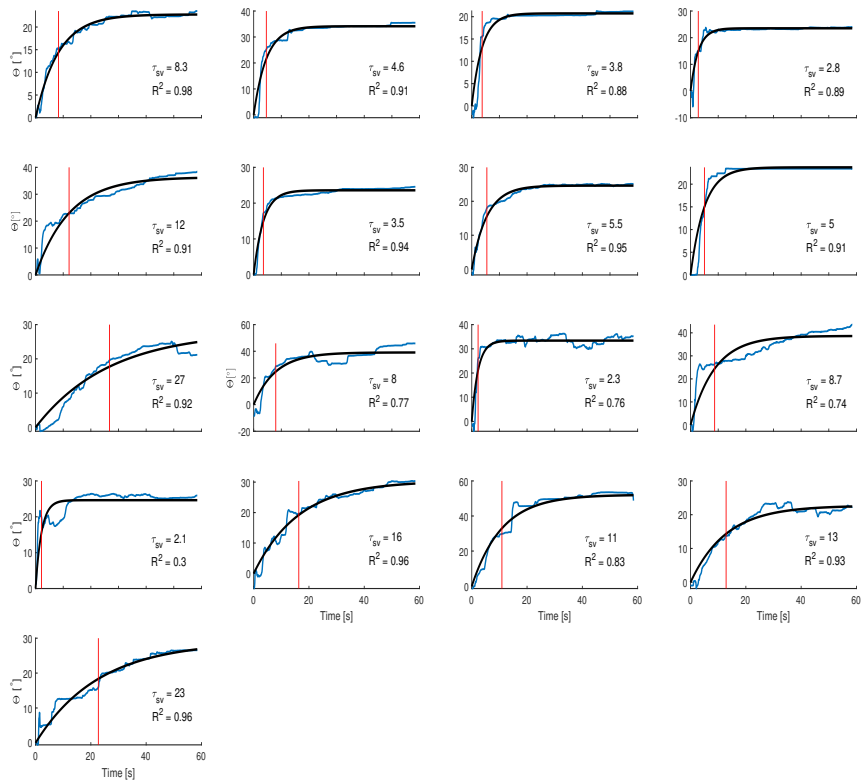


# **B**

## **APPENDIX OF CHAPTER 4**

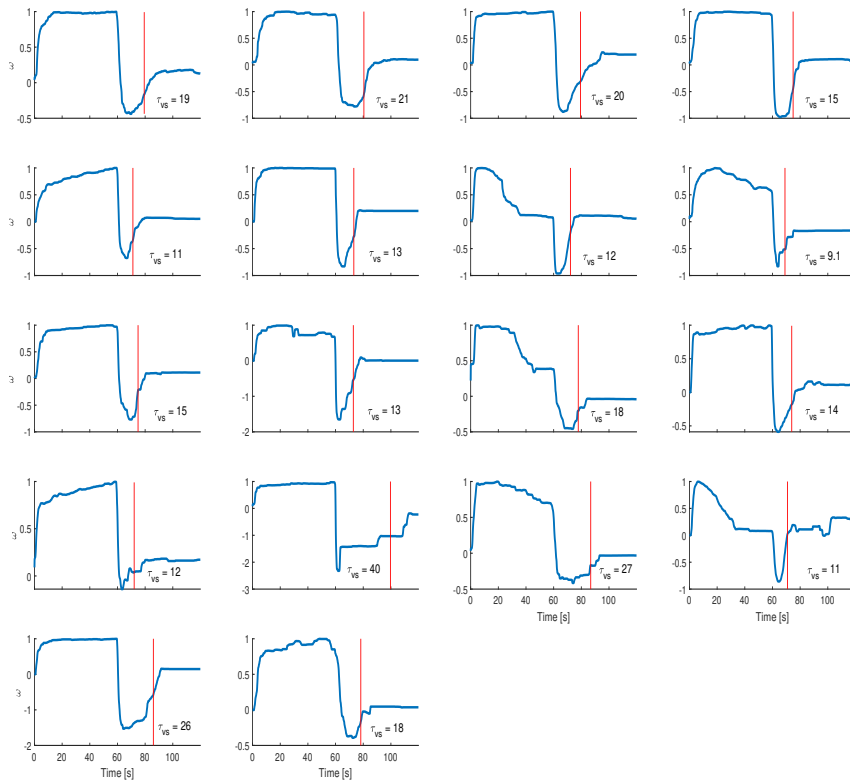
## B.1. PERCEPTION EXPERIMENT RESPONSES

Figure B.1 shows the centrifugation and EVAR responses of each participant for whom data could be collected. Figure B.1a shows the first 60 s of the centrifugation response as indicated by participants using the angular pitch of a metal rod connected to a potentiometer. Figure B.1a shows the entire 120 s of the EVAR response indicated by rotating the rod away from the body or towards the body, depending on the perceived direction and magnitude of angular velocity in yaw. The y-axis has been normalized to the maximum displacement of the rod.



(a) Centrifugation

## B.1. PERCEPTION EXPERIMENT RESPONSES

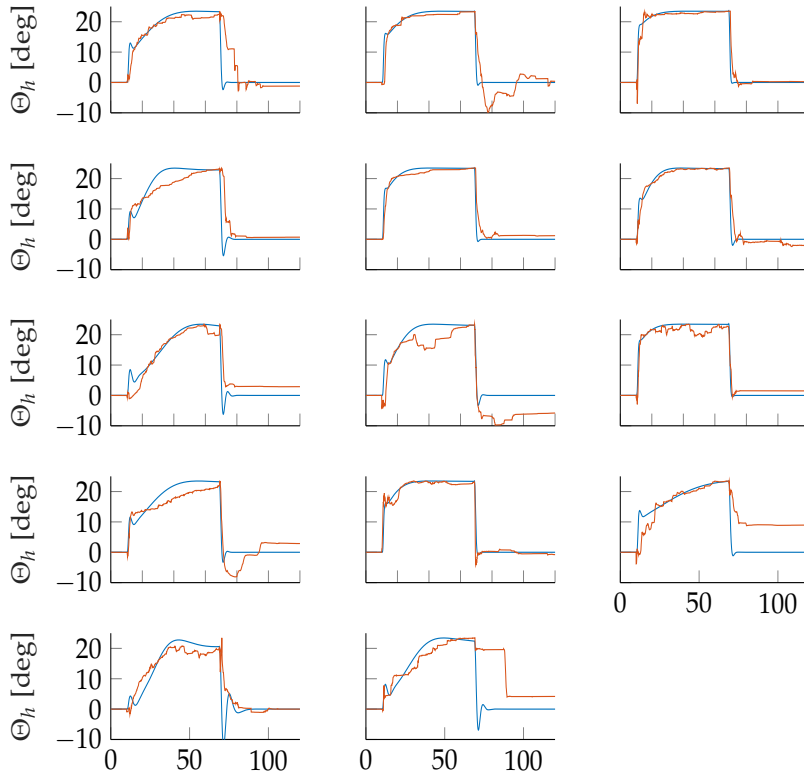


### (b) EVAR

**Fig. B.1** Perceptual responses for all individuals averaged over repetitions. *a* is the subjective vertical tilt in centrifugation. At 0 s, the centrifugation is started and maintained until 60 s, after which it is stopped. At 120 s, another trial is initiated. The black line shows the fitted exponential model, the  $R^2$  value and the time constant  $\tau_{vs}$  is also shown in the text box. The vertical red line shows this time constant on the plot itself. *b* shows the angular velocity after rotation in EVAR. At 0 s the EVAR motion of the simulator is stopped and at 60 s a new trial is initiated. The vertical red line shows the point at which perceived normalized angular velocity decays to 63.2% of the way down to steady state

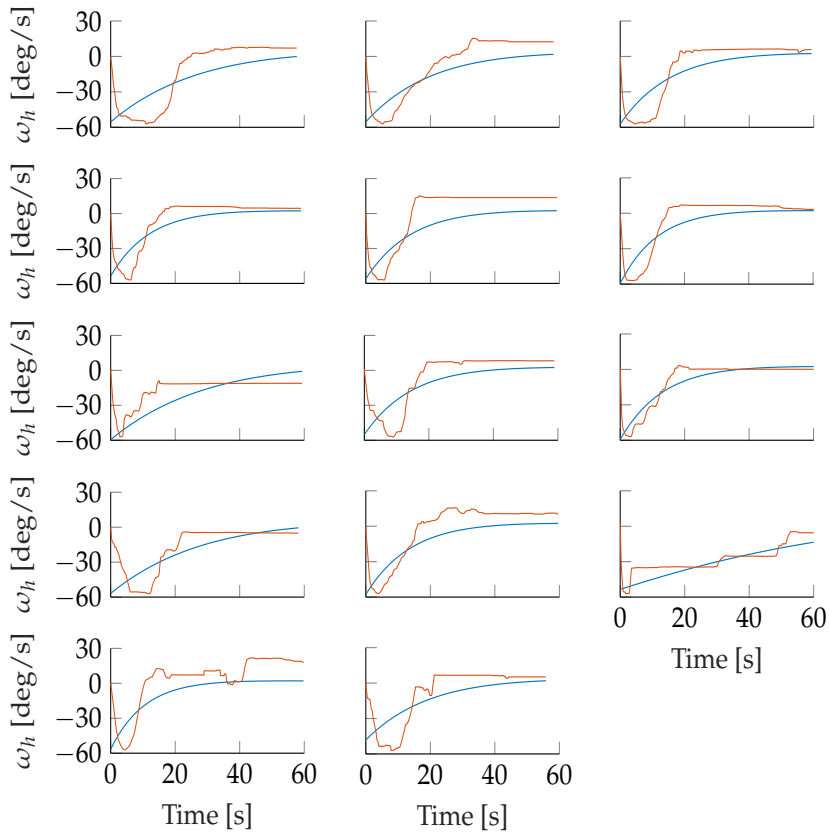
## B.2. MSOM MODEL FITS TO PERCEPTION RESPONSES

Figure B.2 shows the fits of the MSOM to the centrifugation and EVAR after effect responses shown above. Fits were only performed on those participants for whom both EVAR and centrifugation were collected. Figure B.2a shows the fits for centrifugation that are, in most cases, a good fit to the experimental data. Figure B.2b shows the fits for EVAR that does not accurately predict the plateauing effect seen in the experimental data. For this, a more complex model would have to be introduced.



(a) Perceived subjective vertical tilt.

## B.2. MSOM MODEL FITS TO PERCEPTION RESPONSES



(b) Perceived angular velocity.

**Fig. B.2** MSOM fits for all individuals for which both EVAR and centrifugation data exists. *Top* are fits for the subjective vertical tilt for each participant. *Bottom* are fits for the perceived angular velocity after rotation. Only the point after the zero crossing for EVAR was used for the error minimization



### B.3. CROSS-OVER FREQUENCY

Figure B.3 shows the gain of acceleration and gravity estimation with respect to frequency, as computed from the MSOM. At low frequencies, the gravity estimate has the highest gain, which then crosses over at an intermediate frequency, after which the acceleration gain increases. The point where the curves cross is, by definition, the cross-over frequency.

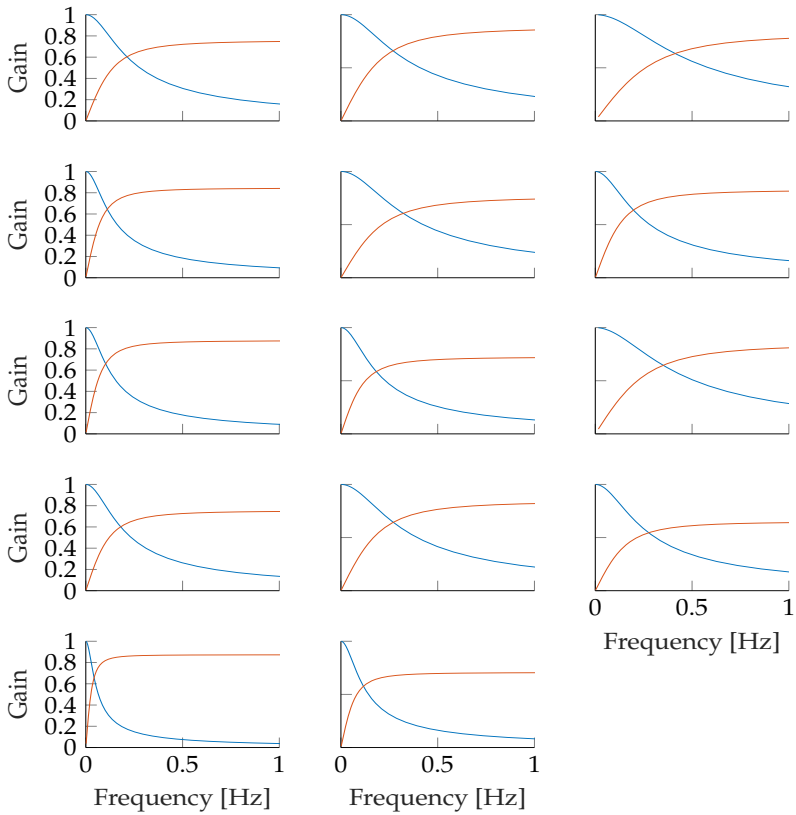


**Fig. B.3** Gravity and acceleration perception frequency responses as obtained from one of the runs of MSOM

## B.4. SICKNESS EXPERIMENT RESPONSES

Figure B.4 shows the MISC as a function of time for all participants and for all frequency conditions. The MISC rating was queried in 30 s intervals. Here, sickness responses are generally seen to converge to a value below the cut-off value of MISC 6.

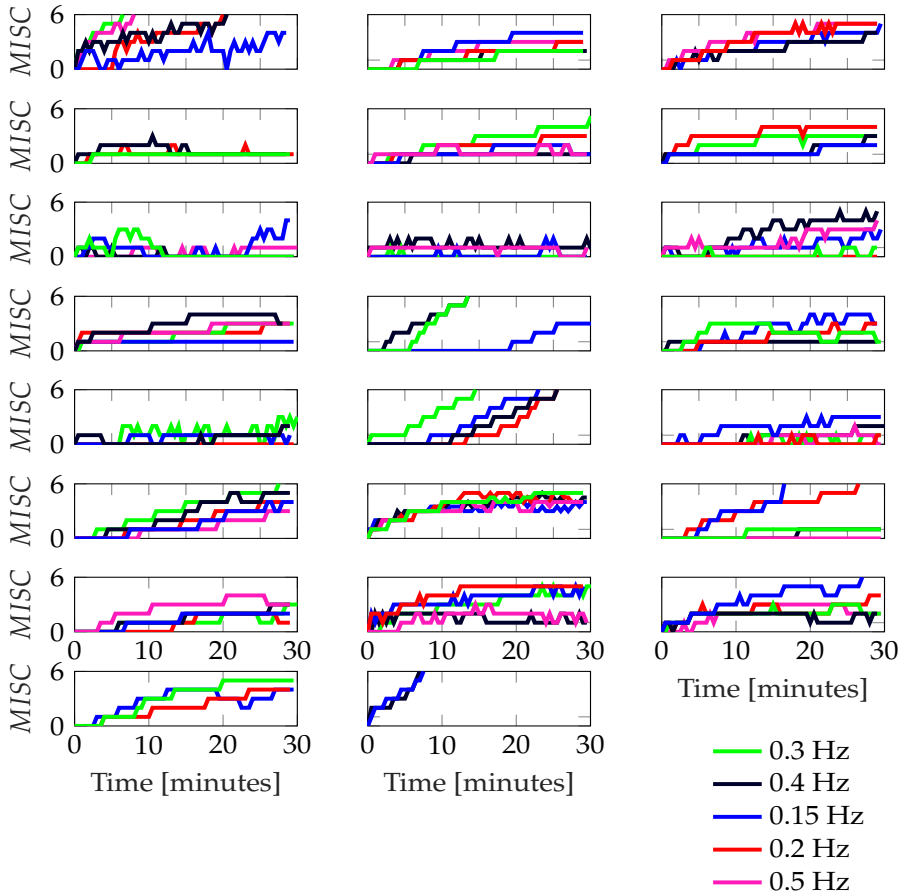
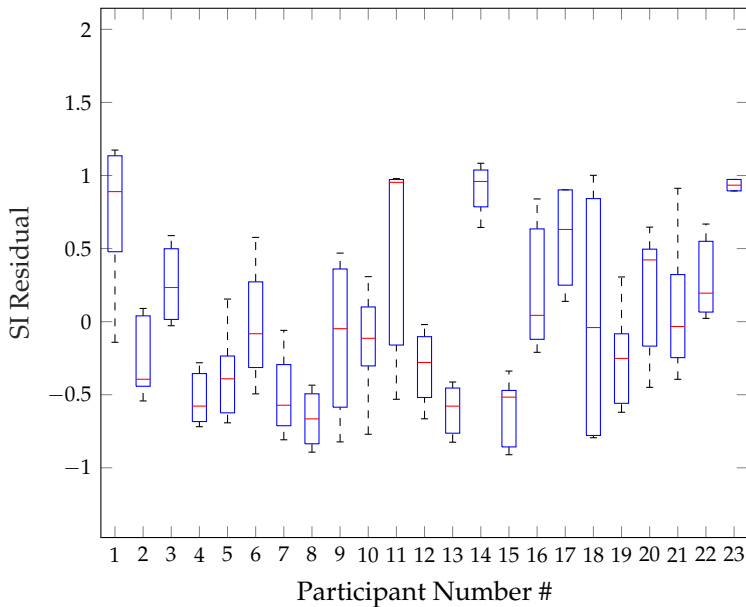


Fig. B.4 MISC Trajectories for all individuals

## B.5. FIXED EFFECT MODEL RESIDUALS

Figure B.5 shows the residuals of the fitted Fixed Effect Quadratic model. An ideal model fit would have residuals centred on zero, with limited variance for each participant. Here the residuals for each participant are centred appreciably above or below zero, with large variances, indicating a poor fit with the Fixed Effect Quadratic model.



**Fig. B.5** Box plot of the residuals for our fitted Fixed Effect Quadratic model. Residuals are, on average, mostly above or below zero, indicating that the model has failed to account for subject-specific effects

# C

## APPENDIX OF CHAPTER 5

### C.1. MOTION IMPLEMENTATION

For this purpose, the following kinematic chain shown in Figure C.1 is used

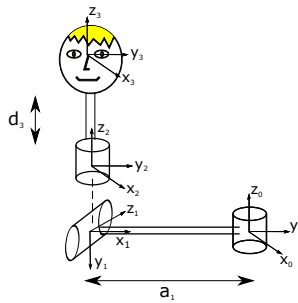


Fig. C.1 Kinematic chain used for complex motion generation

Here  $\mathbf{R}_0$  defines the earth fixed coordinate system, composed of the unit vectors  $\vec{X}_0, \vec{Y}_0, \vec{Z}_0$ . Likewise  $\mathbf{R}_3$  defines the head fixed coordinate system. Using standard Denavit-Hartenberg (DH) formulation one can derive the set of transforms that map  $\mathbf{R}_3$  to  $\mathbf{R}_0$  and likewise  $\mathbf{R}_0$  to  $\mathbf{R}_3$  or any therein between. The DH parameters for this kinematic chain are tabulated in Table C.1

Table C.1 DH parameters for kinematic chain

Link	$\alpha$	a	d	$\theta$
1	$-\pi/2$	$a_1$	0	$\pi/2 + \theta_1$
2	$\pi/2$	0	0	$\theta_2$
3	0	0	$d_3$	$\theta_3$

The parameters  $a_1$  and  $d_3$  are to specify the centrifugation distance and the distance of roll point to the vestibular organs respectively. For centrifugation  $a_1$  is simply defined as the distance of the body from the centrifugation axis.  $d_3$  depends on the nature of the motion. If the motion is such that the roll rotation at the pivot point  $\mathbf{R}_1$  is about the vestibular organ, as is the case for OVAR, then  $d_3$  is set to zero. If

however the roll point is the neck, as is the case for cross-coupled coriolis,  $d_2$  is set to the distance between the neck and the vestibular organs. As a result, the transform which relates the head frame to the earth frame is given by

$$\mathbf{T}_3^0 = \mathbf{T}_1^0 \mathbf{T}_2^1 \mathbf{T}_3^2 \quad (\text{C.1})$$

This transform takes the general form

$$\mathbf{T}_3^0 = \begin{bmatrix} r_{11} & r_{12} & r_{13} & d_x \\ r_{21} & r_{22} & r_{23} & d_y \\ r_{31} & r_{32} & r_{33} & d_z \\ 0 & 0 & 0 & 1 \end{bmatrix} \quad (\text{C.2})$$

Where the elements of the matrix are given as

$$\begin{aligned} r_{11} &= -c_1 s_3 - c_2 c_3 s_1 \\ r_{12} &= c_2 s_1 s_3 - c_1 c_3 \\ r_{13} &= -s_1 s_2 \\ r_{21} &= c_1 c_2 c_3 - s_1 s_3 \\ r_{22} &= -c_3 s_1 - c_1 c_2 s_3 \\ r_{23} &= c_1 s_2 \\ r_{31} &= -c_3 s_2 \\ r_{32} &= s_2 s_3 \\ r_{33} &= c_2 \\ d_x &= -s_1 (a_1 + d_3 s_2) \\ d_y &= c_1 (a_1 + d_3 s_2) \\ d_z &= d_3 c_2 \end{aligned} \quad (\text{C.3})$$

Here for the sake of brevity and legibility  $\sin(\theta_1)$  and  $\cos(\theta_1)$  is denoted as  $s_1$  and  $c_1$  respectively.  $\mathbf{T}_3^0$  relates the head frame to the earth frame, its inverse relates the earth fixed frame to the head frame. The inverse is equivalent to the transpose of the original transform. Therefore

$$\mathbf{T}_0^3 = (\mathbf{T}_3^0)^T$$

With this one can transform earth referenced gravity to the head coordinates to simulate what the gravity component of the gravito-inertial force would be.

$$\vec{g}_3 = \mathbf{T}_0^3 \vec{g}_0$$

The semicircular canals report angular velocity with respect to the head. To acquire the head referenced angular velocity the Jacobian must be evaluated in the head frame of reference. This yields

$$\vec{v}_3 = \mathbf{J}_3(\vec{\theta}) \vec{\theta}$$

Where

$$\vec{v}_3 = \begin{bmatrix} v_x \\ v_y \\ v_z \\ \omega_x \\ \omega_y \\ \omega_z \end{bmatrix}$$

In the head frame. As this is the head frame the velocity terms are zero and so only the angular velocity terms are left. These can be used straight away as inputs to the semicircular canals.

In a similar manner, by expressing the Jacobian in the earth frame, differentiating the linear velocity and transforming back to the head frame one can derive the linear head acceleration in the head frame.

$$\vec{v}_0 = \mathbf{J}_0(\vec{\theta})\vec{\dot{\theta}}$$

This gives linear velocity in the earth frame. Numerically differentiating

$$\vec{a}_0 = \frac{\vec{v}_0(t + \delta t) - \vec{v}_0(t - \delta t)}{2\delta t}$$

Gives the linear acceleration in the earth frame, where  $\delta t$  is the differentiation time step used. In this case, a second order numerical technique is used. The head acceleration in earth frame is then transformed in much the same way as the gravity, in to the head frame.

$$\vec{a}_3 = \mathbf{T}_0^3 \vec{a}_0$$

Therefore the gravito-inertial acceleration in the head frame  $f_3$ , as sensed by the otoliths is given by

$$\vec{f}_3 = \vec{g}_3 - \vec{a}_3$$

This can be used straight away as the input to the otolith model.

## C.2. CONFLICT POWER

Assume a conflict of magnitude  $A$  and angular velocity  $\omega_p$

$$|c(t)| = |A \sin \omega_p t|$$

The Fourier series expansion yields to the following DC ( $A_0$ ) and harmonic amplitude ( $A_n$ ) terms,

$$A_0 = \frac{2|A|}{\pi}$$

$$A_n = \frac{4|A|}{\pi(n^2 - 1)}$$

Where  $n = 2, 3, 4, \dots$

Therefore the conflict signal has most of its power in the DC bias and the first harmonic terms. The second order system applied accumulate sickness filters the signal. The gain for this is given as

$$G = \frac{K}{(1 + \omega\mu)^2}$$

Therefore the end magnitude of the bias and first harmonic of the filtered absolute conflict signal is

$$A_0 = \frac{2|A|K}{\pi}$$

$$A_n = \frac{4|A|K}{3\pi(1 + 4\omega_p\mu)^2}$$

For a constant value of  $|A|$  the lower the frequency of conflict the larger the sickness response, due to the contribution of harmonics. The time constant  $\mu$  used in [Bos and Bles \(1998\)](#) is 12 minutes and  $K$  is equal to 0.85. These free parameters depend on the sickening motion, which for them was pure vertical. A smaller time constant allows for the higher harmonics to contribute but as observed there is quadratically decreasing energies with respect to harmonic position. More importantly, the assumption of constant  $|A|$  is invalid. Accurate prediction of sickness requires smaller sickness at lower and higher frequencies therefore one can expect a parabola in the frequency-domain with centre frequencies ranging between 0.03-0.3 Hz. At such frequencies for the first harmonic to not be filtered by the 2nd order system the time constant must be around 30s. Such small time constants may be observed for cross-coupled Coriolis stimulation and so the frequency of the conflict may become important here, i.e. there may be substantial harmonics added on to the base increase in sickness (waves of nausea with each head rotation). However for the longer time constants observed in majority of cases the first harmonic does not contribute at all and only the DC bias is important.

### C.3. SVM LATERAL AND VERTICAL RESPONSE DERIVATION

Here take only one perturbation direction. As there is no cross-coupling between the input and output direction one can do the analysis on a given component,  $f$  of the gravito-inertial force vector  $\vec{f}$ .

$$f = \frac{K_a}{s} + \frac{K_g}{s} c_g$$

$$c_a = f \frac{\tau_{lp}s}{\tau_{lp}s + 1} - \hat{f} \frac{\tau_{lp}s}{\tau_{lp}s + 1}$$

$$c_g = f \frac{1}{\tau_{lp}s + 1} - \hat{f} \frac{1}{\tau_{lp}s + 1}$$

### C.3. SVM LATERAL AND VERTICAL RESPONSE DERIVATION

---

$$c_a = f \frac{\tau_{lp}s}{\tau_{lp}s + 1} - \left( \frac{K_a}{s} c_a + \frac{K_g}{s} c_g \right) \frac{\tau_{lp}s}{\tau_{lp}s + 1}$$

$$c_a s + c_a \left( K_a + \frac{1}{\tau_{lp}} \right) + K_g c_g = f s$$

Taking the inverse laplace transform with zero ininitial conditions

$$\dot{c}_a + c_a \left( K_a + \frac{1}{\tau_{lp}} \right) + K_g c_g = \dot{f}$$

Similarly for  $c_g$

$$\tau_{lp} \ddot{c}_g + \dot{c}_g + K_g c_g + K_a c_a = \dot{f}$$

This system of ordinary differential equations can be represented in state space form such that

$$\vec{\dot{q}} = \mathbf{A}\vec{q} + \mathbf{B}\vec{f}$$

$$\vec{y} = \begin{bmatrix} c_a \\ c_g \\ \dot{c}_g \end{bmatrix} = \mathbf{C}\vec{q} + \mathbf{D}\vec{f}$$

Where  $\vec{f}$  here is defined as the sole component perturbing the system. For instance if there is only lateral acceleration

$$\vec{f} = \begin{bmatrix} f_y \\ f_y \\ f_y \end{bmatrix}$$

Therefore following through

$$\mathbf{A} = \begin{bmatrix} -K_a - 1/\tau_{lp} & -K_g & 0 \\ 0 & 0 & 1/\tau_{lp} \\ -K_a & -K_g & -1/\tau_{lp} \end{bmatrix}$$

$$\mathbf{B} = \begin{bmatrix} -K_a - 1/\tau_{lp} & 0 & 0 \\ 0 & \frac{1}{\tau_{lp}} & 0 \\ 0 & 0 & -K_a - 1/\tau_{lp} \end{bmatrix}$$

$$\mathbf{C} = \begin{bmatrix} 1 & 0 & 0 \\ 0 & 1 & 0 \\ 0 & 0 & \tau_{lp} \end{bmatrix}$$

$$\mathbf{D} = \begin{bmatrix} -1 & 0 & 0 \\ 0 & 0 & 0 \\ 0 & 0 & -1 \end{bmatrix}$$

Now transforming this back one can obtain the gravito-inertial force to conflict transfer functions.



## C.4. MSOM LATERAL RESPONSE DERIVATION

First the simpler system without the semi circular canals influence is derived. It is assumed that the only forcing terms are  $f_y$  and  $f_z = \hat{f}_z = -k$  where  $b = 9.81$ . Here  $f_x = \hat{f}_x = 0$ .

The conflict terms are defined as

$$\vec{c}_o = \vec{f} - \vec{\hat{f}}$$

$$\vec{c}_{oa} = \frac{\vec{f} \times \vec{\hat{f}}}{|\vec{f}| |\vec{\hat{f}}|}$$

Let us expand the otolith angle conflict in to vector form

$$\begin{array}{ccc|c} i & j & k & (f_y \hat{f}_z - f_z \hat{f}_y) i \\ |f_x & f_y & f_z| & = -(f_x \hat{f}_z - f_z \hat{f}_x) j \\ \hat{f}_x & \hat{f}_y & \hat{f}_z & (f_x \hat{f}_y - f_y \hat{f}_x) k \end{array}$$

As  $f_x = \hat{f}_x = 0$  and  $f_z = \hat{f}_z = k$

$$f_x \hat{f} = -b(f_y - \hat{f}_y) i$$

Where all the other components are zero. As the equation above divides the cross product by the magnitude of the respective vectors this too must be done. Assuming small perturbation for  $f_y$  the product of the magnitude of the two is  $b^2$  Therefore the final otolith angle conflict may be written as

$$\vec{c}_{oa} = \frac{\vec{f} \times \vec{\hat{f}}}{|\vec{f}| |\vec{\hat{f}}|} = -\frac{1}{k} (f_y - \hat{f}_y) i, 0j, 0k$$

$$= -\frac{1}{k} c_{oy} i, 0j, 0k$$

The way the magnitude error evolves can be written as

$$\vec{c}_o = \vec{f} - \vec{\hat{f}}$$

Where

$$\vec{\hat{f}} = \vec{g} - \vec{a}$$

Therefore

$$\vec{c}_o = \vec{f} - \vec{g} + \vec{a}$$

As

$$\vec{a} = K_a \vec{c}_o$$

$$\vec{c}_o = \vec{f} - \vec{g} + K_a \vec{c}_o$$

#### C.4. MSOM LATERAL RESPONSE DERIVATION

---

Therefore the magnitude error can be written as

$$\vec{c}_o = (\vec{f} - \vec{g}) \frac{1}{1 - K_a}$$

The derivative of this with respect to time gives

$$\vec{c}_o = (\dot{\vec{f}} - \dot{\vec{g}}) \frac{1}{1 - K_a}$$

Here  $\dot{\vec{g}}$  can be determined by assuming that the gravity does not tilt substantially away from the vertical. Such an assumption allows for the use of the small angle approximation. Here gravity is tilted about the x axis due to the rotational velocity of the otolith angle error multiplied by the gain  $K_f$ . Therefore the change in gravity is given as

$$\dot{\vec{g}} = 0i, K_f c_{oy}j, -\omega_x bk$$

As the rate of change in gravity  $\dot{\vec{g}}$  is zero in all but the lateral perturbation direction this is the only relevant component of the magnitude conflict. Therefore substituting the above equation

$$c_{oy} = (\dot{f}_y - K_f c_{oy}) \frac{1}{1 - K_a}$$

Rearranging this gives

$$c_{oy} + c_{oy} \frac{K_f}{1 - K_a} = \dot{f}_y \frac{1}{1 - K_a}$$

Taking the Laplace transform yields

$$\frac{c_{oy}}{f_y} = \frac{s \left( \frac{1}{1 - K_a} \right)}{s + \frac{K_f}{1 - K_a}}$$



# ACKNOWLEDGEMENTS

The first and foremost person to be acknowledged is **Sultan Yeşilay**. Without you, I would not be in Delft, nor the Netherlands. Without you, I might very well have quit in my second year. We have shared in much pain, but also in much joy. We have grown up together, and made many fond memories, these I will cherish, and be forever grateful for. I would also like to thank **Aniş Yeşilay**, **Ramazan Yeşilay** and **Deniz Yeşilay** for being a family to me.

I have heard many horror stories about PhD supervision. I am lucky to not count myself among such stories. Indeed, I have instead been very fortunate to have supervisors and mentors who care about their students and not just what we can do for them.

**Riender Happee**, you have been an excellent role model of a senior academic, someone I hope to emulate. Despite the multitude of commitments and higher-level work, you get your hands dirty in the research. But not only my own, but of all your PhDs. You know when to supervise actively, and when to not. Above all, you know how to make everyone shine.

**Daan Pool**, it has always been a pleasure to work with you. You have always grounded my research, cutting neatly to the most impactful parts. Your sharp but gentle guidance has been invaluable in allowing me to finish in the way I have done. I would also like to thank you for the late nights you spent squiggling in red on the  $n^{\text{th}}$  iteration of this thesis.

**Ksander de Winkel**, I am grateful for making your acquaintance. You have been a key contributor to both this thesis and my development on all aspects. From you, I learned how to better do statistical analysis, particularly at the individual level, and how to properly design experiments. You might have felt somewhat a stranger among engineers, as psychologists usually do, but I felt we were in close synergy. We shared a very similar vision for the future of motion sickness and perception research, and I hope we can realise this in the coming years. I will fondly remember our conversations at the MPI, and I hope there will be many more to come.

**Barys Shyrokau**, you have been a guiding figure in my personal development, especially in the end stages of the PhD, towards being an independent researcher. You have always given me honest and firm feedback. I am deeply appreciative of your guidance and the experiences you have shared. I also very liberally recount your stories from Singapore!

**The Broken Ones:** Vishrut Jain and Alberto Bertipaglia. **Vishrut Jain**, I would like to thank you for your company and your joyous spirit, which, despite the naming of this section, seems to be unbreakable. **Alberto Bertipaglia**, I would like to thank you for your friendship, and though I played my part in breaking your heart, yours was always open to be confided in.

**The Mad Ones:** Gerd Kiene, Matt Kielan, Matthew Right and Vivek Suryamurthy. **Gerd Kiene**, I have thoroughly enjoyed our time as friends together, both through illness and health. You have been a trusty rope mate and though you try to distance yourself from the Mad Ones, your effective behaviour places you firmly amongst us. Here is to many more adventures! **Matt Kielan**, the original mad guy and our patient zero. You were the first who dragged me quivering in fear, tied on a rope, up the hill, and that day has slowly but steadily shifted the trajectory of everything thereafter. I am grateful for your friendship and your presence. **Matthew Right**, you are the finest example of a man, a friend and a rope partner. I would like to thank you for your continued friendship. **Vivek Suryamurthy**, free-soloing 5<sup>th</sup> class terrain certainly inducts you in to the Mad Ones. Here is to hoping we enjoy many ice capped peaks together.

**The Ancient Ones:** Jork Stapel, Felix Dreger, Carlos Clemin, Ewoud Pool, Andras Palffy, Thomas Hehn, Ronald Ensing and Sarah Barendswaard. Jork Stapel, you were the first person in Delft that I interacted with, in what now seems like pre-history. You have been there through all cruxes of my PhD, providing insights and good conversation. I will fondly remember these, I will also fondly remember the tick inspections at Fontainebleau. **Felix Dreger**, thank you for all the interesting conversations we had and your insights in to psychology and knowledge on statistics. **Carlos Clemin**, thank you for your company during the start of the PhD, as you were a more senior person, speaking to you was always reassuring. **Ewoud Pool**, there is only one of you. Your reaction to this statement likely illustrates the point. Thank you for the interesting discussions, your final guidance on finishing the PhD and afterwards, and lastly, for all the fun (as well as the tick removal card)! **Andras Palffy**, I had never had someone almost run me over with a car so many times, in such a short duration! You have been a very good friend and all around good person to be around. It's a shame we never had that coffee, but I hope I won't ever need it again. **Thomas Hehn**, I fondly recall our pre-COVID office talks together, thank you for your company. **Ronald Ensing**, you are probably the only person that has not only read the SSC article I sent them, but went on to read most of the top articles! I think that speaks to your intellectual curiosity and your spirit for debate and discussion. I hope for many more lunch specials in this regard! **Sarah Barendswaard**, thank you for all the coffee talks on philosophy and life in general.

**The Boisterous Ones:** Hidde Boekema, Varun Kotian, Wilbert Tabone, Jetze Schuurmans, Yanggu Zheng, Marko Cvetkovic, Mubariz Zaffar, Sandeep Suresh and Andoni Medina. **Hidde Boekema**, thank you being able to take and give back heat in our discussions, most people don't like it, but it makes things interesting sometimes!

**Varun Kotian**, my padwan, thank you for your diligent experimentation and enthusiasm in embracing the topic. Thank you also for your company, and our fruitful discussions. **Wilbert Tabone**, thank you for beaming a bit of shazam in to our tech-bro club. Your missing presence is always felt whenever you are off to wherever you are off to. **Jetze Schuurmans**, thank you for all the conversations to and from the Coop. Thank you also for saving me from being crushed by weights I am too weak to handle. **Yanggu Zheng** you just missed out by a thin margin on being inducted in to the Ancient Ones! You have always been there throughout the PhD, I have and continue to enjoy your company. Indeed, once a week these days there is a “*Yanggu Day*”, that is a good day. **Marko Cvetkovic**, thank you for your company and being always willing to have a talk. Thank you also for opening your home and hosting us, we will surely make börek soon! **Mubariz Zaffar**, thank you for your friendship, you are a good listener and always have a unique and valuable perspective to share. **Sandeep Suresh**, thank you for all the fun, I have embraced your mannerisms and use them liberally. **Andoni Medina**, thank you for keeping me company in the worse days of COVID when everyone was hidden at home. I hope we will again go for a dip in the canal.

**The Driven Ones:** Shriya Hazra, Paulo Colaco Baptista Cerqueira, Monika Salandova and Nianlei Zhang. **Shriya Hazra**, thank you for your steady belay and friendly company. **Paulo Colaco Baptista Cerqueira** you have the honorary position of the person with the longest name in these acknowledgements. Thank you for keeping me company through the end grind of my PhD and beyond. Your unrelenting toxic masculinity has fuelled my growth to new heights! **Monika Salandova**, thank you also for keeping me company through the end grind of the PhD. Your baking skills were thoroughly appreciated, particularly after my accident. **Nianlei Zhang**, thank you for your steadyish belay, it was quite the first time crash course! Thank you also for your good company on those long drives, though at times you only did answer back in snores!

**The Helpful Ones:** Kenny Lie, Yunyi Li, Job Schepers, Pieter Pinson, Tom Goossens and Jonathan Heemskerk and Adarsh Pattanayak. I would like to thank you all for helping with the experiments. Your efforts were highly valuable.

Lastly, I would like to acknowledge all the **participants** who took part in the experiments that constitute this thesis. The participant interaction is one of the favourite parts of my job, and indeed, an often not mentioned advantage of within-participant research! I thoroughly enjoyed hearing a slice of your life story. I also commend you on your selflessness in the name of science. Out of nearly 100 of you, only a handful dropped out. Some came to the experimental venue despite having flat tyres, others puked and continued for the next motion trial! I am grateful to you all.



# CURRICULUM VITAE

**Tuğrul IRMAK**

1995/01/27      Born in Üsküdar, Turkey.

## EDUCATION

2013-2017      Masters in Mechanical Engineering, University of Bristol  
2017-2022      PhD: Cognitive Robotics, Delft University of Technology  
Thesis on *Understanding and Modelling of Motion Sickness  
and its Individual Differences for the Comfortable Control of Au-  
tomated Vehicles*

2022-Present      Researcher (Post-Doc): Studying motion sickness and mo-  
tion perception, Delft University of Technology





# LIST OF PUBLICATIONS

## JOURNAL ARTICLES

1. **Irmak, T.**, Pool, D.M., Happee, R. Objective and subjective responses to motion sickness: the group and the individual. *Exp Brain Res* 239, 515–531 (2021)
2. **Irmak, T.**, de Winkel K.N., Pool, D.M., Bühlhoff H.H., Happee, R. Individual motion perception parameters and motion sickness frequency sensitivity in fore-aft motion. *Exp Brain Res*. (2021)
3. de Winkel, K.N., **Irmak, T.**, Kotian, V. et al. Relating individual motion sickness levels to subjective discomfort ratings. *Exp Brain Res* (2022).
4. **Irmak, T.**, Kotian, V., Happee, R., de Winkel K.N., Pool, D.M. Amplitude & Temporal Dynamics of Motion Sickness. *Frontiers in Systems Neuroscience* (2022).
5. **Irmak, T.**, Pool, D.M., de Winkel K.N., Happee, R. Validation of Perception Models for Motion Sickness Prediction. *Biological Cybernetics* (To be submitted)

## CONFERENCE ARTICLES

1. **Irmak, T.**, de Winkel K.N., Pattanayak A., Happee, R. Motion Sickness, Motivation, Workload and Task Performance in Automated Vehicles Comfort Congress (2021)
2. Mirakhorlo M., Kluft N., **Irmak T.**, Shyrokau B., Happee, R. Simulating 3D human postural stabilization in vibration and dynamic driving Comfort Congress (2021)
3. Mirakhorlo, M., **Irmak T.**, Happee, R. Simulating lateral postural stabilisation in dynamic cornering. *Humanschwingungen* (2020)
4. Pulgarin E.J.L., **Irmak T.**, Paul J., Arisara M., Herrmann G., Leonards U. Comparing Model-Based and Data-Driven Controllers for an Autonomous Vehicle Task. *Lecture Notes in Computer Science* (2018)

Propositions accompanying the dissertation

**UNDERSTANDING AND MODELLING OF MOTION SICKNESS DEVELOPMENT  
AND ITS INDIVIDUAL DIFFERENCES FOR THE COMFORTABLE CONTROL OF  
AUTOMATED VEHICLES**

by

**Tuğrul IRMAK**

1. Deterministic control theoretic modelling cannot explain motion sickness; probabilistic sensory integration models are needed instead.  
*This proposition pertains to Chapter 5.*
2. As a measure of motion sickness, subjective ratings are superior to physiological data.  
*This proposition pertains to Chapter 2.*
3. Optimising vehicle motions using group-averaged metrics will never give optimal group-averaged comfort.  
*This proposition pertains to Chapter 4.*
4. Motion sickness accumulation is best modelled as a bistable system.  
*This proposition pertains to Chapter 3.*
5. Motion sickness research especially suffers from the "*replication crisis*": all new findings should be assumed false until confirmed by multiple replications
6. The difference between engineering and research is that research should not exclusively focus on positive outcomes.
7. A final grade of 6.0 should be given more often for a Master's thesis.
8. Fully automated vehicles will further reduce human autonomy.
9. Science cannot motivate public policy, only our values can.
10. Mask mandates did not have a measurable effect on the trajectory of the COVID-19 pandemic.

These propositions are regarded as opposable and defensible, and have been approved as such by the promoters Dr. ir. R. Happee and Dr. ir. D.M. Pool